The University Of Sheffield.

Nitric Oxide Reduction with Hydrogen over Carbon-Supported Copper-Iron Oxides Catalysts

By:

Ibrahim B Yakub

A thesis submitted in partial fulfilment of the requirements for the degree of Doctor of Philosophy

The University of Sheffield

Department of Chemical and Biological Engineering

DECEMBER 2018

ABSTRACT

Nitric oxide (NO) is an air pollutant generated during fuel combustion which is responsible for ground-level ozone, acid rain and smog formation. Current abatement technologies include reducing NO to nitrogen (N_2) in the presence of a reductant, usually ammonia, and a catalyst. Replacing ammonia with a less-toxic reductant such as hydrogen (H_2-SCR) requires the utilization of expensive precious metal as a catalyst supported on metal oxides. This study aims to evaluate the potential use of hydrogen as a renewable reductant; activated carbon as a sustainable catalyst support; and less-precious metals as a catalyst to selectively convert NO to N_2. Mono- and bimetallic oxide catalysts were synthesized via incipient wetness method using copper, iron and manganese oxides supported over palm kernel shell activated carbon. Copper-based catalysts were proven to totally convert NO (100 %) in an oxidizing condition starting at 250 °C, while co-impregnating with iron oxide (PKSFeCu) improved N_2 selectivity (eg. from 80 to 100 % at 200 °C) as well as lowering the carbon combustion rate (eg. from 3.1 to 2.3 µmol $CO+CO_2$/s). The catalysts were characterized via elemental and metal content analyses, nitrogen adsorption-desorption, ammonia-temperature-programmed desorption, Fourier-Transform infra-red spectroscopy, hydrogen-temperature-programmed reduction, thermogravimetric analysis, and NO-temperature-programmed desorption. The conversion and selectivity were found to correlate strongly with the catalyst reducibility and acidity. Kinetic experiments revealed that the rate of reaction for H_2-SCR using PKSFeCu obeys a power rate law with an order of 0.82 with respect to NO concentration. The stability test showed that the catalyst is susceptible to changes in physical properties under prolonged exposure to high temperatures and feed gas disturbance. Therefore, improvements in terms of catalyst stability should be the main focus of future work for this sustainable H_2-SCR system to become an attractive alternative to NH_3-SCR.

ACKNOWLEDGEMENT

Praise be to God, Lord of the universe. With the completion of this thesis, I shall acknowledge the organizations and persons who make this possible. First and foremost, appreciation is due to Universiti Malaysia Sarawak and Ministry of Education Malaysia for the sponsorship and opportunity given to pursue this study. This project has been partially funded by the Fundamental Research Grant Scheme FRGS/TK04(02)/1138/2014(05).

My heartiest gratitude goes to Dr. James McGregor as an invaluable supervisor who guided me with brilliant ideas, bolstered my confidence and taught me lessons throughout this journey. I am also indebted to the lecturers, technicians and support staffs in the Department of Chemical and Biological Engineering, and technicians in the Department of Chemistry, for their wonderful advices and services, without which this study would have been impossible. To my colleagues and friends, your encouragements and feedback have kept me going this far. Finally, I must dedicate this work to my late father, whose presence I always sense; my mother, whose love I always have; and my family, whose prayers I always hear.

Thank you,
Ibrahim Yakub
Sheffield
12.12.18

CONTENTS

List of Figures

List of Tables

CHAPTER 1. INTRODUCTION

1.1 Nitrogen Oxides

NO_x is the cumulative notation for nitrogen oxides, consisting mostly of nitric oxide (NO) and nitrogen dioxide (NO_2), which are mainly generated during fuel combustion. It has attracted major interest due to its toxicity and capacity to produce secondary pollutants in the atmosphere (Goodsite et al., 2011). It is a strong respiratory irritant and corrosive to the organ at high concentrations. Acid rain formation, through the transformation of nitrogen oxides and water into HNO_3, can cause death to aquatic ecosystems (Holder, 2002). Additionally, ammonium nitrate particles (0.1 to 1.0 µm size range) may be formed by the nitric acid produced by the reaction of NO_x with water and oxygen available in the atmosphere. This particle is responsible for smog formation, which reduces visibility (Nevers, 1995). NO_x is also associated with the formation of ozone, which is unwanted at ground level and is known to cause respiratory problems, eye irritation and bronchoconstriction (equation 1.1) (Goodsite et al., 2011; Holder, 2002; Nevers, 1995);

$$NO + Hydrocarbon + O_2 + sunlight \rightarrow NO_2 + O_3 \qquad 1.1$$

The formation of NO and its further oxidation to NO_2 proceeds according to equations 1.2 and 1.3, respectively (Nevers, 1995). It is normally assumed that all NO emitted from flue gases react with ozone to form NO_2 which is associated with decreased lung function and increased respiratory infection (Goodsite et al., 2011).

$$N_2 + O_2 \leftrightarrow 2NO \qquad \Delta H_{298K} = 180.6\ kJ/mol \qquad 1.2$$

$$NO + 0.5O_2 \leftrightarrow NO_2 \qquad 1.3$$

Major sources for NO_x can be divided into stationary sources such as coal-fired combustion and mobile sources like motorized vehicles (Nevers, 1995). As of 2011 in Europe, road transportation contributed 40.5 % of total NO_x emissions, as compared to energy production and distribution at 22.5 %. However, the NO_x from on-road emission has greatly decreased due to the decreased limit in the European emission standards. For example, Euro 3, introduced in 2000 for diesel vehicles, has a limit of 0.5 gNO_x/km while Euro 5a in 2009 is 0.18 gNO_x/km. From 1990 to 2011, road transportation

contributed 47.3 % reduction of the total Europe NO_x emissions. In 2015, they continued to be more stringent by introducing Euro 6 at 0.08 gNO_x/km. However, the regulation imposed on the energy sectors (flue gas emission) only contributed to 26.8 % of total reduction (European Environment Agency, 2014). NO_x emission contributors also vary based on world region. For instance, the largest NO_x contributor for the US is mobile sources (57.5 %), while China's major contributor is stationary sources (71 %) (Zhang & Samet, 2015). Figure 1.1 shows the variations in NO_x emissions across the globe (selected countries) from 1970 to 2010. It can be seen that while some countries like the UK and Russia showed reduction in total NO_x emission, some developing countries in South East Asia exhibited otherwise.

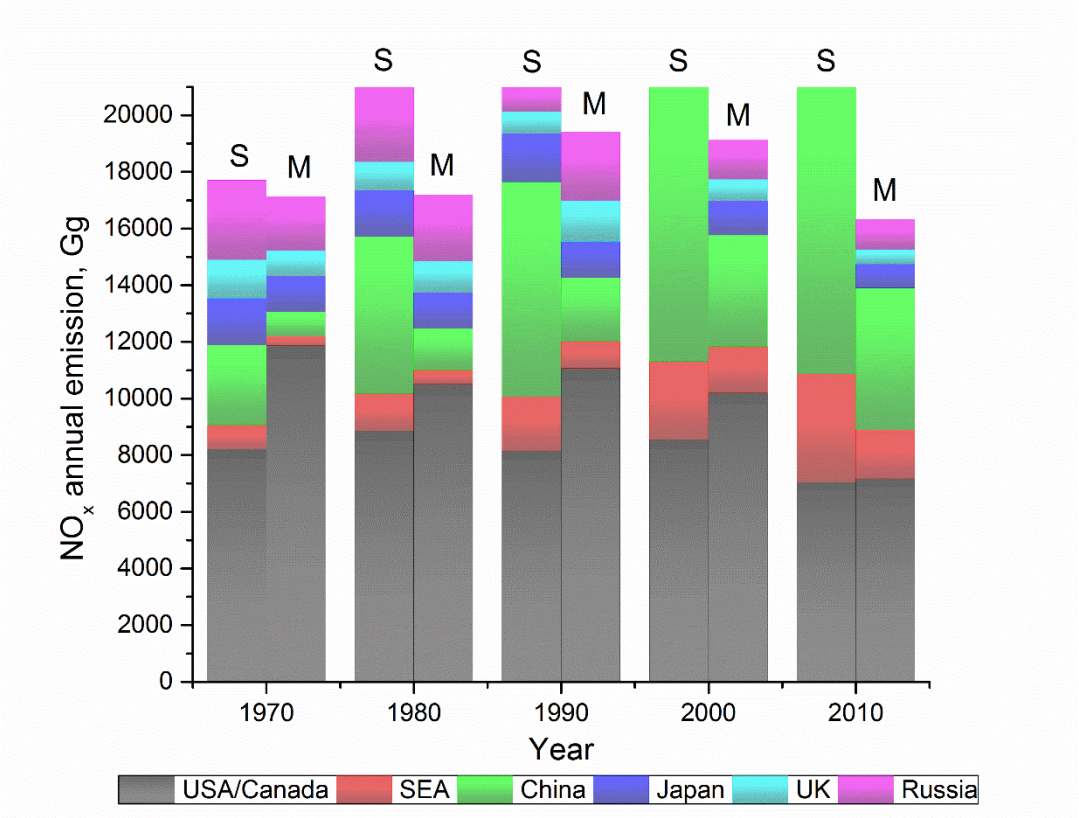

Figure 1.1: Annual nitrogen oxides concentration from 1970 to 2010 for selected countries. S: stationary sources and M:mobile sources. USA: United States of America, SEA: South East Asia, and UK: United Kingdom. Data source: (European Commission, 2016).

The production of NO_x is conditional, as it can be classified as thermal, prompt or fuel NO_x. Thermal NO_x is mostly formed at high temperature (well above 1300 °C such as in combustion) without the need for other molecules while prompt and fuel NO_x can form at low temperature, with proper interaction between nitrogen molecules and the carbon-bearing radicals for the prompt NO_x, and proper NO-to-O_2 ratio for the fuel NO_x. Prompt NO_x is formed by nitrogen contained in the air while nitrogen available in the fuel is the source of the formation of fuel NO_x. To add to the list, the types of fuel and oxidizer used, the size of flame, the degree of fuel-air premixing, the amount of fuel-air pre-heat as well as the formation of intermediates such as free radicals (O, N, OH, H, C, NH, NH_2 and hydrocarbons which have lost hydrogen), water vapor, HCN, oxygen and nitrogen affect the complexity of the prediction of the NO_x generation in a given system (Nevers, 1995).

1.1.1 NO_x emission regulations

Japan, the European Union and the United States are among the pioneering regulators that have established regulations specifically targeted on reducing pollutants from stationary flue gases, especially power stations. For nitrogen oxides, Japan started focused regulation as early as 1973 under the Air Pollution Control Law by the Environmental Standards for Nitrogen Dioxides and Photochemical Oxidants (European Environment Agency, 2010). As for the Europeans, the reduction target was as high as 40 % for NO_x emission within 10 years starting from 1988 (Council of the European Communities, 1988). The 1999 Multi-effect Protocol was introduced thereafter, which included the US and Canada setting limits for the emission of sulfur dioxide, nitrogen oxides, non-methane volatile organic compounds and ammonia by 63, 41, 40 and 17 % respectively in 2010 based on the emission in 1999. The protocol has been renewed in 2012 to achieve reduction target by 2020 (United Nations Economic Commission for Europe, 1979). As of 2012, the treaty had been ratified by 26 parties, including the United States and the European Union (United Nations Economic Commission for Europe, 2012).

Consequently, regulations on NO_x emission have become more stringent in participating countries over the years. For instance, in the U.S, the level of the allowable NO_x emission from boilers using lignite was

0.8 lbs/MMBtu in 1971. This was only applicable to boilers of higher than 73 MW capacity but effective 1997, the regulation was also imposed on boilers of 25 MW or higher capacity with only 0.15 lbs/MMBtu NO_x emission limit (United Nations Economic Commission for Europe, 1979). Besides, Figure 1.2 shows the NO_x emission ceilings targeted by the European Union are mostly lower under the revised United Nations Convention on Long-Range Transboundary Air Pollution (CLRTAP) for 2020 as compared to the targets set for 2010 and under the EU National Ceilings Directive 2001/81/EC (NECD).

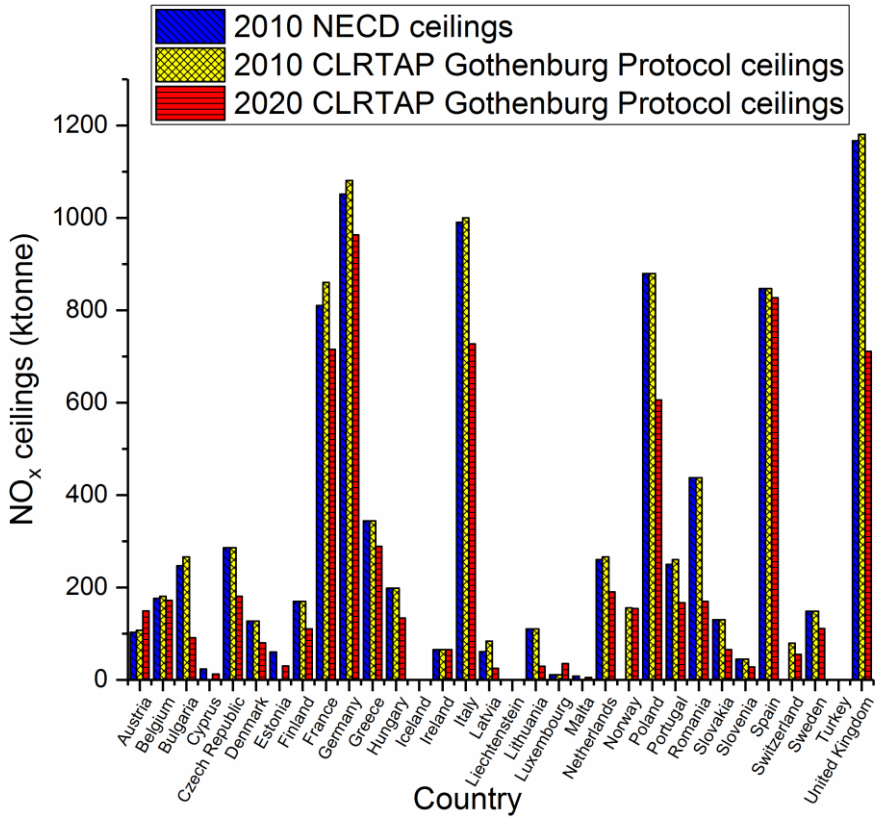

Figure 1.2: NO_x emission ceilings for the EU in 2010 and 2020 (European Environment Agency, 2010).

In the Southeast Asian countries (members of the Association of Southeast Asian Nations, ASEAN), multilateral agreements have been ratified as part of an approach to controlling air pollution caused by agricultural activities such as open burning and deforestation (Khwaja et al., 2012). The ASEAN Transboundary Haze Pollution was developed as a correspondence to the worst episodes of haze in 1997 that consumed over USD 9 billion

economic losses to the region (Khwaja et al., 2012; Goodsite et al., 2011). Haze is caused by the accumulation of particulate matters, usually mixed with the gaseous pollutants including ozone, nitrogen dioxide, carbon monoxide and sulfur dioxide. It reduces visibility, which is dangerous to both land and air traffic besides reducing crop yields and disturbing the earth radiation budget, which affects meteorology (Goodsite et al., 2011).

The World Health Organization's recommended allowable NO_x concentrations in air quality standard are 40 $\mu g/m^3$ and 200 $\mu g/m^3$ for annual mean and 1-hour mean, respectively (Goodsite et al., 2011). For the emission limit values (ELV) from stationary sources, each country uses different methods and units of measurement, so it is difficult to compare emission standards. In addition, most countries impose different ELV between new and existing plants (concerning the starting operational date and the effective date of the regulation) which each have their own criteria. However generally, the new plants have stricter ELV and have been used as the basis of discussion here, alongside the conversion factor produced by Zhu and Wang (2014). European countries set the ELV to 150 mg/m^3 of NO_x emission from a new coal-fired power plants, measured continuously except for the Germany whose measurements are on a daily basis. Australia has the highest ELV (most lenient) at 800 mg/m^3 while China has the lowest value at 50 mg/m^3. Countries in Asia have a wide ELV variation. For example, the levels in Japan, Thailand and Indonesia are in increasing order of 200, 410 and 750 mg/m^3 (Zhang, 2016).

1.1.2 NO_x emission controls

There are generally two ways to control NO_x emissions: by modifying the combustion system or by treating the exhaust gas to convert NO_x into a safer compound before release (Nevers, 1995). Therefore, the Best Available Technologies (BAT) to ensure the reduction targets fulfills the national standards are categorized as follows (European Commission, 2006):

i) Reduction of NO_x formation during the combustion process
   a. Wet combustion controls
   b. Dry combustion controls

ii) Post-combustion NO_x reduction

a. Selective non-catalytic reduction (SNCR)
b. Selective catalytic reduction (SCR)

As thermal NO_x formation becomes significant due to the presence of hot spots in the combustion chamber, water or steam is used to lower the peak flame temperature and subsequently lower the formation of NO_x. The injection can be performed into the furnace during combustion or directly into the flame in the primary combustion zone (European Commission, 2006). Water and steam injection have been shown to reduce up to 42 and 25 ppmv NO_x, respectively with the presence of 15 % O_2. Since water has a higher heat absorbing capacity, less is required to achieve the same effect given by steam. However, this method is associated with increased CO and hydrocarbon formation and reduced turbine efficiency (California Energy Commission, 2002).

The formation of hot zones in the combustion chamber can also be reduced using dry combustion controls such as flue-gas recirculation (FGR), oxygen injection, staged combustion and natural gas injection. In the FGR, the secondary combustion air is replaced with recirculated flue gases that contain lower oxygen concentration which lower the flue-gas temperature. Additionally, pure oxygen or air with enriched oxygen can be used during combustion to limit the supply of nitrogen which leads to NO_x formation. In the staged combustion, oxygen supply in the primary zone is reduced to obtain lower temperature and the subsequent combustion zone is supplied with more air to ensure products of incomplete combustion, such as CO, are kept at a minimum. Finally, natural gas has been used by injection, either into a zone above the primary combustion or directly into the primary zone to inhibit NO_x formation (European Commission, 2006). These options are comparable to the wet combustion controls and are especially preferable if the supply of water is limited and the formation of CO and hydrocarbons could be prevented (California Energy Commission, 2002).

1.1.3 Post-combustion NO_x controls

Another means of reducing NO_x from combustion is treating the flue gas before release into the atmosphere. This is usually preferable either when high conversion is required, or the NO_x content in the flue gas is too low it is

difficult to remove via the methods discussed earlier. Selective non-catalytic reduction (SNCR) is performed by injecting a fluid, mostly amine-based such as ammonia and urea, in the hot zone downstream usually between 850 – 1000 °C (European Commission, 2006). The reaction follows equation 1.4 within this temperature window, whereas NH_3 oxidizes further to NO at higher temperatures, according to equation 1.5 (Tahir et al., 2013).

$$4NO + 4NH_3 + O_2 \rightarrow 4N_2 + 6H_2O \quad 1.4$$

$$4NH_3 + 5O_2 \rightarrow 4NO + 6H_2O \quad 1.5$$

SNCR is very temperature sensitive, as lower temperature would leave most of the ammonia unreacted, called ammonia slip (Tahir et al., 2013). This can also occur when more reagent is required to convert NO_x at more than 80 %. Therefore, a wet scrubber is often used to recover the ammonia and feed back to SNCR. Staged NH_3 injection is also practiced to ensure optimum ammonia consumption at varying temperature zones in the combustion chamber. The key factors in this method are homogeneous mixing and adequate gas residence time (European Commission, 2006).

Alternatively, and sometimes ultimately, selective catalytic reduction (SCR) is used to reduce NO_x especially when the removal required is more than 90 %. SCR is the primary selection installed on stationary sources with desired NO_x reduction unachievable by SNCR (Sorrels et al., 2015).

This technique is discussed in detail in Section 2.1 but it is worth mentioning here that the difference between SNCR and SCR is the need for a catalyst that reduces the temperature requirement for the conversion to take place. Various catalysts have been used in industry and studied in laboratories, especially vanadia- and carbon-based catalysts, in combination with different reducing fluids such as urea, hydrocarbon, hydrogen and carbon monoxide. Choices of catalyst and reductant are dependent on the cost and resource availability. However, it is the current interest to develop a cheaper and sustainable system. Carbon has proven to be functional in the SCR system and it is one of the most sustainable catalyst supports. Hydrogen theoretically would not form additional pollutants such as CO and CO_2 which are produced when using urea and hydrocarbon, and is non-toxic when used in excess in comparison to ammonia and carbon monoxide. With the advent

of sustainable hydrogen production, it is interesting to study the performance of its utilization in SCR.

1.2 Biomass Activated Carbon

Carbon is becoming an alternative to zeolite and metallic oxides supports for catalysts due to its comparatively high porosity and surface area of up to 1,500 m^2/g. It is obtained by carbonizing coal, wood or various other carbonaceous materials, such as biomass and biomass waste including olive stones and coconut shell, in an inert gas. The surface can then be activated by, for example, oxidation via nitric acid or carbon dioxide. This process usually results in various surface entities such as hydroxyl and carboxyl, which make significant contributions to the performance of carbon as a catalyst support (Qian et al., 2015). Therefore, the derivation of carbon from biomass or waste for various purposes including fuel cell, adsorption, gas storage and catalytic reactions has recently becoming popular due to the fact that it is much cheaper, renewable and sustainable (Lam & Luong, 2014).

Activated carbon in particular is widely utilized in wastewater treatment and certain gas purification processes due to its high adsorption capacity. Its potential uses in other applications, especially catalysis, have also been cited and proven. Yang et al. (2011) has reviewed the applications of various forms of carbon as catalyst supports for flue gas treatment, concluding that activated carbon can be a potentially cost-effective solution, especially at a low temperature system (Yang, Chiang, & Burke, 2011). Besides acting as adsorbents to the reactants, biochar also converts the metal oxides into metallic state that increases the catalytic activity. Cotton stalks, coconut shells, rice straw and sewage sludge have all been investigated as catalyst supports in SCR to convert NO_x into inert nitrogen (Singh et al., 2013; Bingnan et al., 2011; Cha et al., 2010).

1.3 Objectives

The main objective of this research is to study nitrogen oxides (NO_x) reduction with the following criteria:

1) Using hydrogen as a renewable reductant;
2) Using palm kernel shell carbons (PKS) as a sustainable catalyst support; and
3) Using earth-abundant and less precious metals (copper, iron, manganese) as a catalyst precursor.

This study aims to achieve the following research outcomes;

1) To evaluate the performance of PKS as a catalyst support for NO reduction with hydrogen;
2) To develop structure-performance relationship by correlating the performance of the catalyst with the measured physico-chemical properties;
3) To evaluate the kinetics parameters and stability of the PKS-derived catalysts in H_2- SCR.

CHAPTER 2. LITERATURE REVIEW

2.1 Selective Catalytic Reduction

In controlling NO_x emissions, selective catalytic reduction (SCR) is the dominant technology typically applied in industry (also considered as one of the BACT, best available control technologies) (Mihet & Lazar, 2014). In earlier patented reactions, methane and hydrogen were used to reduce nitric oxide in an industrial stack gas by contacting those reactants with metallic catalysts producing nitrogen, carbon dioxide and water according to the stoichiometric equations 2.1 and 2.2 which proceed at temperatures greater than 500 °C (Eugene, William, & James, 1959);

$$CH_4 + 4NO \rightarrow CO_2 + 2N_2 + 2H_2O \qquad 2.1$$

$$2H_2 + 2NO \rightarrow 2H_2O + N_2 \qquad 2.2$$

These reactions are fundamental to three-way catalysis under stoichiometric conditions and have been improved for lean-burn condition as in the SCR system. Since then, SCR has found wide application in remediating NO_x from stationary sources such as thermal power plants, chemical plants, municipal waste incinerators, glass, steel and cement industries as well as mobile sources including heavy and medium-duty vehicles (Johnson, 2009; Forzatti, 2001). Over 1,000 SCR units have been installed in the US alone with at least 300 on coal-fired boilers ranging between 100 to 1,400 MWe. It can be utilized solely to control NO_x emission or combined with other technologies such as selective non-catalytic reduction, low NO_x burner and flue gas recirculation (Sorrels et al., 2015).

Capital cost for SCR increased from USD 100/kW in 2000, to USD 250-300/kW in 2011, and was predicted to reach an average of USD 570/kW after 2014 (all costs in 2011 USD). Operating and maintenance costs are typically 0.1 cents/kWh and depend on the capacity of the unit (unit used for multiple combustion sources usually has lower average operating cost but higher reduction target increases this cost) (Sorrels et al., 2015). As many other countries are following the stringent regulations of NO_x emission, several catalysts and reducing agents have been studied to improve the system's

performance for a particular application and to reduce the capital and operating costs of the deNOxing system (Cai et al., 2016).

2.1.1 Process description

There are basically three options for SCR arrangements in an industrial boiler – high-dust, low-dust and tail-end configurations (shown in Figure 2.1). The choice depends on the type of fuel used, technology availability and cost and space constraints. The high-dust configuration is the most widely used due to the availability of metal oxide catalysts, which are reactive at high temperatures and relatively stable against poisons because it is situated prior to any air pollution control devices. On the contrary, the catalyst's stability towards particulate matters (PM) is less important if the second option, low-dust configuration, is used, as PM have been removed prior to the SCR reactor (Jensen-holm, Castellino, & White, 2012). However, the flue gas temperature could drop below the NH_3-SCR optimum operating temperature, requiring an increase in the size of the economizer bypass duct. In the third option, a tail-end configuration requires the flue gas to be heated up to the SCR operating temperature as it is positioned downstream of the other air pollution control devices (Sorrels et al., 2015). Despite the higher costs incurred by this type of arrangement, a low cost catalyst such as carbon catalysts can be used to disregard the effect of particulate matters and poisons such as SO_2 (Singh et al., 2013).

A typical means of introducing ammonia is by injection, either from its anhydrous or aqueous form, with the latter requiring a vaporizer. Gaseous ammonia decomposes into NH_3 and NH_2 and comes into contact with NO_x. As NH_3 is toxic, it is sometimes stored in a more stable form such as urea and solid reductants. The usage of urea requires a complex injection system which is temperature-sensitive, while the size of the droplets formed affects the overall performance. Generally, there are three steps involved in the decomposition of urea in the SCR reactor: evaporation of water from the solution; hydrolysis of molten urea into ammonia and isocyanic acid (HNCO); and hydrolysis of HNCO into ammonia and CO_2. This process is summarized in equation 2.3, where it can be seen that 2 mol of NH_3 is produced for every

mol of urea, which is sufficient for both standard and fast SCR reactions (Guan et al., 2014).

$$NH_2 - CO - NH_2 + H_2O \rightarrow 2NH_3 + CO_2 \qquad 2.3$$

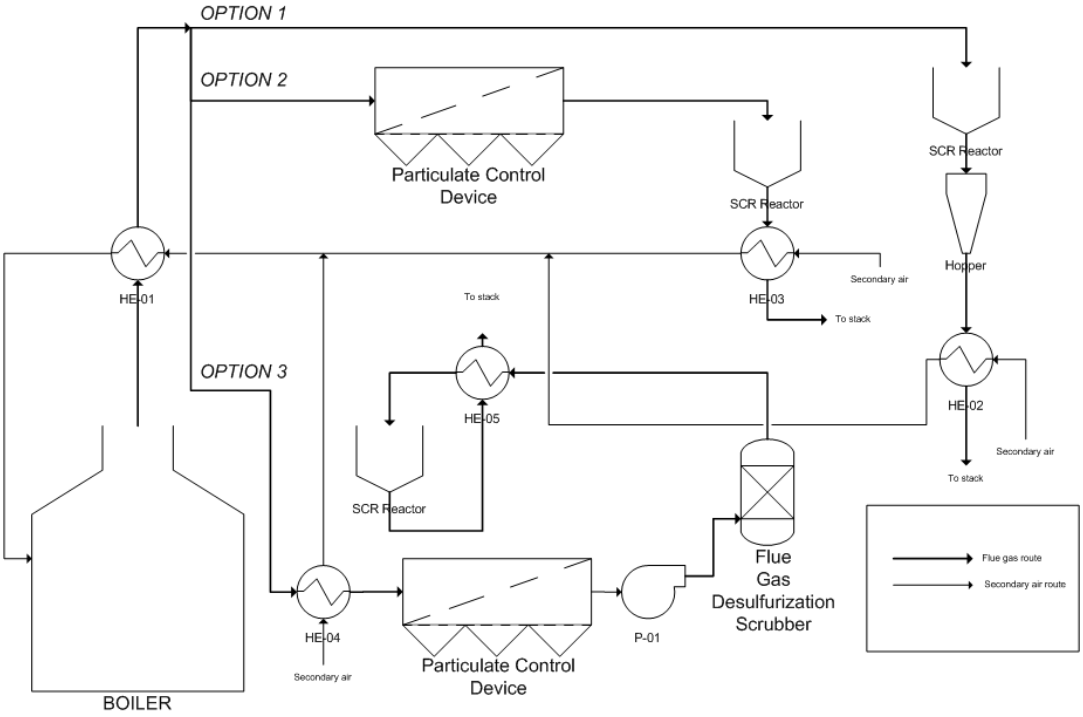

Figure 2.1: Process flow diagram for flue gas treatment with SCR for options; 1) High-dust, 2) Low-dust, and 3) Tail-end SCR. Summarized from (Sorrels et al., 2015; Jensen-holm, Castellino, & White, 2012).

However, a survey conducted on SCR operators revealed that 80 % use ammonia (anhydrous and aqueous) because as more than half of the respondents indicated, cost is their primary criterion. Only a quarter took safety as the priority (Sorrels et al., 2015). On another note, the need for sophisticated ammonia injection causes the non-SCR operators to avoid this technology regardless of its effectiveness. Additionally, there have been arguments over the secondary pollution instigated by using ammonia in this treatment via the slip ammonia (unreacted portion) and reaction with SO_2 producing ammonium sulfates at temperature below 350 °C (Armor, 1992). This is accompanied by increased capital and operating costs, mostly due to the reagent and catalyst replacement. Nevertheless, SCR is preferred over other NO_x-reducing techniques such as SNCR because of its higher efficiency

and the lower and wider temperature window (Roy, Hegde, & Madras, 2009). Therefore, the utilization of other renewable reagents such as hydrocarbon, hydrogen and carbon monoxide, and cheaper catalysts in SCR have been areas of interest (Mrad et al., 2015; Hamada & Haneda, 2012; Liu, Li, & Woo, 2012).

2.1.2 Conventional reactions and catalysts

The reactions of nitric oxide reduced using ammonia are given by equations 2.4 (standard SCR) and 2.5 (without oxygen) while the reduction of nitrogen dioxide is given by equation 2.6. The fastest reaction occurs at equimolar NO and NO_2, as represented in equation 2.7 (fast SCR) (Guan et al., 2014; Forzatti, 2001);

$$4NO + 4NH_3 + O_2 \rightarrow 4N_2 + 6H_2O \quad 2.4$$

$$6NO + 4NH_3 \rightarrow 5N_2 + 6H_2O \quad 2.5$$

$$6NO_2 + 8NH_3 \rightarrow 7N_2 + 12H_2O \quad 2.6$$

$$2NO + 2NO_2 + 4NH_3 \rightarrow 4N_2 + 6H_2O \quad 2.7$$

The reaction temperature depends on the catalyst being used but most commercial catalysts require optimum temperatures between 250 and 430 °C. Some of the industrial catalysts also produce nitrous oxide (N_2O) according to the reaction in equation 2.8 at temperatures higher than 400 °C and ammonia is oxidized into additional NO at temperatures beyond 500 °C, as shown in equation 2.9, both of which are undesirable. Besides, too low a temperature (below 200 °C) can cause the formation of ammonium nitrate (NH_4NO_3), as depicted by equation 2.10 (Guan et al., 2014).

$$4NH_3 + 4NO + 3O_2 \rightarrow 4N_2O + 6H_2O \quad 2.8$$

$$4NH_3 + 5O_2 \rightarrow 4NO + 6H_2O \quad 2.9$$

$$2NH_3 + 2NO_2 \rightarrow NH_4NO_3 + N_2 + H_2O \quad 2.10$$

Formerly, precious metals such as platinum, palladium and rhodium were used as SCR catalysts, but were limited to natural gas combustion and other low-temperature exhaust gas applications because of their ammonia-oxidizing ability at high temperature (Forzatti, 2001). Therefore, base metals such as vanadium, titanium and tungsten have emerged as excellent SCR

catalysts due to the ability to broaden the temperature window. Zeolites and crystalline alumina silicates are also used as supports, usually for high temperature applications (360 – 540 °C), but this would increase the overall cost of the catalyst (Sorrels et al., 2015).

Vanadium-based catalysts demonstrated excellent performance in reducing NO_x gases over wide temperature window such as that shown by V_5-W_3/TiO_2 and V_2O_5/AC, supported by different materials (i.e. titania and activated carbon, respectively) with high NO_x conversion at 400 and 150 °C correspondingly (Camposeco et al., 2014; Hou et al., 2014). However, there have also been reports claiming that toxic vanadium compounds were released at above 600 °C arousing environmental concern over its uses. Hence, numerous studies have formulated new vanadium-based catalysts, including a tungsten-coupled TiO_2-supported catalyst and rare earth modified vanadates which have shown no indication of toxic release at temperatures as high as 850 °C (Guan et al., 2014). Titanium dioxide is a preferred choice of support due to its high tolerance against SO_2 poisoning, which is common in an SCR system (Fang et al., 2015). The incorporation of TiO_2 as W and/or V support has displayed a synergistic effect which promotes the oxidation of hydrocarbon and soot presence in flue gas (Japke et al., 2015).

Generally, the rate of reaction is first order in NO, as well as independent of oxygen, ammonia and water for >2 vol.% O_2 (Forzatti, 2001), NH_3/NO >1 and >5 vol.% H_2O correspondingly (Busca et al., 1998). It has been accepted that N_2 formed via equation 2.4 attains one atom each from NO and NH_3 (Forzatti, 2001). The activity requires both acid-base and redox sites that are responsible for adsorption and activation of ammonia, respectively (Jensen-holm, Castellino, & White, 2012). The activation energy is provided by the high flue gas temperature and the reaction is not limited by the thermodynamic equilibrium, for the amount of heat released is considerably small (Sorrels et al., 2015). The extent of the favoured reactions depends highly on the surface reactivity of the catalysts. For a vanadia-based catalyst, the reactive site can be V-OH, V=O or V(5+)=O group (based on different proposal by different researchers). Regardless of the reactive site, the popular mechanism proposed for these range of catalysts is that of Eley-Rideal, in

which ammonia is adsorbed at these sites before reacting with NO and selectively forming nitrogen (Forzatti, 2001).

The typical reactivity of a V_2O_5-WO_3/TiO_2 catalyst can be explained with a transient response analysis such as that by Lietti et al. (1998), as shown in Figure 2.2. It is clear (from A) that NO is weakly adsorbed on the catalyst as the breakthrough curves resemble the ideal positive step change. Meanwhile, NH_3 is appreciably adsorbed on the catalysts for the delayed breakthrough time as compared to the step change. Feeding in NH_3 into the NO+O_2+He system (in B) indicates a dead time at the beginning before steady-state is reached while the formation of N_2 is specular to the consumption of NO. On the other hand, feeding in NO into the NH_3+O_2+He system (in C) instantaneously brought all components to their steady-state concentration. This strengthened the fact that the reaction proceeds via an Eley-Rideal mechanism, which requires only NH_3 adsorption, while NO is converted in its gas phase/weakly adsorbed molecules.

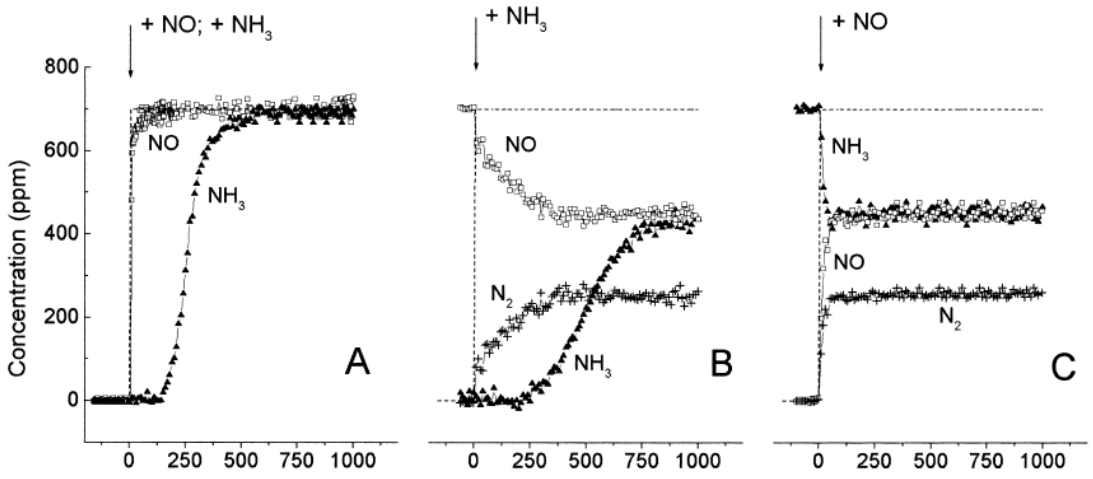

Figure 2.2: Transient response analysis of V_2O_5-WO_3/TiO_2 model catalyst during positive step of (A) NO and NH_3 into He+O_2, (B) NH_3 into NO+O_2+He and (C) NO into NH_3+O_2+He. Reaction condition: 700 ppm NO + 700 ppm NH_3 + 1 % O_2 + He at 120 sccm over 0.16 g catalyst between 220 to 350 °C. Reprinted with permission from (Lietti et al., 1998). Copyright (1998) Elsevier.

2.2 Ammonia-less SCR

As discussed in Chapter 1, many other countries are implementing the stringent regulations of NO_x emission and SCR has been accepted as the best available technology. However, the high capital and operating costs associated with ammonia have hindered SCR deployment especially in developing countries. Alternative reducing agents, and consequently catalysts, have been studied to reduce the costs and eliminate the formation of toxic by-products / ammonia slip while competing with the performance of a conventional method. Additionally, it is worth reviewing the catalytic decomposition of NO_x without the presence of a reductant as an alternative to NH_3-SCR.

2.2.1 Reagentless NO_x catalytic decomposition

Nitric oxide can be decomposed to nitrogen via equation 2.11, but the reaction does not proceed at a perceptible rate because it is spin-forbidden and has high activation energy (364 kJ/mol) (Mrad et al., 2015; Roy, Hegde, & Madras, 2009).

$$NO \rightarrow \frac{1}{2}N_2 + \frac{1}{2}O_2 \qquad \Delta H^{\circ}_{298K} = -86.6\ kJ/mol \qquad 2.11$$

Catalysts have been developed to overcome the activation energy and make decomposition possible under attractive reaction conditions. One of the factors required for a decomposition catalyst is the adsorption of nitric oxide that can be either dissociative or molecularly on the catalyst. Desorption of oxygen from the catalyst surface is preferred to be fast to prevent metal oxidation or the formation of an oxygen adlayer over the catalyst surface, which obstructs subsequent decomposition processes (Roy, Hegde, & Madras, 2009).

Figure 2.3 shows the typical types of NO adsorption states reported so far on transition metal surfaces where it can be dissociative, molecular or both. Though the rule is presented based on the position of the metals in the periodic table, adsorption species formation is rather complex, as it depends on the surface temperature and crystallinity, as well as the presence of surface defects and NO coverage (Brown & King, 2000). The weaker N-O bond as compared to the M-N dissociates the NO molecules into nitrogen and oxygen

adatoms. Most single crystalline metals are permanently oxidized by M=O bonds, which deters the further NO adsorption-dissociation steps. However, metals such as rhodium, ceria and cobalt oxides showed 'oxygen spillover' effect where the dissociated oxygen forms weak bonds with the metals that are easier to desorb (Roy, Hegde, & Madras, 2009). The dissociation of NO as a dinitrosyl species is abundant on Mo surfaces especially Mo{110} and complete dissociation is always seen on W surfaces. However, at very high NO coverage, little molecular NO adsorption occurs on either metals (Brown & King, 2000).

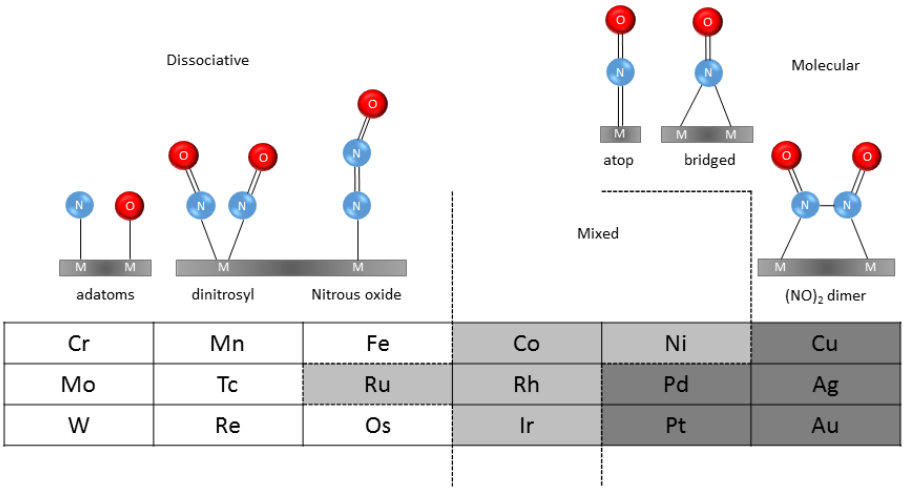

Figure 2.3: Nitric oxide adsorption states on selected transition metals. M: metal, N: nitrogen, O: oxygen atom. Adapted from (Roy, Hegde, & Madras, 2009; Brown & King, 2000).

Molecular adsorption is more prominent as NO interacts with metals of increasing *d* subshell electrons (metals to the right of the periodic table). This can be explained by considering the bonding between CO and the transition metals. As CO is bonded to the metals to the right of the table, overlapping between *d*-metal and CO $2\pi^*$ orbitals decreases such that the dissociation of the C-O bond does not occur spontaneously (Roy, Hegde, & Madras, 2009). Pd evidently allowed complete molecular NO adsorption. Choi et al. (2015), via temperature-programmed desorption (TPD) after exposure of PdO{101} with NO at 90 K, observed no desorption of other species than molecular NO up to 600 K showing no dissociation reaction. Reflection absorption infra-red spectroscopy (RAIRS) showed the presence of linear (or atop) and bridged-NO which requires two adjacent sites to hold one NO molecule.

The adsorption of NO on metal surfaces is fundamental in designing the sorbent material, lean-NO_x trap (LNT) catalysts and NO_x-decomposition catalysts. NO sorbent has many applications including medical, as non-toxic sorbents such as carbon can be used to deliver NO in therapies (Fioretos, Psofogiannakis, & Froudakis, 2011). Selective NO_x recirculation (SNR), developed by Daimler-Chrysler, is using two adsorbing beds that operate alternatively where the desorption returns NO_x into the combustion chamber to decompose NO_x thermally. This is a similar concept to LNT but upon desorption, LNT uses reductants, usually hydrocarbons, carbon monoxide and hydrogen, to chemically reduce NO_x (Gomez-Garcia, Pitchon, & Kiennemann, 2005). On the other hand, NO_x decomposition catalysts convert NO_x into nitrogen without requiring desorption step and reducing agents.

Alumina-silica supported transition metals have shown considerable adsorption capacity at room temperature of up to 0.23 mg NO/m^2. Copper is said to be more adsorptive in its oxidized form than the reduced state, unlike other metals such as iron, nickel, chromium, cobalt and platinum. Adsorption on alumina-supported precious metals also produces NO_2, which is more reactive in reduction reaction (Gomez-Garcia, Pitchon, & Kiennemann, 2005). Other adsorptive supports have also been used with metal oxides including silica, zeolite and carbonaceous materials. SBA-15 silica showed significant adsorption improvement (from 0.3 to 5.0 mmol NO_2/g) when doped with cerium-zirconium mixed oxides. Fe and Cu have also been impregnated onto carbons and shown adsorption capacity up to 320 mg NO/g at 303 K with desorption temperature as low as 393 K. However, traces of CO_2 would have been observed with this sorbent starting at 383 K, making this a trade-off of its optimal performance (Gomez-Garcia, Pitchon, & Kiennemann, 2005).

Winter (1971) found that the NO decomposition mechanism is similar to the decomposition of N_2O (equation 2.12) over metal oxides. However, the NO adsorption is higher than the N_2O, and the presence of oxygen has significant impact on the surface coverage of the metal oxides especially CuO and Cr_2O_3 which shown higher affinity towards O_2. The NO decomposition over 40 metal oxides showed first order kinetics with respect to NO pressure and the rate-determining steps are the NO adsorption on the adjacent anion vacancies and reforming of the sites via oxygen desorption. A similar

mechanism can be seen by using precious metals such as platinum, and zeolite-based catalysts (Haneda & Hamada, 2016).

$$2N_2O \rightarrow 2N_2 + O_2 \qquad 2.12$$

Copper ion-exchanged zeolite ZMS-5 has attracted much attention in SCR since its discovery due to superior NO decomposition to N_2 (conversion and selectivity of at least 90 and 60 %, respectively), and persistence against oxygen of up to 10 % (Li & Armor, 1991). The adsorption species are molecular NO and its dimer $(NO)_2$ on Cu^+ ions that exist alongside Cu^{2+} in zeolite framework. The reversible redox interaction between copper ions ($Cu^{2+} \leftrightarrow Cu^+$) continues the reduction of NO to N_2. However, NO_2 was also reported to form with small amount of N_2O at low temperature and high temperature is required to regenerate the catalysts. As the zeolite structure is altered above 600 °C, this catalyst is preferred for use in low-temperature SCRs (Imanaka & Masui, 2012).

Activated carbon (discussed in Section 1.2) has also been shown to decompose NO in the presence of CuO. NO can be readily adsorbed on the activated carbon due to the high surface area and rich in oxygenated functional groups (Plens, Monaro, & Coutinho, 2015). Inopportunely, NO_2 in the flue gas is also being adsorbed and reduced to NO while oxidizing carbon surface. The addition of copper on carbon alters the adsorption mechanism by forming copper nitrate/nitrite, before completely being reduced at temperatures as low as 270 °C (Levasseur et al., 2011; Xue et al., 2008). The mechanism of NO_x decomposition over activated carbon-supported copper is illustrated in Figure 2.4. As the NO_2 oxidizes the carbon, the CO formed is used to reduce Cu^{2+} to Cu^+, which can be re-oxidized by NO in its reduction to nitrogen (Sager et al., 2013).

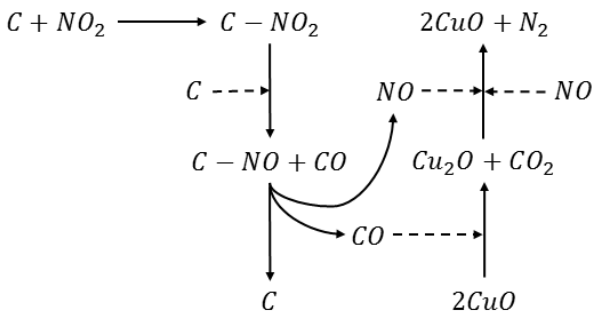

Figure 2.4: NO_x decomposition over Cu-carbon. Adapted from (Sager et al., 2013).

Overall, reagentless decomposition of NO suffers from the high temperature requirement and oxidation by the intrinsic oxygen content in the exhaust/flue gas that hinders the practical application. Therefore, a reagent is added to overcome these problems.

2.2.2 Hydrocarbon and carbon monoxide SCR

In earlier patented reactions, methane and hydrogen were used to reduce nitric oxide in industrial stacks by contacting those reactants with metallic catalysts producing nitrogen, carbon dioxide and water according to the stoichiometric equations 2.13 and 2.14 which occur at temperatures greater than 500 °C. The catalysts used were layered 0.5 wt.% platinum supported over alumina and nickel aluminate and at 25,999 h^{-1}, the reduction is almost 100 % (Eugene, William, & James, 1959);

$$CH_4 + 4NO \rightarrow CO_2 + 2N_2 + 2H_2O \qquad 2.13$$

$$2H_2 + 2NO \rightarrow 2H_2O + N_2 \qquad 2.14$$

Since then, many studies and patents regarding the utilization of hydrocarbons in removing NO_x have been published. These reactions are also fundamental to the three-way catalysis used in the vehicle emission control under stoichiometric conditions. In addition, in a SNCR, hydrocarbon (HC) and carbon monoxide (CO) are used as additives to improve the performance of the system. For instance, the addition of methane (CH_4-to-NH_3 ratio of 1) reduced the maximum temperature from 1200 to a window of 735-800 °C for the maximum 60 % NO_x conversion while increasing the amount of CO up to

1000 ppm in the system reduced the temperature window by 110 °C (Tahir et al., 2013).

Theoretically, the presence of a catalyst could further lower this effective temperature window; this is where the SCR system is applied. Utilizing the intrinsic carbon monoxide and unburned hydrocarbon in the exhaust gases both from mobile and stationary sources to reduce NO_x in the presence of oxygen is a sustainable alternative to NH_3-SCR. Therefore, efforts have been made to find the optimum pair of reductant and catalyst that is effective at lower temperature.

The generalized reactions for HC oxygenation and HC-SCR are shown in equations 2.15 and 2.16 respectively, where $C_xH_yO_z$ represents the oxygenated hydrocarbon (Łamacz, Krztoń, & Djéga-Mariadassou, 2013);

$$HC + NO_2 \rightarrow NO + C_xH_yO_z \qquad 2.15$$

$$C_xH_yO_z + NO_2 \rightarrow N_2 + CO_2 + H_2O \qquad 2.16$$

A review of the patents of HC-SCR catalysts revealed that many HC have been used, including methane, propene and propane, as well as the oxygenated HC such as aliphatic alcohol. The maximum temperature lies between the onset temperature of equation 2.16 and the combustion temperature of the HC (without NO_x presence), and higher selectivity can usually be achieved when these two temperatures have greater difference. Precious metals such as Pt are known to be reactive but HC combustion temperatures are normally low over these catalysts lowering the selectivity (Tabata, Kokitsu, & Okada, 1994). Besides, the formation of N_2O over precious metals is significant, especially at low temperature. However, the bimetallic catalyst Pt-Sn supported over silica showed total N_2 selectivity attributed to the oxygen-deficient SnO_x species. In addition, rhodium and ruthenium-based catalysts were reported to give higher selectivity compared to platinum catalysts but are susceptible to deactivation by sulfur dioxide and limited to reducing condition as in the three-way catalyst (Mrad et al., 2015; Pârvulescu, Grange, & Delmon, 1998).

Many studies using metal ion-exchanged zeolites have established that the selectivity of the catalyst to reduce NO_x depends on the HC used. For instance, Co, Mn, Ni, Ga and In are selective with methane, while Cu and Ce

are selective with C_{2+} hydrocarbons. However generally, CH_4 and C_2H_6 are considered as non-selective while most alkenes and alkynes such as ethene, propene and acetylene were found to be selective. In fact, C_2H_4 was proven to have higher selectivity compared to NH_3 even in the presence of excess oxygen (Pârvulescu, Grange, & Delmon, 1998). Furthermore, the reactivity of the saturated HC was ranked as follows: i-C_4H_{10} > n-C_5H_{12} > 2,2,4-tri-methylpentane > neo-C_5H_{12} > 3,3-dimethylpentane > methane > C_3H_8 > 3,3-diethylpentane. Meanwhile, the reactivity of soluble oxygenated HC such as alcohols, aldehydes, ketone and ethers were comparable to that of propene (Mrad et al., 2015).

Table 2.1 shows the performance of novel catalysts that have been studied on HC-SCR. Bimetallic catalyst Cs-Co supported over zeolite showed high N_2 selectivity in HC-SCR as each metal plays important roles – Cs improved toluene adsorption while Co acted as the reactive site. The zeolite support was reported to lose the adsorption capacity for HC as Ce was exchanged over the surface which is the reason Cs was incorporated (Serra et al., 2015). Another study using activated carbon as the support for Ce catalyst showed similar conversion but achieved at lower temperature due to the presence of oxygenated functional groups and oxygen storage and supply over the metal surfaces. However, the maximum oxygen content in the reaction gas was reported not to exceed 3 % due to the exacerbated support combustion (Chu et al., 2015).

Overall, unsaturated hydrocarbon supplies more electrons than ammonia making it easily forming oxygenates as reactive species but it is less polar compared to NH_3 causing weak adsorption with the metal surface that affects N_2 selectivity (Busca et al., 1998). Even with satisfying conversion and selectivity in the HC-SCR, the unreacted HC and nitrite-nitrate complexes still remain in the flue gas (Pârvulescu, Grange, & Delmon, 1998).

CO and H_2 are also employed in the reduction of NO from automotive exhaust gas but are not considered as selective due to the formation of by-product including N_2O or NH_3. However in a lean flue gas treatment at high temperature, such as that in a fluid catalytic cracking regenerator where the concentration of CO is usually higher than O_2, carbon monoxide is favoured for use as a reductant due to its ability to consume the excess oxygen which

retards the reduction of NO (Hamada & Haneda, 2012). Various catalysts have been investigated to increase the selectivity towards N_2 formation. By using the base metal oxides Fe_2O_3 and Cr_2O_3, the CO-NO reaction (equation 2.17) superseded CO-O_2 reaction (equation 2.18). This was due to the poisoning effects of oxygen by the active site preventing CO combustion (Pârvulescu, Grange, & Delmon, 1998).

$$2NO + 2CO \rightarrow N_2 + 2CO_2 \qquad 2.17$$

$$O_{ads} + CO \rightarrow CO_2 + * \qquad 2.18$$

Patel et al. (2014) compared the activity of various MSM-41-supported base metal oxides with a precious metal (i.e. Ru) and found the latter to be the most reactive (total conversion at 300 °C) in a 250 ppm NO + 750 ppm CO gas flow at 80 mL/min over 0.1 g catalyst, followed by copper. It was also found from the characterization that Ru/MCM-41 possessed the highest reducibility ($1/T_{red}$, T_{red} being the first temperature peak in the TPR experiment), whereas the metal-oxygen bond strength in RuO_2 is the lowest. A relationship plot between these two parameters for the studied catalyst is shown in Figure 2.5 which suggests that a catalyst to the right-hand side of the graph should be reactive in SCR.

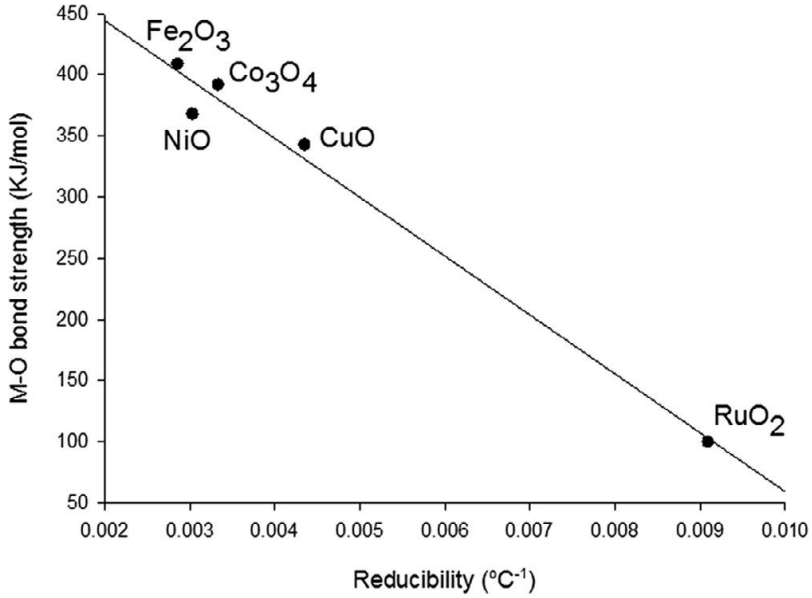

Figure 2.5: Relationship plot between M-O bond strength and reducibility of metal oxides. Reprinted with permission from (Patel et al., 2014). Copyright (2014) Elsevier.

The performance of selected catalysts in CO-SCR is shown in Table 2.1. Among other precious metals used were gold and iridium, both showing total conversion at low temperature (Ilieva et al., 2015; Haneda et al., 2005). Ilieva et al. (2015) attributed the improved conversion from using Au/Ce to using Au/FeCe (from 75 to 100 % at 250 °C) to the participation of Fe_2O_3 in oxidizing CO and thus reducing NO by Fe_3O_4. A similar conclusion on the role of Fe_2O_3 has also been published by Li et al. (2014).

Non-precious metals such as Mn and Cu have also shown great performance when supported over metal oxides. When comparing Cu, Ni, Fe, Mn and Cr supported over TiO_2, Sreekanth and Smirniotis (2008) found that the NO conversion decreased as Mn > Ni > Cu > Cr > Fe. The high Mn reactivity was ascribed to the multiple Mn phases presence on the TiO_2 surface as indicated via a temperature-programmed reduction (TPR) experiment (MnO_2, Mn_2O_3 and Mn_3O_4). Meanwhile, Cu supported over amorphous $AlPO_4$ has been proven to give 100 % NO conversion and N_2 selectivity in CO-SCR. The ion exchange over the support yielded well-dispersed copper (II) amino species was claimed to be responsible for this activity (Kacimi, Ziyad, & Liotta, 2015).

Table 2.1: Review on catalysts performance used in recent HC and CO-SCR studies.

Catalyst	Preparation method (calcination temperature)	Feed gas composition (space velocity/flow rate)	Highest NOx conversion (temperature)	Highest N_2 Selectivity (temperature)	Other performance	Ref
2wt.%Cs-2.9wt.% Co/Mordenite	Ion exchange of Na-mordenite with $Co(CH_3COO)_2$ and $CsCH_3COO$ (500°C, 8h in air)	1000ppm NO + 2% O_2 + 286ppm C_7H_8 + 2% H_2O + He ($20,000h^{-1}$)	~80% (525°C)	-	0.27 toluene retention capacity	(Serra et al., 2015)
7wt.%Ce/activated carbon	Activated with HNO_3 and impregnated with $Ce(NO_3)_3{\cdot}6H_2O$ (400°C, 2h in N_2)	0.1% NO + 0.1% C_3H_6 + 3% O_2 + N_2 (600mL/min)	~70% (300°C)	-	~80% C_3H_6 conversion (300°C)	(Chu et al., 2015)
0.53wt.%Rh/$Ce_{0.62}Zr_{0.38}O_2$	Incipient wetness with rhodium (III) nitrate over $Ce_{0.62}Zr_{0.38}O_2$ (550°C, 2h in air)	250ppm NO + 247ppm HC (50ppm C_3H_8, 133ppm C_3H_6 and 64ppm C_7H_8) + 5% O_2 + Ar ($30,000h^{-1}$)	~60% (280°C)	~50% (280°C)	~100% HC conversion (280°C)	(Adamowska-Teyssier et al., 2015)
1wt.%Au-1wt.%Ag/Al_2O_3	$HAuCl_4$ and $AgNO_3$ co-precipitated over Al_2O_3 using urea (500°C, 6h)	300ppm NO + 300ppm CO + 300ppm C_3H_6 + 2000ppm H_2 + 100ppm $C_{10}H_{22}$ + 10% CO_2 + 10% O_2 + 5% H_2O + He ($50,000h^{-1}$)	~100% (350°C)	~90% (350°C)	-	(More et al., 2015)
Cu_3Ti_1	Titanium sulfate and copper nitrate co-precipitated using urea (450°C, 6h)	1000ppm NO + 1000ppm C_3H_6 + 10% O_2 + He ($20,000h^{-1}$)	~80% (260°C)	-	~65% N_2 yield (270°C) ~100% C_3H_6 conversion (250-300°C)	(Yuan et al., 2014)
4wt.%Pd/SBA	Incipient wetness with $Pd(NH_3)_4(NO_3)_2$ over mesoporous silica SBA-15 (500°C, 2h in air)	1500ppm NO + 1500ppm CH_4 + 7% O_2 + Ar ($22,100h^{-1}$)	~100% (300°C)	-	~100% CH_4 conversion (550°C)	(Boutros et al., 2014)
4wt.%Ag/Al_2O_3+6 wt.%Ba/ZSM5	Wet impregnation of Al_2O_3 with $AgNO_3$ and ZSM5 impregnated with $Ba(NO_3)_2$ (600°C, 3h in air)	500ppm NO + 5% O_2 + 200ppm $C_{10}H_{22}$ + 6% H_2O + 1ppm SO_2 + He ($60,000h^{-1}$)	~55% (450°C)	-	-	(Sultana et al., 2013)
5wt.%Cu/$AlPO_4$	Ion exchange of $AlPO_4$ with $Cu(NO_3)_2.4H_2O$ (500°C in air)	0.2% NO + 0.65% O_2 + 1.5% CO + He (200mL/min over 100mg catalyst)	~100% (325°C)	~100% (325°C)	-	(Kacimi, Ziyad, & Liotta, 2015)
3wt.%Au/FeCe	Deposition-precipitation of 5%Fe_2O_3-loaded ceria with $HAuCl_4.3H_2O$ (400°C, 2h in air)	3000ppm NO + 5% O_2 + 3000ppm CO + 1000ppm H_2 + He (60,000mL/g.h)	~100% (250°C)	~100% (250°C)	0% N_2O formation (250°C)	(Ilieva et al., 2015)
4wt.%Ru/MCM-41	Ru precipitation over MCM-41 (500°C, 5h in air)	250ppm NO + 750ppm CO + He (80mL/min over 100mg catalyst)	~100% (450°C)	-	-	(Patel et al., 2014)
3wt.%Cu/MCM-41	$Cu(NO_3)_2$ precipitation over MCM-41 (500°C, 5h in air)	250ppm NO + 750ppm CO + He (80mL/min over 100mg catalyst)	~75% (450°C)	-	-	(Patel et al., 2014)
3wt.%Fe-Mo/Al_2O_3	$Al(NO_3)_3.9H_2O$ co-precipitated with molybdemum and $Fe(NO_3)_3$ (400°C, 4h in air)	1000ppm NO + 1% O_2 + 4% CO + He ($8,000h^{-1}$)	~80% (700°C)	-	~100% O_2 consumption (700°C)	(Li et al., 2014)
5wt.%Ir/SiO_2	Wet impregnation of SiO_2 with $H_2IrCl_6.6H_2O$ (600°C, 8h in air)	1000ppm NO + 6000ppm CO + 6% H_2O + He ($75,000h^{-1}$)	~80% (500°C)	-	~100% N_2 selectivity (500°C)	(Haneda et al., 2005)

2.2.3 Hydrogen-SCR

The presence of hydrogen has also been shown to improve the HC- and CO-SCR efficiency due to its involvement in the NO adsorption activity, direct gas-phase reaction with the reactants, and facilitation in HC/CO oxidation. The intrinsic content of hydrogen in the vehicle exhaust has also been utilized as a three-way catalytic reductant. Therefore, studies on the utilization of hydrogen as an SCR reductant has attracted special interest.

Hydrogen can react with NO to produce NH_3 that reduces the other NO_x species. This reaction is usually carried out at very high temperature (more than 800 °C) and with limited amount of oxygen (Hamada & Haneda, 2012). However, it has been demonstrated that some catalysts can promote deNO_x using hydrogen at lean-burn combustion and low temperature according to equation 2.19 (Costa et al., 2002). Equations 2.20 and 2.21 also occur as side reactions, giving undesired products (Chiarello et al., 2007; Costa et al., 2002).

$$2NO + 4H_2 + O_2 \rightarrow N_2 + 4H_2O \qquad 2.19$$

$$2NO + 3H_2 + O_2 \rightarrow N_2O + 3H_2O \qquad 2.20$$

$$2H_2 + O_2 \rightarrow 2H_2O \qquad 2.21$$

Noble metals are commonly used in a H_2-SCR studies due to their known ability to activate hydrogen, as well as to increase the acidity and reducibility of the catalyst which is preferable in reducing NO_x gases. Several studies have compared the performance between noble metals in H_2-SCR and selected ones are listed in Table 2.2. Though it is difficult to compare across studies due to the variation in the experimental conditions, it is certain that Pt and Pd are active in converting NO at low temperatures (below 150 °C), while Ru and Rh can give higher N_2 selectivity especially at higher temperature. Shelef and Gandhi (1972) reported the “unfixed” products selectivity for the catalysts, which refers to the selectivity towards N_2 and N_2O that has a stable N≡N bond, and found the selectivity for Pt and Pd fell below 50 % between 200 – 600 °C.

Table 2.2: Performance comparison between noble metal catalysts in H_2-SCR in selected studies.

Reference	Condition	Conversion	Other performance
(Shelef & Gandhi, 1972)	20,000h^{-1} 1000ppm NO + 1.4% H_2	Temperature (°C) at 90% NO conversion; Pd(143) < Ru(215) < Pt(280) < Os(485)	Unfixed products selectivity (%) at 350°C; Ru(85) > Os(65) > Pt(20) > Pd(5)
(Stenger & Hepburn, 1987)	8,820 to 15,420h^{-1} 1.8 to 3.2kPa NO + 63.4 to 74.6kPa H_2 in near-ambient pressure	Temperature (°C) at 90% NO conversion; Pt(114)< Pd(128) < Rh(186)	Highest rate of product N_2 formation (s^{-1}@°C); Ru(0.8@240) > Pd(0.7@170) > Pt(0.2s@130)
(Nanba et al., 2003)	0.12gs/cm^3 1000ppm NO + 1% H_2 + 2% O_2	Temperature (°C) at 50% NO conversion; Pt(40) < Pd(90) < Ir(150) < Rh(200)	-
(Mihet et al., 2012)	4,500h^{-1} 0.5% NO + 0.6% H_2	Temperature (°C) at 50% NO conversion; Pt(62) < Pd(72) < Rh(162)	N_2 selectivity (%) at 150°C; Pd(80) > Rh(60) > Pt(40) N_2 yield (%) at 150°C; Pd(80) > Pt(40) > Rh(10)

Mihet et al. (2012) concluded that Pd was the most efficient noble metal catalyst supported over alumina due to the low formation of N_2O and negligible NH_3 and NO_2 production. A nitric oxide temperature-programmed desorption experiment (NO-TPD) showed that NO was highly adsorbed over all three catalysts with dissociative adsorption (based on the evolution of N_2 signal) being preferred over Pt and Pd, while competitive molecular NO adsorption was observed over Rh. In addition, hydrogen-TPD indicated that Pd has moderate H_2 adsorption capacity but possessed the lowest desorption peak below 300 °C. These two characteristics could be evidence that NO and H_2 chemisorption determine the reactivity of the catalysts.

The performance of Pd-based catalysts is also dependent on the support. Qi, Yang and Rinaldi (2006) studied the performance of Pd supported over mixed oxides (V_2O_5, TiO_2 and Al_2O_3) and found that 1 wt.% Pd/V_2O_5-TiO_2-Al_2O_3 has the highest NO conversion (98 % at 150 °C) and the widest temperature window (>80 % between 140 to 250 °C) as compared to Pd supported over TiO_2-Al_2O_3. This was attributed to the formation of NH_4^+ over the vanadia-containing catalyst especially above 200 °C as seen under Fourier-Transform infra-red (FTIR) spectroscopy at peaks around 1460 and

1680 cm^{-1}. This species is commonly observed on vanadia catalysts in NH_3-SCR and is believed to be the adsorption species of ammonia over Brønsted acid sites (Gruber & Hermann, 2013). Among other catalysts reported to possess this active species are bimetallic catalysts Mn-Fe, Mn-Zn and Mn-Zr supported over TiO_2 (Thirupathi & Smirniotis, 2011), as well as mixed oxides MnO_x-CeO_2-ZrO_2/γ-Al_2O_3 (Cao et al., 2014). In fact, Zhang et al. (2016) incorporated ammonium ions into a Mg/Al/Cu hydrotalcites network and obtained up to 85 % NO_x storage and decomposition which is 75 % higher than those without this ion. Other catalysts recently studied in the literature are listed in Table 2.3.

In addition, the effect of using mesoporous silica as the Pd support has also been studied since silica showed higher surface diffusivities that contributed to the higher hydrogen spillover. 1 wt.% Pd supported over silica SBA-15 showed higher NO_x conversion compared to silica MCM-41-supported Pd (56 and 29 % respectively) at very low NO concentration (50 ppm) and low H_2/NO ratio (10:1). Wang, Yin and Yang (2016) supported these findings with the amount of stored hydrogen over Pd on the two different supports from a transient kinetic experiment and hydrogen adsorption isotherms. It was determined that SBA-15 and MCM-41-supported Pd stored 7.3 and 2.1 μmolH_2/g catalyst, respectively.

Pt catalysts have also been known to convert a higher amount of NO_x among other noble metals, especially in the substantial presence of oxygen. The performance of Pt and Pd supported over Al_2O_3 and TiO_2 in a net-oxidizing condition was reported by Ueda et al. (1998). Both supported Pt showed high activity at low temperature while only Pd supported over TiO_2 showed tolerance against a high concentration of oxygen. However, at higher temperature, 1 wt.% Pd/TiO_2 has the highest activity due to the ability to reduce NO_2 generated *in situ*. Moreover, Burch and Coleman (1999) reported that only Pt catalysts (as compared to Pd, Rh and Ir supported over Al_2O_3 and SiO_2) were reactive in a H_2-SCR with gas mixture of 500 ppm NO + 2000 ppm H_2 + 6 % O_2 where about 75 % NO conversion was achieved at 90 °C. However, at this temperature, the formation of N_2O is so high that the selectivity towards N_2 fell below 30 %. It was found that the formation of this

toxic by-product is preferred at low temperature and increased with hydrogen and water concentration.

The improvement of Pt-based catalysts has since been focused on increasing the selectivity towards N_2 formation. Shibata et al. (2004) reported that N_2 selectivity was highly affected by the acidity of the support. By using different supports (zeolitic materials MFI, Y and BEA, and non-zeolitic materials SiO_2 and Al_2O_3), it was found that zeolites which have high acidic strength provided more N_2 formation due to the capacity for ammonium ion storage. The rate of N_2 formation was correlated to the intensity of NH_4^+ adsorption on Brønsted acid sites (determined during an in-situ IR experiment at bands between 1404 and 1447 cm^{-1}) for the catalysts and was found to be strongly proportional as shown in Figure 2.6. In the same figure, it can be observed that the mixed oxides SiO_2-Al_2O_3 supporting Pt catalyst possessed more NH_4^+ intermediates compared to the single oxides, which suggests the presence of synergistic effects between the oxides that contributed to the N_2 formation.

Noble metals have also been incorporated into perovskites, which show competitive N_2 selectivity. The performance was said to be dependent on the composition of the perovskite structure. For instance, Pt supported over $La_{0.7}Sr_{0.2}Ce_{0.1}FeO_3$ had a consistent N_2 selectivity of 90 % at low temperature range while Pt/$La_{0.5}Ce_{0.5}MnO_3$ had a varied N_2 selectivity between 80 to 95 % (Liu, Li, & Woo, 2012).The formed oxygen vacancies adjacent to the metals (i.e. Pt), due to the interaction between perovskite and noble metals, are attributed as the O-anchoring sites for NO adsorption with N atom attached to the Pt (Roy, Hegde, & Madras, 2009).

Table 2.3: Review on catalysts performance used in recent H_2-SCR studies.

Catalyst	Preparation method (calcination temperature)	Feed gas composition (space velocity/flow rate)	Highest NO_x conversion (temperature)	Highest N_2 Selectivity (temperature)	Other performance	Ref
8%Pt/C	Hydrothermal method at 250°C of carbon black powder and H_2PtCl_6	1000ppm NO + 1.5% H_2 + 2% O_2 + N_2 ($32,000mLh^{-1}g^{-1}$)	~90% (160°C)	-	-	(Tu et al., 2017)
0.2%Pd/Al_2O_3-ZSM5-TiO_2	Incipient wetness with $Pd(NO_3)_2$ over Al_2O_3-ZSM5-TiO_2 (500°C, 6h in air)	500ppm NO + 5% O_2 + 5% H_2O + 0.3% H_2 + 0.1% CO + Ar ($95,000h^{-1}$)	~90% (150°C)	~90% (150°C)	-	(Caravaggio, Nossova, & Burich, 2016)
1%Pd/SiO_2	Incipient wetness with $Pd(NH_3)_4Cl_2.H_2O$ over SiO_2 (500°C, 6h in air)	50ppm NO +2000ppm H_2 + 1.5% O_2 + 17.5% H_2O + He (100mL/min over 0.2g catalyst)	~65% (150°C)	-	-	(Yin et al., 2015)
10%Ni-0.5%Pd/Al_2O_3	Incipient wetness with $Pd(NO_3)_2.xH_2O$ and $Ni(NO_3)_2.6H_2O$ over Al_2O_3 (550°C, 3h in Ar)	0.5% NO + 0.6% H_2 + Ar ($4,500h^{-1}$)	~100% (200°C)	~90% (200°C)	~90% H_2 conversion (200°C) ~90% N_2 yield (200°C)	(Mihet & Lazar, 2014)
3wt.%W/ZrCe	Wet impregnation with $(NH_4)_6H_2W_{12}O_{40}.xH_2O$ over ZrCe at 50°C overnight (150°C, 1h; 350°C, 2h; 600°C, 1h in static air)	520ppm NO_x ($NO:NO_2$~9:1) + 1.0% H_2 + 5% O_2 + 10% CO_2 + He ($51,000h^{-1}$)	~55% (300°C)	~90% (300°C)	~70% H_2 conversion (500°C)	(Väliheikki et al., 2014)
2wt.%Pt/SiO_2	Incipient wetness with $H_2PtCl_6.xH_2O$ over SiO_2 (500°C, 4h)	480ppm NO + 5% O_2 +0.8% H_2 + He (100mL/min over 0.1g catalyst)	~100% (50-200°C)	~20% (50°C)	-	(Park et al., 2011)
2wt.%Pt/MnO_x	Incipient wetness with $H_2PtCl_6.xH_2O$ over MnO_x (500°C, 4h)	480ppm NO + 5% O_2 +0.8% H_2 + He (100mL/min over 0.1g catalyst)	~90% (200°C)	~20% (50°C)	-	(Park et al., 2011)
0.5%Pt/ZSM-35	Incipient wetness with K_2PtCl_6 over ZSM-35 (500°C, 3h in air)	0.1% NO + 0.5% H_2 + 6.7% O_2 + He ($80,000h^{-1}$)	~80% (110°C)	~70% (140°C)	~50% H_2 conversion (120°C)	(Yu et al., 2010)
2wt.%Cr-0.5wt.%Pt/ZSM-35	Incipient wetness with $Cr(NO_3)_3$ over 0.5wt.%Pt/ZSM-35 (500°C, 3h in air)	0.1% NO + 0.5% H_2 + 6.7% O_2 + He ($80,000h^{-1}$)	~90% (140°C)	~80% (180°C)	~60% H_2 conversion (140°C)	(Yu et al., 2010)
1wt.%Pd/TiO_2-Al_2O_3	Wet impregnation with $Pd(NH_3)_4Cl_2$ over TiO_2-Al_2O_3 (500°C, 6h in oxygen)	500ppm NO + 4000ppm H_2 + 5% O_2 + He ($100,000h^{-1}$)	~100% (150°C)	-	~100% H_2 conversion (250°C)	(Qi, Yang, & Rinaldi, 2006)
5wt.%V_2O_5/TiO_2-Al_2O_3	Wet impregnation with NH_4VO_3 over TiO_2-Al_2O_3 (500°C, 12h in oxygen)	500ppm NO + 4000ppm H_2 + 5% O_2 + He ($100,000h^{-1}$)	~70% (250°C)	-	~100% H_2 conversion (130°C)	(Qi, Yang, & Rinaldi, 2006)
1wt.%Pd-5wt.%V_2O_5/TiO_2-Al_2O_3	Wet impregnation with NH_4VO_3 and $Pd(NH_3)_4Cl_2$ over 5wt.%V_2O_5/TiO_2-Al_2O_3 (500°C, 6h in oxygen)	500ppm NO + 4000ppm H_2 + 5% O_2 + He ($100,000h^{-1}$)	~100% (150°C)	~95% (170°C)	~100% H_2 conversion (130°C)	(Qi, Yang, & Rinaldi, 2006)

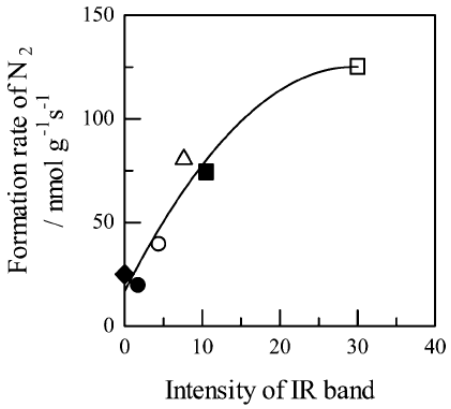

Figure 2.6: Correlation between N_2 rate of formation and intensity of ammonium ions on Brønsted acid sites. (□) Pt/MFI, (∆) Pt/BEA, (○) Pt/Y, (■) Pt/SiO_2-Al_2O_3, (♦) Pt/SiO_2, and (●) Pt/Al_2O_3. Reprinted with permission from (Shibata et al., 2004). Copyright (2004) American Chemical Society.

Alongside the catalyst support, the metal oxidation state is also an important factor in N_2 selectivity (Pârvulescu, Grange, & Delmon, 1998). A relationship between Pt oxidation states and turnover frequency regardless of the catalyst support has been established. The Pt oxidation states were measured using X-ray absorption near edge spectroscopy (XANES) where the white line intensity indicates the electronic state of Pt – the higher intensity, the more oxidized the Pt. Figure 2.7 shows that higher TOF was obtained over reduced Pt (Shibata et al., 2004).

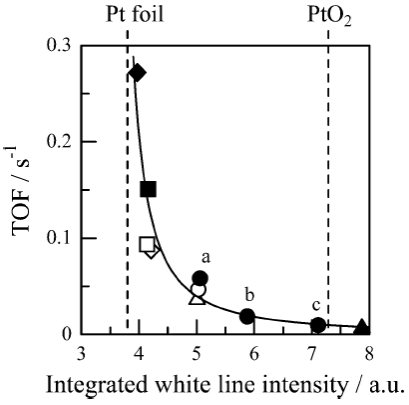

Figure 2.7: Correlation between NO TOF and Pt white line intensity estimated from Pt L_{III}-edge XANES. (◊) Pt/MOR, (□) Pt/MFI, (∆) Pt/BEA, (○) Pt/Y, (■) Pt/SiO_2-Al_2O_3, (♦) Pt/SiO_2, (●) Pt/Al_2O_3, and (▲) Pt/MgO. Reprinted with permission from (Shibata et al., 2004). Copyright (2004) American Chemical Society.

The classical mechanism reported for Pd was that of dual-site reaction where both NO and H are adsorbed prior to conversion (Qi, Yang, & Rinaldi, 2006). Recently, Huai et al. (2015) published a microkinetic model of H_2-SCR over Pd(111) catalyst which stated that H adsorbed on the surface reduces the energy barriers of NO dissociation via equations 2.22 and 2.23 which become the precursors to NH_3 responsible for reduction of NO_x gases. It is also said to effectively remove O molecule from catalyst surfaces which contribute to the surface poisoning (Huai et al., 2015).

$$M - NO + M - H \rightarrow M - N + M - OH \quad 2.22$$

$$M - NO + M - H \rightarrow M - NH + M - O \quad 2.23$$

The reaction mechanism on a platinum via the formation of ammonia can be described as either Eley-Rideal (ER) or Langmuir-Hinshelwood (LH) types. The former refers to the reaction taking place when only one of the reactant is being adsorbed while the other in the gaseous phase, while the latter is a mechanism involving the adsorption of all the reactant species over the catalyst surface prior to the reaction (Wilkinson, 1980). In this case, ER has been reported to lead to the formation of water and ammonia while the latter only of ammonia, as shown in equation 2.24-2.25 and 2.26-2.27, respectively. Therefore, the formation of ammonia, which is an important intermediate, depends highly on the dissociation of NO molecule on the metal surface and the interaction with molecular hydrogen or dissociated atomic hydrogen on the metal surface. The dissociation of hydrogen could prevent the formation of more water that is usually unwanted in a product stream. The onset of hydrogen dissociation is associated with the polycrystallinity of the metal and the partial pressure of the gas (Pârvulescu, Grange, & Delmon, 1998).

$$M - O + H_2 \rightarrow M + H_2O \quad 2.24$$

$$M - N + {}^{3}/_{2}\, H_2 \rightarrow M + NH_3 \quad 2.25$$

$$H_2 + 2M \rightarrow 2M - H \quad 2.26$$

$$M - N + 3M - H \rightarrow 4M + NH_3 \quad 2.27$$

The reaction order in NO-H_2-O_2 system has been scarcely reported, with microkinetics being more of recent interest, incorporating density functional theory studies. Some of the reported rate equations and apparent activation energies are summarized in Table 2.4, additionally enlisting those from the conventional NH_3-SCR system. It can be seen that the activation energy for H_2-SCR system is comparable to conventional SCR. However, NO adsorption is much stronger with precious metals in H_2-SCR (chemisorption) as opposed to the transition metals in NH_3-SCR system. The adsorption of the reductant, on the other hand, is stronger in NH_3-SCR, which is dependent on the adsorption and activation of ammonia at the active sites (Forzatti, 2001).

Table 2.4: Selected rate equations and the apparent activation energy in SCR studies.

System	Rate equations	Parameter values	Ref
Pt/MgO-CeO_2 catalyst in NO-H_2-O_2 reaction	$r_{NO} \propto p_{NO}^{-0.97} p_{H_2}^{1.34} p_{O_2}^{-0.17}$	E_a = 87.4 kJ/mol	(Costa et al., 2007)
Pt-Mo-Co/α-Al_2O_3 catalyst in NO-H_2-O_2 reaction	$r_{NO} = 2\left(k_{N_2} + k_{N_2O}\right)\left[\frac{K_{NO}p_{NO} \times K_{H_2}\left(p_{H_2} - p_0\right)}{\left(1 + K_{NO}p_{NO} + K_{H_2}\left(p_{H_2} - p_0\right) + K_{O_2}p_{O_2}\right)^2}\right]$	E_a = 63.16 kJ/mol $\Delta H_{ads,NO}$ = -77.2 kJ/mol $\Delta H_{ads,H2}$ = -58.6 kJ/mol	(Frank, Emig, & Renken, 1998)
V_2O_5-WO_3/TiO_2 honeycomb monolith in NO-NH_3-O_2 reaction	$r_{NO} = k_1 C_{NO}$	E_a = 27 kJ/mol	(Yang et al., 2013)
Commercial catalyst containing TiO_2. WO_3, SiO_2, CaO, Al_2O_3 and V_2O_5 in NO-NH_3-O_2 reaction	$r_{NO} = k_1 c_{NO} \frac{K_{NH_3} c_{NH_3}}{1 + K_{NH_3} c_{NH_3}}$ $r_{NO} = k_{NO} \frac{K_{NO} p_{NO}}{1 + K_{NO} p_{NO}}$	E_a = 69-86 kJ/mol $\Delta H_{ads,NO}$ = -21.3 kJ/mol $\Delta H_{ads,NH3}$ = -137 kJ/mol	(Koebel & Elsener, 1998)

Furthermore, the effects of Pt loading and reaction temperature on the mechanism have also been investigated. Selectivity towards N_2 formation decreased from 85 to 67 % from using 0.1 to 1.0 wt.% Pt loading, which may be attributed to the different reduction kinetics by hydrogen on the active species. Despite being similar under a wide range of Pt loading (0.1 to 1.0 wt.%) on MgCeO support, the adsorption species vary on temperature. For example, between 120 and 200 °C, unidentate or bidentate nitrates and nitrosyls are the active intermediates while from 200 to 300 °C, the formation of chelating nitrite was more apparent than unidentate or bidentate nitrates (Savva & Costa, 2011). Figure 2.8 shows an illustration of the adsorption species suggested in most of the H_2-SCR.

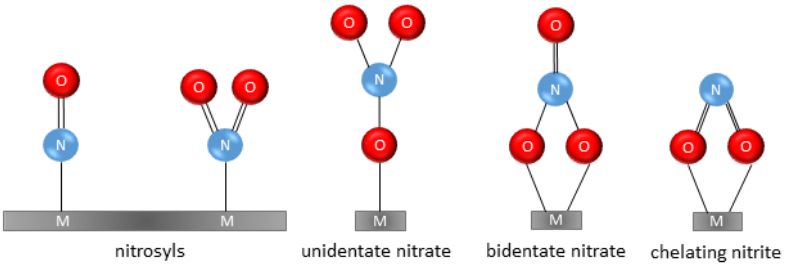

Figure 2.8: Structure of adsorbed NO_x species in H_2-SCR. Adapted with permission from (Savva & Costa, 2011). Copyright (2011) Taylor & Francis.

2.3 Precious Metals Replacement in NO_X Treatment Studies

The application of precious metals are usually limited to mobile NO_x sources due to the high cost, low-range temperature window, oxygen inhibition and sensitivity to poisons such as SO_2 (Gao et al., 2017). Even then, the search to replace precious metals in the three-way catalytic converter catalyst is still an interest. This catalyst consists of the oxidation catalysts Pt and Pd, which consume the unburned hydrocarbons and carbon monoxide, and the reduction catalyst, Rh to convert NO_x gases. Rh, as the scarcest element among the three, was the main focus for replacement. Different bimetallic systems have been investigated, such as Pt-Mo, Pd-Mo and Pd-W, but these have been found to be inferior in terms of NO_x reactivity (as compared to the Rh-containing catalyst) though the hydrocarbon oxidation improved (Adams & Gandhi, 1983).

Growing industrialization and demand for vehicles worldwide would increase the consumption of the depleting precious metals. World production of platinum and palladium increased by 11 and 29 %, respectively from 2014 to 2015, while the recycling rate of the platinum-group metals (PGM) was only 30 % in 2014. The primary source of recycled PGM is catalytic converters, as this accounts for 45 and 65 % of the application of Pt and Pd, correspondingly (Loferski, 2014).

Precious metals are usually preferable in the catalysis market due to their high selectivity, simple catalyst design and low metal loading requirements. It is typical to obtain similar performance between platinum-group metals and cheaper metals with higher loading and more complex ligands of the latter. Therefore, there has been a lack of studies focusing on replacing precious metals especially in industries where the precious metals-based catalyst is not the cost-determining factor such as in the pharmaceutical industry due to the low usage of the catalysts. In NO_x treatment from both mobile and stationary sources, increasing NO_x emission regulation worldwide demands larger production of NO_x removal catalysts which could impose a great threat on the availability of precious metals (NRCCSR, 2012). Continuing efforts to develop cheaper and more sustainable NO_x-removal catalysts allows the exploration of non-precious metals (NPM). In the industrial context, NPM includes the major industrial metals and rare earth elements which are at least 200 times more abundant than precious metals, as depicted in Figure 2.9 (Haxel, Hedrick, & Orris, 2002).

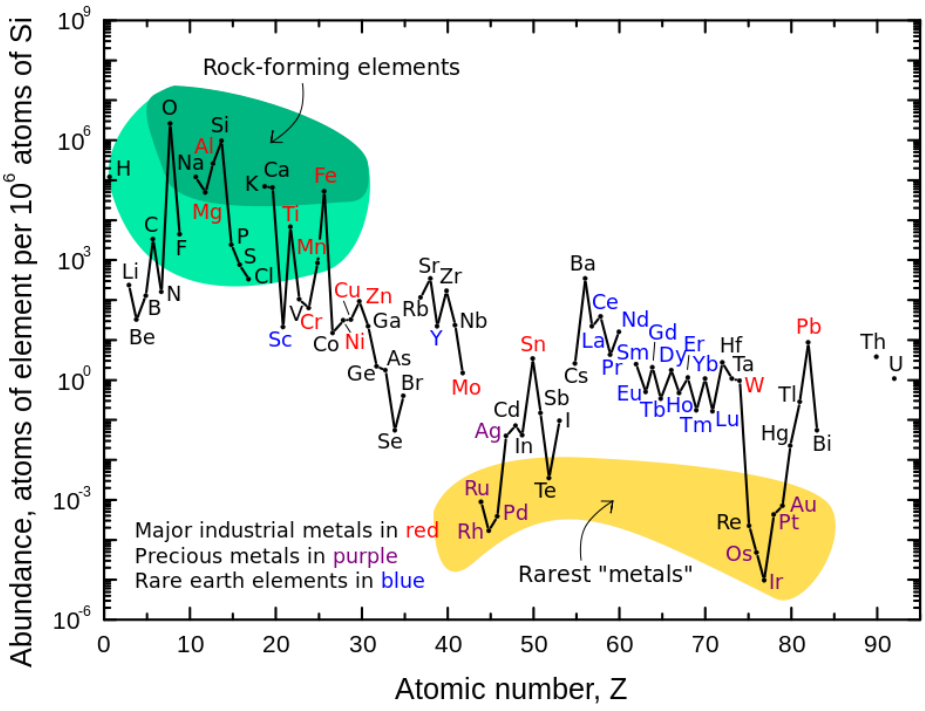

Figure 2.9: Classification of metals based on the elemental abundance (Haxel, Hedrick, & Orris, 2002).

In 2012 it was reported that mullite, a natural silicate mineral discovered on the Scottish Isle of Mull, is the most promising alternative to Pt used in catalytic converter. Nanostellar Inc. has since developed a synthetic material based on mullite and studied its performance in reducing NO_x (Canter, 2012). The Mn-mullite ($Mn_7SrSmCeO_{14.83}$) was reported to better oxidize NO into NO_2 as compared to Pt by 20 %. This is attributed to the synergistic effects contributed by the mixed components – Ceria dissociatively adsorbs oxygen to supply atomic oxygen to the Mn-Mn dimers, Sr increases the surface area to expose more active sites and Mn_3O_4 stabilizes the catalyst activity at high temperature up to 350 °C (Wang et al., 2012). The formation of NO_2 from NO is essential, as NO_2 is used to oxidize soot formed in an exhaust system and is easily reduced to N_2 by a subsequent SCR catalyst.

Transition metals have quickly replaced the role of precious metals in NH_3-SCR because of the superiority in inhibiting NH_3 oxidation at high temperature (Gao et al., 2017; Liu, Yu, & He, 2014; J. Li et al., 2011; Thirupathi & Smirniotis, 2011; Consul et al., 2004; Forzatti, 2001; Busca et al., 1998). Therefore, this group of metals have been studied in a wide range of

applications, from NO decomposition to reduction with hydrogen. Shelef and Ghandi (1972) studied the NO-H_2 reaction for both LPM and noble metals, and the selectivity towards unfixed nitrogen products are shown in Figure 2.10. Most of the tested metal oxides were able to achieve more than 90 % selectivity and the activity threshold for the catalysts are comparable to the noble metals, for instance MOD (undisclosed metal types and composition) and Pd, which started at about 100 °C. The minima for the base metal oxides started at higher temperature than the noble metals (350 as compared to 250 °C). In their study, they ranked the reactivity of base metal oxides as MOD > copper chromite = copper oxide >> nickel oxide > iron oxide. The reduced selectivity is attributed to the increasing formation of NH_3 over the catalysts at increasing temperature. However, it was shown in the same studies that the addition of oxygen up to 0.27 % in the inlet gas affected the selectivity over noble metals only slightly, while the maximum NO conversion and NH_3 formation over the LPM shifted to a higher temperature.

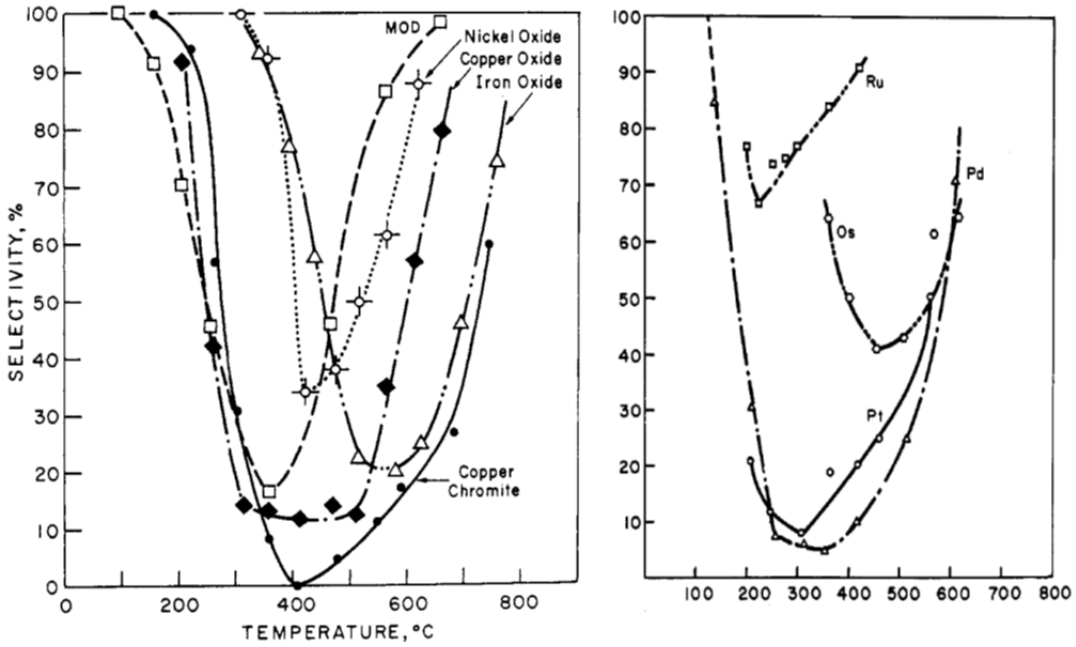

Figure 2.10: Selectivity for unfixed nitrogen-products in 1000-1200 ppm NO + 1.4 % H_2 over base metal oxide and noble metal catalysts. Reprinted with permission from (Shelef & Gandhi, 1972). Copyright (1972) American Chemical Society.

Copper is known to be reactive in NO_x decomposition and reduction, making it one of the most studied transition metals. Supported copper over zeolite has been extensively used in NO_x reduction, which is attributed to the strongly stabilized Cu^+ ions in the ZSM5 structure. In addition, the redox properties of the supported copper are also believed to play important roles in the catalytic activity. Therefore, the performance levels of copper over different supports should also be explored. Aritani et al. (1997) found that TiO_2-supported Cu had the highest performance compared to other supports (Al_2O_3, SiO_2, MgO and ZnO), also showing that pre-treating 8 wt.% copper supported over TiO_2 in 100 torr of H_2 at 473 K for 1 h could give a superior performance (83 % conversion and 95 % N_2-selectivity). The co-existence of Cu^0 and Cu^{2+} has been reported to be responsible for this high activity. In addition, CuO in its oxidized state is not preferable for a sulfur-containing exhaust gas treatment even for its high sorption capacity, as it consumes SO_2 to form $CuSO_4$ (Gomez-Garcia, Pitchon, & Kiennemann, 2005).

Several attempts have been made to evaluate the performance of singularly supported transition metals in NO_x reduction with hydrogen. Wang et al. (2014) tested impregnated zinc on ZMS5 and compared the performance to the catalysts containing Pd and Ru, with the results shown in Figure 2.11. This study revealed that monometallic zinc supported over the zeolite structure is active in reducing NO and the selectivity towards N_2 formation is competitive to those of noble metals. In fact, coupling of zinc with palladium produced better selectivity (~100 % in a wider range of temperature) compared to Pd-Ru catalyst. In a separate study, Qi, Yang, & Rinaldi (2006) compared the performance of Pd and V in H_2-SCR and found that 5 wt.% V_2O_5 supported over TiO_2 was able to consume NO and hydrogen at a high percentage at over 250 °C (results are shown in Table 2.3). Even though no N_2-selectivity was reported for the catalyst, it was found via FTIR studies that the formation of NH^+ over the catalyst surface contributed to the removal of NO.

Further studies comparing the performance between LPM and noble metals evidently should be published in order to explore the sustainability of non-ammoniacal SCR. Some researchers have argued that the LPM oxidation by the presence of oxygen is a limitation to its application (Gomez-Garcia,

Pitchon, & Kiennemann, 2005) but some reported the reaction does happen but via Mars-van Krevelen mechanism which utilizes redox sites (Busca et al., 1998). As redox sites are also contributed by the catalyst support, the detailed interaction between transition metals supported over different kind of materials should also be explored.

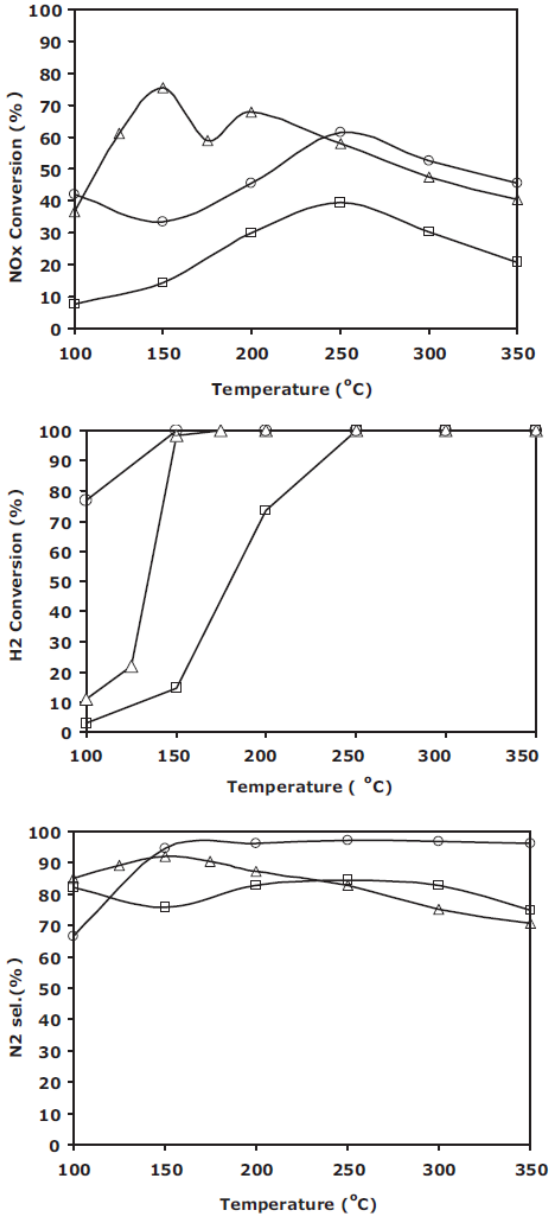

Figure 2.11: Catalysts performance in 50 ppm NO + 2000 ppm H_2 + 1.5 % O_2 at 200 mL/min for (Δ) 0.25 g 0.8 wt.% Pd/0.11 wt.% Ru/W-(ZrO_2-SiO_2)SO_4, (○) 0.2 g 1 wt.% Pd/2 wt.% Zn/ZMS5 and (□) 0.2 g 2 wt.% Zn/ZMS5. Reprinted with permission from (Wang et al., 2014). Copyright (2014) Elsevier.

2.4 Carbon-based Catalysts and Sorbents for NO_x Treatment

Carbon materials are known to possess excellent characteristics as sorbents and catalyst supports. They can be synthesized via carbonization of carbonaceous materials, or through the preparation of ordered mesoporous or nano-structured materials. Examples of carbon polymorphs can be classified as in Figure 2.12.

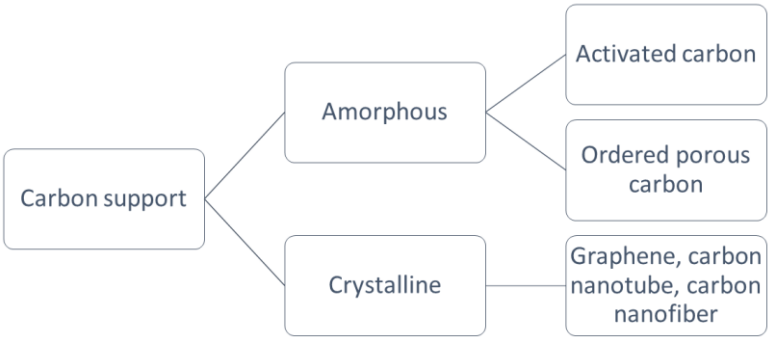

Figure 2.12: Carbon polymorphs for application as sorbent and catalyst support. Adapted with permission from (Yang, Chiang, & Burke, 2011). Copyright (2011) Elsevier.

The simplest form of carbon support is activated carbon, which can be either powdered or granular. The basic structural unit comprises of microtextured carbon, and the ligands bonded at the edge of the microtexture. The pores of the activated carbon are made of the interstices and irregularities of the microtexture, formed during the combustion, activation and calcination process (Alfarra, Frackowiak, & Béguin, 2004). Oxygen, nitrogen, hydrogen and sometimes inorganic elements coexist in the microtexture, influencing aspects of surface chemistry such as the acidity and hydrophobicity of activated carbon. Due to the high electronegativity of oxygen molecules, their presence at the edge of the structure forms important surface functional groups, some of which are illustrated in Figure 2.13 (N. Li et al., 2011; Marsh H. & Rodriguez-Reinoso F., 2006).

In industrial applications, a packed-bed catalyst imposes considerable high pressure drops; a different configuration with higher voidage could solve this drawback. The activated carbon can be coated on a template or extruded to form ordered porous carbon such as honeycomb monolith. The first application of this structure is in treating exhaust gas of automobiles. Though

ceramic was the first material used, its low surface area requires the inner surface of the channel to be coated with other high surface area material such as carbon, which was then known as carbon honeycomb monolith (CHM). This can be prepared either by dip-coating in resin or by chemical vapour deposition. CHM has the monolith retaining its mechanical strength, while the carbon washcoat provides adsorptive and catalytic properties. Another type of CHM can be prepared by extruding a mixture dough of carbon, binder and filler (Moreno-Castilla & Pérez-Cadenas, 2010).

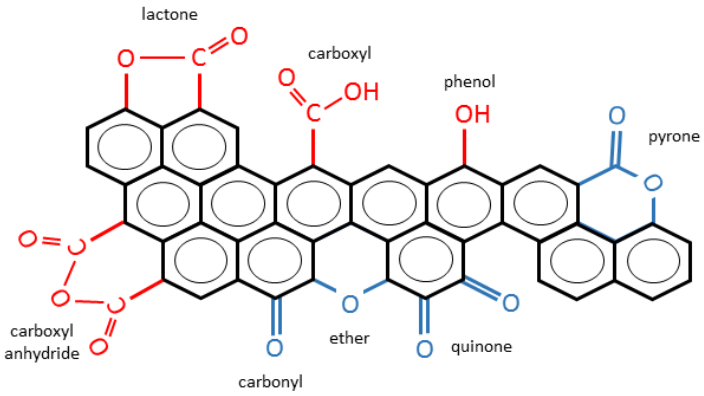

Figure 2.13: Surface functional groups commonly found on activated carbon: red-acidic group and blue-basic or neutral group. Adapted with permission from (N. Li et al., 2011). Copyright (2011) Elsevier.

Graphene, the basis for many nanocarbon materials, has been used as a catalyst support. It has been agreed that graphene sheet is superior compared to the other carbon supports in terms of surface-weight ratio, surface availability, and flexible surface doping (Taheri Najafabadi, 2015). Layers of graphene enveloped into a cylindrical shape have also been used as a catalyst support in the form of carbon nanotubes (CNT). The development of CNT from a tubular form in 1950, to multi-walled CNT in 1991, to the recent interest in single-walled CNT, are all attributed to its strong mechanical and electronic properties. It can be synthesized via chemical vapour deposition, arc discharge and laser ablation (Tan et al., 2013). Functionalised CNT involves the removal of impurities that grew along with the carbon network such as graphite and fullerene as well as modification with amino and sulfonic groups. It has attracted special interest as a supporting catalyst because it can

overcome common issues related to using conventional catalysts such as pore diffusion limitation, low structure stability due to organic compounds, catalyst leaching and high catalyst costs (Shuit et al., 2013). As graphene and CNT are 2D structures, carbon nanofibers (CNF) resemble 1D structures of fibrous material synthesized via electrospinning or catalytic thermal chemical vapour deposition growth. It also differs from the conventional carbon fibres, as the diameter is 50 – 200 nm instead of micrometres, which leads to large differences in their properties. In an application to remove NO and NO_2, CNF without other embedded metallic catalysts acted as both catalyst and adsorbent to facilitate the reaction due to the increased redox properties (Feng, Xie, & Zhong, 2014; Zhang et al., 2014).

2.4.1 NO_x adsorption with activated carbon

One of the most common methods to separate toxic industrial compounds from air is adsorption. Its efficiency is influenced by the number of adsorption sites and the energy retaining the molecules. Larger molecules that can fit the pores in the sorbent surfaces at temperatures below its critical imposed stronger retaining energy (Bandosz, 2012). Therefore, as NO_x gases pre-dominantly consist of NO with a critical temperature of -93 °C and N-O distance of 1.2 Å, oxidizing this to for example NO_2 is more preferable (NO_2 critical temperature is 158 °C) (Claesson, Donohue, & Schomaker, 1948). This is called reactive adsorption, as an oxidation/reduction happens before the resulting molecules are adsorbed, as opposed to chemisorption, which refers to the stronger bonds of adsorbate and the sorbent sites.

Activated carbons have been reported to be able to oxidize NO and adsorb the subsequent NO_2 into the pores. Neathery, Rubel, & Stencel (1997) tested several types of commercially available activated carbons, mostly produced from coal and pitch, in bench and pilot-scale rigs. The temperature window was reported to be 35 – 120 °C and desorption (at temperature below 200 °C to avoid carbon consumption) showed NO_2 as the primary products. Below this temperature range would allow competitive adsorption with CO_2, while lower NO_2 is produced above this range. Experiments using the pilot-scale have produced similar conclusions to those from the bench-scale experiment. Detail mechanism of NO adsorption over activated carbon has

been reviewed by Shen, Ge, & Chen (2016) where it was concluded that the adsorption was mainly contributed by the surface functional groups and oxygen concentration in the gas phase.

The types of NO adsorbed species on activated carbon from palm oil shell have also been studied. Klose & Rincón (2007) showed in their study that the four types of adsorbed species existed in a carbon-NO-oxygen-water system are: 1) weakly adsorbed NO which desorbed during 12 - 15 h of purging at the adsorption temperature; 2) adsorbed NO_2 formed via oxidation over the carbon surface having a desorption peak from 175 to 200 °C; 3) strongly adsorbed NO with a desorption peak around 250 °C; and 4) $(NO)_2$ dimer desorbing at temperature higher than 300 °C. The evolution of these adsorbed species throughout the adsorption process is shown in Figure 2.14.

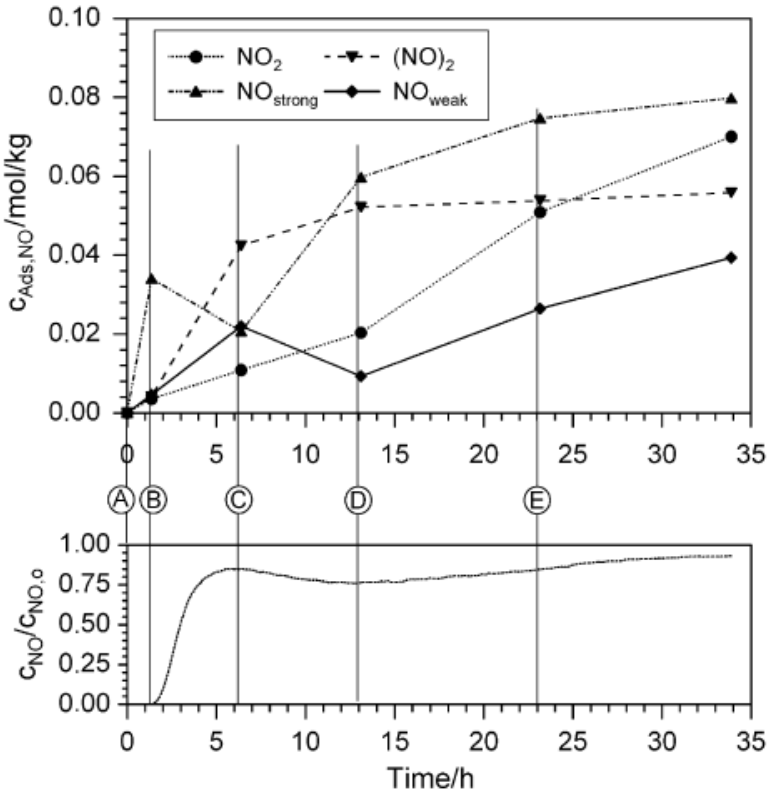

Figure 2.14: Adsorbed species evolution over activated carbon (palm oil shell steam activated at 850 °C) with respect to time-on-stream. Reaction condition: 800 ppm NO + 6 % O_2 + 10 % H_2O +N_2, 120 °C at 692 h^{-1}. Reprinted with permission from (Klose & Rincón, 2007). Copyright (2007) Elsevier.

One of the key findings from the figure is that NO was strongly adsorbed over the carbon from the start until a breakthrough (A-B), followed by the formation of $(NO)_2$, until a maxima was reached at C. This means that during the high concentration of adsorbed NO, there is a higher probability for the two adjacent NO molecules to form a dimer $(NO)_2$. As more of these dimers were formed, more sites were liberated which provided more sorption sites for NO, causing a minima at D. It can be seen that the strongly adsorbed NO was preferable to the weakly adsorbed NO. Additionally, NO_2 is produced due to the interaction between the weakly adsorbed NO with gaseous O_2, as the rate of the course for the two is similar until a steady-state was achieved (D-E) (Klose & Rincón, 2007).

The reduction of NO_2 at the carbon active sites (C*) have also been studied and proposed to follow equation 2.28. The oxygenated surface groups formed via this reduction also react with gaseous NO_2 to form nitrogen-oxygen functional groups on the carbon according to equation 2.29. The $–C(ONO_2)$ surface complexes desorb as –C(O) and NO_2 at around 110 °C, to CO_2 and NO around 200 °C, and to CO and NO_2 up until 250 °C. The decomposition of –C(O) groups can be determined above this temperature to form both CO and CO_2 (Jeguirim et al., 2004).

$$-C* + NO_2 \rightarrow C(O) + NO \qquad 2.28$$

$$C(O) + NO_2 \rightarrow -C(ONO_2) \qquad 2.29$$

The re-formation of NO over activated carbon is certainly unfavourable. A study performing simultaneous adsorption of NO and NO_2 over coconut-based activated carbon, pre-treated with KOH, found that the NO production rate decreased as more NO_2 was produced via oxidation over the sorbent, as can be seen from Figure 2.15, where the slope is decreasing against NO_2 concentration. The same study also showed that inlet gas rich in NO_2 (115 ppm NO + 793 ppm NO_2) produced more adsorbed NO_x compared to the NO-rich mixture (973 ppm NO + 26 ppm NO_2) due to the affinity towards NO_2 adsorption. The presence of oxygen increased the NO_x adsorption amount, due to the conversion of NO to NO_2 by the chemisorbed atomic oxygen on the sorbent surface (Lee et al., 2003).

In a recent study, the performance between commercial carbons and the ones prepared from waste was compared. Al-Rahbi et al. (2016) found that waste-derived carbons adsorbed NO_x less than the commercial carbons by at least 20 %. Elemental analysis showed that all commercial carbons used in the study possessed higher carbon content (about 90 %), while carbon derived from date seeds was the highest among the waste-derived carbons (about 70 %). This can be correlated to the similar adsorption rate of the carbons prepared from date to the commercial carbons. In addition, the biomass carbon also had high nitrogen content, which has been reported by other researchers to contribute to NO adsorption because it can provide basic properties. Deliyanni & Bandosz (2011) introduced N-containing functional groups over a wood-based activated carbon via exposure to dimethylamine vapours (DMA). A reaction between the DMA and carboxylic groups formed carboxylic acids salts and amides, which interacted with NO_2 to form nitramine and nitrosoamine as indicated using FTIR spectroscopy, DTG and elemental analysis. These compounds are said to be strongly retained on the carbon surface at room temperature.

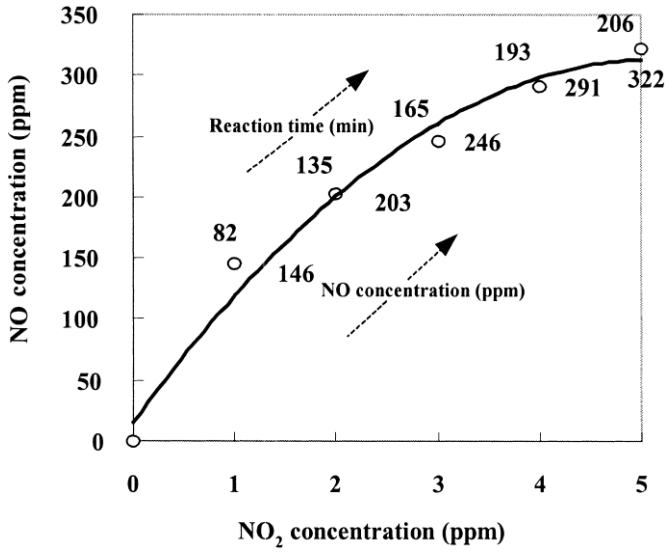

Figure 2.15: NO production versus NO_2 production with regard to the breakthrough time. Reaction condition: 122 ppm NO + 787 ppm NO_2 + N_2 at 130 °C and 0.67 s contact time in a fixed-bed column. Reprinted with permission from (Lee et al., 2003). Copyright (2003) Elsevier.

2.4.2 NO_x adsorption over metal-impregnated activated carbon

The efficiency for NO adsorption on activated carbon can be improved through the incorporation of metallic catalysts. For instance, copper impregnated over activated carbon was reported to increase the adsorption of NO with the presence of oxygen at room temperature. López et al. (2007) recorded the findings in Figure 2.16 where the copper-carbon material adsorbed approximately 94 % of the inlet NO. They also postulated the two stages of NO adsorption over this sorbent: 1) occupation of the internal surface of the carbon; and 2) adsorption on the active sites on the surface, which was believed to be enhanced by the presence of oxygen. In addition, characterisation of the sorbents revealed that copper increased the oxygen and nitrogen surface groups over the carbon.

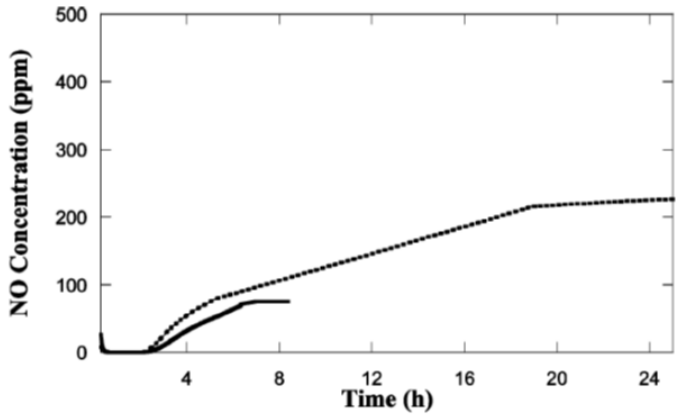

Figure 2.16: NO outlet concentration profiles on (- - -) activated carbon and (——) 10 wt.% copper supported over activated carbon. Reaction condition: 500 ppm NO + 5 % O_2 + He at 100 mL/min over 0.1 g sample at 30 °C. Reprinted with permission from (López et al., 2007). Copyright (2007) American Chemical Society.

Levasseur et al. (2011) studied the mechanism of NO_2 adsorption over copper doped on a wood-based activated carbon. Without the metal, they found that NO_2 oxidized the active carbon sites to form carboxylic acids and lactones which were further oxidized by NO_2 as NO, NO_2, CO and CO_2. This process reduced the porosity of the sorbent but incorporating copper was seen to reduce this effect. They suggested that oxidation mostly occurred over copper metals, while adsorption produced stable copper nitrates/nitrites.

2.4.3 NO_x reagentless reduction over activated carbon

Studying the adsorption behaviour and capacity is important for the design of a sorbent or NO_x storage as in the lean-NO_x trap system where the adsorbed species are released in the subsequent stage for reduction. Ultimately, the conversion to nitrogen, be it in one or multiple stages, is the goal and is preferably performed on-site to eliminate transportation cost. Previous sections have addressed adsorption over carbon materials without the report on the N_2 formation even though it was not completely ruled out. This section includes studies that have reported the formation of NO reduction products over carbon materials without the use of reducing agents as required in SCR.

Xue et al. (2008) investigated the formation of N_2 with respect to CO_2 after NO reduction over copper supported on activated carbon prepared from coconut shells. In the absence of oxygen, it was found that the evolution of N_2 was proportional to CO_2. As the reduction was proposed to follow equation 2.30, the higher concentration of CO_2 as compared to N_2 observed in this study indicated the consumption of carbon by the oxygenated functional groups in addition to by NO. This was further supported by the findings that increasing the oxygen-containing groups on the carbon surface via pre-oxidation treatment with nitric acid or hydrogen peroxide increased the CO_2 formation, especially at temperatures above 250 °C.

$$2NO + C \rightarrow N_2 + CO_2 \qquad 2.30$$

The mechanism of NO_x decomposition over Cu supported on carbon has been discussed, demonstrating the synergistic role of carbon and copper. As oxygen-containing groups are crucial as NO adsorption sites as well as metal-anchoring sites, Shi et al. (2017) proposed a synergistic effect between the carbon-metal species and surface anhydride group on the carbon in reducing NO. They impregnated iron on the oxidized graphite powder prior to pyrolysis at 400 °C, then exposed the catalyst to 990 ppm NO in argon gas at 14300 h^{-1} GHSV. At 300 °C, anhydride and C-Fe(O) formed active sites, C_f and carbon-metal bonds, C-Fe with a release of CO_2. C_f was responsible for reducing NO based on equation 2.30, while a couple of C-Fe dissociatively adsorbed NO. A pair of adsorbed atomic nitrogen was said to spontaneously

form N_2 while O was being transferred to the carbon releasing CO_2 while regenerating both C_f and Ce-Fe sites.

2.4.4 NO_x reduction with carbon-based catalysts

SCRs operating at low temperatures are becoming an important topic lately due to its significant advantages in both mobile and stationary applications. This is true for the former, as current vehicle technology has adopted a low temperature combustion system which results in low exhaust temperature (Guan et al., 2014). Moreover, it is always accepted that recovering heat from the downstream process, for example in a chemical plant, is attractive economically due to the optimized energy utilization. Thus, both mobile and stationary sources of NO_x now each require that the catalysts be reactive at low temperature. Some of these catalysts have been discussed in the previous sections. Maximum performance was attained at temperatures lower than 250 °C, but as the temperature is lowered, the catalytic activity dropped for almost all of the cases. A catalyst that can give high NO_x conversion and N_2 selectivity at wide and low temperature window is urgently needed (Fu et al., 2014).

In a low temperature range, the use of carbon-based catalysts is beneficial because of the thermal stability and comparable surface properties to the metallic and zeolitic materials. García-Cortés et al. (2001) compared the performance of Pt supported over different supports including activated carbon, alumina and zeolites in a C_3H_6-SCR. The performance is summarized in Table 2.5, in which it is evident that the conversion over carbon-supported catalyst (Pt/ROXN) was competitive while the selectivity towards N_2 formation was the highest. The characterisation of the catalysts revealed that Pt/ROXN has the largest surface area and is the most acidic which contributed to the high propene adsorption. Via C_3H_6-TPD experiment with a mass spectrometer, it was reported that propene adsorbed dissociatively into $C_2H_2^+$, $C_2H_3^+$ and $C_2H_5^+$ over the carbon-supported catalyst. As NO is dissociated over Pt surfaces, the adsorbed atomic oxygen is removed by these intermediates to allow the Pt surface to continue reducing NO.

Table 2.5: Conversion and selectivity of Pt (1 wt.%) supported over different supports. Reaction condition: 1000 ppm NO + 1500 ppm C_3H_6 + 5 % O_2 + He balance at 12,000 mL/g.h. Reprinted with permission from (García-Cortés et al., 2001). Copyright (2001) Elsevier.

Catalyst	BET surface area (m^2/g)	pH	C_3H_6 adsorbed (µmol/g)	T(°C)	X_{NOx} (%)	S_{N2} (%)
Pt/ROXN	850	2.3	40.3	200	85	30
a-Pt/Al_2O_3	90	9.3	4.78	250	55	20
c-Pt/Al_2O_3	90	9.3	4.78	250	60	20
Pt/ZMS-5	385	2.5	58.5	225	80	15
Pt/USY	800	2.8	42.7	200	95	20

*a and c refer to the precursor used for the Pt catalysts; anionic platinum complex (H_2PtCl_6) and cationic platinum complex ($[Pt(NH_3)_4]Cl_2$), respectively.

The author has reviewed various types and characteristics of carbon-supported catalysts for the application of SCR at low temperature: (Yakub et al., 2013). Lázaro et al. (2008) compared the performance of vanadium deposited over different types of carbon support including activated carbon (AC), carbon briquette (CB) and carbon corderite monolith (CM). At 150 °C in a stream of 1000 ppm NO + 1500 ppm NH_3 + 3.5 % O_2 + Ar, pre-oxidized AC, CB and CM converted NO by 88, 79 and 72 % respectively (these values are based on the highest conversion achieved by each type of support among various preparation methods used in this study). Even though there are no distinct explanations as to what causes these differences, it was noted that both AC and CB have a mainly microporous structure while CM is mesoporous. Improving microporosity increased NO conversion over AC and CB but did not influence the activity of the CM. However, all types of catalyst supports described in this study showed increases in NO reduction with increased amount of oxygenated functional groups, which were responsible for the adsorption of NH_3 and fixation of V catalyst on the surface.

Table 2.6 summarizes the performance of selected activated carbon-supported SCR catalysts. Copper was used in a NH_3-SCR and compared to the conventional catalyst. The results are shown in Figure 2.17. At a lower temperature range (below 180 °C), copper-carbon catalysts converted a higher amount of NO even at low copper loading. However, all carbon-supported catalysts in this experiment experienced a maxima, reportedly due

to: 1) the gasification of the support that changed the dispersion and structure of the catalyst; and 2) change of selectivity towards NH_3 oxidation at higher temperature (based on the fact that the conversion decreased while NH_3 consumption continued, results not shown here). In addition, the formation of N_2O has also been reported to increase up to 100 ppm at 300 °C (Singoredjo et al., 1990).

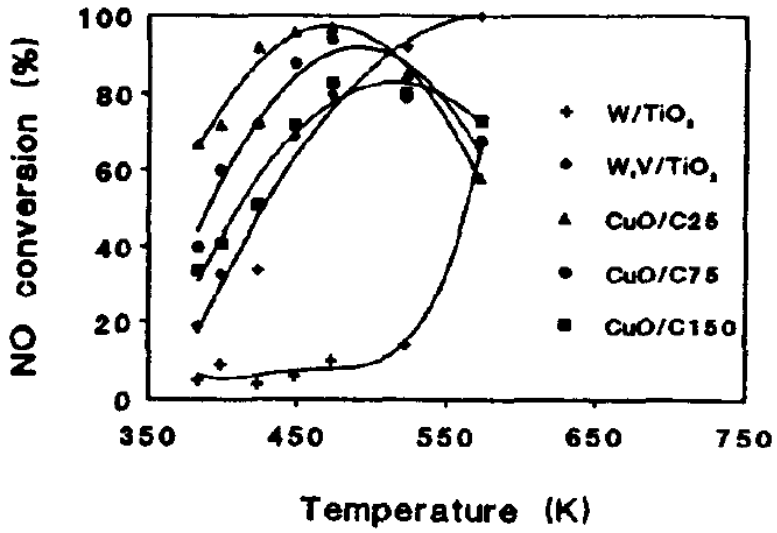

Figure 2.17: NO conversion over copper-based and conventional catalysts in NH_3-SCR. 25, 75 and 150 refer to C/M ratio. Reaction condition: 540 ppm NO + 680 ppm NH_3 + 2 % O_2 + He balance at 60,000 h^{-1}. Reprinted with permission from (Singoredjo et al., 1990). Copyright (1990) Elsevier.

In a separate study, Pasel et al. (1998) compared the formation of N_2O over Cu, Fe and Cr supported over active carbons with respect to temperature. The results in Figure 2.18 showed that N_2 yield was affected by the formation of N_2O over all transition metals used above 220 °C, except for copper at 280 °C. However, they concluded that Fe/AC was the best catalyst because of the wider temperature range of the high N_2 selectivity. Though no correlation can be made between the catalyst characteristics and the activity, it was determined that Cu and Fe supported over the active carbons possessed the highest NO and NH_3 adsorption capacity (more than 75 μmol NO/g and 400 μmol NH_3/g).

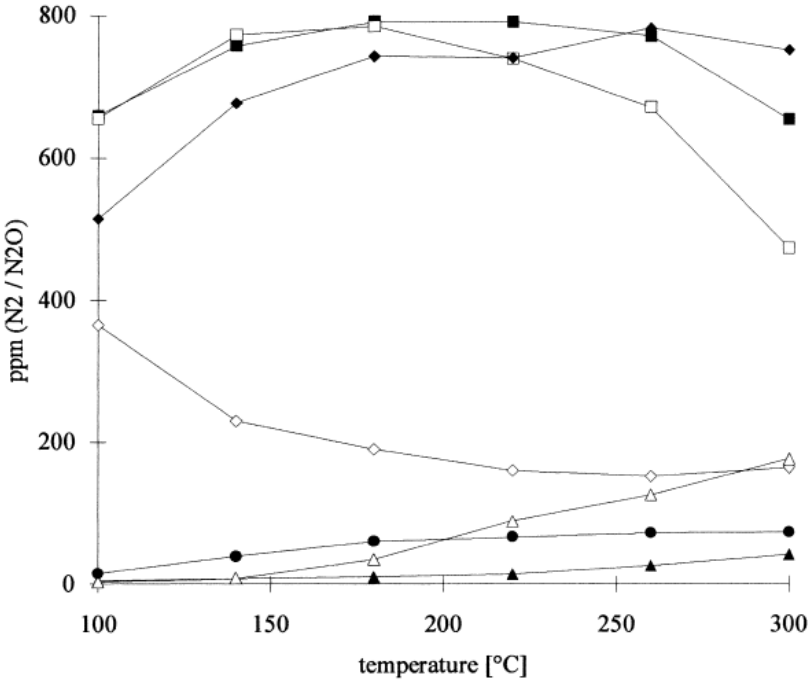

Figure 2.18: Nitrogen and nitrous oxide yield over Fe, Cr and Cu supported on active carbons. (■) N_2 over Fe/AC, (□) N_2 over Cr/AC, (♦) N_2 over Cu/AC, (◊) N_2 over AC, (▲) N_2O over Fe/AC, (Δ) N_2O over Cr/AC, and (●) N_2O over Cu/AC. Reaction condition: 800 ppm NO + 800 ppm NH_3 + 3 % O_2 + He balance at 100 mL/min over 0.4 g catalyst. Reprinted with permission from (Pasel et al., 1998). Copyright (1998) Elsevier.

Another mono-metallic catalyst is commonly used with carbon support is manganese. Cha et al. (2010) found that impregnating Mn over the two carbon catalysts (derived from rice straw and sewage sludge) led to an increase in NO_x removal at higher temperature (150-250 °C). This could be correlated with an increase in NH_3 adsorption over the catalysts with the presence of Mn (determined from NH_3-TPD), which is also a Lewis acid site. However, as the low-temperature NO_x removal was subjected to the adsorption on carbon surface, Mn was observed not to contribute to any additional removal below 150 °C. Liu et al. (2016) reviewed Mn supported over carbonaceous supports and concluded that this catalyst is not yet practical, as it also catalyses the combustion of the support with the presence of oxygen. Besides, the conversion was still less than other supported Mn such as over Mn/alumina, which converted 98 % NO_x at 200 °C (Lee, Kim, & Kwon, 2017).

NO_x reduction at low temperature can be influenced by the presence and/or formation of water vapour and SO_2. Deactivation due to H_2O is reversible if NO or the reducing agent is competing with it to adsorb on the catalyst and it is irreversible if chemisorption occurs where a hydroxyl is created by H_2O (Fu et al., 2014). Some studies on carbon-supported catalysts have shown that the catalysts can tolerate the presence of water up to 10 % (Santillan-Jimenez et al., 2011), but SO_2 poisoning of the active sites is common for most metallic catalysts due to undesirable oxidation at the surface (Fu et al., 2014). On the other hand, Bai *et al*. (2015) concluded that the reverse is true when the catalyst used was vanadium oxide impregnated onto carbon nanotubes. In fact, a synergistic interaction between the vanadium and the carbon support further enhanced the conversion of the oxidized SO_2 into SO_4^{2-}, which acts as an active site for the reductant adsorption (Bai et al., 2015).

Table 2.6 shows that activated carbons derived from biomass waste have been utilized as SCR catalysts. Recently, Singh et al. (2013) and Shen et al. (2015) used cotton stalk as a precursor to an SCR catalyst support. They concluded that in addition to promoting sustainability in the catalysis industry, cotton stalks have promising properties to be used in SCR systems due to their high surface area, rich surface acidity, high metal catalyst dispersion and oxygen species that function as NO oxidizer, which governs the increased rate of NO_x reduction (Shen et al., 2015; Singh et al., 2013). This offers a new alternative to carbon source for the application of catalyst support.

Table 2.6: Review on activated carbon-supported catalysts used in low-temperature SCR studies.

Carbon support	Metal catalyst (wt.%)	Preparation method (calcination condition)	Feed gas composition (space velocity/flow rate)	Max NO_x conversion (%)	Temperature at max conversion (°C)	Temperature window (°C)	Reference
Non-pitch coal-based activated coke	Mn-Ce-Fe (4,8&7)	Wet impregnation with $Mn(CH_3COO)_2$, $Ce(NO_3)_3.6H_2O$ and $Fe(NO_3)_3$ at room temperature for 12h	0.04% NO + 0.04% NH_3 + 7.2% + N_2 (1.6L/min over 15g catalyst)	84	220	80-240	(Li et al., 2018)
Sargassum oxidized with H_3PO_4, heated to 500°C for 1h in N_2 flow	Cr (2)	Wet impregnation with sonication for 2h and held at room temperature for 1h. (500°C, 5h in N_2 flow)	500ppm NO + 500ppm NH_3 +5% O_2 + N_2 ($80,000h^{-1}$)	90	125	100-250	(Li et al., 2017)
Cotton stalk co-activated in 1.5% H_2PO_4 for 1h, heated to 800°C for 2h in steam/N_2 flow	Mn-Ce (4&8)	Wet impregnation with nitrates of Mn and Ce. (500°C, 5h in N_2 flow)	0.06% NO + 0.06% NH_3 + 3% O_2 + N_2	65	280	250-280°C	(Singh et al., 2013)
Coconut shell carbonized in N_2 and activated in steam	K_2O CuO 2Cu-K	Wet impregnation with nitrates of Cu and K at room temperature for 4h. (300°C, 2h in N_2)	0.2% NO + Ar	100	430 430 390	380 330 315	(Bingnan et al., 2011)
Rice straw char activated with KOH for 2h and heated to 700°C for 1h	Mn (3)	Incipient wetness with $Mn(NO_3)_2$ (350°C, N_2 flow)	1000ppm NO + 1000ppm NH_3 + 5% O_2 + N_2	250	85	50-250	(Cha et al., 2010)
Commercial activated carbon	Pt (1)	Impregnated with H_2PtCl_6 (110°C, 12h)	1000ppm NO + 1500ppm C_3H_6 + 5% O_2 + He ($12,000h^{-1}$)	95	450	170-500	(García-Cortés et al., 2001)
Commercial activated carbon oxidized with nitric acid at 90°C for 1h	Fe (10)	Wet impregnated with $Fe(NO_3)_3$, heated at 80°C till dryness (350°C, 2h in He)	800ppm NO + 800ppm NH_3 + 3% O_2 + He (100sccm over 0.4g catalyst)	100	420	220-500	(Pasel et al., 1998)
Peat char activated with steam	Cu (4)	Incipient wetness with $Cu(NO_3)_2.3H2O$ (300°C, 3h in N_2 flow)	540ppm NO + 680ppm NH_3 + 2% O_2 + He ($60,000h^{-1}$)	99	200	100-200	(Singoredjo et al., 1990)

CHAPTER 3. METHODOLOGY

3.1 Experimental Framework

This chapter describes the theory and development of the experimental setup and methods of this project. The flow and the interdependencies of the experiments are shown in Figure 3.1. The activity of the catalyst in a simulated flue gas system can be studied in a fixed-bed reactor, which is the main equipment used in this project.

The flow of gas mixture into the reactor was controlled via mass flow controllers, while the concentrations of the gases were analysed using a mass spectrometer. The mass and heat transfer limitation of the reactor must be evaluated by fulfilling the Weisz criterion, which requires the measurement of reaction rates under various operating conditions (Haber, Block, & Delmon, 1995). Therefore, catalyst screening was performed prior to this experiment to select a catalyst that possesses the highest reactivity towards nitric oxide and hydrogen. However, at this stage, no oxygen was added in order to avoid catalyst oxidation which creates uncertainty to the conversion. After that, all of the catalysts that showed reactivity in the screening were further used in a lean-burn condition to take into account the effects of oxygen (Chapter 4). The catalysts from this stage were also used in studying the effects of metal composition in catalyst design (Chapter 5).

The catalysts were also characterised in order to understand the properties that govern the reactions. Theories and standard procedures are outlined in this chapter. Consequently, one of the catalysts was chosen from Chapter 5 to study the kinetic parameters and stability in extended reaction time, which forms the major discussion in Chapter 6.

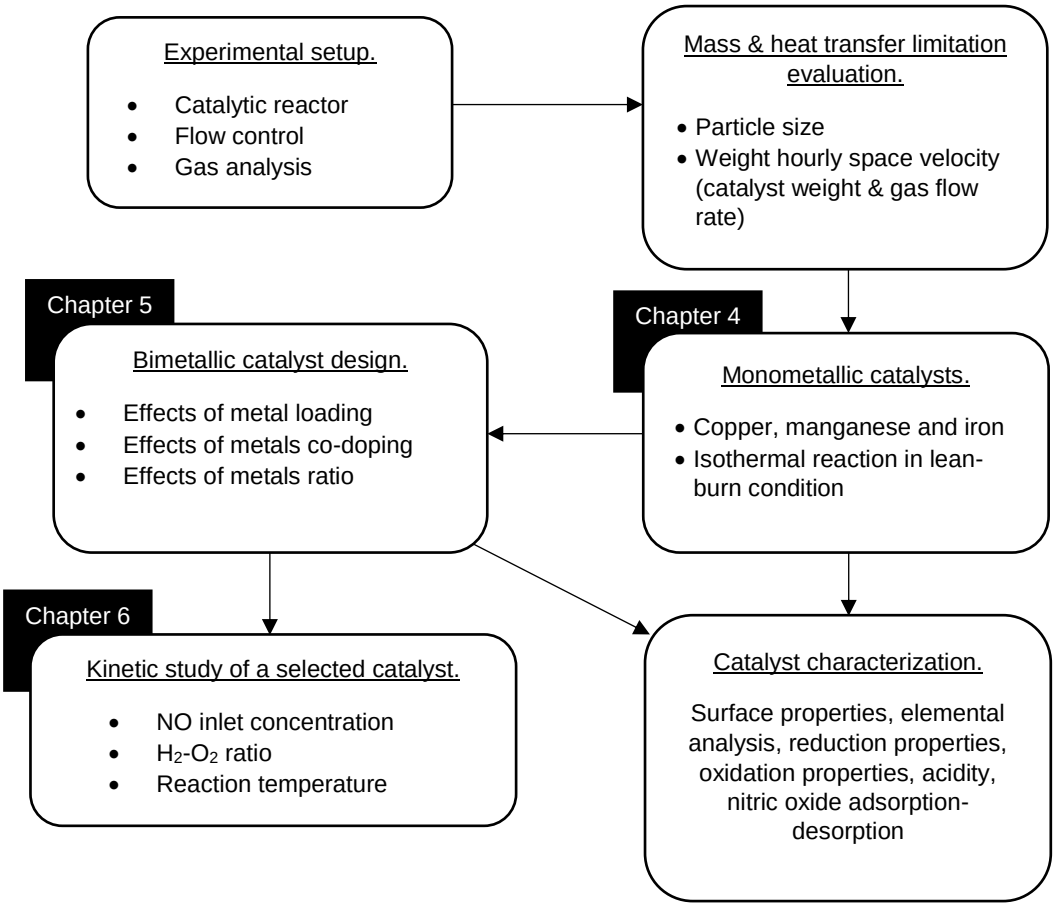

Figure 3.1: Experimental framework for this work.

3.2 Experimental Set-up

A lab-scale reactor was designed to investigate the heterogeneous catalytic reaction of a gas-solid system. This reactor configuration was chosen based on the commercialized SCR reactor and some patented test rigs, as summarized in Table 3.1. This reactor consists of an inlet point with a mixture of a carrier gas and reactant gases, a mixing bed (optional), a reaction bed, an exhaust gas sampling point and a purge point. To ensure appropriate heat transfer, a furnace and two heating sections (one upstream and another one downstream) are required. Reactants are introduced via the inlet point and mixed in an additional tube consisting of glass beads (optional), coming in contact with the catalyst bed in the primary bed tube, going to the outlet tube, and finally are released from the reactor via the product outlet.

Table 3.1: Patents related to SCR reactor.

Title	Inventor	Patent #	Components
Minitype test and evaluation device foe testing whole reaction performance of selective catalytic reduction (SCR) denitration catalyst	Yang Zhi; Wang Dezhi; Lu Jinfeng; Xiao Yuting; Zhang Tao; Li Jianfeng; Jia Man; Xie Qi	CN203941143 (U)-2014-11-12	Gas mixing device, preheating pipe, catalyst filling pipe, sampling device, flue gas component analysis system, flow controller, temperature controller
Model-based controls for selective catalyst reduction system	Robert Frank Hoskin	US201101921 47A1- 2011-08-11	Inlet, outlet, catalyst bed, open-loop control upstream injector, mass flow controller, thermocouple, concentration sensor
Selective catalytic reduction (SCR) reactor assembly to remove fine particles from poisoning or interfering with SCR catalyst activity in biomass fuel applications	Joseph Edward Cichanowicz; Lawrence Muzio	US201101949 86A1- 2011-08-11	Turning vane disposed in a plenum chamber, rectifier layer disposed downstream, catalyst layer, rectifier layer to ensure even flow distribution, a plurality of channels to promote turbulent flow and collection of aerosol particles.
System and method for selective catalytic reduction of nitrogen oxides in combustion exhaust gases	Anatoly Sobolevskiy; Joseph A. Rossin	US200802990 16A1- 2008-12-04	Upstream unit for NO_x reduction and downstream for NH_3, CO and VOC oxidation
Process and device for the purification of waste gases	Christian Mulleder	US201402123 49A1- 2014-07-31	Regenerators for post-combustion system, combustion chamber, gas inlet, gas outlet.
Device for SCR (Selective Catalytic Reduction) denitration system of coal-fired power plant reboiler	Lu Zuoji; Qin Xudong; Zhong Xuejin; Chen Kai	CN203829919 (U)- 2014-09-17	Inlet, outlet, Upper part rectification device, lower part rectification device (with several parallel catalyst layers), ammonia spraying device, temperature controller.
Exhaust emission control device	Murazaki Takanori	2014-159776-2014-09-04	Spiral internal urea water supply pipe, DPF and SCR compartments, plurality of discharge points, heat accumulator.

3.2.1 Reactor sizing and instrumentation

Reactor sizing was based on the requirement (see the following) recommended by the IUPAC (Haber, Block, & Delmon, 1995) and the resulting specification is summarized in Table 3.2. The assembly and exploded dimension of the reactor are shown in Figure 3.2.

1) *Volume of the bed must be only a few cm^3,*
2) *Cross-sectional area of the bed must be less than a cm^2,*
3) *Mass of the catalyst to be tested is between 0.05 to 3 g, and*
4) *Optimum size; Height(bed):Diameter(bed):Diameter(particle) = 100:10:1*

Table 3.2: Reactor specification.

Reactor internal diameter	7.1 mm
Reactor outer diameter	9.5 mm
Primary bed tube height	50 mm
Maximum allowable temperature	600 °C
Maximum catalyst capacity (activated carbon)	1.0 g
Maximum WHSV (activated carbon)	45,000 h^{-1}

Figure 3.3 shows the process instrumentation of the fabricated reactor. The bed temperature is monitored using a type-K thermocouple inserted from the top of the reactor, while the pressure is measured using a pressure transducer. All gases introduced into the reactor are controlled by the mass flow controllers (MFC) installed upstream of the reactor. Thermocouple, pressure transducer and MFC are controlled and monitored via a data acquisition system. Pressure regulators are used to manually control the inlet pressure from the gas bottles to the MFC. The isolation valves fitted between the pressure regulator and MFC prevent continuous MFC pressurization and protect the MFC from corrosive gas when not in use, while check valves prevent the backflow of the gases. As the inlet pressure into the mass spectrometer (MS) is limited to below 10^{-5} torr and 10^{-7} torr for the Faraday and SEM detectors respectively, two gas sampling valves are allocated for 1) control of the pressure into the MS; and 2) purging to the extractor to avoid pressurizing the reactor and the MS.

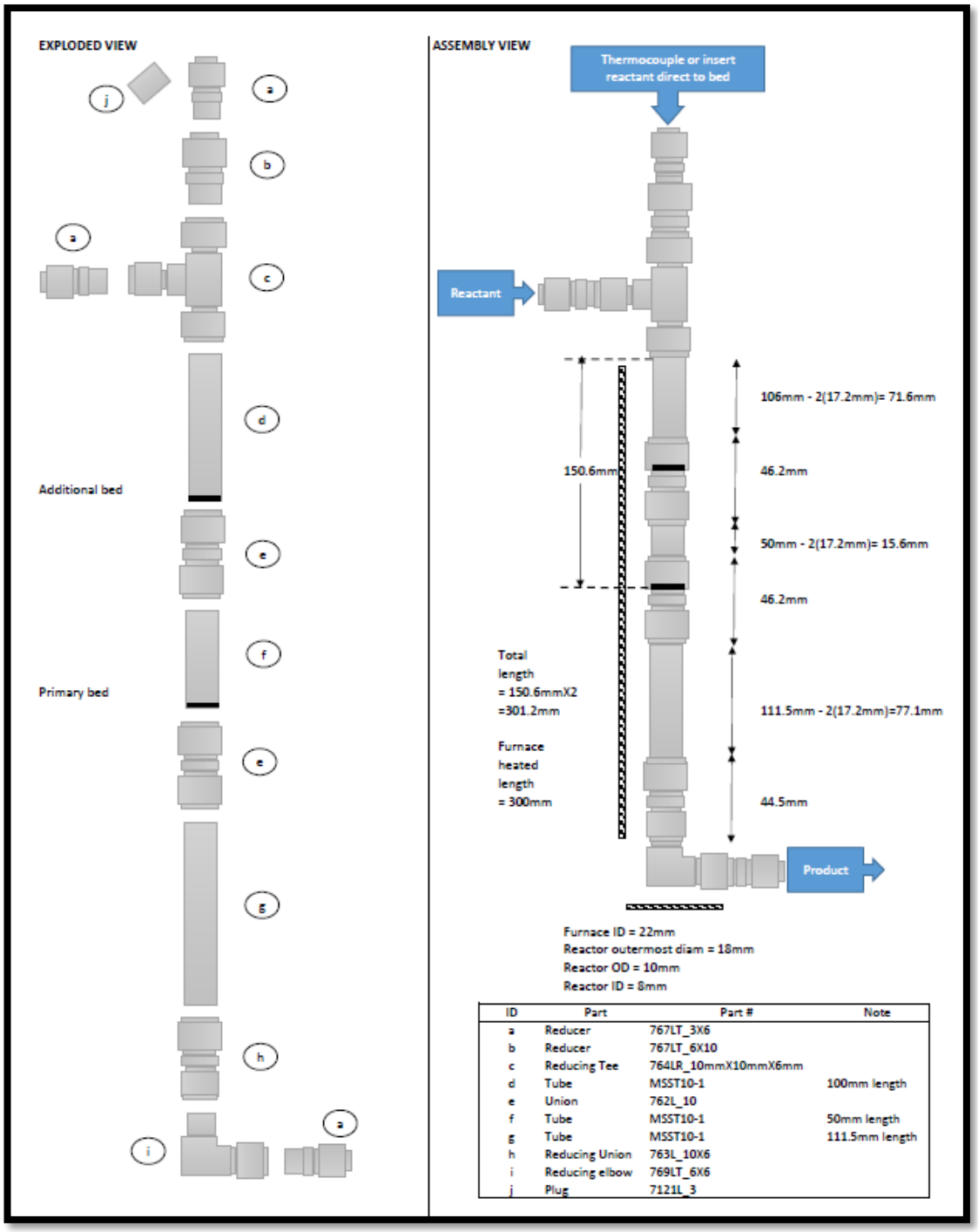

ID	Part	Part #	Note
a	Reducer	767LT_3X6	
b	Reducer	767LT_6X10	
c	Reducing Tee	764LR_10mmX10mmX6mm	
d	Tube	MSST10-1	100mm length
e	Union	762L_10	
f	Tube	MSST10-1	50mm length
g	Tube	MSST10-1	111.5mm length
h	Reducing Union	763L_10X6	
i	Reducing elbow	769LT_6X6	
j	Plug	7121L_3	

Figure 3.2: Exploded-view drawing of the packed-bed reactor.

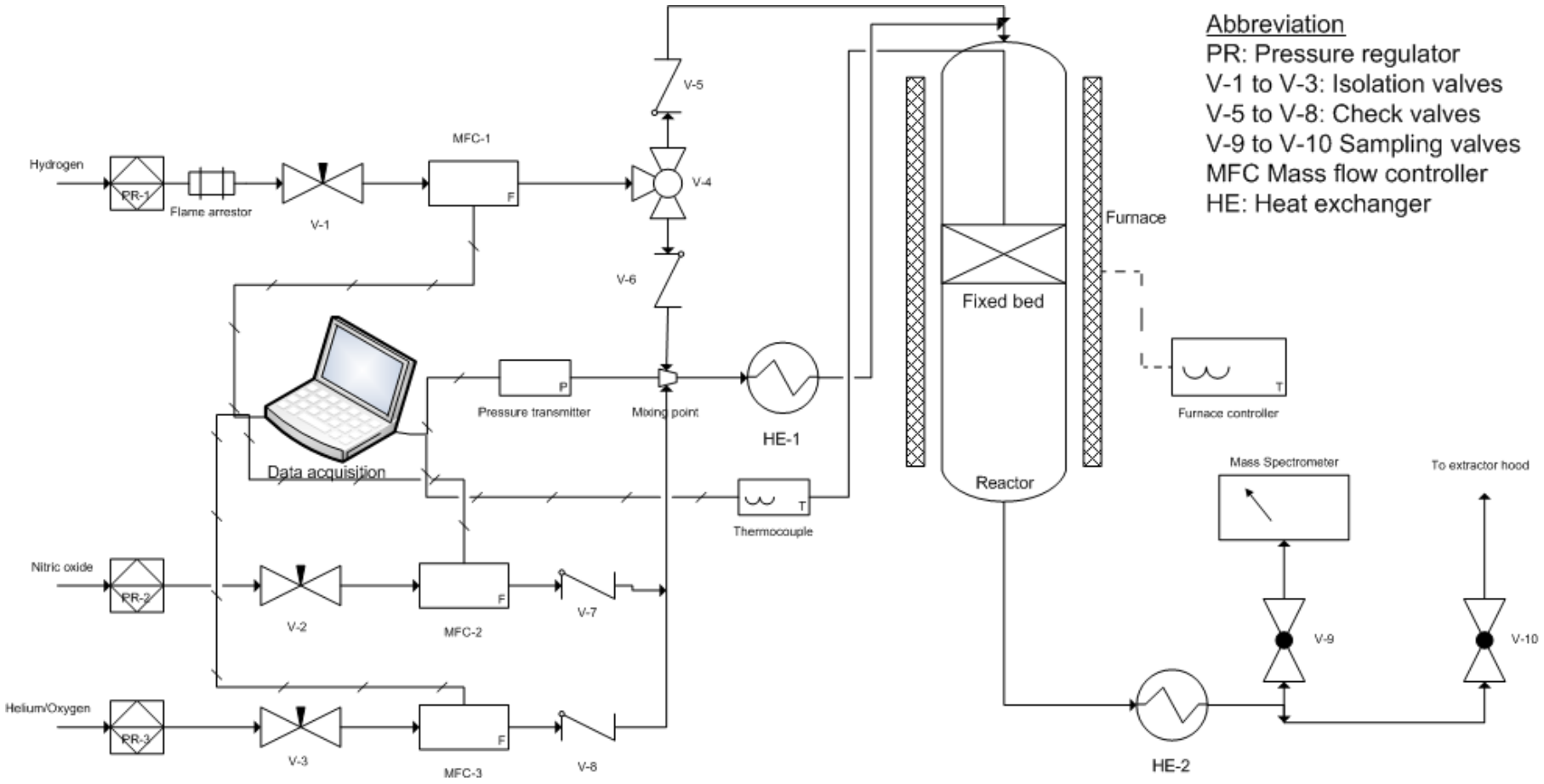

Figure 3.3: Process instrumentation diagram for the experimental set-up.

3.2.2 Mass flow controller and mass spectrometer calibration

The mass flow controllers (MFC) work on the basis of thermal mass measured as differential heat transfer between heater elements, which is related to mass flow by the specific heat capacity of a gas (MKS Instruments, 2013). The specification for the MFC (MKS Automation, UK) is shown in Table 3.3.

Table 3.3: Mass flow controller specification.

MFC #	Flow range (sccm)	Accuracy (sccm)	Repeatability (±%)	Resolution (sccm)
1	5.2 - 260	0.52	0.3	0.26
2	5.6 - 280	0.56	0.3	0.28
3	5.6 - 280	0.56	0.3	0.28

A mass spectrometer (MS) is used for continuous concentration measurement of NO, NO_2, N_2, N_2O, NH_3, CO, CO_2, O_2 and H_2. The gas entering the MS is ionized through thermionic emission from a hot filament, resulting in a mixture of ions depending on the species present. The ions are then extracted via a mass filter which differentiated the fragments based on their mass-to-charge (m/z) ratio in a vacuum environment. M/z ions are deflected at different trajectory before reaching the detector which then displays the intensity of the ions. This intensity, together with the knowledge of the gas fragmentation pattern, can be used to identify the compound and its concentration (Harris, 2010). In this study, secondary electron multiplier (SEM) was selected for the detector due to high sensitivity towards the very low NO concentration used and the faster measurements. The settings for the quadrupole mass spectrometer HPR20 (Hiden Analytical, UK) used in this study are shown in Table 3.4.

The calibration of the MFC and MS was carried out simultaneously. The types of gas for each MFC was selected based on the calibrated correction factor available from the supplier's library. The calibration gas (BOC, UK) was then allowed to flow through the valve and the partial pressure was detected by the MS. As only one gas bottle was used at one time, the partial pressure must be that of the concentration in the bottle, regardless of the valve opening.

Therefore, the relative sensitivity (RS) of the MS for a particular gas can be calculated per equation 3.1. Then, the flow rate was changed and the RS calculated was applied to find the true partial pressure. The deviation percentage of the partial pressure is the flow rate correction factor (CF), as illustrated in equation 3.2. The CF was applied to the MFC every time the gas bottle was used, as summarized in Table 3.5.

Table 3.4: MS setting for SCR experiments.

Parameter	Value
Minimum pressure, Torr	1 X 10^{-13}
Operating pressure, Torr	6 X 10^{-6} ± 5 X 10^{-7}
Detector voltage, V	875
Electron energy, eV	70
Electron emission, µA	20

$$RS = \frac{(pp\ at\ a\ particular\ m/z - pp\ at\ background) \times 100\%}{gas\ vol\%\ in\ bottle} \quad 3.1$$

$$CF = \frac{vol\%/_{RS}}{obtained\ vol\%} \quad 3.2$$

Table 3.5: MS detection details and MFC correction factor.

Species	Bottle concentration (% in helium as balance)	Base peak (m/z ratio)	Relative sensitivity (RS)	MFC correction factor (CF)
NO	1	30	2.24	1.00
N_2	100	28	1.70	-
NO_2	1	30	0.37	1.00
N_2O	1	44	1.39	-
NH_3	5	17	1.30	-
CO_2	100	44	1.54	-
H_2	5	2	3.19	0.96
O_2	10	32	1.57	0.95
H_2O	0.05	18	8.48	-
He	100	4	1.00	1.00

- : not applicable as CF is only for feeding gases

3.2.3 Gas analysis

As described in the previous section, the main gas analysis equipment used is the mass spectrometer. The gas fragmentation pattern was determined by comparing the MS signal of a particular gas with the carrier gas helium. The fragment intensities relative to the base peak (m/z ratio that of the molecular weight) was found by normalizing the signal with respect to the base peak. The fragmentation pattern and relative fragment intensities for each species are tabulated in Appendix A (Table A.1). This is useful in the deconvolution of a signal during the experimental analysis. The deconvolution was carried out by subtracting the overlapping signal based on the knowledge of the gases present. The unique m/z ratio of a particular gas is used as an indication of the gas presence, as indicated in Table A.1. Therefore, an algorithm for the gas analysis with the MS is developed as in Figure 3.4.

Other methods of gas concentration measurement common in SCR studies include the gas chromatography-thermal conductivity detector (GC-TCD), non-dispersive infra-red (IR) and the chemiluminescence detector (CD). GC-TCD separates the compounds based on the retention time in a particular column which are then measured at the TCD, a detector comparing the analyte conductivity to the reference conductivity of helium (Harris, 2010). N_2, N_2O, and CO can be separated in a molecular sieve column while CO_2 is retained in a porous-layer open-tubular (PLOT) column. A comparison between the measurement of N_2O and N_2 by using MS and GC-TCD was reported by Costa et al. (2002), who found an agreement of within 3 % (Costa et al., 2002). Therefore, measurements of N_2, N_2O, CO and CO_2 were cross-checked with GC-TCD with two different columns (details included in Table 3.6) for a particular experiment to ensure the formation of the by-products. The measurement comparison is summarized in Table 3.7; the highest error is ~ 0.02 vol.%. Gas calibration with GC-TCD is included in Appendix A (Figure A.1 and A.2).

IR and CD are the two most commonly used method to measure NO_x concentration. While IR operates based on the fact that molecules absorb infra-red at discreet wavelengths, CD reacts the NO_x with ozone to produce light emission detectable by the photomultiplier tube (Norris, 2002). In this

study, NO and NO_2 measurement was independently analysed with a commercial NO_x analyser, KANE 940 which uses the non-dispersive infra-red to detect NO and NO_2. These species have distinctive absorption energies at about 1800 and 1600 cm^{-1} respectively. This analyser is equipped with a particulate and water trap to avoid absorbance interference at the particular wavelength (Kane International, 2006). The NO_x analyser was factory-calibrated. Its specifications as well as the NO_x calculation procedure are shown in Appendix A (Table A.2 and Section A.1). Comparisons with the MS measurement are included in Table 3.7, where it is shown that the highest error is 30 ppm.

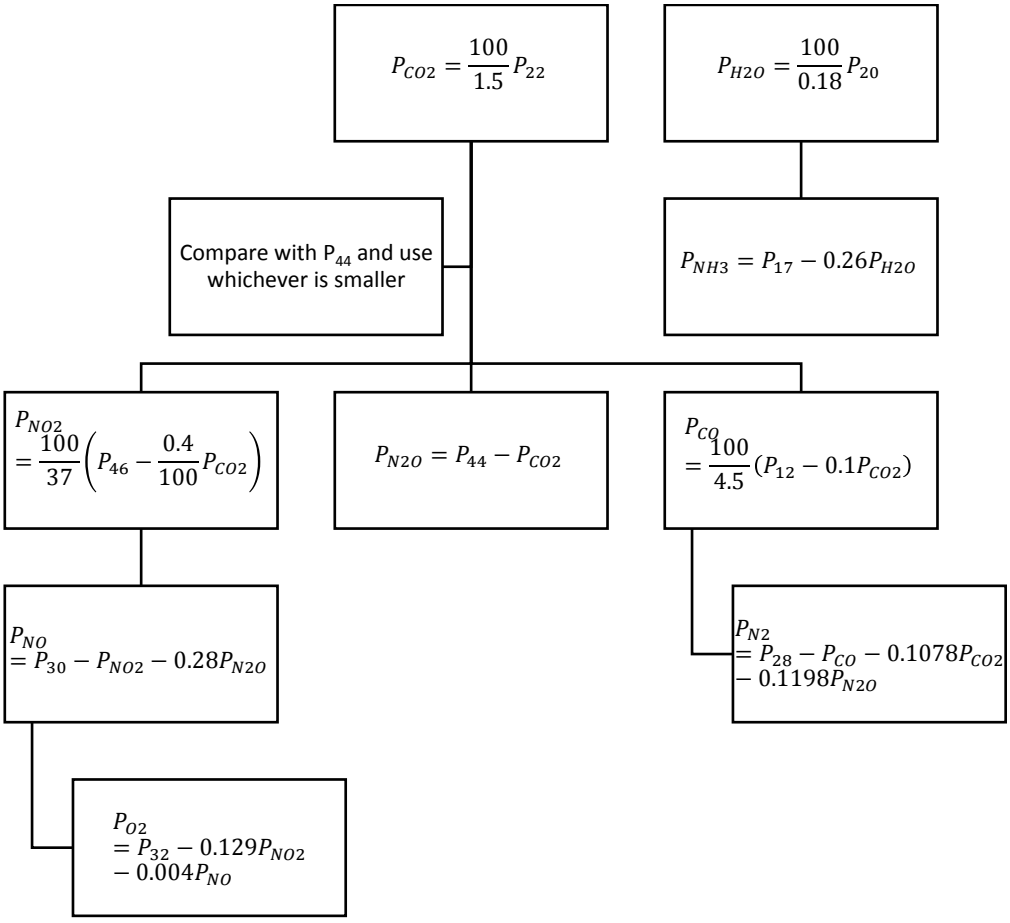

Figure 3.4: MS deconvolution algorithm for species concentration calculation.

Table 3.6: GC columns specifications.

GC Column	Properties	Analysis conditions
Molecular sieve 5A capillary column (RT-Msieve 5A, Restek, USA)	30 m, 0.53 mm ID	Detector: TCD (100 °C) Carrier: Pure hydrogen (5 mL/min) Oven ramp: 30 °C for 8 mins, increase to 300 °C at 40 °C/min and hold for 10 min
Divinylbenzene PLOT column (Elite PLOT-Q, PerkinElmer, USA)	30 m, 0.53 mm ID	Detector: TCD (100 °C) Carrier: Pure hydrogen (5 mL/min) Oven ramp: 30 °C for 5 min

3.2.4 Conversion, selectivity and combustion rate

The mole balance for nitrogen (as NO_x is the limiting reactant) can be written as in equation 3.3, where *F* is the molar flow rate; F_p is the molar flow rate of the N-products including N_2, N_2O, NO_2 and NH_3; *a* is the number of nitrogen moles in the product molecule; P_{ads} is the mole of adsorbed NO_x or N-product which are not emitted from the reactor; and $NO_{x,gen}$ is the generated NO_x during the process with the carbon catalyst. A positive mole difference between the measured inlet NO_x and the outlet NO_x, as well as the outlet N-products, is indicative of the adsorbed species while a negative indicates the generated NO_x. The NO_x conversion is calculated as the ratio of the total NO_x consumed to the amount of NO_x introduced into and generated within the system as shown in equation 3.4 at steady-state condition (at least after 60 minutes, as observed in this study). However, an efficient SCR catalyst should be able to convert the adsorbed NO_x and release the N-products fast enough to avoid permanent occupancy of the active sites (Pârvulescu, Grange, & Delmon, 1998). This is taken into consideration when calculating the efficiency of a new catalyst, termed here as selectivity towards N_2 formation, which is taken as the ratio of N_2 formed over the other products including the adsorbed species, as in equation 3.5.

$$F_{NO_x,in} = F_{NO_x,out} + \sum aF_p + \sum P_{ads} - NO_{x,gen} \qquad 3.3$$

$$Conversion, X\ (\%) = \frac{F_{NO_x,in} + NO_{x,gen} - F_{NO_x,out}}{F_{NO_x,in} + NO_{x,gen}} \times 100\% \qquad 3.4$$

$$Selectivity, S_{N_2}(\%) = \frac{2 \times F_{N_2}}{\sum aF_p + \sum P_{ads}} \times 100\% \qquad 3.5$$

Another important feature of a carbon catalyst is the carbon gasification during the application at elevated temperature. Carbon can react with NO_x to burn off according to equation 2.30 and also with the intrinsic oxygen content in the flue gas. The total combustion rate in this process can be quantified from the sum of CO_2 and CO formation (µmol/s).

Table 3.7: Comparison of components measurement with MS and other gas analysers in a selected experiment: $PKSCu_{20}$ at 7,175 h^{-1} WHSV and 500 ppm NO + 4% H_2 + 1.5% O_2.

Component	**MS**	**NOx analyzer**	**GC-TCD (Msieve column)**	**GC-TCD (Plot column)**	**Standard error**
Reaction temperature: 200 °C					
NO (ppm)	446	510	-	-	32.4
NO_2 (ppm)	0	0	-	-	0
N_2 (vol.%)	0.00340	-	0.00486	-	0.720×10^{-3}
N_2O (vol.%)	0	-	0	-	0
CO (vol.%)	0	-	0	-	0
CO_2 (vol.%)	0.0343	-	-	0.0392	2.44×10^{-3}
Reaction temperature: 250 °C					
NO (ppm)	4	0	-	-	1.75
NO_2 (ppm)	0	0	-	-	0
N_2 (vol.%)	0.0215	-	0.0318	-	5.15×10^{-3}
N_2O (vol.%)	0	-	0	-	0
CO (vol.%)	0	-	0	-	0
CO_2 (vol.%)	0.0924	-	-	0.0791	6.66×10^{-3}
Reaction temperature: 300 °C					
NO (ppm)	5	0	-	-	2.70
NO_2 (ppm)	0	0	-	-	0
N_2 (vol.%)	0.0249	-	0.0422	-	8.62×10^{-3}
N_2O (vol.%)	0	-	0	-	0
CO (vol.%)	0	-	0	-	0
CO_2 (vol.%)	0.1776	-	-	0.137	20.1×10^{-3}

3.3 Mass and Heat Transfer Limitations Evaluation

It is important to certify that the reaction performance (i.e. NO conversion, equations 3.4) as measured using the fabricated reactor is not affected by the mass and heat transfer properties that could enhance or depreciate the true reaction parameters such as the conversion and reaction rate. For a solid-fluid system, the molecule and heat transport regions can be divided into two regions: external transport from the bulk fluid to the fluid-solid interphase, and internal transport from the interphase to the inner surface of the catalyst (Haber, Block, & Delmon, 1995).

3.3.1 Internal diffusion evaluation

A well-known method used to determine the effects of species diffusion into and out of a porous catalyst on the catalytic conversion is by determining the rate of reaction at varying particle size. Should the conversion remain constant at different particle sizes, the internal diffusion effects can be neglected (Murzin et al., 2005a). At this stage, the catalyst was prepared from palm kernel shell activated carbon and copper nitrate trihydrate via incipient wetness with approximately 10 wt% metal loading. The catalyst was calcined at 350 °C in helium flow for 2 h and reduced under 5 % hydrogen/helium flow at the same temperature for the same duration. The catalysts were then crushed and sieved to obtain particle sizes of 500-600 μm, 600-710 μm, and 710-850 μm. The reaction tested for this purpose was at 130 sccm total flow of 330 ppm NO and 8,000 ppm H_2 at 300 °C and the conversion was calculated as 1-h average values. The result is presented in Figure 3.5 where it can be seen that the conversion does not significantly change when the size is larger than 600 μm, but lower particle size resulted in enhanced conversion due to the internal diffusion effects at lower particle sizes (Murzin & Salmi, 2005)[1]. Therefore, 600-710 μm was chosen as the particle size to eliminate this influence.

[1] It must be noted here that the conversion used for the purpose of evaluating mass transfer limitation must be lower than 20 %.

3.3.2 External diffusion evaluation

External mass transport is influenced by the reactor geometry and size as well as the space velocity. This can be minimized by following the recommended reactor size discussed in Section 3.2. An experimental means for validating the absence of external mass transfer effects is by evaluating the change in NO conversion over a range of flow rates and catalyst weights. For a fixed residence time, constant conversion at varying flow rate implies the absence of external mass transfer limitation (Murzin et al., 2005a).

Prior to this experiment, the residence time was chosen by varying the flow rate (from 130 to 250 sccm) at two selected catalyst weights: 0.7 and 1.0 g. The catalyst synthesis and reaction conditions have been described in Section 3.3.1. The result is shown in Figure 3.6 where the change in NO conversion can be seen almost overlapping between weight-to-flow rate ratio W/F of 1.65 and 1.75 g.h/mol. Therefore, 1.7 g.h/mol was chosen in the succeeding experiments where the catalyst weights and total flow rates were varied between 0.7 – 1.0 g and 170 – 250 sccm, respectively. The result is shown in Figure 3.7 and it is evident that increasing the catalyst weight above 0.85 g at this residence time does not change the NO conversion. Therefore, 1.0 g and 250 sccm were chosen as the catalyst weight and total flow rate, respectively, to eliminate the external diffusion effects[2]. This gives a Reynold number of 36 (transitional region for a flow in a packed-bed column) which means the catalytic activity is not enhanced by a turbulent flow.

[2] It must be noted here that the conversion used for the purpose of evaluating mass transfer limitation must be lower than 20 %.

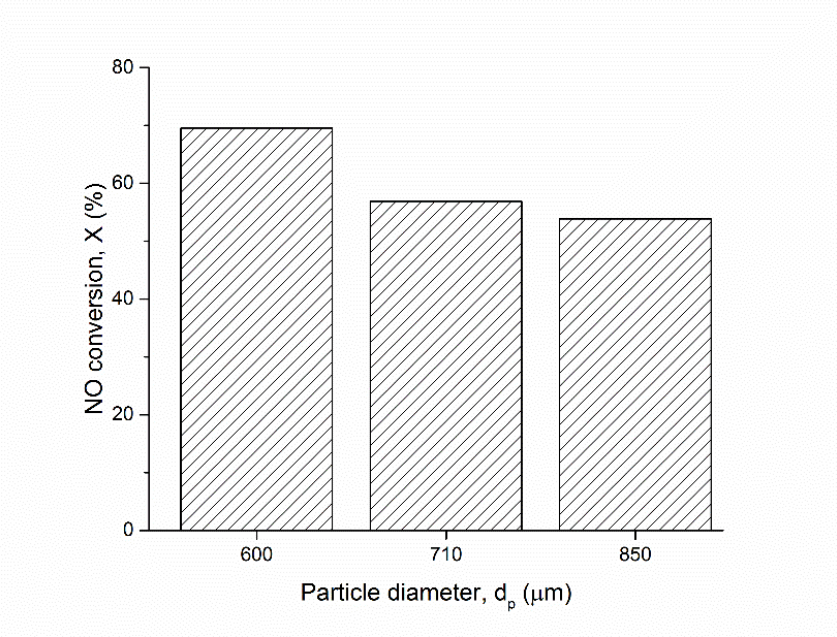

Figure 3.5: Effects of particle size on the conversion in 330 ppm NO + 8000 ppm H_2 at 3,731 h^{-1} and 300 °C.

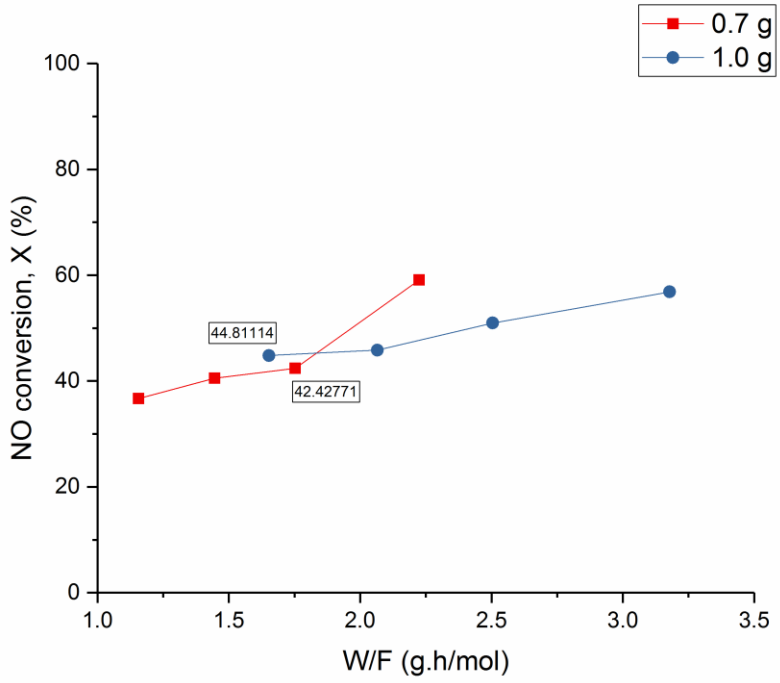

Figure 3.6: Selection of a fixed W/F in 330 ppm NO + 8000 ppm H_2 at 300 °C.

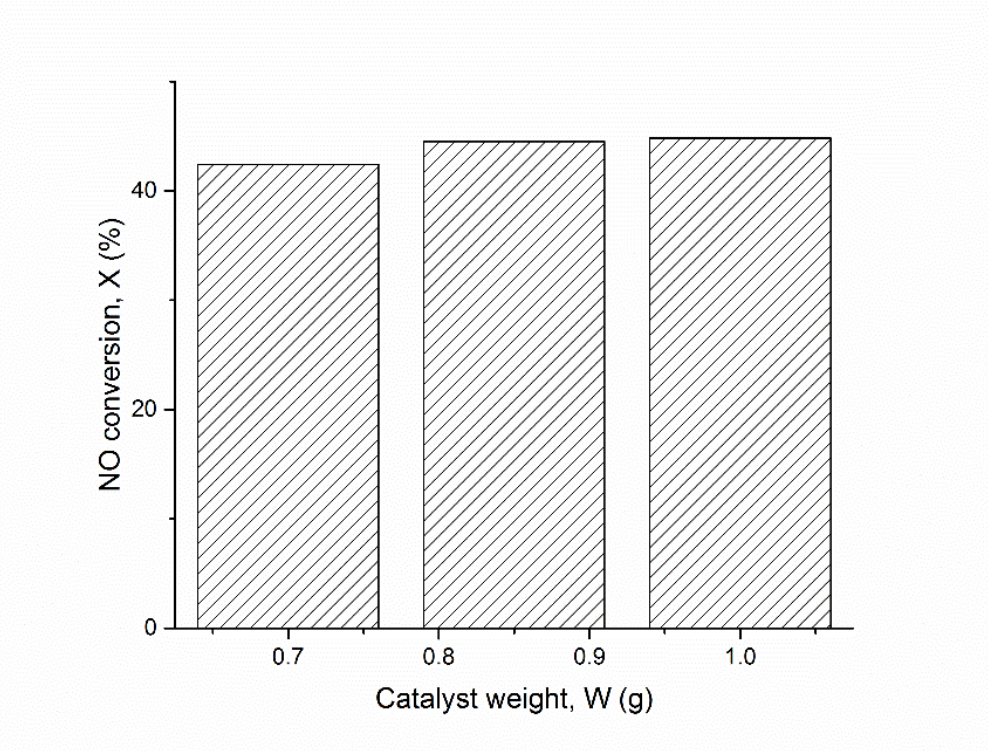

Figure 3.7: Effects of catalyst weight on conversion in 330 ppm NO + 8000 ppm H_2 at 7,175 h^{-1} (equivalent to 1.65 g.h/mol) and 300 °C.

3.3.3 Heat transfer evaluation

Mears (1971) developed the diagnostic criteria for heat transfer limitations in fixed bed reactors for kinetic determination purpose. The interphase transport limitation is always expected for a fast reaction with high heat of reaction and low Reynold number (Mears, 1971). Though H_2-SCR is an exothermic reaction, the amount of NO is too small for this limitation to exist as can be proven using equation 3.6 with the parameters explained in the "Note" column in Table 3.8. Referring to the calculation of values in Table 3.8, the criteria for the interphase transport has been satisfied. Likewise, the criteria for interparticle heat transport limitation evaluation (equation 3.7) were also fulfilled (with no heat transfer limitations).

$$\frac{(-\Delta H_R) r_{obs} d_p \rho_b}{hT} < 0.15 \frac{RT}{E} \qquad 3.6$$

$$\frac{(-\Delta H_R) r_{obs} {d_p}^2 \rho_b}{\lambda_p T} < 0.75 \frac{RT}{E} \qquad 3.7$$

Table 3.8: Calculation for equation 3.6 and 3.7.

Parameter	Value	Note
$-\Delta H_R$	1.44 X 10^3 kJ/kmol	Heat of reaction without oxygen. See Appendix A (Table A.3) for calculation
r_{obs}	3.00 X 10^{-8} kmol/kg.s	Highest observed reaction rate
d_p	7.10 X 10^{-4} m	Particle diameter
ρ_b	478.3 kg/m^3	Bed density
h	kJ/m^2.K.s	Calculated heat transfer coefficient ($h = \frac{q}{\Delta T}$) where *q* is the heat supplied by the furnace and ΔT is the temperature difference between the furnace and the middle of the catalyst bed
T	573 K	Reaction temperature
R	8.314 kJ/K.kmol	Gas constant
E	8.9 X 10^4 kJ/kmol	Estimated activation energy from linear determination at 523 – 573 K reaction temperature
λ_p	0.374 kJ/s.m.K	Lowest value of copper thermal conductivity (Touloukian et al., 1975)
Equation 3.6 *right-hand term*	8.05 X 10^{-3}	Criteria for external mass transport
Equation 3.6 *left-hand term*	1.65 X 10^{-6}	Lower than the criteria value
Equation 3.7 *right-hand term*	4.02 X 10^{-2}	Criteria for internal mass transport
Equation 3.7 *left-hand term*	4.87 X 10^{-11}	Lower than the criteria value

3.4 Catalyst Synthesis

Palm kernel shell activated carbon (PKS) was obtained from the Universiti Malaysia Sarawak, Malaysia. No further pre-treatment was required besides drying at 110 °C for 72 h to remove adsorbed water and carbon dioxide. The carbon was ground using a ball mill and sieved to a particle size of 600-710 μm (refer Section 3.3 for the particle size selection). The incipient wetness method was used to prepare the catalyst as this is one of the most established ways in producing catalysts from metal salt solution. In this method, the metal salts were dissolved in deionized water based on the PKS pore volume, instead of in excess solution volume such that in the wet impregnation method (Haber, Block, & Delmon, 1995). Therefore, the wastewater produced via this method is largely reduced. The metal salts used were $Cu(NO_3)_2.3H_2O$, $Mn(NO_3)_2.xH_2O$, and $Fe(NO_3)_3.9H_2O$ (Sigma Aldrich, UK). The material was then washed (to remove physisorbed metal nitrates) and filtered using deionized water and dried at 80 °C for 24 h before calcination

at 350, 510 and 540 °C for Cu-, Fe- and Mn-based catalysts, respectively (based on the decomposition temperature of the metal nitrates), under helium ambient (to avoid excessive carbon combustion which could lower the carbon mass). Two types of catalyst design were investigated: mono- and bimetallic catalysts. The former involved impregnating the metals individually over carbon while the latter was synthesized by combining two metals in a sequential impregnation. The synthesis was discussed in Chapter 4 for monometallic and Chapter 5 for bimetallic catalysts.

3.5 Catalyst Characterisation

Characterisation is a technique used to determine the surface and bulk properties of a material which are often correlated to the performance or behaviour of the materials in a particular application. In general, there are two classes of properties – physical and chemical. Physical properties are used to describe matter such as the appearance and size, while chemical properties represents the quality of the material in a particular chemical reaction such as toxicity and flammability (Ertl; et al., 2008). Figure 3.8 shows the types of characterisation technique used in this study to enable the determination of properties which are influential and important to H_2-SCR reaction.

3.5.1 Elemental analysis

The composition of a carbon catalyst can be determined by performing elemental and metal content analysis. The former gives information on the carbon, hydrogen, nitrogen, oxygen and ash content while the latter on the metal content which is a part of the ash. Two equipment were used to quantify elemental composition; CHNS elemental analyser and thermogravimetric analyser (TGA), while metal content was determined using modified dry ashing coupled with atomic adsorption spectrometer, as discussed in the following section. Quantification for the elemental analysis is illustrated in Figure 3.9. The residual percentage obtained from C, H, N and S composition consists of the ash and oxygen. By determining the level of ash content in a thermogravimetric analysis, the oxygen content can be determined from the percentage balance.

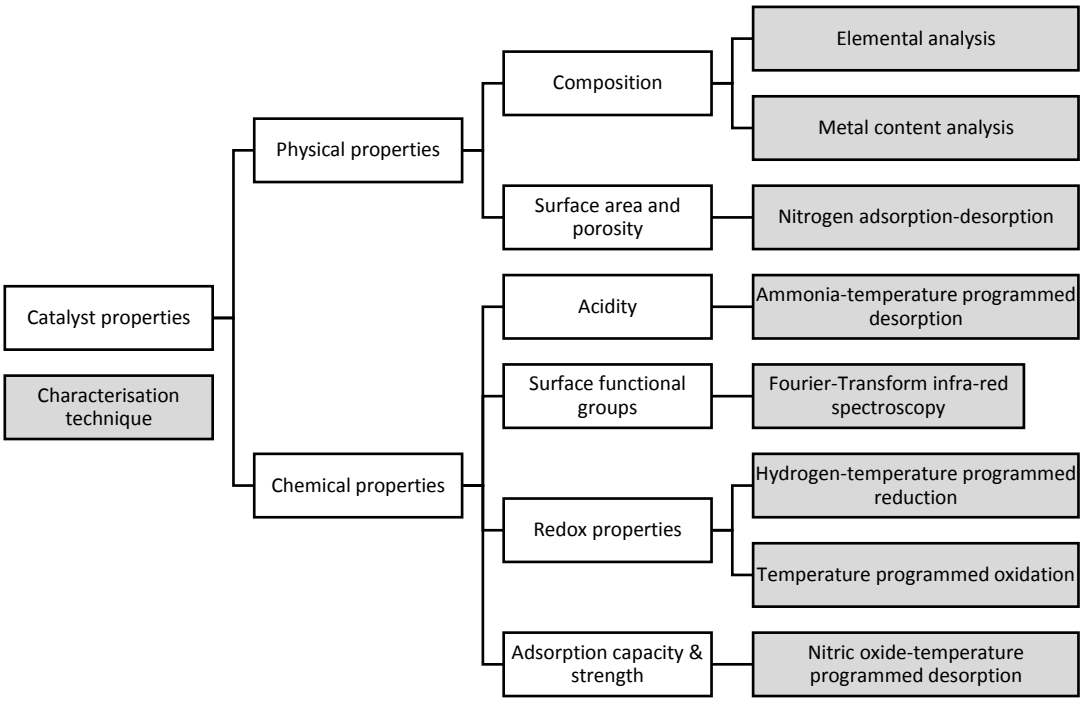

Figure 3.8: Catalyst characterisation scheme in this study. Based on Ertl, et al., (2008).

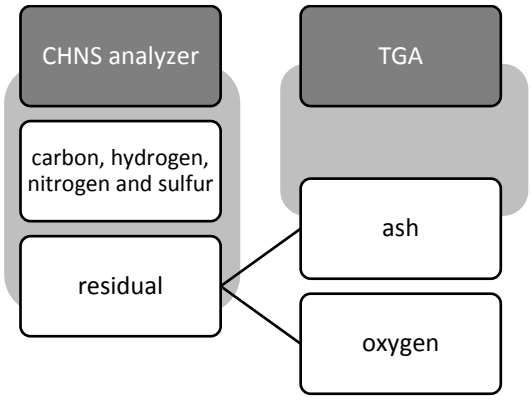

Figure 3.9: Elemental analysis determination of C, H, N, S, O and ash content by using two equipment.

CHNS elemental analyser combusts the sample in a high-temperature chamber and filter the combustion products into carbon dioxide, water, nitrogen and sulfur dioxide (depending on the elements existing in the sample) prior to quantification by a gas analyser such as TCD and MS. These gaseous products are calibrated to the amount of the element by the combustion stoichiometric relations (Harris, 2010). Likewise, the weight of the sample is

closely monitored in a TGA during a combustion and the final weight is taken as the ash content (mass loss plateau). This equipment requires a small amount of sample to be placed in a combustion chamber equipped with micro-balance sensitive enough to detect changes in weight (ASTM, 2014).

Elemental Analyser Flash 2000 (CE Instrument, UK) was used to quantify the concentration of C, H, N and S. About 5 mg of samples was placed in an aluminium capsule and combusted at 900 °C in 50% oxygen atmosphere. The gaseous products were analysed by an equipped GC-TCD which was calibrated with a standard material, 2,5-(bis(5-tert-butyl-2-benzo-oxazol-2-yl) thiophene (BBOT) having a chemical formula $C_{26}H_{26}N_2O_2S$ and 72.56 wt% C, 6.11 wt% H, 6.49 wt% N and 7.40 wt% S. The MS calibration peak for this standard is shown in Appendix A (Figure A.3).

TGA 4000 (PerkinElmer, UK) was used to measure ash content using a microbalance with a ± 0.01% precision and 1 μg sensitivity. 5 mg sample was loaded into the micro-crucible and placed on the micro-balance in the combustion chamber. The temperature was increased to 950 °C and held at this temperature until mass loss plateau was obtained (about 15 minutes) under 20 mL/min air flow. The final weight was taken as the ash content.

3.5.2 Metal content determination

The composition of metal in the carbon catalysts can be measured by digesting the catalyst in acidic solution for chemical element analysis such as atomic absorption spectroscopy (AAS) and inductively coupled plasma-mass spectrometry (ICP-MS). In an AAS, samples containing metals are atomized in air-acetylene flame to produce an analyte at an excited state which absorbs a specific wavelength unique to a particular element. The source of the wavelength emission is a hollow-cathode lamp made of cobalt-chromium-copper-iron-manganese-nickel (depending on the element of interest) and the intensity of absorbance relates to the concentration of the analyte via the Beer-Lambert law (Ball, 2006). For ICP-MS, the analyte is atomized and ionized in an argon plasma, inductively coupled with a high-frequency electrical field. These ions are transported to the MS via a sampler orifice prior to the separation based on the energy, momentum, and velocity of the ions (representative of the m/z value of an element) (Evans, 2007).

The modified dry ash method was chosen to be the digestion method because it was reported to be safer and more effective as compared to the conventional method, which uses high amount of *aqua regia* in determining Cu, Fe and Mn in biochar samples. This modified method can be simplified as follows (Enders & Lehmann, 2012):

1) 100 mg of the sample was heated in a furnace to 500 °C in 2 h before kept at this temperature for another 8 h;
2) The residue from (1) was mixed with 1.43 mL 65% HNO_3 (Sigma-Aldrich, USA) and evaporated at 120 °C;
3) The residue from (2) was mixed with 5 mL 35% HCl (Sigma-Aldrich, USA) and evaporated at 120 °C;
4) The residue from (3) was mixed with 1 mL HNO_3 and 4 mL HCl and evaporated at 120 °C; and
5) The residue from (4) was solubilized in 5 mL HNO_3 before vortexed, filtered and further diluted to a suitable concentration for use in an Atomic Adsorption Spectrometer (AAS).

The modified method published by Enders & Lehman (2012) used H_2O_2, but this study uses HCl, showing acceptable metals recovery from the activated carbon – based catalysts. As the calibration standards for the AAS were prepared in 1% HNO_3, the sample must be diluted to the same acidic concentration. About 5 mL of sample was injected into the AAS AAnalyst 400 (PerkinElmer, UK) which automatically calculate the concentration of the metal based on the calibration carried out prior to the sample run. The concentration reading by AAS was cross-checked with an ICP-MS for PKSCu(10 wt%) as the comparison sample and the standard difference was 1.8 wt% (refer Appendix A (Table A.4) for detail values obtained using ICP-MS).

3.5.3 Surface area properties

The surface properties of a catalyst are measured to understand the attributes of the material and their contributions to the chemical potential, such as adsorption and reaction. This includes the surface area and porosity, the two most important physical properties. The understanding of adsorption and desorption phenomenon allows the study of these properties in a single experiment, called gas adsorption analysis. In this experiment, a gas is used

as a probe molecule of known purity and properties to be adsorbed over a material surface while either the amount of volume adsorbed is being evaluated throughout the change of the relative pressure (P/P_0 where P_0 is the adsorbate saturation pressure) (Thommes et al., 2015). In this project, Surface Characterization 3Flex (Micromeritics, USA) was employed for this experiment. Prior to analysis, the samples were vacuum-dried at 150 °C overnight using VacPrep 061 sample degas system (Micromeritics, USA) to remove moisture and impurities from the catalyst surfaces. About 0.1 g of the sample was loaded into a quartz tube and installed in the equipment. Nitrogen is used as the gas probe at 77 K. The surface area was calculated using the Brunauer-Emmett-Teller (BET) method which assumes multilayer adsorption over a solid surface while the pore volume and width are evaluated using t-plot and Barrett-Joyner-Halenda (BJH) methods respectively (Attard & Barnes, 2001). The equipped software (3flex 4.05) calculated these parameters automatically upon obtaining the results.

3.5.4 Catalyst acidity analysis

It has been discussed in Chapter 2 that catalyst acidity, contributed by the support and the metal catalyst, plays an important role in H_2-SCR. Therefore, this property is characterised here to determine the extent of the acidity of the carbon catalysts.

By exploiting the fact that acidic sites react with a base analyte, basic gases can be used in a chemisorption experiment to quantify the amount of acidic sites and then expose the chemisorbed species to a linear ramp of temperature to determine the acidic strength (Fadoni & Lucarelli, 2006). Ammonia-temperature programmed desorption (NH_3-TPD) uses this method to quantify acidic sites, but it is unable to differentiate the nature of the acidic site (Brønsted or Lewis acid). Depending on the interest of a study, NH_3-TPD could be an acceptably good and repeatable method to determine total acidic sites as it was reported that ammonia even adsorbs on weak Lewis acid sites (Hemmann, Jaeger, & Kemnitz, 2014). The calibration of the instrument with a known quantity of ammonia allows the calculation of the acidic site by integrating the area under the desorption curve.

In this study, NH_3-TPD was carried out in a Chemisorb 2720 Pulse Chemisorption System (Micromeritics, USA) equipped with a TCD, diagram shown in Figure 3.10. The general procedure for a NH_3-TPD experiment consists of catalyst pre-treatment, ammonia adsorption and ammonia desorption:

1) Pre-treatment – About 50 mg of samples was dried at 110 °C for 10 min under helium flow;
2) Ammonia adsorption – The flow was switched to 20 mL/min 5 % NH_3/He for 1 h to achieve adsorption equilibrium; and
3) Ammonia desorption – The flow was switched back to helium to purge the system from physisorbed NH_3 for 1 h prior to increasing the temperature to 600 °C at 10 °C/min.

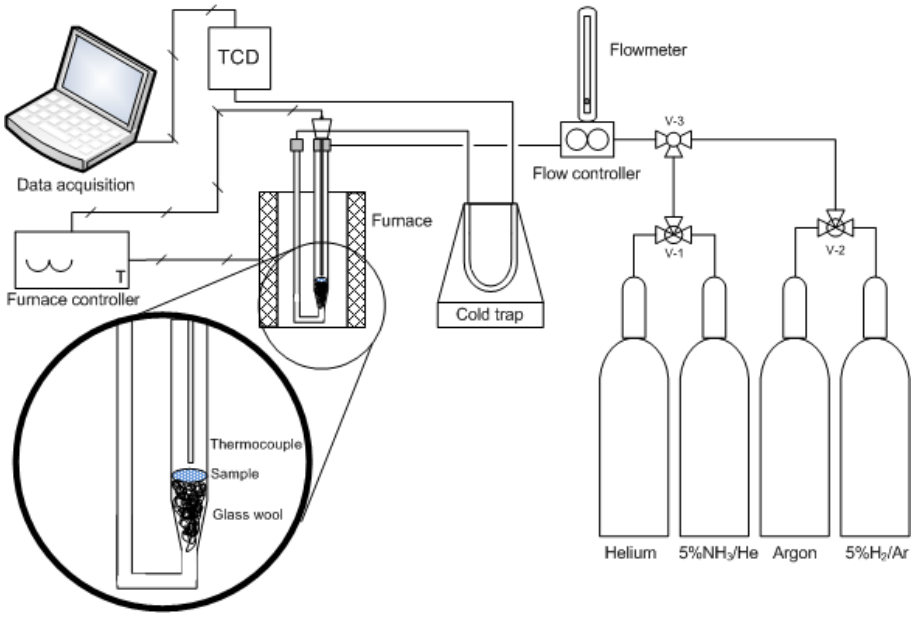

Figure 3.10: Chemisorb 2720 Pulse Chemisorption system. TCD: Thermal conductivity detector; V-1,2,3: Switch valves.

As the acidity of a carbon catalyst can also be attributed to the surface functional groups of the activated carbon as the support, attenuated total reflection Fourier-Transform infra-red spectroscopy (ATR-FTIR) was also utilized to observe the microtexture properties of the catalyst surface. This analysis has been made easier with the capability of the ATR to extend the IR wave directly onto the specimen surface with less sample preparation. The powdered sample was pressed against the ATR crystal that receives and

reflects a beam of IR light which propagates the evanescent waves into up to 2 m in depth over the specimen surface. The beam exiting the crystal was collected at a detector to record the transmittance of light over a wide range of wavenumber. FT is used to convert the raw data (in the form of cosine waves) into spectra. These spectra are used by chemists to identify chemical bonds and structures, but complex specimens require experience to interpret (Harris, 2010). In this project, IRAffinity-1S FTIR spectrophotometer (Shimadzu, UK) was used to perform this analysis.

3.5.5 Redox properties

The interaction in a supported catalyst and bimetallic catalyst is often observed as a bulk phenomenon because of the accumulative effects between the support and the catalyst, or between the two catalysts. Robertson et al. (1975) first used temperature-programmed reduction (TPR) to evaluate the alloying effect of nickel-copper supported over silica as opposed to the unsupported and monometallic systems (Fadoni & Lucarelli, 2006).

In a TPR experiment, hydrogen mixed in inert gas is usually used as the reducing gas and flowed over the catalyst at increasing temperature of constant ramp rate. The concentration of hydrogen in the outlet gas, detected using a detector such as TCD, can be used to determine the consumption of a gas at the reduction sites of a catalyst at a particular temperature (when plotted against temperature). Hence, the area under the peak can be correlated to the amount of hydrogen consumed at a particular site (Fadoni & Lucarelli, 2006). There are also known peak temperatures (temperature at which hydrogen is consumed) published in the literature which give knowledge of the metal phases present on the catalyst (Regalbuto & Ha, 1994).

In this study, TPR was carried out using a Chemisorb 2720 Pulse Chemisorption System (Micromeritics, USA), diagram shown in Figure 3.10, and the general procedure used to determine the catalysts reducibility is as follows; About 60 mg of the dried sample was loaded into a quartz tube. The tube was then electrically heated to 110 °C to dry off the sample in argon flow before ramping the temperature at 10 °C/min to 450 °C in 5% H_2/Ar. Hydrogen consumption was recorded by the equipped thermal conductivity detector (TCD) and plotted against temperature.

In similar sense, temperature-programmed oxidation (TPO) can be used to determine the oxidation sites, or as a bulk property, the catalyst oxidizability (Fadoni & Lucarelli, 2006). The interpretation from these data must be carefully applied, as a system such as a carbon catalyst would imply additional phenomena related to the gasification of the carbon support. As the interest in this study is to characterise the total oxidizability of the catalyst in terms of the catalyst stability under oxidative operating conditions which can be related to the combustion rate during the reaction (explained in section 3.2.4), TPO was carried out using a thermogravimetric analyser TGA 4000 (PerkinElmer, UK) and the general procedure is as follows; About 5 mg of samples was dried at 110 °C for 10 min under nitrogen flow. Then, the flow was switched to 20 mL/min air at increasing temperature at 10 °C/min until 600 °C. The derivative of the sample weight change with temperature (DTG) was automatically calculated by the machine and plotted against increasing temperature. The offset-temperature, defined as the temperature at which the material combustion starts, was determined using onset-of-slope package in OriginPro 2017. This software application finds an intersection between two straight lines on the TGA curve. An example is shown in Appendix A (Figure A.4).

3.5.6 NO-temperature-programmed desorption experiment

The nature of NO adsorption could either be dissociative or non-dissociative, where the former could lead to the formation of different species over the catalyst surface (refer Section 2.2.1). These products can be identified by desorbing those species at increasing temperature and monitored using a detector such as TCD or MS (the latter is preferred to differentiate a complex mixture of products). Prior to this stage, a significant amount of NO must be adsorbed over the catalysts surface, usually at room temperature. 0.2 g of the samples was exposed to 1 % NO/He at 100 mL/min for 30 mins (at this duration the system has reached equilibrium where the outlet NO is equal to the inlet NO). Then, pure helium was used to remove the physisorbed NO for 1 h prior to ramping the temperature at 3 °C/min until 400 °C in pure helium flow.

CHAPTER 4. Catalytic Reduction of Nitric Oxide with Hydrogen using Carbon-supported *d*-metal Catalysts

4.1 INTRODUCTION

Selective catalytic reduction is one of the best available technologies used to remove nitrogen oxides (NO_x) from flue gases. As the common method utilizes ammonia or urea (Piumetti et al., 2015), an alternative to this reducing agent may be applied to avoid safety and environmental issues. Using hydrogen as the reductant ensures no ammonia slip, which is unacceptable in many countries (Tu et al., 2017). However, H_2-SCR currently requires noble metals such as Pt, Pd and Rh to be used as a catalyst. As the NO $2\pi^*$ orbital consists of an unpaired electron and the transition metals have valence electrons in the *d*-subshell, the metal-NO backbonding takes place from metal *d*-orbital to NO $2\pi^*$ orbital which is stronger than the N-O bond (Roy, Hegde, & Madras, 2009). Many transition metals have been studied and showed promising results, but some lead to health and environmental issues, such as Cr, Co and Ni. In fact, Ni is known to react with CO in the exhaust gas to form nickel tetracarbonyl, a product more toxic than CO (Mondt, 2000). Among other transition metals, Cu, Fe and Mn showed promising and practical use as H_2-SCR catalysts. These *d*-metals are also abundant in the earth's crust as compared to the precious metals belonging to the same group. For instance, copper is at least 4000 times cheaper than palladium, while iron is 2000 times cheaper than ruthenium (NRCCSR, 2012). Furthermore, the supported metal oxides catalyst also showed enhanced performance due to the surface chemistry of the support and synergistic effects imposed by the support-metal bonding. Activated carbon is one of the catalyst supports studied in SCR. Its high surface area and rich surface functional groups are expected to contribute to the reduction of NO. However, the utilization of *d*-metals supported over activated carbon has not yet been extensively explored in H_2-SCR. Therefore, this chapter explores the potential utilization of these catalysts in terms of the conversion and selectivity, given by equations 3.4 and 3.5. The characteristics of the monometallic oxide catalysts are also determined based on the adsorption-desorption behavior of NO over the catalyst.

4.2 MATERIALS AND METHODS

4.2.1 Catalysts preparation

Monometallic oxide catalysts were prepared via incipient wetness as described in Section 3.4. As the pore volume of the PKS is about 0.5 ml/g (refer Table 4.1), 1 mL of deionized water was used for impregnation of every 2 g of PKS. The hypothetical metal loading chosen at this stage was 10 wt.%. The resulting catalysts were designated as PKSM where M = Cu, Fe and Mn.

4.2.2 Catalyst characterisation

The carbon support (i.e. PKS) and the derived catalysts (PKSM) were characterised based on the elemental composition, surface area and pore volume, catalyst acidity, redox properties, and nitric-oxide adsorption-desorption.

Carbon, hydrogen, and nitrogen content were determined using a CHNS Flash elemental analyser and the oxygen content was obtained by the difference between the balance of the mass in this analysis and the ash content determined from TGA (refer Section 3.5.1). The metal loading on all synthesized catalysts were measured in comparison to the hypothetical loading using an AAS. The digestion of the solid catalysts was performed according to the modified dry ash method, as explained in Section 3.5.2. The surface area properties for the PKS and the derived catalysts were determined using nitrogen adsorption-desorption method in a surface characterization equipment (refer Section 3.5.3).

The catalyst acidity was analysed from the desorption profile of NH_3 gas (NH_3-TPD) at elevated temperature. NH_3 was pre-adsorbed on the catalyst surface prior to the experiment as a basic probe (refer Section 3.5.4). The type of the metal species (oxidation states) on the catalyst and the catalyst reducibility were determined using temperature-programmed reduction (H_2-TPR) analysis (refer Section 3.5.5). In addition, the nature of NO adsorption over the catalyst was also investigated to identify the types of adsorption species formed over the different metal species supported over carbon. This was achieved via a NO-temperature-programmed desorption (NO-TPD) experiment (refer Section 3.5.6).

4.2.3 Catalyst activity testing

For determination of the conversion and selectivity, an isothermal reaction was performed on the catalysts at selected temperatures. 1 g of the pre-dried catalyst was loaded into the fixed-bed reactor (refer Figure 3.3), and purged using helium prior to any reaction. The catalyst was reduced in-situ at 250 °C under 5 % H_2/He at 250 sccm (equivalent to 7,175 h^{-1}). Then, the system was purged and cooled under pure helium flow to 40 °C. After increasing the temperature to a desired value, a gas mixture of 500 ppm NO + 4 % H_2 + 1.5 % O_2 in helium (see Table 2.3 for the range of gas composition used in H_2-SCR studies) at 250 sccm was fed into the reactor and the reaction was allowed to reach steady-state at the reaction temperature for at least 2 h. The effluent was analysed continuously using a MS (Hiden HPR-20, UK) and the quantification method used was discussed in Section 3.2.3. On top of the NO conversion and N_2 selectivity, the combustion rate was also calculated based on the cumulative production of CO and CO_2.

4.3 RESULTS AND DISCUSSION

4.3.1 Characteristics of the carbon catalysts

The surface properties of the catalyst support (PKS) and the derivative catalysts are included in Table 4.1. The surface area of PKS was more than 1000 m^2/g (common value for activated carbon as reported by Yahya et al. (2018)) in which 80 % was contributed by micropores – apertures of less than 2 nm in diameter including the walls of the cracks, pores and cavities which are deeper than they are wide. The total pore volume was approximately 0.5 cm^3/g. In addition, the nitrogen adsorption-desorption curve hysteresis loop (included in Appendix B (Figure B.1)) indicated that the pores were mostly narrow slit-like (Sing et al., 1985) which can also be observed in the SEM image (insert image of Figure B.1). The surface area of the resulting catalysts can be seen to reduce due to the incorporation at the PKS surface by the metal oxides. It was evident that the metal oxides were doped over the external surfaces, as all catalysts showed a reduction in the external surface of about 90 %, while the micropore volume remained constant (as compared to the PKS as the precursor).

Table 4.1: Surface properties for PKS and the derivative catalysts.

Properties (unit)	PKS	PKSCu	PKSFe	PKSMn
BET surface area (m^2/g)	1126	850	715	800
t-plot micropore area (m^2/g)	910	830	697	777
t-plot external surface area (m^2/g)	216	20	18	23
t-plot micropore volume (cm^3/g)	0.361	0.421	0.360	0.401
BJH adsorption average pore width (Å)	64	4	4	4

The elemental composition of PKS and the derivative catalysts are summarized in Table 4.2. The carbon support possesses high carbon content (~90 %) which is comparable to the commercial activated carbon reported by Al-Rahbi et al. (2016). As metal was impregnated, the C, H, N and O content of the PKS lowered mainly due to liberation during high-temperature calcination stage of the catalyst synthesis. Meanwhile, ash content increased due to the presence of metals and incombustible matters after catalyst synthesis. It can be reported here that the incipient technique employed in this study successfully impregnated the theoretical amount of metal over the activated carbon evident by the close metals wt% values obtained via elemental analysis.

Table 4.2: Elemental composition for PKS and the derivative catalysts.

Element	Mass percentage (%) ± standard deviation (%)			
	PKS	PKSCu	PKSFe	PKSMn
C	82 ± 4	78 ± 2	75 ± 1	80 ± 1
H	1.15 ± 0.44	0.45 ± 0.01	0.52 ± 0.08	0.34 ± 0.02
N	0.89 ± 0.04	0.54 ± 0.03	0.49 ± 0.01	0.51 ± 0.05
O*	14.97	10.81	14.00	7.81
Ash	1.2 ± 0.8	10.6 ± 0.7	10.3 ± 1.3	11.3 ± 1.3
Doped metal percentage (%)	-	8.3 ± 0.2	7.6 ± 1.2	6.1 ± 0.1

*From balance.

The chemical properties of the catalysts and the support were also investigated and are summarized in Table 4.3. Generally, the PKS has an intrinsic acidity contributed by the ash content and surface functional groups (as determined using FTIR spectroscopy). However, impregnating the metal

oxides reduced the acidity of the carbon support due to the heat treatment that destroyed the acidic sites (Yahya et al., 2018). On the other hand, the presence of metal oxides increases the hydrogen consumption which is useful in H_2-SCR reaction, but the offset temperatures were largely reduced because the metal oxides catalysed the carbon gasification. Therefore, the utilization of the catalysts beyond this temperature should be performed with caution as the performance might be deteriorating at the loss of the carbon mass.

Table 4.3: Chemical properties for PKS and the derivative catalysts.

Properties (unit)	PKS	PKSCu	PKSFe	PKSMn
Acidity				
Concentration of desorbed NH_3 (mmol/g)	8.02	8.15	1.44	4.35
Redox properties				
Total H_2 consumption (mmol/g)	0	2.34	0.38	0.27
Reducibility ($X10^{-3}$/°C)	-	5	2.9	4.5
Offset temperature (°C)	500	350	370	335

To observe the contribution of the surface functional groups to the acidity-basicity of a catalyst, FTIR spectra for the PKS and the carbon catalysts are obtained and displayed in Figure 4.1. The spectra are divided into three regions (this is shown by the dotted line in Figure 4.1a); 3500 to 2500 cm^{-1} for the single bond stretch functional groups, 2500 to 1400 cm^{-1} for the double and triple bonded groups and the compounds fingerprints from 1400 to 500 cm^{-1}. The detailed stretch indexing in these regions are shown separately at the bottom part of the figure. The presence of carboxylic acid (α) can be observed at stretches around 2660 cm^{-1} for the O-H stretch, broad stretches from 1970-1620 cm^{-1} for the C=O bond and stretches around 900 cm^{-1} for the bending O-H bond (White, 1971). Carboxylic acids are known as Brønsted -Lowry acids because of their tendency to donate protons (H^+). The other functional groups generally presence on the catalysts include various sharp stretches from 2380 to 2000 cm^{-1} belonging to alkyne (β), stretches around 1550 cm^{-1} assigned for aromatic compounds (χ), N-containing functional groups such as aliphatic amines (δ) were observed at around 1200 cm^{-1} and alkene (ε) was observed at around 670 cm^{-1} (White, 1971).

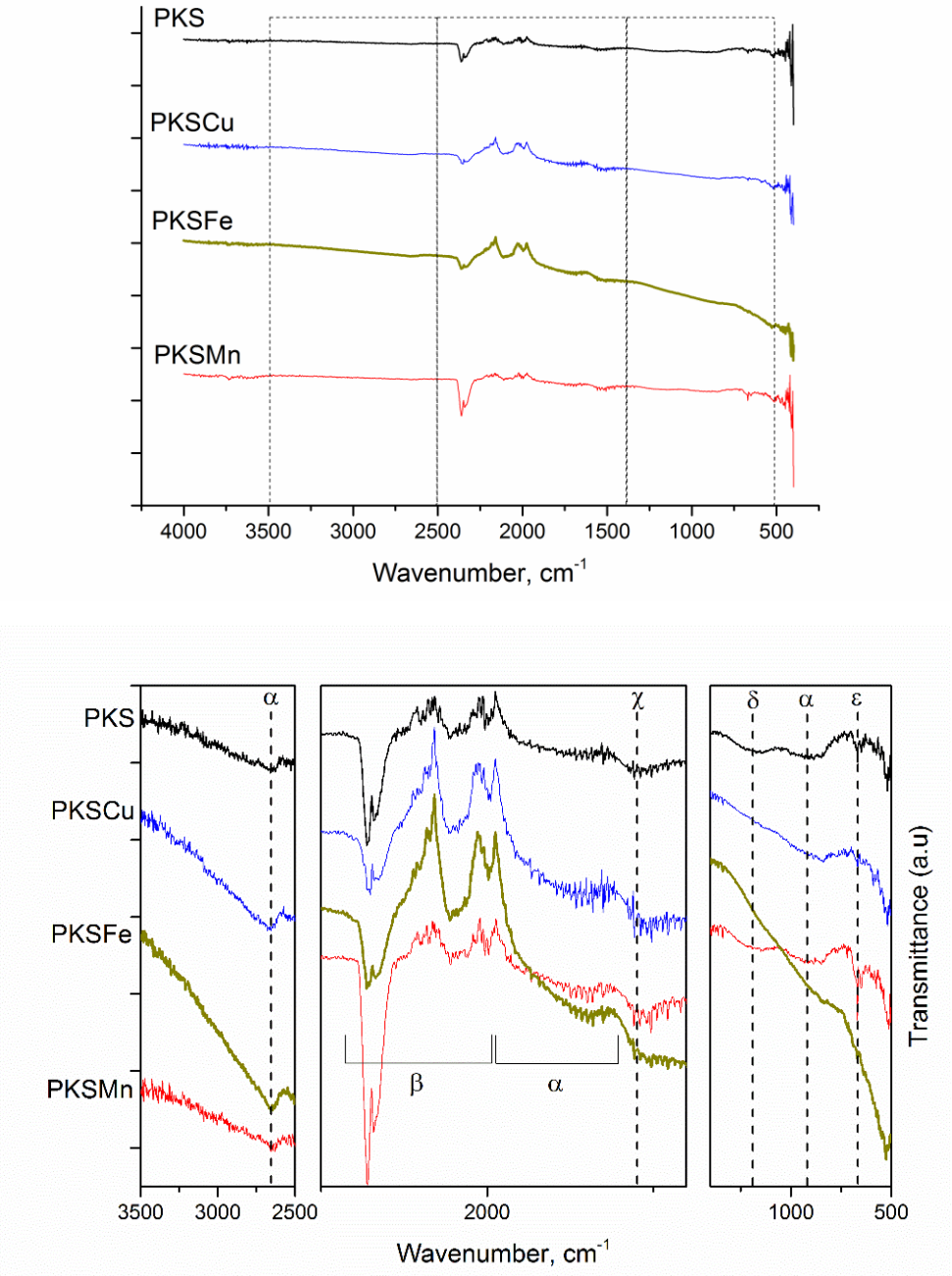

Figure 4.1: FTIR spectra for PKS and the derivative catalysts. α: carboxylic acids, β: alkyne, χ: aromatics, δ: aliphatic amines and ε: alkene.

As the intensity of the transmittance in FTIR is the amount of photons at a particular stretching frequency, the change of the intensity could imply a change in the compound concentration. Overall, carboxylic acid can be seen to be enhanced in PKSCu and PKSFe as compared to PKSMn that has similar peak intensity with the unsupported PKS. On the other hand, the other

functional groups can be seen to reduce if not remain the same over PKSCu and PKSFe as compared to the PKS. Therefore, it can be claimed that carboxylic acids may play a role in the acidity of the catalysts, as determined via NH_3-TPD.

NH_3-TPD profiles for the PKS and the carbon catalysts are shown in Figure 4.2. The TCD signal represents NH_3 concentration and increasing the temperature of the sample showed desorption of NH_3 that was pre-adsorbed by the samples prior to this stage. PKS exhibited the largest NH_3 desorption (area under the peak) implying the largest NH_3 adsorption due to the high acidity of the activated carbon. The acidic property of activated carbon has been reported in the literature as due to the oxygenated functional groups (Chen et al., 2015). The one large peak on the PKS NH_3-TPD profile indicates the acidic site is exclusively that of the carbon surface.

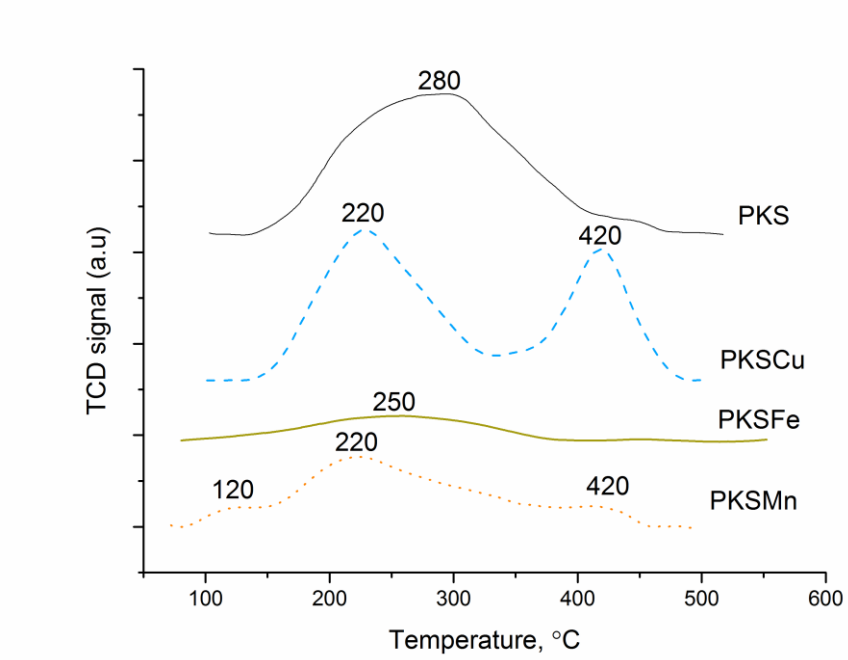

Figure 4.2: NH_3-TPD profiles for PKS and the derivative catalysts in 20 sccm pure helium and 10 °C/min.

Multiple desorption peaks can be observed on the derivative catalysts, especially for PKSCu, which has two distinct peaks centred around 220 and 410 °C. A study on the acidity of copper supported over SAPO-34 showed the desorption peaks had shifted to lower temperature. The two peaks around 150 and 450 °C originally found on the support material had shifted to 140 and

320 °C respectively (Yu et al., 2014). Therefore, it can be reported here that the first peak is due to the shifting effect of the TPD peak for PKS by the presence of copper, while the second one is due to an additional stronger acidic site promoted by copper oxide.

The acidity of PKS was reduced after impregnation with iron and manganese due to the high calcination temperature used (higher than copper, refer Section 3.4). This was also reported by Lee et al. (2012) that the manganese TPD peaks decreased when increasing the calcination temperature from 300 to 700 °C. On the NH_3-TPD curve for PKSFe, only a wide and low desorption peak can be seen on PKSFe stretching from 100 to 350 °C which is a similar range to the peak found on raw PKS. The desorption peak for Fe supported over ZSM-5 was reported in the literature to be around 300 °C (Lindholm, Sjövall, & Olsson, 2010; Long & Yang, 2001). This means Fe may have partially contributed to the adsorption of NH_3 at this site alongside the carbon surface functional groups.

However, manganese showed the appearance of three NH_3 desorption peaks at 120, 220 and 420 °C. The first peak could be due to the physisorbed NH_3, which is very weakly attached to the catalyst surface and can be disregarded as an acidic site (Lee et al., 2012). Meanwhile, Deng et al. (2016) examined MnO_x/TiO_2 catalyst in a NH_3-TPD experiment and found two peaks associated with MnO_x acidic sites at 220 and 360 °C indicating the weak and strong acidic sites. This means the second peak in the NH_3-TPD curve for PKSMn could be assigned to both PKS and Mn acidic property while the third one to the strong acidic MnO_x sites.

The reducibility of the catalyst was determined via TPR experiment. Figure 4.3 shows the TPR profiles for the PKS and the carbon-supported metal oxides. TCD signal in the figure is an inverse of hydrogen concentration detected which means increasing signal implies the consumption of hydrogen by the samples. Over all temperature ranges, PKS is not readily reducible without the presence of a metallic catalyst which is the reason for no hydrogen consumption. As reducibility is defined as $1/T_{first}$ (reciprocal of the first reduction temperature) (Patel et al., 2014), PKSCu is the most reducible catalyst, followed by PKSMn and PKSFe. However, based on the amount of

hydrogen consumption (area under the curve), PKSCu used up the most hydrogen followed by PKSFe and PKSMn. Note that the stoichiometric amount of metals based on the consumed hydrogen over the three catalysts is different from the values obtained via metal content determination experiment. This is because the peak height in TPR depends highly on the heating rate and flow rate used in the experiment, as opposed to a pulse chemisorption experiment which is preferably performed for metal content/surface area determination .

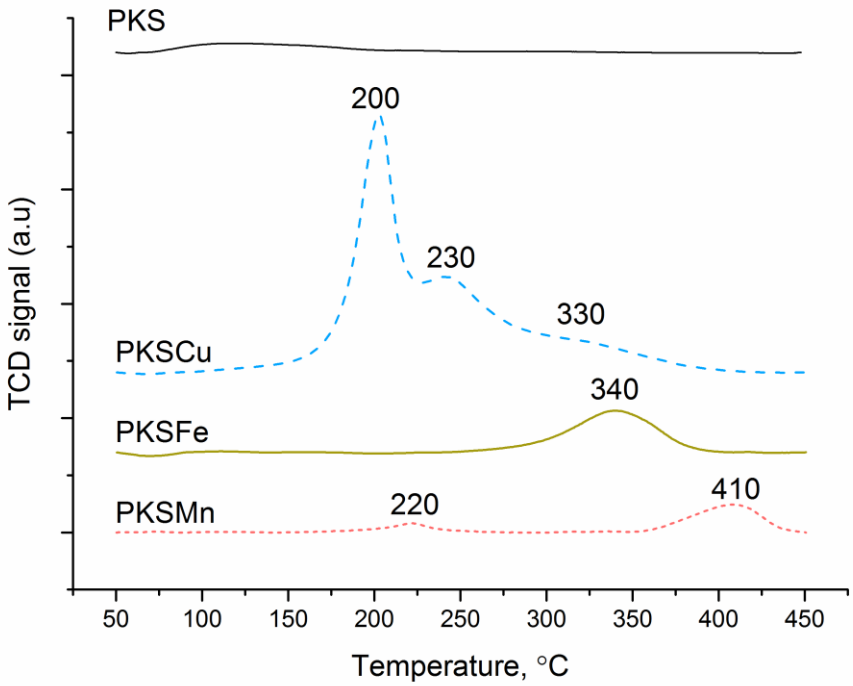

Figure 4.3: H_2-TPR profiles for the PKS and carbon catalysts in 5 % H_2/He at 20 sccm and 10 °C/min.

Furthermore, the presence of metal and the oxidation states can also be determined from a TPR profile. The reduction of H_2 over PKSMn resulted in two peaks at 220 and 410 °C. According to Deng et al. (2016), the reduction of pure manganese oxide can be observed at two temperatures – 350 °C for MnO_2 to Mn_2O_3, and 520 °C for the successive Mn_2O_3 to MnO reduction. Therefore, upon impregnation over PKS, both reduction temperature shifted to lower values and because more hydrogen was consumed at the second peak, this means that some Mn_2O_3 was already present on the catalyst due to the calcination process.

Reduction over PKSFe showed only one peak at 340 °C which can be attributed to the reduction of Fe_2O_3 to Fe_3O_4. This is based on a TPR experiment carried by Patel et al. (2014) over Fe/MCM-41 which exhibited peaks at 390 and 590 °C for the reduction of Fe_2O_3 to Fe_3O_4 and Fe_3O_4 to FeO, respectively.

Generally, for copper oxide, a reduction temperature of below 300 °C is attributed to the reduction of highly dispersed Cu^{2+} to Cu^{+} while the higher temperature is due to the direct reduction of agglomerated CuO to Cu metal (Patel et al., 2011). Li et al. (2012) studied copper species when impregnating copper nitrate over activated carbon via TPR experiment and assigned the reduction peaks around 240 and 550 °C to the reduction of isolated Cu^{2+} to Cu^{+}, and Cu^{+} to Cu^{0} respectively. An intermediate peak at around 430 °C was attributed to the direct reduction of CuO to Cu metal. However, Moreno-Piraján et al. (2010) reported a lower reduction temperature for copper species when impregnating copper nitrate over coconut shell activated carbon. The range of the reduction peaks was 150-300 °C with stepwise CuO reduction ($Cu^{2+}\rightarrow Cu^{+}\rightarrow Cu^{0}$). Upon deconvoluting of the TPR curve for PKSCu, three peaks can be observed (see Figure 4.4).

The two consecutive peaks (the curve for Peak 3 starts after the curve for Peak 1) can therefore be assigned to the reduction of Cu^{2+} to Cu^{+} and Cu^{+} to Cu^{0} respectively. Meanwhile, the intermediate peak can be assigned to the direct reduction of CuO to Cu, encompassing the dominant species according to the area under the curve (about 63 % of the total integrated area). The assignment of metal species from TPR experiment should be corroborated with other analyses, such as WAXS or XRD.

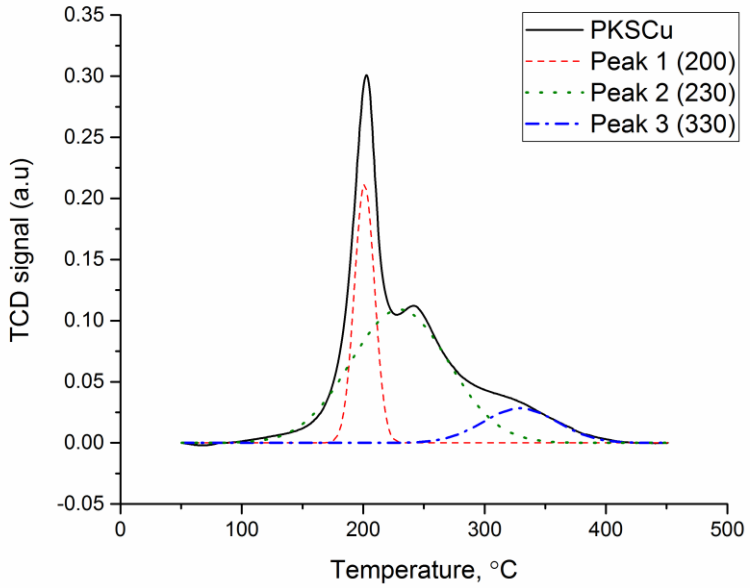

Figure 4.4: H_2-TPR peak deconvolution for PKSCu using OriginPro 2017 with Gaussian peak model and Levenberg Marquardt iteration algorithm.

The behaviour of the catalysts under oxidizing conditions can be observed via a differential thermogravimetric analysis (DTG) which shows the rate of weight change over temperature. This is displayed in Figure 4.5. The change of weight (negative) implies that carbon was gasified, and the temperature at which this occurs the most is called the inflection point (Dollimore et al., 1992). The inflection point for the PKS is beyond 600 °C which is typical for carbon gasification temperature in air (Radic et al., 2017). With the presence of the transition metals, the inflection point was lowered to about 400, 410 and 450 °C for PKSMn, PKSCu and PKSFe respectively. This shows that the reactivity of the metal oxides present on the catalysts in oxidizing condition decreases in that particular order.

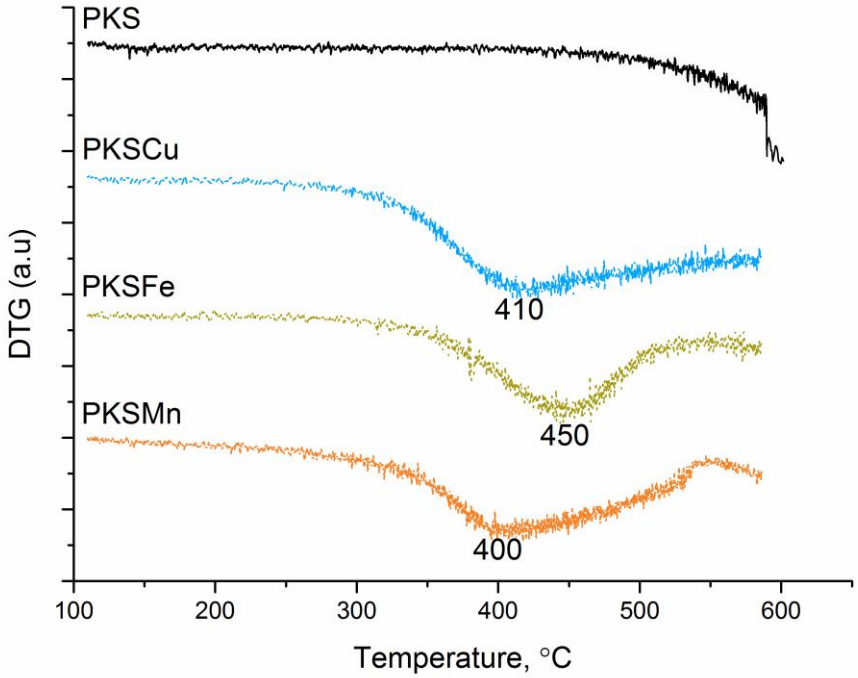

Figure 4.5: DTG curves for PKS and the derivative catalysts in 20 sccm air and 10 °C/min.

The characterisation of *d*-metals supported over PKS revealed that the catalysts synthesis altered the properties of the carbon support. Different metal oxide catalysts with different calcination temperatures have different chemical properties. Even the presence of carboxylic acids on the carbon support was retained in all catalysts; the acidity changed depending on the acidity at the metallic sites. Furthermore, the presence of the metallic species in the catalysts can be determined via elemental analysis and H_2-TPR. The corroboration of these characterisation techniques indicates that the metal species influenced both the hydrogen consumption and acidity of these catalysts.

4.3.2 Nitric oxide adsorption-desorption experiment

NO-TPD experiments were performed both on the bare carbon support (without metal oxide) and the *d*-metal supported catalysts. After exposure of 1 % NO/He until equilibrium, PKS was purged for at least 1 h to remove the physisorbed and trapped NO in the system. Upon desorption at increasing temperature, the evolved gases were detected by a mass spectrometer. For

PKS, two types of gases can be detected – nitric oxide and nitrogen dioxide. The evolution of NO and NO_2 curves for PKS are shown in Figure 4.6a and b, respectively. The curve deconvolution was performed separately for NO and NO_2 using Gaussian distribution method in OriginPro 2017 (refer Appendix B (Table B.1)).

It was evident that NO was readily adsorbed by the carbon at room temperature. However, no other N-products such as nitrogen and nitrous oxide were detected during the desorption stage indicating the non-dissociative adsorption of NO on the carbon support. This is similar to the findings by López et al. (2007) using pyrolyzed sub-bituminous coal as NO sorbent. NO was reported to desorb with a wide peak centred at 300 °C and a shoulder at 400 °C. However, for PKS (Figure 4.6a), the curve deconvolution revealed two peaks of NO desorption on the carbon support; a sharp peak at 165 °C and a wide peak at 270 °C. The former can be associated with the desorption of "adsorbed NO_2", formed via oxidation over activated carbon while the higher temperature peak can be assigned to the "strongly bonded NO" (Klose & Rincón, 2007).

The desorption of NO_2 at a peak around 130 °C also showed the oxidation ability of the carbon support. It has been discussed in Section 2.4.1 that the desorption of NO_2 around 110 °C is due to the decomposition of – $C(ONO_2)$ surface complexes. It is noteworthy to report here that CO_2 and CO also evolved during NO-TPD for PKS (curves not shown). As carbon is not readily oxidized in the absence of oxygen at low temperatures, it can be confirmed here that it was a result of the surface complex decomposition according to equations 4.1-4.3, as proposed by Jeguirim et al. (2004).

$$-C(ONO_2) \rightarrow CO_2 + NO \qquad 4.1$$

$$-C(ONO_2) \rightarrow C(O) + NO_2 \qquad 4.2$$

$$-C(ONO_2) \rightarrow CO + NO_2 \qquad 4.3$$

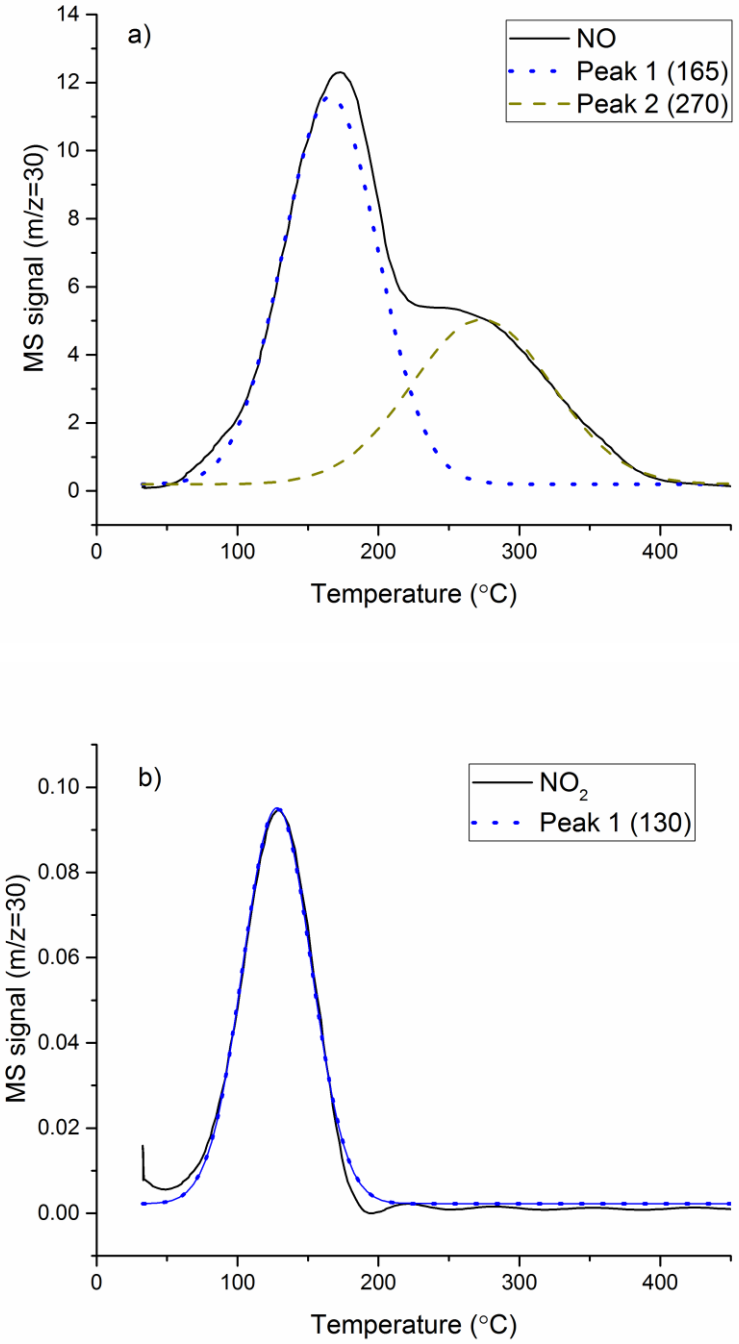

Figure 4.6: NO-TPD peak deconvolution for PKS showing evolved; a) NO and b) NO_2 in 20 sccm pure helium and 10 °C/min.

The high NO adsorption on the carbon support can be attributed to the high carbon and nitrogen levels that provide basic sites on the surface. Figure 4.7 shows the NO signal obtained during NO-TPD of the carbon supported *d*-metal catalysts. In all cases, the amount of adsorbed NO reduced at least 3-

fold compared to the area under the peak of NO-TPD of PKS. Additionally, no other N-products can be observed during desorption stage other than NO. This means, incorporating the *d*-metals onto activated carbon reduced the capacity for NO adsorption by the carbon support. The main reason for this was the losses of carbon and nitrogen content, which contributed to the adsorption sites for NO and the bond between NO and *d*-metals was not as strong as NO with the carbon support. The latter can be proven by evaluating the desorption temperature peaks of each catalyst. The peak properties obtained from Gaussian deconvolution are summarized in Table B.1, where the full width at half maximum (FWHM) was used as the peak characteristic.

For PKSCu, NO was desorbed at peaks of around 85, 115 and 160 °C (Figure 4.7a). Wang et al. (2015) reported a desorption peak around 100 °C over Cu/CeO_2 catalysts designating the presence of nitrosyls species bonded with copper. Thus, the first two peaks can be assigned to the bonds between NO and the impregnated copper. The third peak which has similar peak characteristic with the peak at the same temperature in Figure 4.6a can be assigned to the "adsorbed NO_2".

As for PKSFe and PKSMn, each possessed an additional low-temperature peak at 90 and 70 °C, respectively. This is attributed to the physisorbed NO_x with the metal oxides as being reported by Long & Yang (2001) and Lee et al. (2012) for the peaks at 75 and 100 °C over Fe/ZSM-5 and Mn/TiO_2 respectively. As for the peak assigned to $–C(ONO_2)$ on PKS, taking FWHM ± 10 would infer that this peak shifted to lower temperature for PKSMn, for a desorption temperature of 115 °C. The second peak in Figure 4.7b resembles the "strongly adsorbed NO" peak in Figure 4.6a (FWHM ± 10) more than the "adsorbed NO_2" peak (FWHM ± 30).

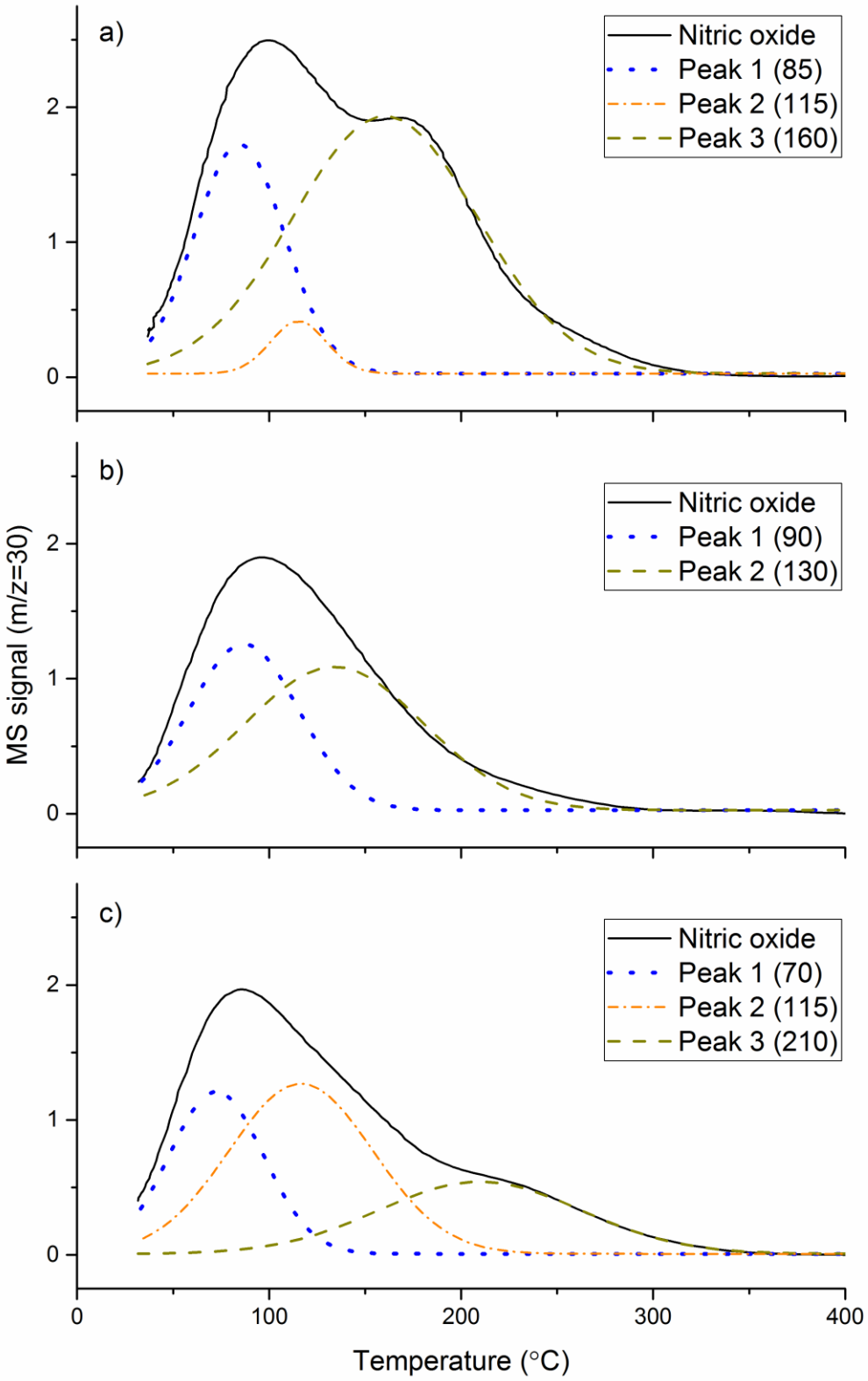

Figure 4.7: NO-TPD peak deconvolution for; a) PKSCu, b) PKSFe and c) PKSMn in 20 sccm pure helium and 10 °C/min.

There is a high-temperature peak observed for PKSMn at 210 °C (Figure 4.7c), which can be postulated to be either the shifted “adsorbed NO” peak (from Figure 4.6a), or the strong NO_x-Mn bond as reported by Kijlstra et al. (1997) at a peak of around 207 °C when studying NO-TPD over MnO_x/Al_2O_3 catalyst. Lower desorption temperature is known to possess lower adsorption energies which means C-N surface complexes possessed lower adsorption energy over metal-impregnated catalysts as compared to the bare carbon support.

In addition, there were no NO_2 gases evolved during NO-TPD for all three catalysts. This suggests that the desorption of the formed NO_2 was reductive due to the presence of reductive sites (S_{red}), according to equations 4.4 and 4.5, based on Klose & Rincón (2007).

$$(NO_2)_{ads} + S_{red} \rightarrow NO + CO \qquad 4.4$$

$$2(NO_2)_{ads} + S_{red} \rightarrow NO + CO_2 \qquad 4.5$$

The area under the peak indicates the amount of NO adsorption species at a particular site. By taking the amount of nitrosyls formed per gram of metal, it can be inferred that the formation of this species is most pronounced over PKSCu, followed by PKSFe and PKSMn. This is not correlated to the order of decreasing acidity even for the fact that NO is reported to adsorb at Brønsted acid sites. Therefore, the formation of nitrosyls over carbon-supported catalyst is rather complex; its contributions as a reaction intermediate are not the focus of this project.

However, it is conclusive that NO was readily adsorbed over PKS. The bond was stronger than the nitrosyls species formed over *d*-metals catalysts. The weak nitrosyls bond would allow further dissociation with a reductant in gaseous phase, and avoid permanent occupation of the adsorption sites (ease of regeneration).

4.3.3 Gasification of catalysts in NO-H_2-O_2 system

An important feature of a carbon-supported catalyst is the rate of carbon combustion due to oxidation by intrinsic oxygen content in the flue gas and/or oxides of nitrogen. This is because the catalyst could experience deteriorating performance over the loss of carbon that serves as the basic structure of the

catalyst. It was shown previously that the offset temperature of the carbon catalysts reduced considerably with the impregnation of metals. In this experiment, the gasification of carbon was calculated based on the accumulative rate of CO_2 and CO formation in μmol/s during the H_2-SCR reaction. Figure 4.8 shows the combustion rate over the catalysts in H_2-SCR. Generally, the combustion rate for all catalysts increased with increasing temperature.

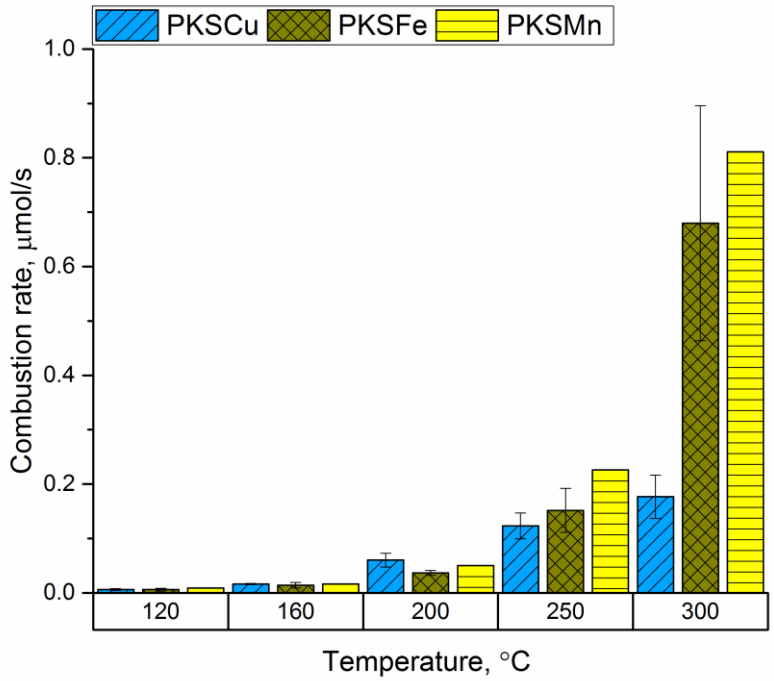

Figure 4.8: Combustion rate by the catalysts in 500 ppm NO + 4 % H_2 + 1.5 % O_2 at 7,175 h^{-1}.

As the offset temperature for all the catalysts is near 300 °C, the combustion rate between the catalysts can be compared at this temperature. The order of decreasing combustion rate at 300 °C is PKSMn ≈ PKSFe > PKSCu[3]. This may be correlated to the decreasing electropositivity of the reduced metal states (as the catalysts were reduced in hydrogen flow prior to this experiment) in that particular order. Castoldi et al. (2009) explained this

[3] Note the standard deviation for PKSFe is only significant at high temperature 300 °C. This might be due to another factor, such as catalyst dispersion, contributing to the combustion rate. This was not investigated further due to the absence of this effect in other samples.

phenomenon as follows: high electropositivity indicates a higher tendency for the metal to donate electrons which increases the electron density of neighbouring carbon sites (C). This leads to the increased affinity of this site for binding an oxygen atom, denoted as C_f. As a result, C-C_f bonds are weakened and carbon gasification is promoted. The information provided by the combustion rate can be a determining factor for the catalyst application in a particular oxidizing condition.

4.3.4 Catalyst activity

Prior to quantification of the catalyst activity, a control experiment was carried out using the bare PKS in the same condition stated in Section 4.2.3. Figure 4.9 shows the evolution of NO in a wide range of temperature. The formation of a product is negligible because the carbon support did not induce NO reduction/decomposition without the presence of metal oxides. However, at low temperature, (below 150 °C), there was a decrease in NO signal, indicating adsorption over carbon surfaces. Therefore, to discount adsorption at low temperature and further explore the activity at higher temperature, the selected temperatures for the isothermal reaction experiments were 120, 160, 200, 250 and 300 °C.

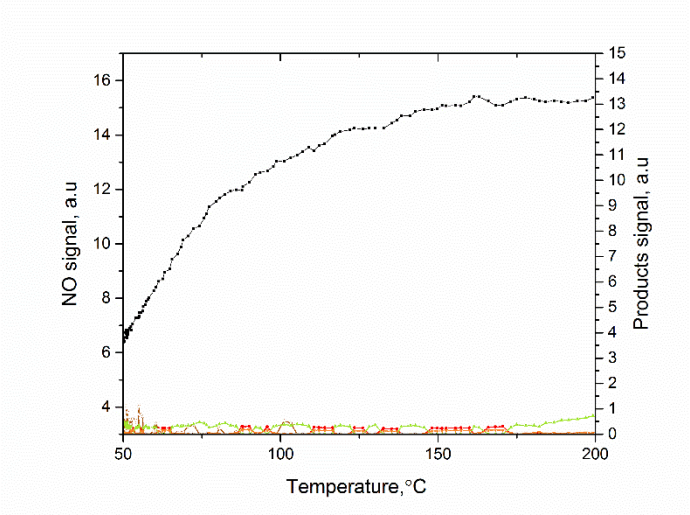

Figure 4.9: Temperature-programmed reactions for PKSblank at 7,175 h^{-1} and 1 °C/min in; 500 ppm NO + 4 % H_2 + 1.5 % O_2. (■) Nitric oxide, (●) nitrous oxide, (♦) nitrogen, (◊) ammonia, (○) nitrogen dioxide, (▲) carbon dioxide, and (▼) carbon monoxide.

Figure 4.10 shows the NO conversion over the three catalysts in a NO-H_2-O_2 system. All catalysts can be seen to achieve higher conversion at elevated temperatures, but only PKSCu was able to totally convert NO below 300 °C. PKSMn has the lowest conversion activity at low temperature until at least 250 °C, with a perceptible rate of 9 %. PKSCu and PKSFe showed similar and constant conversion (~10 %) until at the same temperature where the conversion caused by PKSCu peaked to 100 %. These findings indicate that the *d*-metals supported over activated carbon are able to facilitate the reduction of NO using hydrogen as the alternative reducing agent but at varying levels of efficiency.

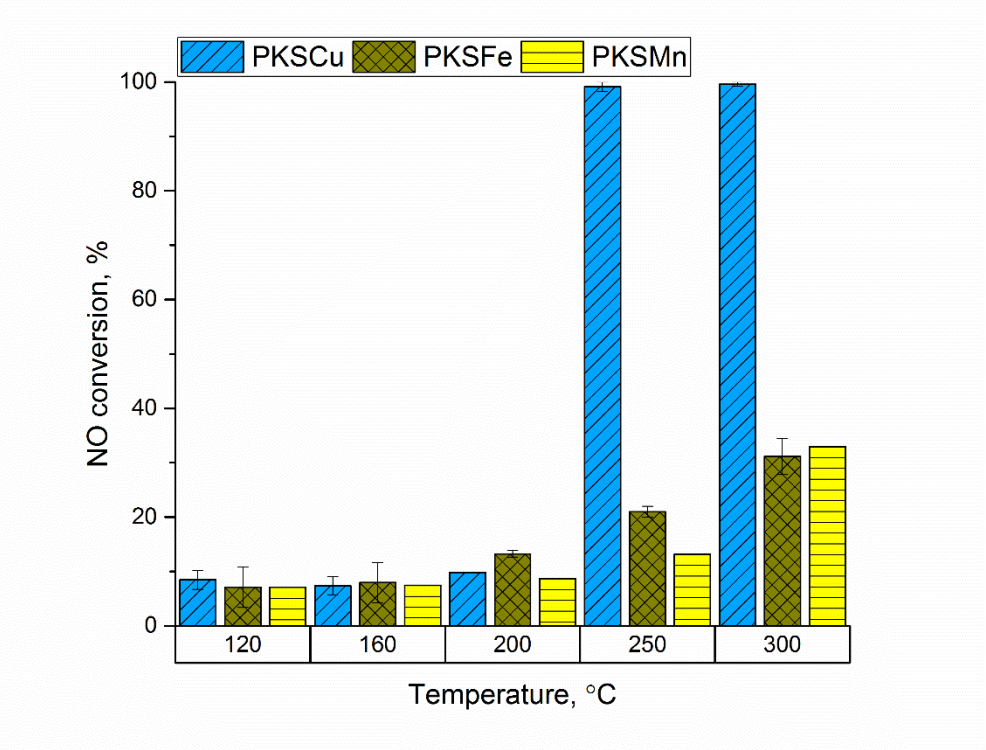

Figure 4.10: Nitric oxide conversion by the catalysts in 500 ppm NO + 4 % H_2 + 1.5 % O_2 at 7,175 h^{-1}.

Above 200 °C, PKSCu gave the most NO conversion followed by PKSFe and PKSMn but at 300 °C, the activity of the catalysts decreased as follows; PKSCu > PKSMn ≈ PKSFe. This is consistent with the findings on the catalysts' reducibility order discussed previously. It is known that catalyst reducibility is an important factor in NO_x reduction. As oxygen mobility is increased on a reducible metal surface, oxygen vacancies are easily

generated (Cheng et al., 2017; Ji et al., 2017). This is required for the dissociation of adsorbed NO over metal surfaces. The removal of oxygen from this vacancy will keep the metal reduced for the next reaction cycle (Ilieva et al., 2015).

In addition, this trend may also correspond to the acidity of the catalysts as shown by NH_3-TPD analysis and the amount of nitrosyls formation as shown by NO-TPD. As NH formation during NO-H_2 reaction over metallic surfaces is a well-known mechanism (as discussed in Section 2.2.3), PKSCu which showed the highest amount of adsorbed ammonia among the three catalysts in NH_3-TPD provided more sites for the intermediates to be adsorbed and consumed. In the meantime, PKSCu exhibited the highest nitrosyl formation (NO adsorbed over metal oxides) which also contributed to the high conversion.

Figure 4.11 shows the variation of N_2 selectivity over the catalyst. The decrease in selectivity was due to the release of ammonia in the outlet where ammonia is known to be an important intermediate in H_2-SCR. The formation of NO_2 and N_2O is negligible across the entire experiment (not shown). As can be seen from the graph, PKSCu showed the formation of NH_3 the most and followed by PKSFe. The selectivity towards N_2 formation over PKSCu peaked to about 100 % at 200 °C and reduced at 250 °C. However, at 300 °C, selectivity for PKSCu increased and achieved almost 100 %. PKSFe followed a similar trend, except that beyond 250 °C the selectivity was constant.

The high selectivity achieved by PKSMn throughout the temperature range does not implicate the high reactivity in H_2-SCR compared to the other catalysts, as the conversion rate is very low below 300 °C. It probably does not produce enough NH intermediate which prevents the release of excess NH considering the low nitrosyl formation. Therefore, selection of a catalysts in terms of the selectivity must be made with caution. In fact, it must solely be used to make sure the catalysts do not produce additional toxic gases in addition to NO_x.

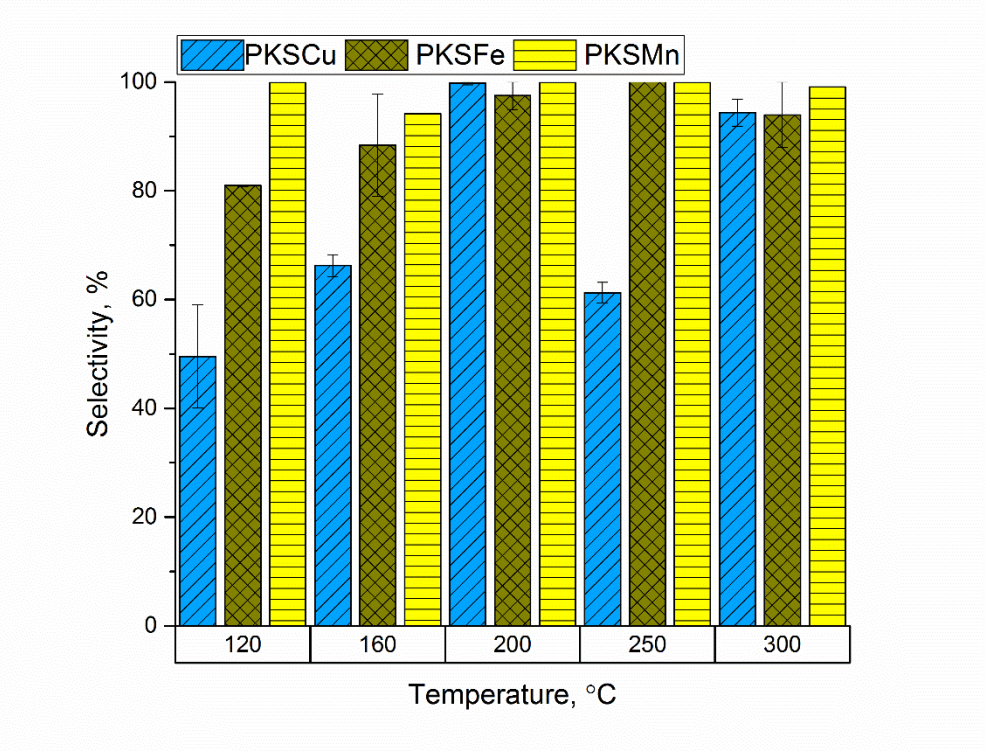

Figure 4.11: Nitrogen selectivity by the catalysts in 500 ppm NO + 4 % H_2 + 1.5 % O_2 at 7,175 h^{-1}.

4.4 CONCLUSIONS

Carbon-supported *d*-metal catalysts were synthesized using palm kernel shell activated carbon as the support and copper, iron and manganese as the catalysts. NO was found to adsorb over the carbon support as the "adsorbed NO_2" and the "strongly adsorbed NO" species. Upon impregnating the carbon with metal oxides, the extent of NO adsorption reduced as does the extent of NO oxidation, while the formation of nitrosyl species over the metal surfaces was evident. The impregnation and calcination in the synthesis stage produced Cu, Cu_2O and CuO species over PKSCu, MnO_2 and Mn_2O_3 species over PKSMn and Fe_2O_3 species over PKSFe as determined from TPR. PKSCu was the easiest to be reduced followed by PKSMn and PKSFe which was related to the increased in NO conversion. The catalyst acidity and the amount of nitrosyls formation were also seen to affect the activity in H_2-SCR. High catalyst acidity (as found in PKSCu) provided more sites for NH (an intermediate in H_2-SCR) adsorption and reaction with the formed nitrosyls

over the catalyst surface. In addition, PKSMn showed the highest carbon combustion activity due to high electropositivity compared to the other two *d*-metals. This information is useful to achieve the second objective of this project that is to develop structure-performance relationship in H_2-SCR. Moreover, copper will be used as the core catalyst in the next chapter in order to optimize the performance of the catalyst. Improvements such as increasing metal loading and co-catalyst must be explored before the kinetics of the reaction can be evaluated in detail.

CHAPTER 5. Bimetal Oxides Effects of Copper Co-doped with Manganese or Iron Supported over Activated Carbon in Reduction of Nitric Oxide with Hydrogen

5.1 INTRODUCTION

Multicatalysis is a technique employed in a catalytic reaction to achieve what would be a difficult transformation by a mono-catalytic system. Bimetallic catalysis is an example of such a system which involves the application of two metal catalysts in one system which can act either in double activation (both catalysts are required to activate a reagent) or cascade (activation of a reagent is sequential between the two catalysts) or synergistically (each catalyst activates different reagent) in a reaction (Allen & Macmillan, 2012). Oh & Carpenter (1986) discovered an improvement of the catalyst activity in an exhaust treatment (NO + CO + O_2) when using bimetal Pt-Rh, compared to using physically mixed Pt and Rh catalysts supported over silica. It was found that the 50 % CO conversion temperature for the bimetal catalyst prepared via stepwise impregnation reduced by 30 °C at CO concentration higher than 2 % compared to the physically-mixed Pt and Rh catalysts. This is due to the increased probability of reaction between surface CO (adsorption affinity on Pt) and adsorbed oxygen (readily forms oxides with Rh) in a randomly distributed Pt and Rh over the catalyst surface. This is an example of synergism as each metal activated different reagent.

Studies of the effect of bimetallic catalysts in NO_x treatment are important to develop a catalyst with optimum performance. Most of these studies however focused on the application in NH_3-SCR. The application of hydrogen as the reductant and biomass activated carbon as the catalyst support could change the means of bimetallic effects between the catalysts, which of interest in this chapter. For a pair of catalysts to be synergistic, the total effect needs to be better than the individual effects. As it was shown in Chapter 4 that all three carbon-supported metallic catalysts demonstrated considerable NO conversion and selectivity in H_2-SCR in a wide temperature range, all metallic catalysts will be further investigated in this chapter in terms of the compositional effects and characteristics of the bimetallic system.

5.2 MATERIALS AND METHODS

5.2.1 Catalyst preparation

The preparation of the catalyst using PKS as the catalyst support was performed as described in Section 3.4. The investigation of the bimetallic effects can be performed in a sequence shown in Figure 5.1. Since copper showed the best monocatalytic performance in Chapter 4, it was chosen as the principle catalyst. The total metal loading using copper supported over PKS was examined at 10, 20 and 30 wt% prior to observing the effect of adding another metal oxide in the catalyst system. The catalysts are denoted as $PKSCu_y$, with y representing the hypothetical metal loading. A fixed total metal loading was chosen after this stage to study the effect of pairing copper with a different catalyst – iron and manganese which were then termed as $PKSFe_xCu_y$ and $PKSMn_xCu_y$, respectively with *x* and *y* representing the hypothetical metal loadings. The bimetallic oxide catalysts were synthesized via sequential impregnation, which involves impregnation-calcination of one metal oxide after another. Finally, the effect of metals ratio on the characteristics and performance of the catalysts were studied by preparing the catalysts based on the hypothetical composition listed in Table 5.1.

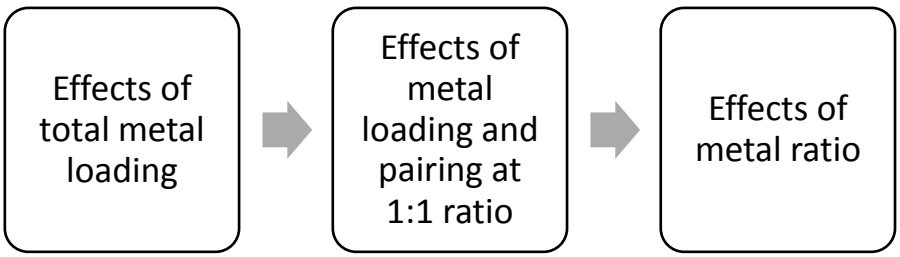

Figure 5.1: Sequence for studying bimetallic effects in H_2-SCR.

Table 5.1: Values for preparation of bimetallic catalysts with different ratio.

No.	Metal 1 wt.% (M1)	Metal 2 wt.% (M2)	Total metal loading	Designation
1	10	10	20	$PKSM1_{10}M2_{10}$
2	10	20	30	$PKSM1_{10}M2_{20}$
3	10	30	30	$PKSM1_{10}M2_{30}$
4	20	10	40	$PKSM1_{20}M2_{10}$
5	30	10	40	$PKSM1_{30}M2_{10}$

5.2.2 Catalyst characterisation

The derived catalysts were characterised based on the elemental composition, catalyst acidity, and redox properties. The methods and procedures used are described in Section 4.2.2.

5.2.3 Catalyst activity testing

The method and procedure used are similar to the ones in Section 4.2.3.

5.3 RESULTS AND DISCUSSION

5.3.1 Effects of metal loading

Prior to studying the effect of the bimetal oxides approach, the effect of increasing the mono-metal oxide content in the catalyst was evaluated to understand the contribution of the total metal loading on the performance and characteristics of the catalysts. The concentration of copper was increased to 20 and 30 wt% and the chemical properties have been summarized in Table 5.2.

Table 5.2: Physical and chemical properties of Cu-impregnated PKS at increasing copper loading.

Properties (unit)	$PKSCu_{10}$	$PKSCu_{20}$	$PKSCu_{30}$
Elemental analysis (%)			
C	78	60	56
H	0.45	0.59	0.41
N	0.54	0.44	0.57
O	10.81	18.56	17.58
Ash content	10.6	20.3	25.4
Metal content	8.3	13.4	14.5
Acidity			
Concentration of desorbed NH_3 (mmol/g)	8.15	12.49	11.67
Redox properties			
Total H_2 consumption (mmol/g)	2.34	4.59	4.81
Reducibility ($X10^{-3}$/°C)	5	5	5
Offset temperature (°C)	350	360	360

The carbon content decreased with the increase in metal loading due to the replacement of the carbons for the metal oxides as also can be seen from the increase in the ash content. All catalysts were calcined at the same temperature and duration, so the effect of high temperature treatment could be ruled out, except that Chapter 4 has shown copper to accelerate carbon combustion, also contributing to the loss of more carbon at the same

temperature. However, the successful rate of metal loading decreased at higher concentrations, as preparing the catalysts for 20 and 30 wt% only impregnated about 13 and 14 wt%, respectively. This phenomenon can be explained at the microscopic level as pore size, adsorption capacity and solubility of the metal precursors in water (used in the incipient wetness) play important roles, which are however not of interest in this study. Therefore, the catalysts are still denoted with the intended concentration value because the preparation condition (including moles of nitrates involved) might affect the chemical properties of the catalysts such that can be seen for the increasing ash content. In the meantime, the acidity in terms of the adsorbed NH_3 and the offset temperature improved at high copper loading whereas the reducibility remained constant. Similarly, copper concentration has no effect on the total hydrogen consumption by the catalyst when increasing loading from 20 to 30 wt%.

The effects of increasing copper loading on CuO species can be studied via TPR experiment. Figure 5.2a shows the TPR profiles for the copper impregnated over PKS at increasing loading. It is evident that all three peaks (200, 230 and 330 °C) originally observed over $PKSCu_{10}$ (refer Chapter 4) can be found at the same temperatures for $PKSCu_{20}$ and $PKSCu_{30}$, indicating similar copper species. However, an additional peak appeared for $PKSCu_{30}$, as determined from the deconvolution of the TPR curve shown in Figure 5.2b.

As it is known that the intermediate-temperature peak in TPR for copper species is an indicative of the direct reduction of CuO to Cu (Li et al., 2012), it is reasonable to assign this species to the new peak found at around 280 °C over $PKSCu_{30}$. The deconvoluted area-under-the-peak for each species in the TPR profiles are correlated with the hydrogen consumption and summarized in Table 5.3. The third peak which was assigned to Cu_2O (refer Chapter 4) showed an increase in the magnitudes as the copper loading increased.

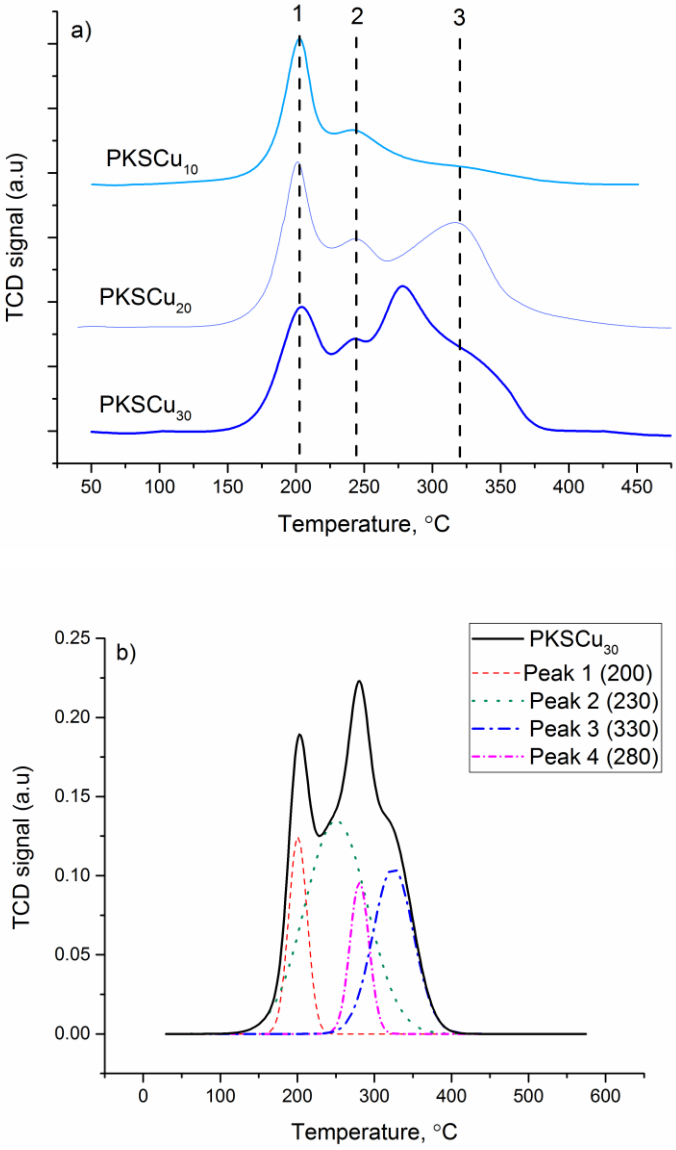

Figure 5.2: a) TPR profiles for Cu-impregnated catalysts at increasing copper loading; and b) deconvoluted TPR profile for PKSCu$_{30}$ using OriginPro 2017.

Table 5.3: H_2 cosumption at each peak for TPR experiment of Cu-impregnated catalysts at increasing copper loading.

(mmol/g)	**Peak 1**	**Peak 2**	**Peak 3**	**Peak 4**
PKSCu$_{10}$	0.60	1.78	0.39	-
PKSCu$_{20}$	0.63	2.09	1.86	-
PKSCu$_{30}$	0.66	2.42	1.23	0.53

Changes in the catalyst acidity with respect to metal loading were also observed via FTIR spectroscopy and NH_3-TPD, showed in Figure 5.3 and Figure 5.4, respectively. Figure 5.3 shows the regional analysis of FTIR spectra for the catalysts at increasing metal loading. By evaluating the peak intensity (by using Curve Translate function in OriginPro 2017), $PKSCu_{20}$ exhibited a reduction in the carboxylic acid stretch at around 2660 cm^{-1} and the broad peak from 1970 to 1620 cm^{-1} while peak at 900 cm^{-1} disappeared. However, the peaks attributed to the alkyne groups also decreased. Meanwhile, $PKSCu_{30}$ showed an improved carboxylic acids peak intensity at 2660 cm^{-1} and from 1970 to 1620 cm^{-1}.

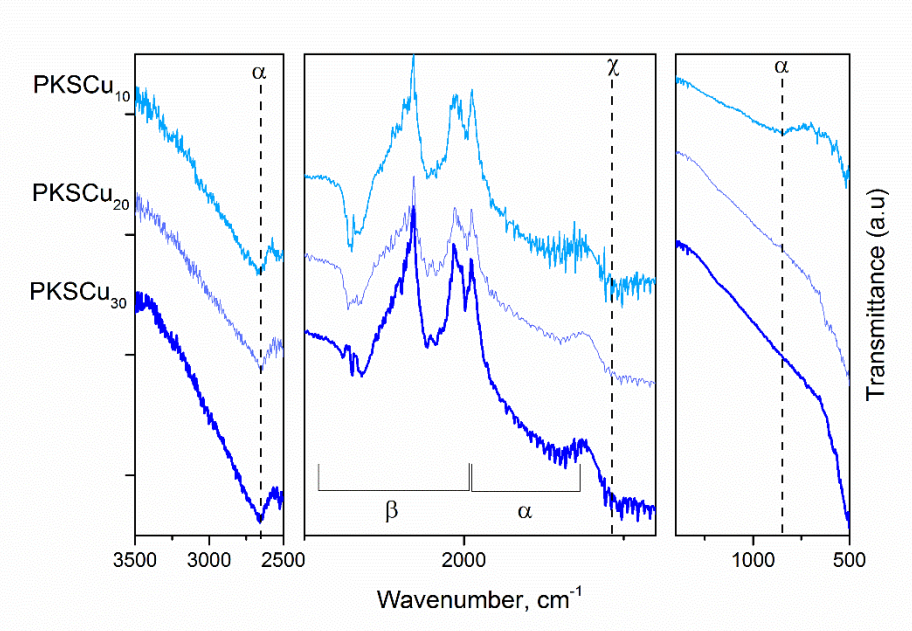

Figure 5.3: FTIR spectra for Cu-impregnated catalysts at increasing copper loading. α: carboxylic acids, β: alkyne, and χ: aromatics.

As discussed in Chapter 4 for NH_3-TPD, the two important sites for PKSCu are denoted as the low-temperature peak (LTP) contributed by the carbon support – copper interaction and the high temperature peak (HTP), assigned to coper oxides. The TPD curve can be deconvoluted to determine the contribution to the adsorption of NH_3 by each acidic site. In this case where the sites are referred to as LTP and HTP, the area under each curve was determined based on the minima that occurs at the curve, where desorption

at the LTP changed to the desorption at the HTP, as shown by a straight line in Figure 5.4.

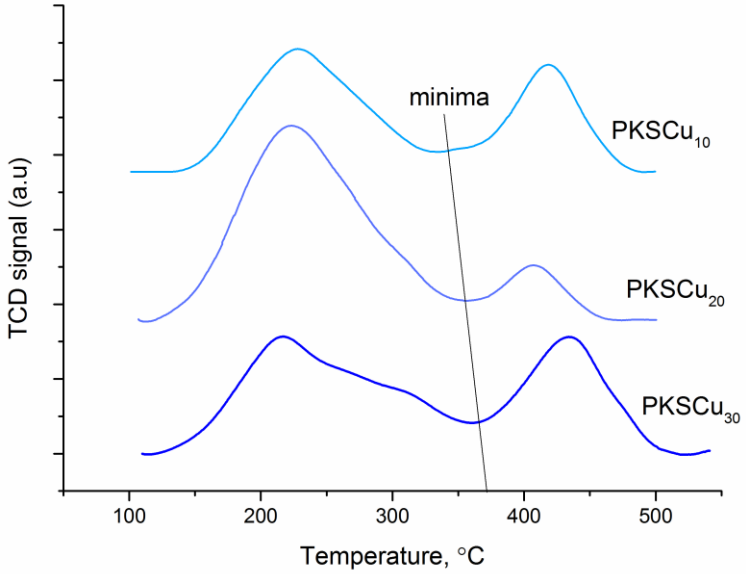

Figure 5.4: NH_3-TPD profiles for Cu-impregnated catalysts at increasing copper loading in 20 sccm pure helium and 10 °C/min.

The peaks deconvolution of NH_3-TPD (not shown) revealed that increasing the copper loading from 10 to 20 wt% increased the amount of NH_3 desorbed at LTP twofold while further increasing to 30 wt% only changed the amount slightly (from 5 mmol/g to 7 mmol/g). This contradicts the FTIR findings that showed lower carboxylic acid (pKa 4) concentration in $PKSCu_{20}$ but is in agreement with the higher carboxylic acids peaks on $PKSCu_{30}$. The contradiction might be due to the increased Cu_2O crystallinity as shown in TPR (as the LTP is contributed by both PKS and copper). Additionally, the disappearance of an alkyne (pKa 25) group stretch in $PKSCu_{20}$ (from FTIR spectra) might have compensated for the total degree of acidity. However, the area under the HTP was halved when increasing the loading from 10 to 20 wt% while increasing by half upon higher loading of 30 wt%. This informed the negative effects of metal agglomeration on the acidity at HTP when increasing the copper loading from 10 to 20 wt%. On the other hand, for $PKSCu_{30}$, the successful metal loading was 14 wt% which is almost twice that of PKSCu, explaining the increased in the HTP concentration due to the increase in metal

loading. However accumulatively, the NH_3 desorption concentration increased with increasing copper loading.

The isothermal conversion, selectivity and carbon combustion rate for the higher copper loading are shown in Figure 5.5, in comparison to the 10 wt% copper-loaded catalyst. The NO conversion did not show significant enhancement over the temperature range, but the low-temperature reaction showed a slight improvement when increasing the metal loading. However, the selectivity towards nitrogen formation exhibited mixed effects. At temperatures lower than 200 °C, the selectivity typically decreased with increasing copper loading while increased at higher temperature. However, at 300 °C, selectivity remained constant. As for the combustion rate, it was almost constant until 300 °C, at which a significant increase of 50 % can be observed for $PKSCu_{20}$ as compared to $PKSCu_{10}$.

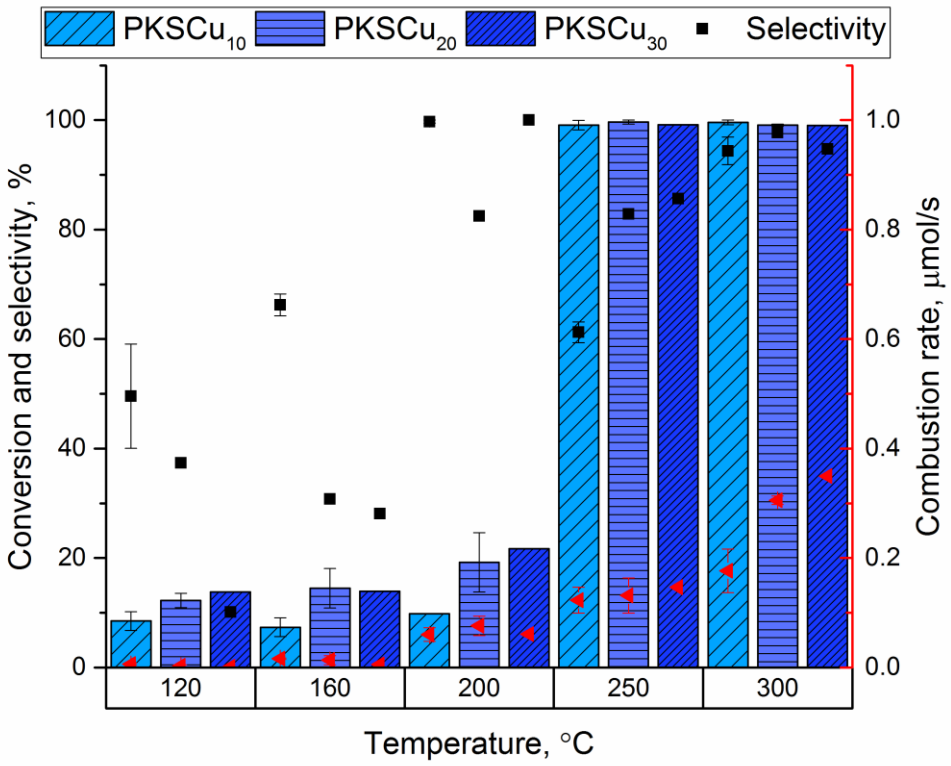

Figure 5.5: Conversion, selectivity and combustion rate for Cu-impregnated catalysts at increasing copper loading in 500 ppm NO + 4 % H_2 + 1.5 % O_2 at 7,175 h^{-1}.

The retained capacity for NO_x conversion by all catalysts is attributed to the identical reducibility factor, as shown in Table 5.2. This strengthens the dependency of NO conversion in H_2-SCR to the catalyst reducibility. As for the selectivity at low temperature, it was observed that the formation of nitrous oxide became detectable at higher copper loading (not shown) even though the signal for ammonia disappeared. The formation of N_2O is known to occur over many metal oxides, especially precious metals, at temperatures as low as 90 °C (Burch & Coleman, 1999). This effect vanished starting at 200 °C for $PKSCu_{10}$ and $PKSCu_{30}$ and at 300 °C for $PKSCu_{20}$. The low in selectivity for $PKSCu_{10}$ at 250 °C was caused by the undesorbed NO or products which have been taken into account by equation 3.5. Increasing copper loading reduced this effect which makes the higher loading metals preferable. However, for carbon-based catalysts under oxidizing conditions, carbon combustion places a limitation on this application. Figure 5.5 shows the combustion rate increased with increasing metal loading and become prominent at higher temperature. The combustion rate of 0.4 µmol/s would mean that a 1 g catalyst with 60 % carbon content could lose the entire carbon mass in only about 35 h. It can be shown that the enhanced carbon gasification was due to the reaction of carbon with NO_x, because as determined by TGA experiment, the stability of the catalysts remained approximately the same as the copper loading was increased. This is shown by the nearly constant offset temperature in Table 5.2 and the inflection points in Figure 5.6.

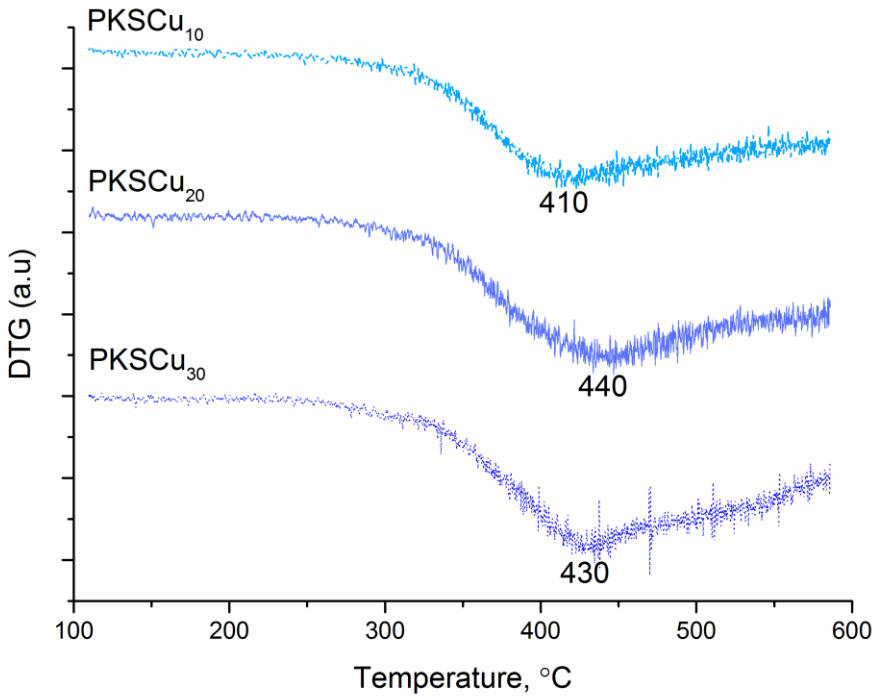

Figure 5.6: DTG curve for Cu-impregnated catalysts at increasing copper loading in 20 sccm pure helium and 10 °C/min.

5.3.2 Effects of metals pairing and loading

The effect of bimetal oxide catalysts on the characteristics and performance in NO_x reduction was investigated by co-impregnating the metals at 1:1 ratio. Chapter 4 showed the potential of singly-impregnated copper, iron and manganese oxide in H_2-SCR at varying degree of performance and Section 5.3.1 has explored the possibility of improving the performance by increasing metal loading with certain limitations. Co-impregnating iron and manganese with copper would theoretically induce different effects on the characteristics and performance which motivates this chapter. The chemical properties of the monometallic copper oxide and the bimetallic Cu-Fe and Cu-Mn oxides supported over PKS are summarized in Table 5.4.

Table 5.4: Physical and chemical properties of $PKSCu_{20}$ and the bimetallic oxide catalysts.

Properties (unit)	$PKSCu_{20}$	PKSFeCu	PKSMnCu
Elemental analysis (%)			
C	60	48	49
H	0.59	0.46	1.14
N	0.44	0.53	0.01
O	18.56	29.94	32.58
Ash content	20.3	20.6	16.9
Cu	13.4	7.0	5.4
Fe	-	5.7	-
Mn	-	-	4.5
Acidity			
Concentration of desorbed NH_3 (mmol/g)	12.49	15.74	9.56
Redox properties			
Total H_2 consumption (mmol/g)	4.59	3.07	2.61
Reducibility ($X10^{-3}$/°C)	5	5	5
Offset temperature (°C)	350	350	340

The similar ash content between $PKSCu_{20}$ and PKSFeCu indicated the similar amount of total metals in the catalyst as also can be proven by the metal content obtained from AAS analysis. PKSMnCu showed less ash content because of the low metal content but the carbon loss due to the preparation method was similar to that of PKSFeCu. Even when reducibility remains constant, the total hydrogen consumption in TPR analysis decreased when using two different metal oxides. The acidity in terms of NH_3 adsorption increased when incorporating Cu and Fe oxides, but reduced with Cu-Mn oxides couple. The latter also showed lower offset temperature indicating lowered stability in oxidizing condition.

The presence of different metal species can be investigated via TPR experiments, and the profiles shown in Figure 5.7 and Table 5.5 for the hydrogen consumption at each peak. It can be seen that the peaks related to CuO (1 and 2) are retained in all catalysts. The first peak increased when using PKSFeCu but decreased for PKSMnCu. Meanwhile, the second peak, which is related to the direct reduction of CuO to Cu, showed decreasing H_2 consumption when co-impregnating copper oxide with iron or manganese oxide. The third peak, associated with further reduction of Cu_2O to Cu, disappeared in both bimetallic oxide catalysts. The reduction peaks originally found over the monometallic oxides PKSFe and PKSMn (refer Chapter 4) are

noticeable at approximately the same temperature in the bimetallic oxide catalysts (peak 4 for Fe_2O_3, 5 for MnO_2 and 6 for Mn_2O_3).

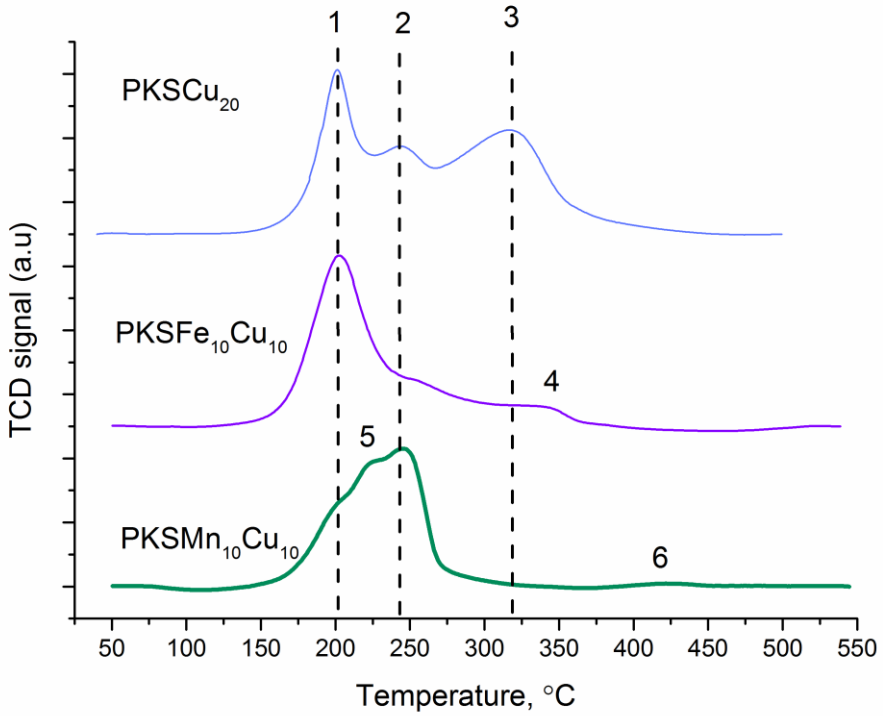

Figure 5.7: TPR profiles for monometallic and the bimetallic oxide catalysts in 5 % H_2/He at 20 sccm and 10 °C/min.

Table 5.5: Hydrogen consumption for monometallic and the bimetallic oxide catalysts.

mmol/g	**Peak 1**	**Peak 2**	**Peak 3**	**Peak 4**	**Peak 5**	**Peak 6**
*$PKSCu_{10}$	0.60	1.78	0.39	-	-	-
*$PKSFe_{10}$	-	-	-	0.38	-	-
*$PKSMn_{10}$	-	-	-	-	0.01	0.26
$PKSCu_{20}$	0.63	2.09	1.86	-	-	-
$PKSFe_{10}Cu_{10}$	1.41	1.52	-	0.24	-	-
$PKSMn_{10}Cu_{10}$	0.84	0.45	-	-	1.50	0.37

*TPR profiles shown in Chapter 4

Despite the lower copper content in the bimetallic oxide catalysts, the integrated area under the first peak was larger than $PKSCu_{20}$, with double the copper loading. However, the total area under the peaks related to copper is lower compared to the $PKSCu_{20}$, mostly due to the loss of the third peak which

is the reduction of Cu^{+} to Cu. By comparing peak 4 over PKSFe and PKSFeCu, the hydrogen consumption almost halved, due to the dominance of peaks 1 and 2 in PKSFeCu. Meanwhile, the increased in hydrogen consumption under the peaks related to manganese species (5 and 6) showed the enhancement effects by the Cu-Mn oxides interactions.

The effect of bimetallic oxides behavior can be further investigated in terms of the change in the catalyst acidity-basicity properties. By evaluating the FTIR spectra with Curve Translate feature in OriginPro 2017, as shown in Figure 5.8, PKSFeCu showed increased in carboxylic acid (α) transmittance at 2660 cm^{-1} and at the broad peak from 1970 to 1620 cm^{-1} while PKSMnCu exhibited otherwise. In addition, the peak associated with alkyne (β) from 2400 – 2000 cm^{-1} can be seen to decrease on PKSFeCu while strongly increasing for PKSMnCu. Meanwhile, the aromatics peak (χ) centered around 1550 cm^{-1} increase for both bimetallic oxide catalysts as compared to $PKSCu_{20}$.

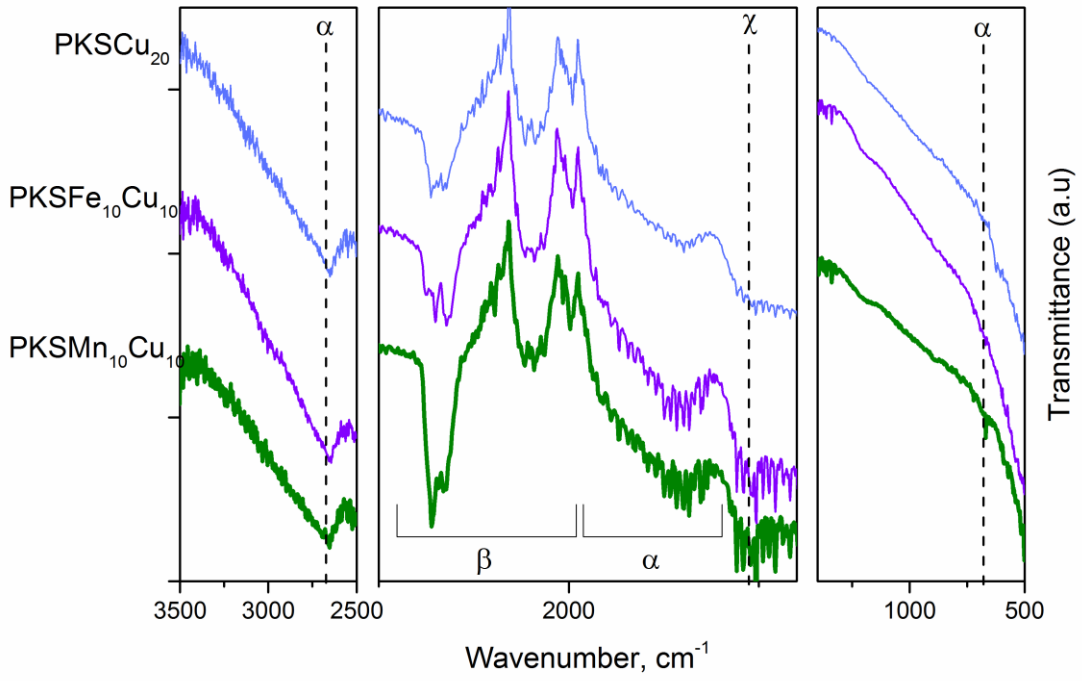

Figure 5.8: FTIR spectra for $PKSCu_{20}$ and the bimetallic oxide catalysts. α: carboxylic acids, β: alkyne, and χ: aromatics.

To evaluate the effect of changing in the surface functional groups to the acidity of the catalysts when co-impregnating the metal oxides, NH_3-TPD was performed. The NH_3-TPD profile is shown in Figure 5.9, with the minima point indicated by the straight line. All three curves show the occurrence of two distinct peaks: one at the low temperature range and the other at the higher temperature range.

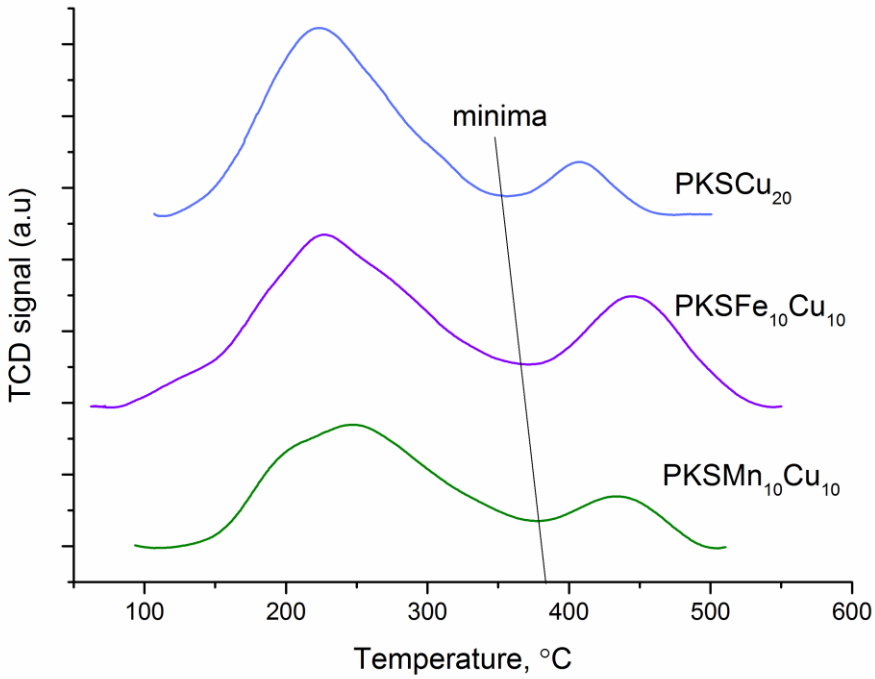

Figure 5.9: NH_3-TPD profiles for $PKSCu_{20}$ and the bimetallic oxide catalysts in 20 sccm pure helium and 10° C/min.

Integration under each peak deconvoluted from the NH_3-TPD curves (based on the minima point) showed that the magnitude of the concentration at the LTP decreased in the order PKSFeCu (11 mmol/g) = $PKSCu_{20}$ > PKSMnCu (7.8 mmol/g) while at HTP, the decreasing order is PKSFeCu (4.7 mmol/g) > PKSMnCu (1.7 mmol/g) = $PKSCu_{20}$. As LTP is also contributed by the acidity of the carbon surface functional groups, the order of the highest to the lowest magnitude at this peak is in agreement with the changing of the carboxylic acid transmittance obtained via FTIR spectroscopy, even though the increased effect (on PKSFeCu as compared to $PKSCu_{20}$) is not very significant.

The performance of the bimetallic oxide catalysts was also compared to $PKSCu_{20}$ as the monometallic oxide catalysts with similar total metal loading. Figure 5.10 shows the conversion, selectivity, and carbon combustion rate for $PKSCu_{20}$, PKSFeCu and PKSMnCu. The conversion over both catalysts is comparable to $PKSCu_{20}$ over most of the temperature range of study. This can be attributed to the similar reducibility of the catalysts as can be seen from Table 5.4. However, the conversion of NO over PKSMnCu at a temperature lower than 250 °C can be seen to be slightly lower.

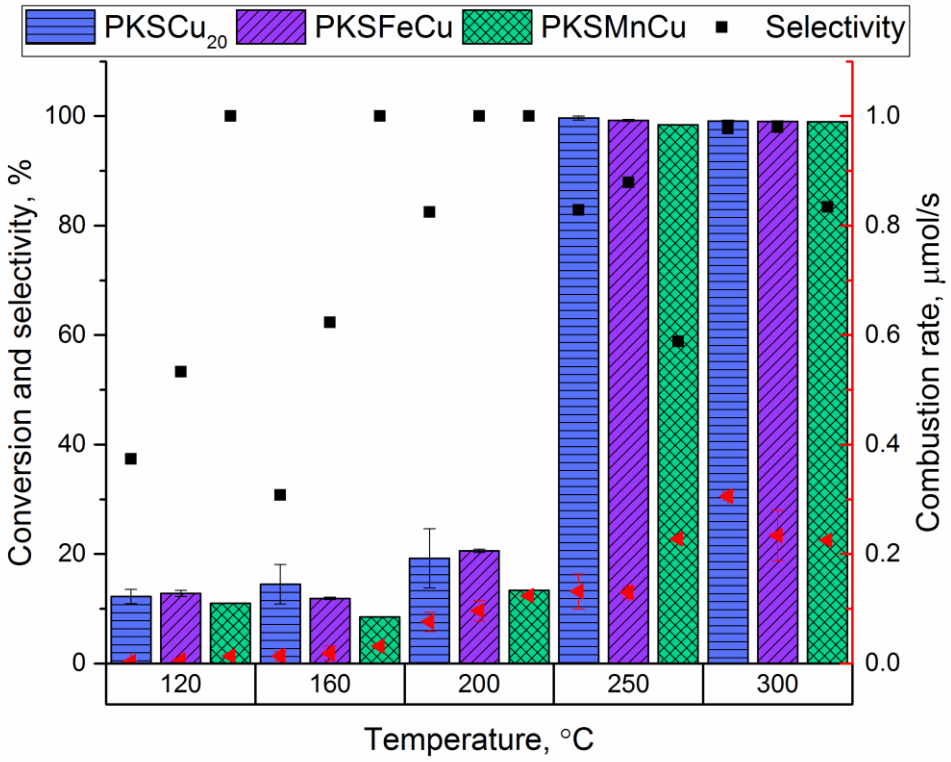

Figure 5.10: Performance of $PKSCu_{20}$ and the bimetallic oxide catalysts in 500 ppm NO + 4 % H_2 + 1.5 % O_2 at 7,175 h^{-1}.

As the conversion of PKSMnCu is low, the selectivity is 100 %, indicating less reactivity of the catalysts in H_2-NO-O_2 system at low temperature. The formation of N_2O can be seen to decrease when co-impregnating iron with copper, as compared to using copper alone. This effect can be seen in the increased selectivity of PKSFeCu at a low temperature window. At temperature higher than 200 °C, the selectivity of PKSMnCu was lower than the other two catalysts due to the undesorbed NO or products over

the catalyst surface (not shown). Slow desorption of products from the catalyst surface is undesirable, due to poisoning effects and fewer vacant sites for continuous reaction (Pârvulescu, Grange, & Delmon, 1998).

The improvement in the conversion and selectivity by the bimetallic oxide catalysts as compared to monometallic oxide catalysts can be illustrated in Figure 5.11. Note that only data at temperature lower than 250 °C were used to accommodate low-temperature H_2-SCR system and to disregard complete conversions. As can be seen from the figure, monometallic oxide catalysts suffered from low selectivity and conversion especially PKSMn and PKSCu (located to the left and bottom part). As the catalysts were co-impregnated (PKSMnCu and PKSFeCu), the selectivity and conversion moved to the top right of the figure indicating an improvement in the selectivity-conversion performance.

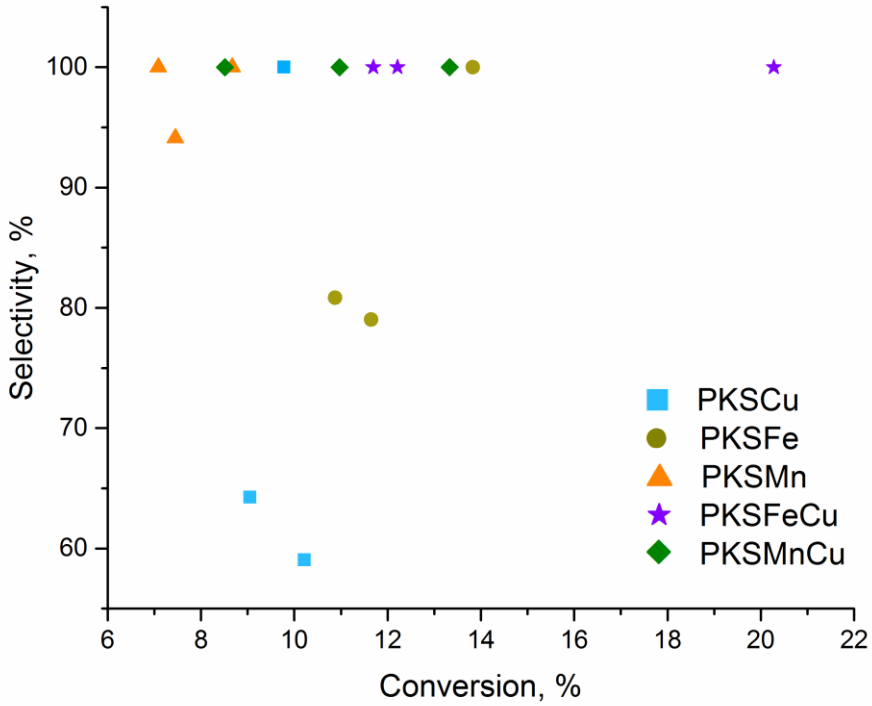

Figure 5.11: Selectivity as a function of conversion for mono- and bimetallic oxide catalysts in 500 ppm NO + 4 % H_2 + 1.5 % O_2 at 7,175 h^{-1} and 120 – 200 °C

The combustion rate of PKSMnCu is higher in most of the temperature range compared to the other two catalysts, resembling a similar effect on PKSMn. This is attributable to the high electropositivity of manganese. However, at 300 °C, the combustion rates of both bimetallic oxide catalysts are lower than $PKSCu_{20}$, showing the improvement by the co-impregnation on the stability of the catalyst in H_2-O_2-NO system. This is because under oxidizing conditions without the presence of NO, PKSMnCu would decompose more easily compared to $PKSCu_{20}$. This is shown by the DTG curve in Figure 5.12 obtained during a TG analysis of the catalysts, where the inflection point shifted to a lower temperature, indicating the maximum loss of mass at lower temperature.

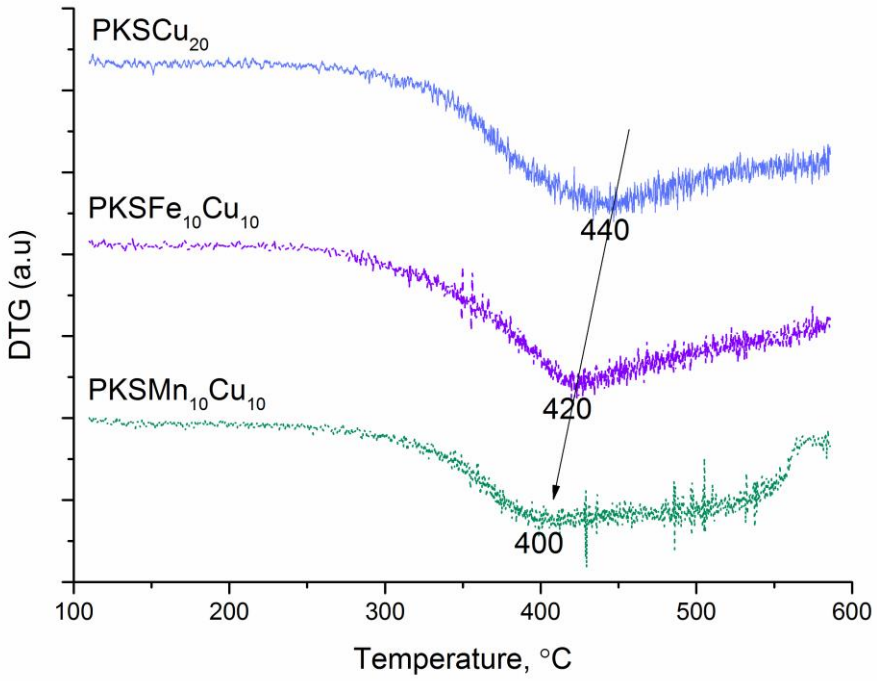

Figure 5.12: DTG curve for $PKSCu_{20}$ and the bimetallic oxide catalysts in 20 sccm pure helium and 10 °C/min.

5.3.3 Compositional effects of Fe-Cu on N_2 selectivity

Cooperation between copper and iron oxides in NO_x reduction was reported by Ma et al. (2012), who reported that bimetallic catalysts increased the NO oxidation to NO_2 as well as the adsorption of NO_2 and NH_3, which accelerated the reaction. However, the dependency of the performance of this

bimetallic oxides catalyst (Fe-Cu-O_x) supported over activated carbon in H_2-SCR on the composition of the two metals has not been reported in the literature. This sub-chapter will reveal the effects of different combination of Fe-Cu impregnation loading on the performance of the catalyst. The catalysts were prepared as per Table 5.1 but the ratio was taken based on the metal content obtained via metal loading determination experiment (explained in Section 3.5.2).

The evaluation of all of these catalysts with different Fe/Cu ratio in H_2-SCR system revealed that the conversion performance (not shown) is unaffected especially at temperature higher than 200 °C where total conversion was achieved. However, selectivity can be lowered by the production of by-product that is N_2O at low temperature and the undesorbed products from the catalyst surface at high temperature[4]. The selectivity of the catalysts can thus be seen to vary depending on the composition of iron and copper in the catalysts. Therefore, the performance of the catalysts with different Fe-to-Cu ratios is observed in terms of the selectivity towards N_2 formation as a collective term for the formation of by-products and the occurrence of undesorbed products. This is shown in the 3-D graph in Figure 5.13, taking into account the metals ratio and the temperature as the independent variables.

[4] The latter phenomenon was proven to occur by heating the used catalysts after reaction to a higher temperature in pure helium flow and measuring the desorbed species with MS as discussed in Section 4.2.3. The desorption profile for an example is included in Appendix C (Figure C.1).

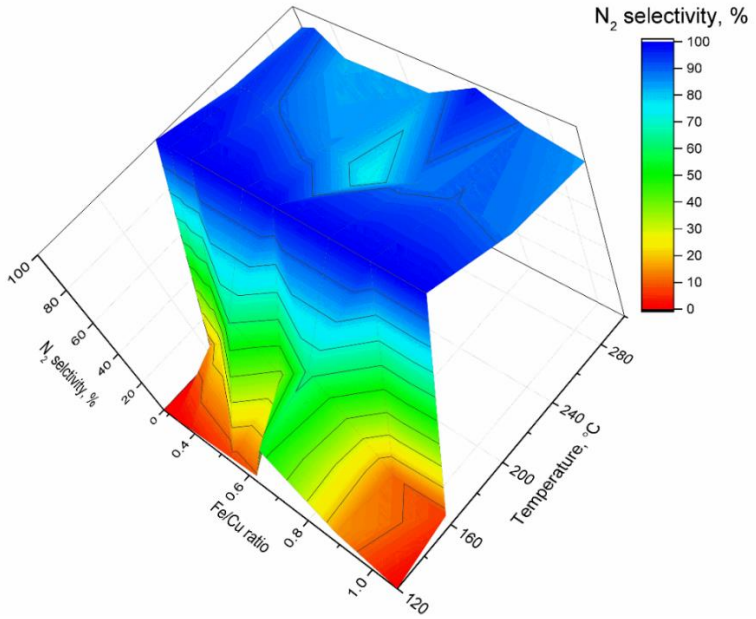

Figure 5.13: Compositional effects of Fe/Cu ratio at different temperature in in 500 ppm NO + 4 % H_2 + 1.5 % O_2 at 7,175 h^{-1}. Perspective view from the right top.

The selectivity towards N_2 formation generally increased with increasing temperature and the release of N_2O can be avoided at temperatures higher than 200 °C. There appeared to be a local minima that the selectivity falls below 80 % which is undesirable due to the poisoning effects of the undesorbed products – at metal ratio between 0.5 to 0.8 and around 240 °C. On the other hand, at temperature below 160 °C, the selectivity is low at ratio lower than 0.5 and higher than 0.8. This implicates the formation of N_2O could be avoided at low temperature with Fe/Cu ratio between 0.5 and 0.8. In H_2-SCR over Pt-based catalyst, Savva & Costa (2011) reported a decrease in N_2 selectivity with increasing Pt particle size. However, they explained that this phenomenon was not due to the geometrical effect of the catalyst on the chemisorption of reactants or intermediates, but rather the influence it has on the rate of hydrogen spillover from Pt to the active sites where adsorbed NO_x is located.

5.4 CONCLUSIONS

The effects of co-impregnating copper oxide with iron or manganese oxide over activated carbon to produce bimetallic oxide catalysts have been studied. Generally, the conversion of NO_x with hydrogen as the reducing agent was provided mostly by copper due to the low reducibility factor. Increasing copper loading increased conversion at low temperature but lowered N_2 selectivity due to the formation of N_2O. Additionally, the gasification of carbon at high copper loading was also enhanced. TPR analysis showed that increasing Cu loading increased the hydrogen consumption. At 20 wt% copper loading over PKS, NH_3-TPD shows the weak acidic sites (LTP) increased even the reduced in carboxylic acid as shown by FTIR spectroscopy confirming the contribution of the additional copper species on the acidity. However, the strong acidic sites (HTP) were reduced due to agglomeration effects at high copper loading. The agglomeration is also observable when co-impregnating Cu with Mn or Fe at the same total metal loading, which means that copper loading was half that of $PKSCu_{20}$. Nevertheless, the acidity for both weak and strong sites increased for PKSFeCu. For PKSMnCu, the acidity at LTP was decreased with an increasing HTP. The change in the magnitude at LTP is directly related to the change in the carboxylic acid, as determined via FTIR spectroscopy, and the change at HTP with the appearance of copper oxides species over PKSFeCu and PKSMnCu as shown via TPR. This also lowered the hydrogen consumption by the bimetallic oxide catalysts even though the reducibility remains unchanged. Evidently, these properties contributed to lower N_2O formation at low temperatures (increasing N_2 selectivity), especially for PKSFeCu. The carbon combustion at higher temperature was also reduced as compared to the monometallic oxide catalyst. This demonstrated the occurrence of synergistic effects between copper and iron oxides in H_2-SCR which is a significant finding of this chapter. Further examination of the effect of Fe/Cu ratio revealed that the ratio of Fe/Cu loading in the bimetallic oxides system affects the formation of N_2O and desorption rate of the products.

CHAPTER 6. Kinetics and Stability Studies of NO_x Reduction using Hydrogen over Iron-Copper Oxides Catalyst Supported over Activated Carbon

6.1 INTRODUCTION

Chapters 4 and 5 have shown the potential of using activated carbon and earth-abundant metals as catalysts to reduce NO_x, with hydrogen as the reducing agent. The kinetics and mechanism for H_2-SCR over precious metals (i.e. Pt and Pd) supported over mixed-oxides (such as $LaCoO_3$ and TiO_2-Al_2O_3) have been established in the literature (Section 2.2.3). Furthermore, Aarna & Suuberg (1997) compiled kinetic parameters available in the literature on the NO-carbon system. This includes the use of activated carbon and coconut char as the carbon catalysts (and in some cases a reactant as carbon was consumed in the reaction) in treating NO_x gases at temperatures between 200 and 900 °C. It was concluded that the reaction is generally first order, even though some have also reported values from 0.22 (Rodriguez-Mirasol et al., 1994) to 1.0 (Chan, Sarofim, & Beér, 1983) with respect to NO while the activation energy between 40 (Aarna & Suuberg, 1997) to 200 kJ/mol (Johnsson, 1994) in the low temperature regime. However, the reaction kinetics of NO-carbon with hydrogen as the reductant in oxidizing condition have not been reported. The addition of hydrogen (as reductant) and transition metals (as catalysts) could enhance the rate of NO consumption as compared to the NO-carbon system. This is because those elements would induce different mechanisms and kinetics due to the different nature of the gas-solid interactions. The presence of oxygen has also been known to affect the performance of a catalyst in H_2-SCR (Liu, Li, & Woo, 2012). Therefore, it is important to study the kinetics of these newly developed catalysts in an unconventional system. Finally, the stability of the newly developed catalyst is presented for future improvement and the consideration of applications.

6.2 MATERIALS AND METHODS

6.2.1 Catalyst preparation

Copper and iron were impregnated over PKS via the incipient wetness method described in Section 4.2.1 at 1:1 ratio and 20 wt% total loading. The catalyst is denoted as PKSFeCu.

6.2.2 Transient and kinetic studies

A transient experiment was carried out to examine the general mechanisms of the reaction over PKSFeCu. The fixed-bed reactor used is shown in Figure 3.3. Approximately 1 g of catalyst was pre-reduced under 5 % H_2/He at 250 °C for 2 h. Then, the reactor temperature was set to 200 °C prior to feeding a gas or gas mixture in helium at 7,175 h^{-1}. Each gas was introduced into the stream stepwise, while the effluent was analysed continuously using an MS (Hiden HPR-20, UK). The component quantification method was as discussed in Section 3.2.3. For the kinetic studies, the reaction was allowed to reach steady-state for at least 2 h. The effects of oxygen on the kinetics parameters were also investigated. This was performed by varying the concentration of oxygen while adjusting the hydrogen feed to keep the volumetric flow rate at STP constant that gave 7,175 h^{-1} WHSV.

6.2.3 Stability test

The catalyst was exposed to the highest reaction temperature (300 °C in this study) for approximately 36 h in 500 ppm NO + 4% H_2 + 1.5% O_2 in helium at 7,175 h^{-1} WHSV. The characteristics of the catalyst before and after the reaction are compared to observe the changes to the properties after a long reaction time. The methods and procedures used for this characterization are as explained in Sections 4.2.2 and 4.2.3.

6.3 RESULTS AND DISCUSSION

6.3.1 Transient experiment and reaction order

A transient experiment is used to determine the behavior of a system during start-up, transition state and upon shut-down (important for determining time to reach equilibrium). It also has been interpreted as indicative of the nature of the reactants-catalyst interaction and the sequence of the steps in a global reaction (O.Bennett, 1999). The isothermal temperature chosen for this

experiment was 200 °C, because at temperatures higher than this, NO might experience total conversion as the MS signal is unobservable. Meanwhile, too low of a temperature (below 100 °C) would only exhibit an adsorption process rather than the reduction by hydrogen.

Once the reaction temperature was achieved and the MS signal under helium flow was stabilized, a step input of hydrogen was initiated. This is shown in Figure 6.1a, while Figure 6.1b shows the response signal when step input of NO was started. Reaction kinetics are discussed in Section 6.3.2. Finally, oxygen was introduced stepwise and the response is shown in Figure 6.1c. The effects of oxygen concentration in H_2-SCR are discussed in Section 6.3.3.

It was observed that the hydrogen signal responded closely to the positive step change, with a slight delay of about 100 ms. This suggests that hydrogen is not readily adsorbed over the catalyst. It is therefore adequate to accept that at this level of concentration (4 %) and temperature, hydrogen adsorption is negligible.

NO, on the other hand, took longer to be detectable at the outlet, with a time of ~ 20 mins. This was due to adsorption, because no N-products such as nitrogen appeared. The NO adsorption phenomena over PKS-supported catalysts have been shown in Section 4.3.2. The occurrence of a breakthrough curve (or simply called a knee) approaching a limiting value indicates that the adsorption took place over a microporous material and the adsorption was governed by the accessible micropore volume (Thommes et al., 2015). After NO was introduced into the reactor, hydrogen was seen to decrease in concentration and quickly achieve steady-state. As there were no products besides water, the decreased hydrogen signal can be attributed to H_2 consumption via the reduction of the metal species that have been re-oxidized by NO and achieved equilibrium on the catalyst surface. Ström et al. (2018) also reported the oxidation of Ag/Al_2O_3 by NO upon analyzing the active species under diffuse reflectance UV-vis spectroscopy. The reaction was carried out in 500 ppm NO + 500 ppm NH_3 at 300 °C and 33,400 h^{-1}.

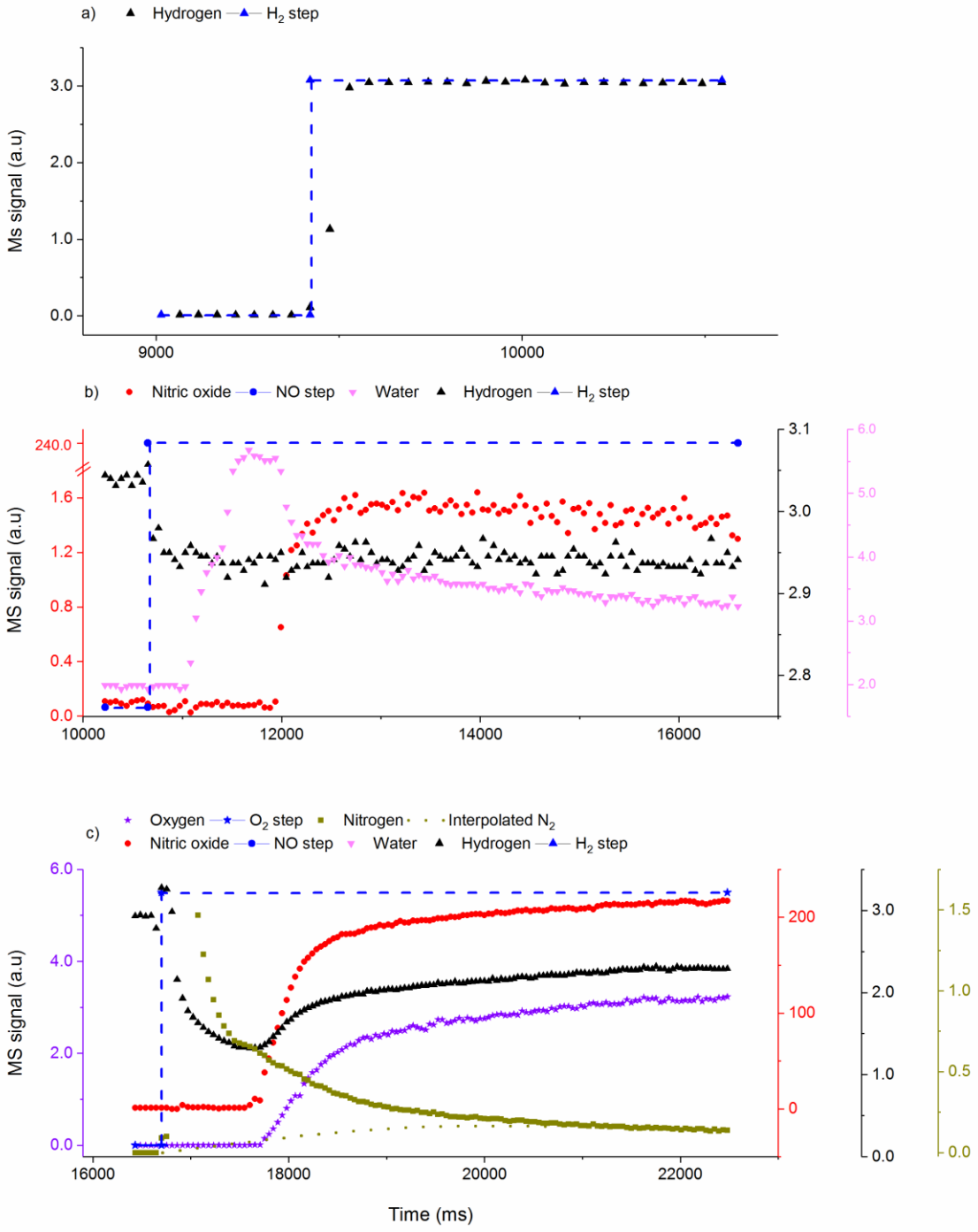

Figure 6.1: Transient response for: a) 4 % H_2 step; b) 500 ppm NO step; and c) 1.5 % O_2 step at 7,175 h^{-1} and 200 °C over PKSFeCu.

The transient response of oxygen is similar to NO with the delayed time of a few minutes earlier. There were no signs of competitive adsorption at the early stage by NO and O_2, because NO was still being adsorbed after oxygen was fed into the system. At exactly the point at which O_2 breakthrough occurred, NO can also be observed to desorb from the catalyst surface. It is well-known that O_2 oxidizes the metal surface and alters the carbon surface for NO_2 (after NO oxidation) adsorption as nitrates/nitrites (Klose & Rincón, 2007; Spivey, 1994). Therefore, this point indicates the saturation of nitrates/nitrites formation over the PKSFeCu surface. Additionally, the stretched knee on oxygen breakthrough curve indicates that physisorption occurred with a significant amount of multilayers (Thommes et al., 2015). Additionally, NO reached a new steady-state, showing that there were two types of sites – one that saturates in the first equilibrium, with the second susceptible to desorption in the presence of oxygen. Figure 6.2 illustrates the different types of adsorbed species without (a) and with (b) the presence of oxygen.

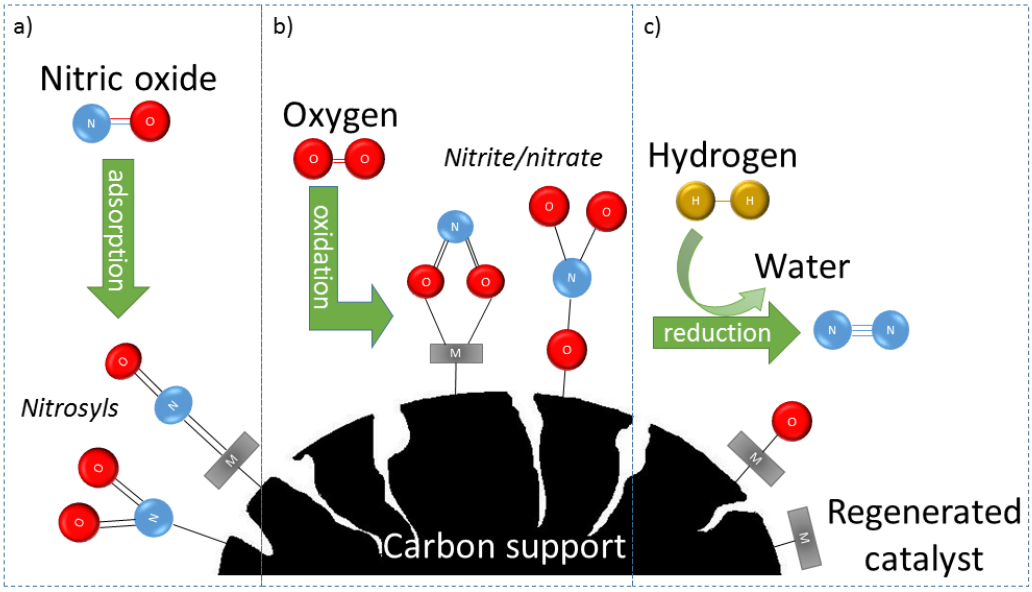

Figure 6.2: Proposed adsorbed species over PKSFeCu in: a) NO-H_2 system; and b) NO-O_2-H_2 system. c) Illustration of reduction and regeneration of metal catalysts by hydrogen.

In the meantime, H_2 experienced an instantaneous decrease in concentration upon a positive oxygen step change that created a minimum before attaining steady-state condition. The point of NO and O_2 breakthrough also saw the starting point of H_2 approaching steady-state. This means that the minimum was due to the reduction of the re-oxidized metal (water formation is not shown in Figure 6.1c) and reaction with NO to form N_2 in the presence of O_2. A sharp peak of the N_2 signal was due to the release of air trapped in the valve. Despite several attempts were made to avoid this disturbance, it persisted. The interpolated N_2 signal is shown Figure 6.1c where instantaneous formation can be observed. The formation of N_2 is known to generate oxidized metal surface as the N-species decreases and depending on the degree of reduction of H_2 at a particular reaction temperature, some regenerated metal surfaces (as depicted in Figure 6.2c) (Pârvulescu, Grange, & Delmon, 1998). This is also evident as the reaction can reach equilibrium with a decreased NO signal (as compared to the inlet signal) and formation of N_2, which signified the continuing reaction. This also suggests that only NO was required to be adsorbed on the catalyst for the reaction to occur, implying an Eley-Rideal mechanism.

The reaction between H_2 and O_2 over this catalyst could not be totally ruled out because it has been reported that the formation of water via this route is a side reaction for H_2-SCR (refer Section 2.2.3). It is therefore interesting to investigate the selectivity of hydrogen towards reacting with NO and O_2. In a separate experiment, NO was introduced after the H_2-O_2 system have reached an equilibrium (shown in Figure 6.3). With 4 % H_2 and 1.5 % O_2, almost complete consumption of oxygen can be seen at the system's equilibrium. However, upon NO injection, MS signal for oxygen can be seen to gradually increase towards its feed value (5.5). Signal for hydrogen immediately decreased upon NO injection due to an instantaneous reaction with NO (signal for NO is absent due to a complete reduction at 300 °C). This means, hydrogen is being highly selective in reacting with NO instead of O_2 over PKSFeCu.

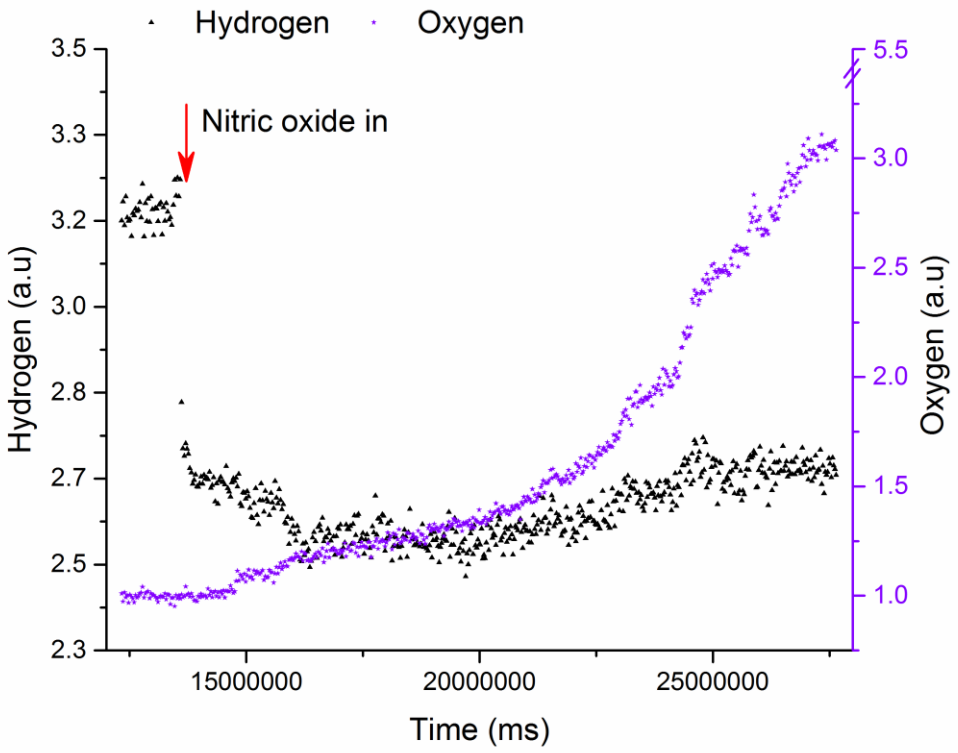

Figure 6.3: Transient response after injection of 500 ppm NO in a 4 % H_2 + 1.5 % O_2 system at at 7,175 h^{-1} and 300 °C over PKSFeCu.

6.3.2 Kinetics of NO reduction using hydrogen over PKSFeCu

Based on the transient experiment, the heterogeneous rate equation per unit volume for NO consumption can be written as in equation 6.1 where NO concentration, *[NO]* being the only limiting factor with an order of α and *k'* as the apparent rate constant (cm^3/g.s). The reaction rate can be experimentally quantified with equation 6.2 at a steady-state reaction condition where; X_{NO} is NO conversion; F_{NO} is flow rate (L/s); m_{cat} is catalyst mass (g); and taking 24.5 L/mol as molar volume at STP. This allows the determination of the reaction order by varying the inlet NO concentration while keeping hydrogen at excess (Murzin et al., 2005b).

$$r_{NO}(mol/cm^3.g.s) = -\frac{1}{m_{cat}}\frac{dn_{NO}}{dt} = k'[NO]^{\alpha} \qquad 6.1$$

$$Reaction\ rate, r_{obs}\ (mol/g.s) = \frac{X_{NO} \times F_{NO}}{m \times 24.5} \qquad 6.2$$

By evaluating the reaction rates from 200 to 1200 ppm NO, the plot in Figure 6.4a was obtained. This is a typical intermediate Langmuir plot (between first-order and zero-order) where a reactant is adsorbed on the catalyst surface during reaction (House, 1997). Linearization of this curve gives Figure 6.4b in which the order of reaction, α can be found from the slope. The value of 0.82 is well within the range of NO order of reaction (from 0.22 to 1.0) over activated carbon and biochars reported by Aarna & Suuberg (1997). However, all of the reactions were achieved at least at 400 °C without the presence of reducing gas, while the temperature used in this H_2-SCR study was 200 °C. Most of the reaction orders in H_2-SCR were reported to be first order over commercial vanadia-based catalysts (Yang et al., 2013), but Costa et al. (2007) also reported a negative order (-0.97) over Pt/MgO-CeO_2 catalyst at 140 °C indicating the poisoning effect of NO. In NH_3-SCR, Tufano & Turco (1993) reported a decreasing order of reaction (with respect to NO) with decreasing temperatures. Using V_2O_5/TiO_2, the reaction order was first order at 300 °C and 0.85 at 200 °C.

The y-intercept from Figure 6.4b gives the apparent reaction constant, k' of about 0.027 $cm^3/g.s$, which is very slow compared to the industrial catalysts in NH_3-SCR. The linearized reaction rate plot also gave an order of 0.82, but a slightly lower rate constant (0.023 $cm^3/g.s$) at reaction temperature of 170 °C (plots are not shown). This suggests the applicability of the power rate law to the temperature range of the study (House, 1997).

Considering the contribution of the reactant adsorption, the rate of reaction can be written as in equation 6.3, where *f* is the fraction of the surface covered by the adsorbed reactants, as given by equation 6.4 for the Langmuir isotherm. The adsorption constant K can be estimated by numerical methods upon plotting reaction rates against reactant partial pressure (House, 1997).

$$r_{NO} = k_{NO} f_{NO} \qquad 6.3$$

$$f_{NO} = \frac{K_{NO} p_{NO}}{1 + K_{NO} p_{NO}} \qquad 6.4$$

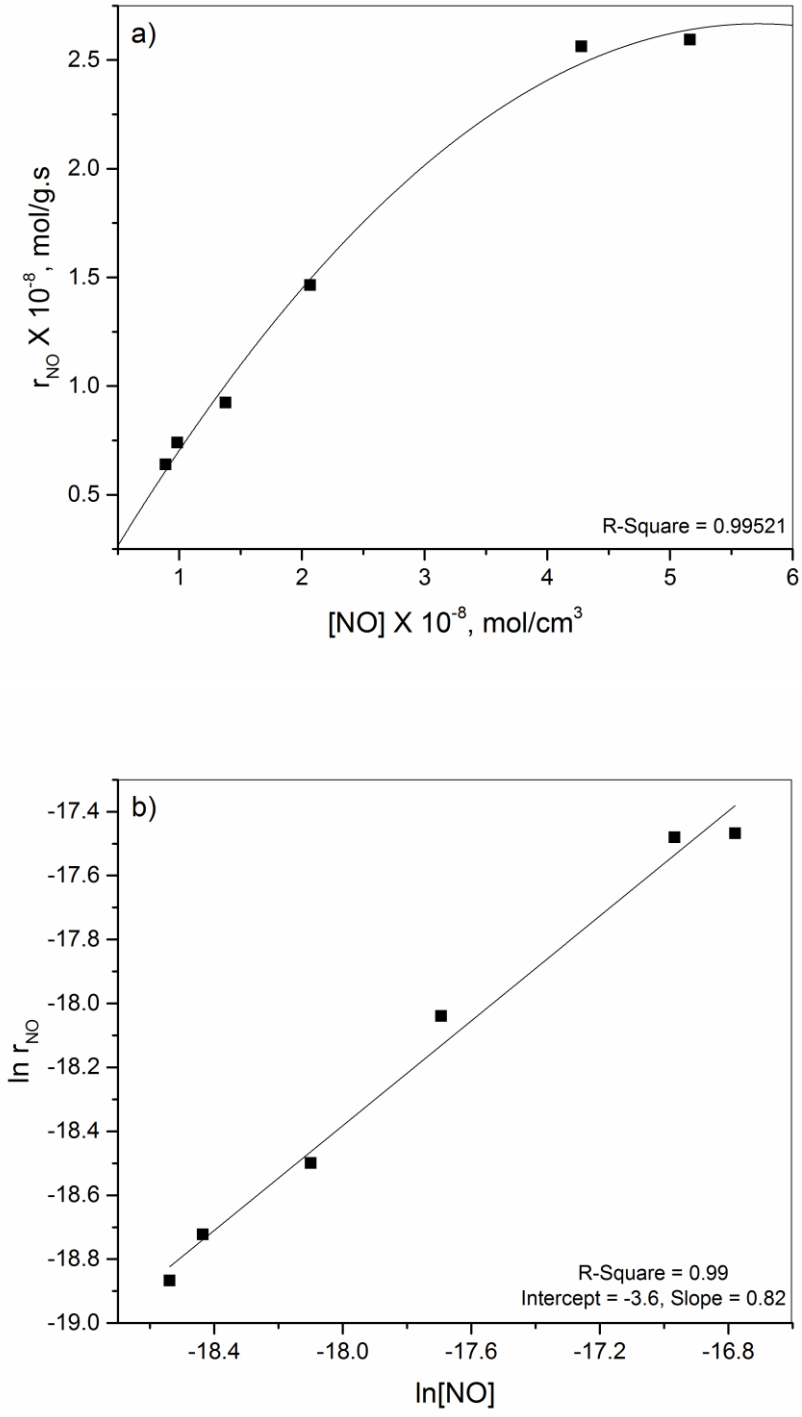

Figure 6.4: Determination of reaction order via initial concentration method from 200 to 1200 ppm NO in 4 % H_2 + 1.5 % O_2 at 7,175 h^{-1} and 200 °C over PKSFeCu. a) Reaction rate plot against concentration and b) linearized plot. (■) experimental data and (–) fitted curve.

Substituting equation 6.4 into 6.3 gives equation 6.5, which resembles that of Michaelis-Menten. This allows the determination of the kinetics parameters via Lineweaver-Burk plot shown in Figure 6.5. Note that the unit for k_{NO} is mol/g.s instead of cm^3/g.s (as in k'), indicating that the adsorption attribute is now embedded into the equilibrium constant, K_{NO} (Pa^{-1}) (Koebel & Elsener, 1998). As NO pressure approaches zero, the term $K_{NO}p_{NO} << 1$ can be neglected but the approximation would overestimate the reaction rate by 10 % due to non-unity reaction order. However, this parameter is useful in determining the heat of adsorption by plotting K_{NO} in a linearized plot against temperature (not shown):

$$r_{NO} = k_{NO}\frac{K_{NO}p_{NO}}{1 + K_{NO}p_{NO}} \qquad 6.5$$

When evaluated between 170 and 200 °C, the estimated heat of adsorption was -240 kJ/mol. This is highly exothermic chemisorption compared to the reported values for NO adsorption over other types of catalysts such as -51 kJ/mol for molecular sieve 13 X in 250 – 400 °C (Rezaei et al., 2015), -63 kJ/mol for Pt-Mo-Co/α-Al_2O_3 in 140 – 160 °C (Frank, Emig, & Renken, 1998) and -21 kJ/mol for commercial catalyst in 225 – 250 °C (Koebel & Elsener, 1998). The known ΔH_{ads} for NO adsorption over iron oxide and copper oxide are -21 kJ/mol (Otto & Shelef, 1970) and -10 kJ/mol (Gandhi & Shelef, 1973), correspondingly. The increased heat of adsorption in this study indicates that enhanced adsorption energy is supplied by the bimetallic oxides catalyst.

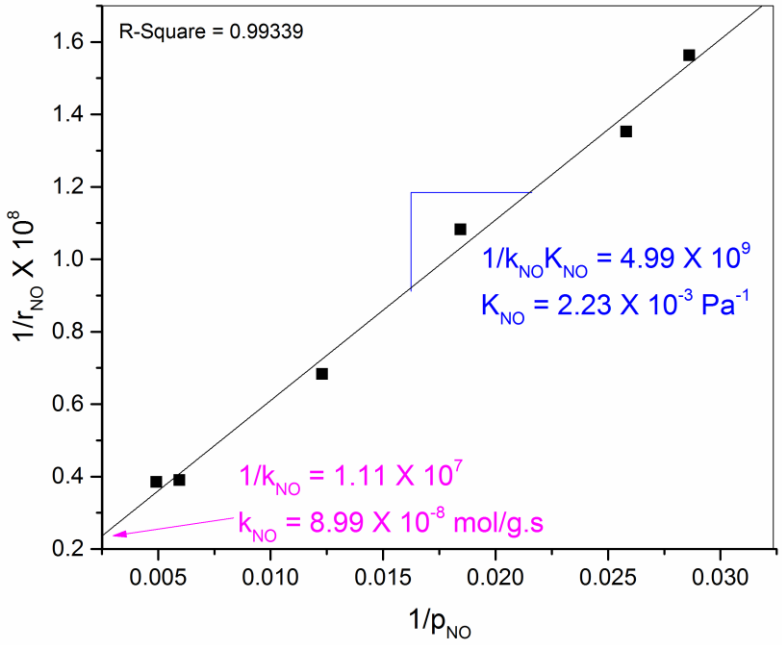

Figure 6.5: Lineweaver-Burk plot for equation 6.5 determining kinetic parameters of H_2-SCR over PKSFeCu from 30 to 200 Pa NO in 4 % H_2 + 1.5 % O_2 at 7,175 h^{-1} and 200 °C. (■) experimental data and (–) fitted curve.

The activation energy, E_a can be determined from an Arrhenius plot of rate constants against temperature (see equation 6.6). At this stage, the temperature ranged from 110 to 215 °C, in which the conversion of NO is at least 10 % but less than 20%. Lower conversions at low temperature would only imply the adsorption of NO instead of conversion, as observed in previous studies (refer Section 4.3.4). Conversely, at higher conversion, the heat of reaction resulting from the high amount of NO converted would underestimate the activation energy. This limits the evaluation of the rate equation over the reaction temperature studied. Figure 6.6 shows the Arrhenius plots at 250, 500 and1000 ppm NO.

$$k = A_0 e^{-E_a/RT} \qquad 6.6$$

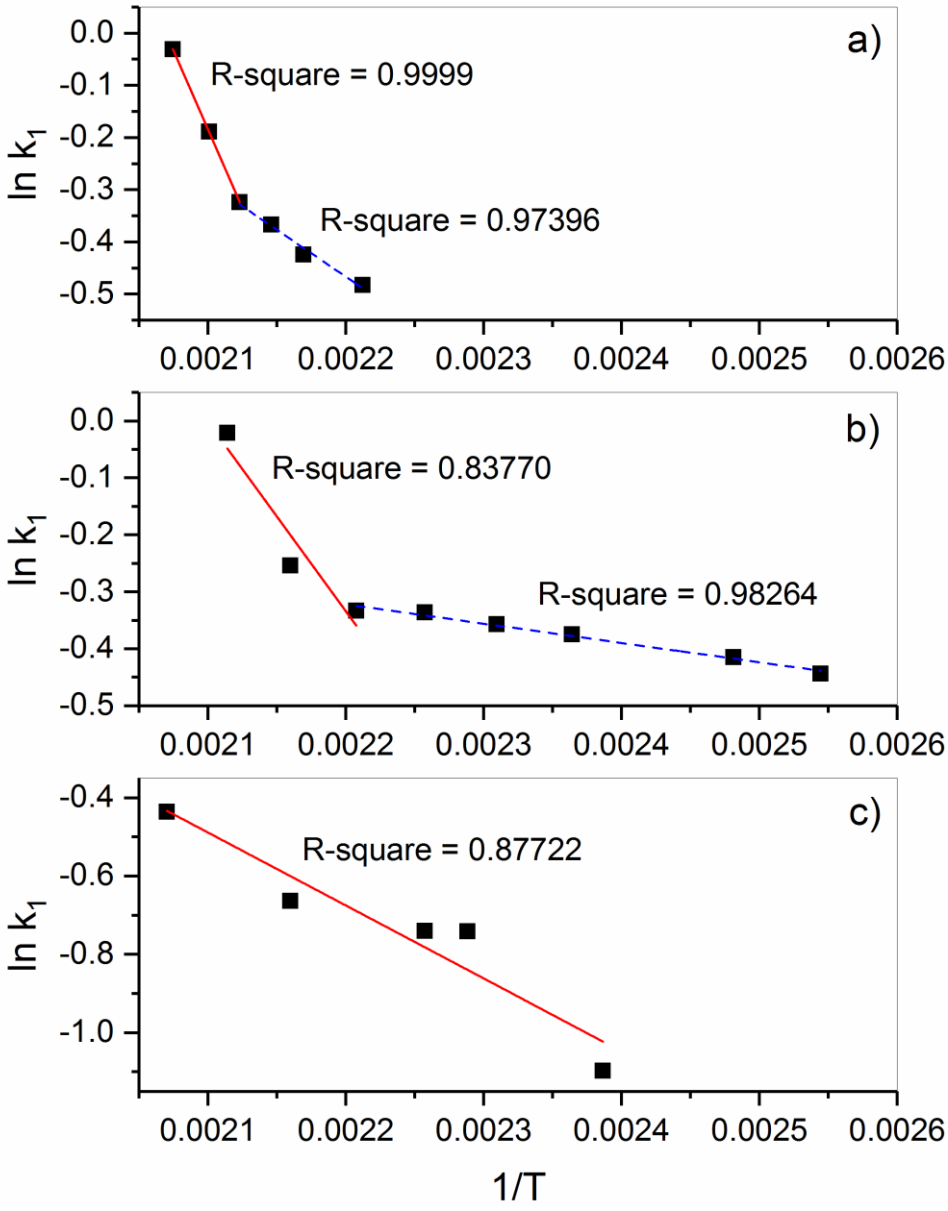

Figure 6.6: Arrhenius plots at: a) 250 ppm NO; b) 500 ppm NO; and c) 1000 ppm NO in 4 % H_2 + 1.5 % O_2 from 110 to 215 °C at 7,175 h^{-1} over PKSFeCu. (■) experimental data, (–) fitted curve for the first region and (– –) fitted curve for the second region.

It is evident that two regions of linear Arrhenius plots exist over the carbon catalyst below 1000 ppm. This break in the Arrhenius plot is commonly reported in the literature, as reviewed by Aarna & Suuberg (1997), for the reaction of NO with carbons. The temperature at which this splitting occurred was calculated by solving simultaneous equations between the two regions. It can be seen that the temperature shifted to a lower temperature when increasing the NO concentration (from 200 °C at 250 ppm NO to 180 °C at 500 ppm). This effect seemed to disappear at higher NO coverage when the activation energy was low. The kinetic parameters from the Arrhenius plots are summarized in Table 6.1.

Table 6.1: Summary of kinetic parameters form Arrhenius plots in Figure 6.6.

Parameter	250 ppm NO	500 ppm NO	1000 ppm NO
Region 1			
A_0 (cm^3/g.s)	3 X 10^5	1080	30
E_a (kJ/mol)	50	30	15
Region 2			
A_0 (cm^3/g.s)	33	1.5	N/A*
E_a (kJ/mol)	15	3	

*Not available.

All of the kinetic parameter values decreased with increasing NO concentration. At 250 ppm, the reaction is active (based on the pre-exponential factor), but the activation energy is higher, which was the reason for the very low and absence of conversion below 175 °C. The decrease in A as the concentration increased to 1000 ppm, or as the reaction temperature decreased to lower temperature (region 2), indicates that the reaction was easily achieved at low temperature, but at a perceptible rate, whereas a higher energy barrier needs to be overcome at higher temperature with higher activity.

6.3.3 Influence of oxygen concentration

The transient experiment has shown that oxygen was also adsorbed over the catalyst surface and was involved in desorption of NO, which allowed the conversion to N_2 to increase. Therefore, it is important to study the

influence of oxygen concentration on the reaction. This was denoted as the ratio of hydrogen volume as a reductant to that of oxygen as an oxidant. Figure 6.7 shows the performance of PKSFeCu at different H_2:O_2 ratios.

The conversion of the reaction in the absence of oxygen can be seen to always be very high (~ 100 %). However, the formation of nitrogen was only observed over a narrow temperature window (100-150 °C). This has also been shown via the transient experiment in Section 6.3.1 which was performed at 200 °C. Furthermore, the temperature at which NO conversion exceeded 20 % was about 200 °C for 1:1 H_2-to-O_2 ratio, and higher (above 250 °C) for higher oxygen concentrations. In addition, the reaction in which the highest O_2 concentration was used (4.5 % O_2 in the 1:2 H_2-to-O_2 ratio) did not experience total conversion over the temperature range studied. This is proposed to be due to the fact that at this concentration, metal oxidation is faster than metal reduction. Similar findings were reported by Lindholm, Sjövall, & Olsson (2010), who compared the performance of a hydrogen-deficit system (2000 ppm H_2 + 8 % O_2) and hydrogen-rich system (16000 ppm H_2 + 8 % O_2); the former was reported to unable to regenerate the Pt/Ba/Al catalyst at 200 °C.

However, N_2 selectivity at high oxygen concentration increased with temperature, and no formation of NO_2 or N_2O was detected. This may be due to the low reactivity resulting from the low NH intermediate formed during the reaction as also has been pointed out by Lindholm, Sjövall, & Olsson (2010). The low selectivity in the reaction at lower oxygen concentration was accompanied by the formation of N_2O which was also observable at low temperature. This showed that the formation of N_2O not only is preferable at low temperature but also in oxygen-poor condition. Väliheikki et al. (2014) also reported the reduced formation of N_2O in a high O_2 content (up to 10 %) in H_2-SCR over W/CeZr catalyst.

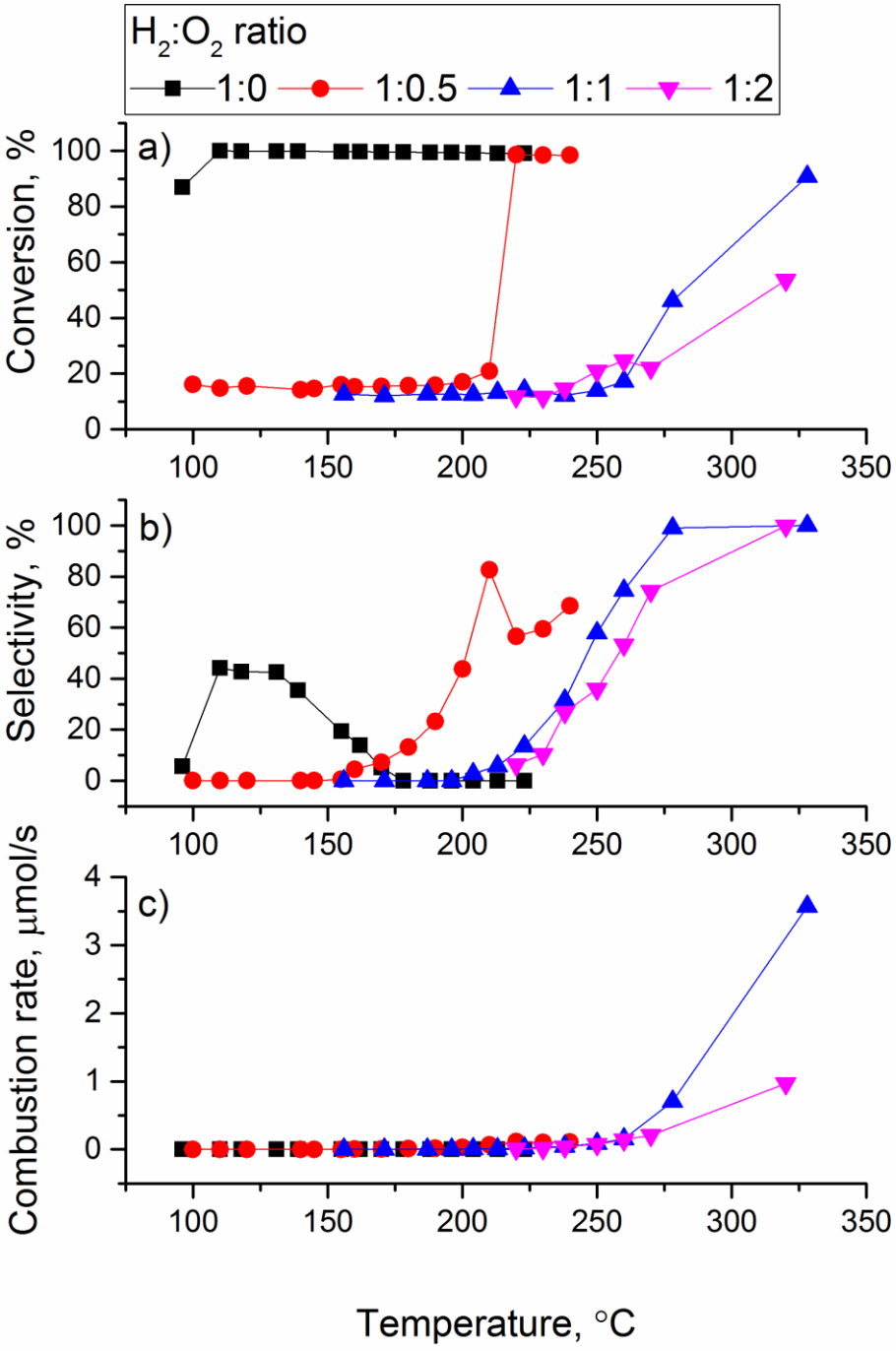

Figure 6.7: Influence of H_2:O_2 ratio in H_2-SCR of 500 ppm NO at 7,175 h^{-1} with PKSFeCu. a) NO conversion, b) N_2 selectivity and c) combustion rate.

There was no combustion observed for the reaction in the absence of oxygen over all temperature range studied even during the formation of N_2, showing that the reduction to N_2 was solely that of H_2-NO reactivity over PKSFeCu. This differs from the conventional reactions using NH_3 as a

reductant (Shi et al., 2017) or decomposition at high temperatures (Singoredjo et al., 1990) involving the carbon molecule in the reduction mechanism. Therefore, using hydrogen as a reductant in a non-oxidizing SCR makes it preferable that the carbon mass be conserved while NO is reduced at low temperature. Meanwhile, the combustion rate in the reaction with equimolar H_2 and O_2 showed more dramatic increase at higher temperature compared to the reaction with the highest O_2 concentration. This may indicate that the 1:1 H_2:O_2 ratio is the optimum gasification condition in H_2-SCR over PKSFeCu, resembling the effect of oxidant enrichment in industrial carbon gasification.

The Arrhenius plots for the different H_2:O_2 ratios are shown in Figure 6.8. Note that there is no plot for the reaction without oxygen due to the very high NO conversion over all temperature range investigated in this project. The plot for 1:0.5 can be found in Figure 6.6b. The dissecting temperature for the plots in the reaction with 1:1 H_2:O_2 ratio was 220 °C which is higher than when using 1:0.5 ratio. This temperature could not be obtained at higher oxygen concentration because of the absence of conversion at temperature lower than 220 °C. Aarna & Suuberg (1997) determine that E_a is high beyond this temperature; typically, gasification occurs in this high-temperature region (no general value for this threshold). From this experiment, the phenomenon of disappearance of this temperature appears highly dependent on the levels of O_2 and NO; doubling NO concentrations reduced the temperature by 20 °C, while doubling oxygen concentrations increased the temperature by 40 °C. However, further increasing the O_2 concentration to a 1:2 ratio with respect to H_2 and higher NO concentration removed this effect.

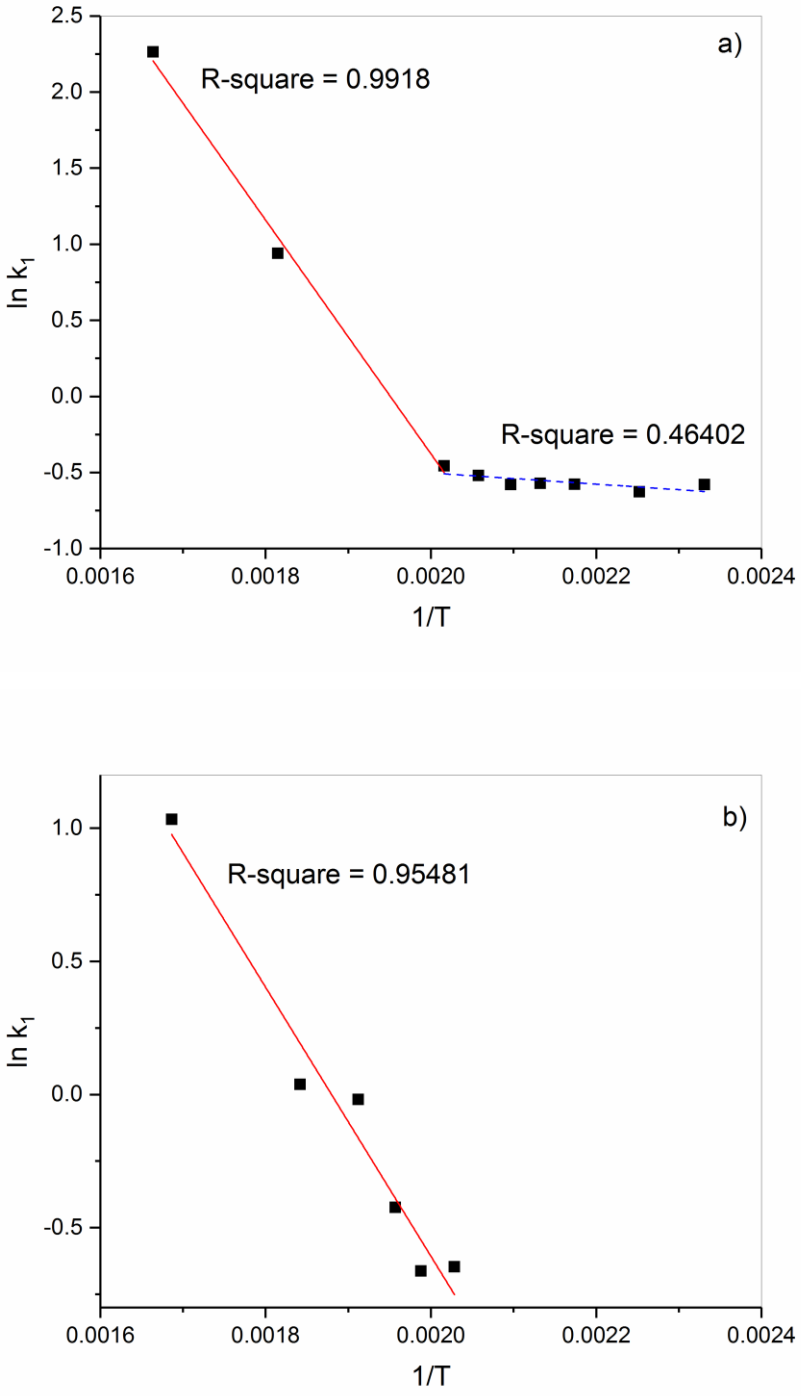

Figure 6.8: Arrhenius plots for: a) 1:1 ; and b) 1:2 H_2-to-O_2 ratio of 500 ppm NO at 7,175 h^{-1} with PKSFeCu. (■) experimental data, (–) fitted curve for the first region and (– –) fitted curve for the second region.

The activation energy for the first region in Figure 6.8 is about 64 kJ/mol and 42 kJ/mol for reactions with 1:1 and 1:2 ratios, respectively. The pre-exponential factor was also larger (3.2 X 10^6 versus 1.3 X 10^4 cm^3/g.s) with a 1:1 ratio in the reaction condition, showing the higher activity in H_2-SCR. This is why the catalyst in this condition surpassed the reaction with higher O_2 content in terms of conversion and selectivity especially at higher temperature (above 220 °C). However, gasification in this condition also increased (see Figure 6.8c), creating a trade-off to stability when using this catalyst under these conditions. Further analysis was performed to determine the stability factor.

6.3.4 Stability of PKSFeCu over extended reaction period

It has been shown that the condition used in Chapter 4 and 5 is an intermediate case with high NO conversion and N_2 selectivity, and considerably low carbon combustion. However, the performance of the catalyst (PKSFeCu) could vary with a longer reaction period. Stability in this case refers to both the long-time performance and the catalyst structure against the oxidizing condition. The duration of a stability test varied from 5 h (Yoshinari et al., 2003) to 167 h (Shen, Ge, & Chen, 2016), but a more practical approach would include a disturbance in the gas composition during this period, which is lacking in the literature. This disturbance mimics the fluctuation of oxygen concentration in flue gas (Liu et al., 2010). Figure 6.9 shows the conversion, selectivity and by-products formation over PKSFeCu in a selected H_2-SCR condition. The highest temperature in the study was used (300 °C) to accelerate the effects of carbon combustion. It can be seen that the first 2 – 3 h demonstrated that a nearly ideal steady-state was reached, implicating the duration used to obtain data of studies in Chapter 4, 5 and 6 (except this section). Thus, N_2 selectivity can be seen to decrease by 10 % from the 4^{th} to 10^{th} hour, with NO conversion remained total. By reducing O_2 concentration gradually at 1 %/s at the 10^{th} hour (a), the conversion and CO_2 production exhibited reductions of 10 and 80 %, respectively. The selectivity showed high disturbance due to the complex formation of by-products such as NO_2 (with a peak from 10^{th} to 20^{th} hour). Feeding in O_2 at the 10^{th} hour at 100 %/s (b) brought the conversion back to around 100 %, but the selectivity

and carbon combustion remained low, though some increased in N_2 selectivity can be seen at about the 33rd hour.

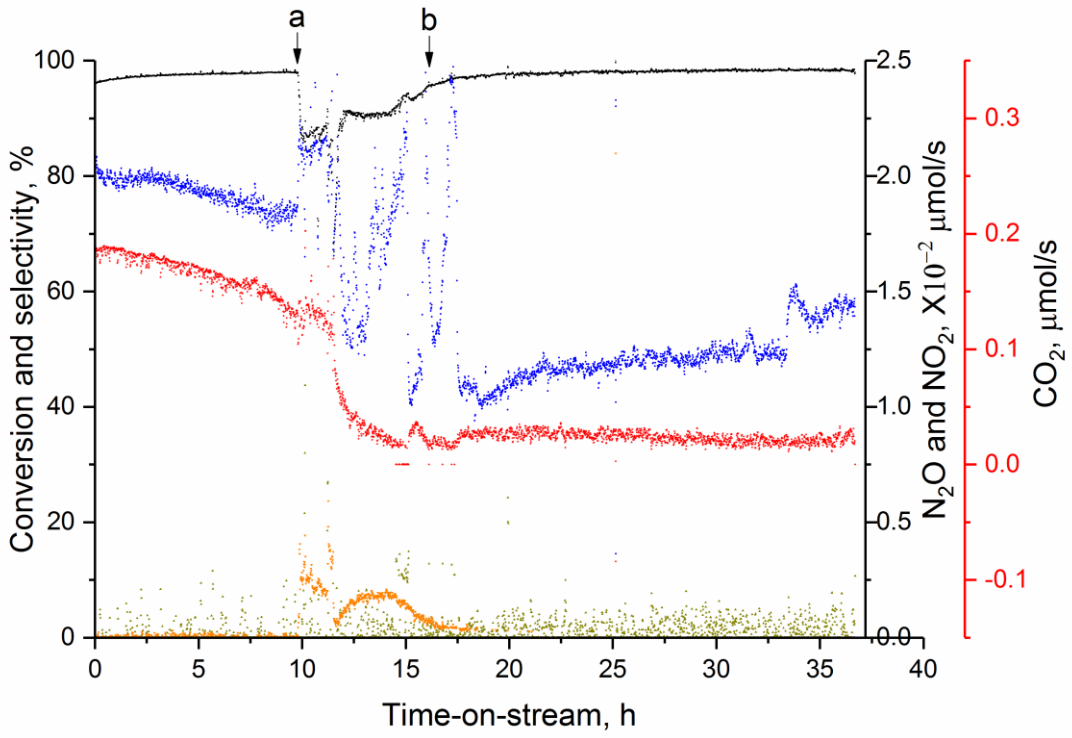

Figure 6.9: Performance of PKSFeCu in 500 ppm NO + 4 % H_2 + 1.5 % O_2 at 300 °C and 7,175 h^{-1}. a) Gradual decrease of O_2 concentration at 1 %/s and b) Step increase of O_2 concentration.

The physical properties were reported to be changed throughout the reaction period, which would also affect the chemical properties. Wang et al. (2015) studied the stability of copper-coupled catalysts supported over CeO_2 for 20 h and found significant changes in physical properties, including surface composition. Therefore, comparisons of the physical properties before and after the reaction are summarized in Table 6.2. The carbon burn-off was 70 % where the loss was contributed mostly by carbon and oxygen. The ash percentage content increased due the adjustment of the composition with the lowered carbon and oxygen portions. However, the mass of copper and iron loaded was conserved. The parameters in the surface properties can also be seen to reduce by 50 % except for the external surface area and average pore

size width that were greatly enlarged. These changes can be attributed to the pro-longed effect of exposure at 300 °C.

Table 6.2: Comparison of the physical properties for PKSFeCu before and after 36 h reaction in 500 ppm NO + 4 % H_2 + 1.5 % O_2 at 300 °C and 7,175 h^{-1}.

Properties (unit)	Fresh PKSFeCu	Used PKSFeCu
Mass in reactor (g)	1.0	0.30
Elemental analysis (%)		
C	48	32
H	0.46	1.38
N	0.53	0.29
O	29.94	6.53
Ash content	20.6	59.56
Metal content (%)		
Cu	7.0	25.7
Fe	5.7	18.6
Surface properties		
BET surface area (m^2/g)	767	443
t-plot micropore area (m^2/g)	763	397
t-plot external surface area (m^2/g)	4	46
t-plot micropore volume (cm^3/g)	0.379	0.197
BJH adsorption average pore width (Å)	3	4

6.4 CONCLUSIONS

A transient experiment was performed prior to kinetic experiment analysis to evaluate the general mechanism of H_2-SCR over PKSFeCu. Apparently, the reaction obeys Eley-Rideal mechanism; only NO was adsorbed over the catalyst surface while H_2 reacted in the gaseous phase. NO showed strong adsorption with two distinguishable sites: one over the microporous surface and another over the metal oxide or the external surface. The latter is prone to formation of nitrites/nitrates species in the presence of O_2. Oxygen adsorption was weaker (physisorption) in which upon contacting with metals oxidizes the surfaces. Hydrogen played two roles – reducing nitrates/nitrates species into N_2, and regenerating oxidized metal surfaces for continuing bonding with O_2 and NO. Kinetic experiments revealed that a power rate law is adequate in expressing the reaction rate that has the order of 0.82. A Langmuir isotherm was also adequate in expressing the adsorption coverage fraction, revealing that the nature of NO adsorption was that of chemisorption (-240 kJ/mol). The dependency of the rate constants on temperature was also examined via Arrhenius plots. It was shown that a break

in Arrhenius plots separates the low and the high temperature regime. At low temperature, the activation energy is as high as 50 kJ/mol, but this decreases with increasing NO concentration. Similarly, in the high temperature region, E_a decreased to a point that it disappeared (at 1000 ppm NO). Furthermore, high O_2 content reduced gasification (based on 1:1 H_2:O_2 ratio), but a lack of oxygen induced the formation of N_2O, especially at low temperatures. The stability test for PKSFeCu under oxidizing conditions showed that the physical properties changed after 36 h in H_2-SCR operation. The disturbance in the oxygen content in the feed lowered the selectivity and carbon combustion. It has been proven that this happened due to changes in physical properties, and the carbon burn-off was about 70 %. This means that this catalyst has yet to be industrially ready. Further development should be made in terms of the stability of the catalyst.

CHAPTER 7. GENERAL CONCLUSIONS AND FUTURE WORK

7.1 General Conclusions

This study aims to explore an SCR system using hydrogen as a renewable reductant, a sustainable catalyst support (activated carbon developed from biomass waste), and earth-abundant and less precious metals (copper, iron and manganese) as catalysts. The NO conversion, selectivity towards nitrogen formation and carbon combustion in the system were investigated. The catalysts were also characterised in terms of the elemental composition, surface area and porosity, acidity, surface functional groups, redox properties and NO adsorption-desorption behavior.

Two types of catalyst design have been synthesized and investigated in H_2-SCR – mono- and bimetallic oxide catalysts supported onto activated carbon (developed from palm kernel shell). For monometallic catalysts, copper, iron and manganese were impregnated (via incipient wetness method) over carbon at 10 wt% metal loading and calcined at 350, 510 and 540 °C for copper, iron and manganese, respectively, giving catalysts denoted as PKSCu, PKSFe and PKSMn. In 500 ppm NO + 4 % H_2 + 1.5 % O_2 and helium as balance flow of 7,175 h^{-1}, PKSCu showed the highest NO conversion (100 % above 250 °C). However, the catalysts were not able to achieve 20 % conversion at temperatures lower than 250 °C. Increasing copper content to 20 wt% improved the NO conversion at low temperature (25 % at 200 °C). However, selectivity towards N_2 formation decreased due to the formation of N_2O. Carbon combustion was enhanced at high copper loading. Co-impregnating of copper and either iron or manganese (PKSFeCu and PKSMnCu) at 20 wt% total metal loading and a 1:1 mass ratio was seen to eliminate this effect. PKSFeCu showed better performance in a wide temperature window, with high N_2 selectivity (80 to 100 % over 120 to 300 °C) and low carbon combustion (0.2 µmol/s at 300 °C). The low selectivity at low temperature was attributed to the formation of N_2O, while at high temperature this was caused by the undesorbed NO and reaction products. To understand the factors governing these performances, the catalysts were physico-chemically characterized.

The extent of NO conversion was found to be correlated with the reducibility of the catalysts. This was measured using the hydrogen-temperature programmed reduction (TPR); PKSCu showed the lowest reduction temperature. High reducibility means that the metal species over the catalyst surface are easily regenerated for the continuing conversion of NO. Increasing the copper content and co-impregnation with iron or manganese do not change the reducibility factor. Additionally, TPR revealed the types of metal species present on the catalyst surface that contributed to the hydrogen consumption. It was evident that Cu, Cu_2O and CuO existed on PKSCu, Fe_2O_3 over PKSFe, and MnO_2 and Mn_2O_3 over PKSMn. Higher copper content and bimetallic oxide catalysts showed an agglomeration effect. This lowered the hydrogen consumption but the conversion was improved, which means there is another factor that is governing the conversion and selectivity.

Acidity of the catalysts is known to provide adsorption sites for the NH as an intermediate in H_2-SCR. It was determined via ammonia-temperature-programmed desorption (NH_3-TPD), in which high ammonia desorption is correlated to high acidic sites. Doubling the copper concentration increased the NH_3 desorption at low-temperature region (LTP) while decreasing the high-temperature peak (HTP); PKSMnCu showed the opposite effect. Conversely, PKSFeCu showed an increase in desorption at both regions. This is highly related to the change in ammonia desorption intensity where the LTP affects the selectivity at high temperature while HTP affects the selectivity in a low temperature reaction. By corroborating NH_3-TPD with FTIR spectroscopy data, it is evident that LTP was contributed to by the carbon support functional groups and the interaction with copper. Therefore, this property is proposed to be responsible for the desorption of N-containing products, as the low selectivity at high temperatures was due to the undesorbed products (including NO). These structure-performance relationships may indicate the synergistic effects of the bimetallic oxide system. Further investigation into the effects of metal ratio on PKSFeCu has shown that the formation of N_2O and desorption of N-products are rather complex depending both on temperature and Fe-Cu loading ratio over PKS. Ratio between 0.5 and 0.8 reduced the formation of N_2O at low temperatures (below 160 °C), while abstaining the desorption of N-

products at high temperatures. At this point, PKSFeCu has shown promising performance. Its applicability has thus been evaluated.

The kinetic experiments revealed that the rate of reactions for H_2-SCR over PKSFeCu is in the order of 0.82 with respect to NO concentration. Only NO was required to be adsorbed while H_2 reacts in gaseous phase, suggesting an Eley-Rideal mechanism. The heat of adsorption was ~ -240 kJ/mol which is the most exothermic among the values ever reported in the literature indicating the high chemisorption bonding energy with PKSFeCu. This is beneficial when a system is able to regenerate the catalyst, but becomes a drawback when NO poisons the active sites against the further conversion and formation of N_2. Additionally, the effects of temperature, NO concentration and oxygen content were studied via Arrhenius plots. It was shown that the activation energy is high at low temperatures and decreases with increasing NO concentration. Increasing oxygen content (H_2:O_2 ratio of 1:1 and 1:2) increased the activation energy with 1:1 ratio having the highest (E_a = 64 kJ/mol). The increase in activation energy lead to an increase in the temperature window as indicated by the break in Arrhenius plots.

The combustion of the catalyst under reaction conditions has also been evaluated. Thermogravimetric analysis (DTG) revealed the offset temperature of PKSMn to have the lowest offset temperature and inflection point, indicating its highly combustible character. This is most likely due to the high electropositivity of manganese making it a challenging metal to apply with a carbon support. The combustion rate in terms of CO_2 production was also measured, taking into account the effect of oxidation by NO_x. Increasing the copper content increased CO_2 production, but co-impregnating the copper with iron reduced this shortcoming. Additionally, the stability test was also performed on PKSFeCu at 300 °C in 500 ppm NO + 4 % H_2 + 1.5 % O_2 at 7,175 h^{-1} for 36 h. The disturbance in the oxygen content for about 5 h lowered the selectivity by ~ 20 %. This is due to change in the physical properties (such as reduced in carbon and oxygen content, BET surface area, micropore area and volume). This indicates that further improvement on the stability of the catalyst in oxidizing condition is required prior to application in industry.

In conclusion, an H_2-SCR with carbon-supported Fe-Cu catalyst is able to reduce NO under oxidizing conditions with promising performance. However, future work is urgently needed to develop a durable catalyst from sustainable resources to attract industrial interest in adapting such a system.

7.2 Future Work

7.2.1 Methods

It was proven that the catalyst crystallinity is an important factor. Therefore, the synthesis of the catalyst should be able to grow crystals of desired size over carbon surface. For instance, Gong et al. (2015) demonstrated that atomic layer deposition method can be applied to activated carbon with the presence of various functional groups in order to specifically grow a controlled size of Pd nanoparticles over the carbon surface. This method involves flowing the catalyst precursors in vapor form over the catalyst surface.

The detailed mechanism in the NO-H_2-O_2 system over platinum-based catalysts can be investigated using a steady-state transient kinetic analysis (SSTIKA). In the experiment, the molecule sources are switched using its different stable isotopes, for instance from ^{14}NO to ^{15}NO, after an initial steady-state was reached. This reveals the knowledge on which N atoms (adsorbed or gaseous) reacts together to form N_2. The dominant route of N_2 formation is known to be formed by two different N species, which is called the “impact” route. Burch, Shestov and Sullivan (1999) utilized this method and reported that about 85 % of the N_2 generated over a 5 wt.% Pt/SiO_2 was via the interaction between physisorbed NO with the reduced N-containing species on the metal surface, while the rest resulted from the combination of two similar N-species on the surface. In addition, Costa and Efstathiou (2004) stated that one of the species involved in the impact route should be reversibly chemisorbed. With the corroborative experiments of temperature-programmed surface reaction (TPSR) and in situ FTIR spectroscopy, the authors concluded that this species is exclusively that of nitrosyls on metal (Savva & Costa, 2011).

Mechanistic studies have also explained the formation of one toxic by-product in this reaction, namely nitrous oxide. In a lower temperature experiment (below 100 °C) and lower Pt dispersion (30 %), N_2O is formed via

the generation of a dimeric $(NO)_2$ from two identical adsorbed N-species while higher temperature and Pt dispersion lead the nitrosyls and unidentate nitrates to react quickly with the gaseous NO to form N_2O (Savva & Costa, 2011). Therefore, it is interesting to apply this method on carbon-supported catalyst that possessed different functional groups contributing to different types of nitrates/nitrites species.

As for the characterization, it is interesting to quantify the metal/metal oxides particle size, oxidation state and contribution of metals and activated carbon in the acidity of the catalyst. The particle size can be determined using transmission electron microscope (TEM) as being performed by Su et al. (2015) for MnO_x particle size distribution over TiO_2-graphene oxide support, and Santillan-Jimenez et al. (2011) for Pt over carbon nanotubes. The oxidation state of the metal/metal oxides presence on the catalyst can be found using X-ray absorption near edge spectroscopy (XANES) (refer page 43). Furthermore, the contribution of metals and activated carbon in the total acidity of the catalyst can be determined by varying the acidity of the carbon support. This can be achieved by varying the calcination temperature as higher temperature resulted different surface functional groups which affected the acidity (refer page 95). The resulting variant of catalysts can be evaluated using NH_3-TPD and FTIR that could show the contribution of the carbon acidity while taking the balance as the acidity contributed by the metal species.

7.2.2 Stability improvement

The study on ceria-containing materials have shown that NO reduction occurred at the reduced ceria sites. The NO consequently oxidizes the sites and the lattice oxygen of the CeO_2 moves freely between the ceria and adjacent metals (such as Pt and Pd) completing the oxidation-reduction cycle. The dissociated N atoms are then released as N_2 or N_2O even at room temperature, as observed in a Ce-Pd system (Cordatos & Gorte, 1996). This is an example of a material that governs the oxygen mobility on catalyst which can be applied to prevent carbon combustion.

In a separate study by Illán-Gómez et al. (2000), comparing the activity of copper, cobalt, iron and nickel coupled with potassium-impregnated carbon, concluded that the alkali metal imposed synergistic effect with the transitional

metals because of increased NO_x conversion as compared to the monometallic catalysts. K-Ni showed the most interesting effects, because despite a similar starting NO_x decomposition temperature of 200 °C with Cu and Co, the carbon burn-off at this temperature is half than those of its counterparts. However, as the concentration of oxygen is increased to 5 %, the carbon burn-off of K-Ni/AC increases from 23 to 32 %. Nevertheless, it is worth studying the multimetallic effects of Cu-Fe-K supported over activated carbon in a pursuit to develop a durable catalyst.

Transitional metals were also used as additives including W, Mo, Ag, Cr and V. Tungsten was reported to activate Pt by increasing the electron density over the surface, molybdenum to reduce the oxygen affinity of the catalyst, and silver to provide higher antioxidant capacity, hence keeping the noble metals in a reduced states even in high oxygen concentration, while chromium and vanadium to promote the formation of ammonium ions as the intermediate species (Liu, Li, & Woo, 2012).

7.2.3 Other less precious metals

Potassium was also studied and found to increase N_2 selectivity over Pd/TiO_2 by about 100 % (40 to 80 % N_2 selectivity over $PdTiO_2$ and Pd/K_2O-TiO_2 respectively at 175 °C). It was observed under DRIFTS that the intensity of Pd^0-NO increased which is believed to be the key intermediate in this H_2-SCR (Li et al., 2008).

Sodium has been reported to be one of the best among alkali metals promoted on Pt-ZSM5. In a 0.08 % NO + 0.28 % H_2 + 10 % O_2 gas inlet mixture at 0.24 $gscm^{-3}$ catalyst weight-to-flowrate ratio, 15 wt.% Na was found to be the optimal addition, producing up to 50 % N_2 selectivity as compared to below 20 % over non-promoted catalyst at temperatures below 110 °C. This was claimed to be due to the increased NO_2^- formation, as observed under the diffusive reflectance infrared Fourier Transform spectroscopy (DRIFTS) (Machida & Watanabe, 2004).

Furthermore, Co_3O_4 was thought to be one of the best single-component decomposition catalysts, but Haneda et al. (2003) clarified that the interaction of cobalt with the residual Na left upon the preparation of the catalyst is what govern the reaction. Singular cobalt oxide only produces

0.01 μmolN_2 $min^{-1}g^{-1}$ at 873 K, while the presence of 0.032 Na-to-Co ratio increased the reaction rate to 1.72 μmolN_2 $min^{-1}g^{-1}$. The alkali metals have been suggested to increase the rate of oxygen desorption from cobalt oxide by weakening the Co-O bond, rather than providing a synergistic effect via composite metal oxides.

7.2.4 Other components in flue gas

An SCR system is often exposed to other components in flue gas depending on the location of the reactor. PKSFeCu is suitable for the applications at the tail-end configuration (refer Section 2.1.1) when poisonous gases such as SO_2 are absent. However, water vapor, carbon monoxide and carbon dioxide may still be present at concentrations that could affect the performance of the catalyst.

The presence of H_2O at 0 – 10 % in H_2-SCR over $Ir/WO_3/SiO_2$ did not affect adversely NO conversion. It was claimed that H_2O even aided the stabilization of reduced Ir sites by producing H_2 *in-situ* via water-gas shift reaction (Hamada & Haneda, 2012). Tu et al. (2017) explained that over a dry Pt/carbon catalyst, water adsorption limits NO adsorption on both Pt and carbon surfaces, but promotes H_2 adsorption to react with adsorbed NO. The water concentrations used were 1 - 3 % at 150 °C, leading to an increase in NO_x conversion by 10 %. On the other hand, the presence of H_2O at about 5 % was reported to decrease 10 % NO_x conversion over $1wt\%Pt/Al_2O_3$ due to NO-H_2O competitive adsorption. This is especially true at temperature as low as 200 °C (Liu, Li, & Woo, 2012).

The presence of CO in flue gas due to incomplete combustion was also reported in the literature on its effects towards NO_x conversion. Negative effects were observed with a Pt/MgCeO catalyst below 200 °C with increasing CO concentration of up to 3 %. This was attributed to the competitive adsorption between CO and H over Pt sites (Costa et al., 2007). On the contrary, CO had positive effects on Pd/Al_2O_3, as a maximum NO_x was achieved at an optimum CO-to-H_2 ratio of 3:1 and at 150 °C. However, a higher ratio would decrease the NO_x conversion and N_2 formation (Savva & Costa, 2011). There is lack of reports on the effects of CO_2 in H_2-SCR, but generally, Savva & Costa (2011) claimed that CO_2 has no significant effects (with

concentration in flue gas of up to 10 %) on NO_x conversion over metal oxide supported catalysts such as Pt/MgCeO. However, as CO_2 is readily adsorbed over activated carbon at room temperature (Zulkurnai et al., 2017), it is expected that it would compete with NO for adsorption sites. The accumulative effects of multi-components in flue gas are therefore a specific study pertinent to a particular flue gas of a specific composition.

REFERENCES

Aarna, I. & Suuberg, E. M. (1997). A Review of the Kinetics of the Nitric Oxide-Carbon Reaction. *Fuel*, 76(6), 475–491.

Adamowska-Teyssier, M., Krztoń, A., Costa, P. Da & Djéga-Mariadassou, G. (2015). SCR NOx Mechanistic Study with a Mixture of Hydrocarbons Representative of the Exhaust Gas from Coal Combustion over Rh/Ce0.62Zr0.38O2 Catalyst. *Fuel*, 150, 21–28.

Adams, K. M. & Gandhi, H. S. (1983). Palladium-Tungsten Catalysts for Automotive Exhaust Treatment. *Industrial and Engineering Chemistry Product Research and Development*, 22, 207–212.

Al-Rahbi, A. S. S., Nahil, M. A., Wu, C. & Williams, P. T. (2016). Waste-Derived Activated Carbons for Control of Nitrogen Oxides. *Proceedings of the Institution of Civil Engineers - Waste and Resource Management*, 169(1), 30–41.

Alfarra, A., Frackowiak, E. & Béguin, F. (2004). The HSAB Concept as a Means to Interpret the Adsorption of Metal Ions onto Activated Carbons. *Applied Surface Science*, 228(1–4), 84–92.

Allen, A. E. & Macmillan, D. W. C. (2012). Synergistic Catalysis: A Powerful Synthetic Strategy for New Reaction Development. *Chemical Science*, 633–658.

Aritani, H., Tanaka, T., Akasaka, N., Funabiki, T., Yoshida, S., Gotoh, H. & Okamoto, Y. (1997). Reduction of NO over TiO2 -Supported Cu Catalysts. *Journal of Catalysis*, 168, 412–420.

Armor, J. N. (1992). Environmental Catalysis. *Applied Catalysis B: Environmental*, 1, 221–256.

ASTM. (2014). *Standard Test Method for Compositional Analysis by Thermogravimetry*.

Attard, G. & Barnes, C. (2001). *Surfaces*. Oxford: Oxford University Press.

Bai, S., Jiang, S., Li, H. & Guan, Y. (2015). Carbon Nanotubes Loaded with Vanadium Oxide for Reduction NO with NH3 at Low Temperature. *Chinese Journal of Chemical Engineering*, 23(3), 516–519.

Ball, D. W. (2006). *Field Guide to Spectroscopy*. Society of Photo Optical.

Bandosz, T. J. (2012). Towards Understanding Reactive Adsorption of Small Molecule Toxic Gases on Carbonaceous Materials. *Catalysis Today*, 186(1), 20–28.

Bingnan, F., Guanzhong, L. U., Yanqin, W., Yun, G. U. O. & Yanglong, G. U. O. (2011). Promoting Role of Potassium on the Catalytic Performance of Copper Oxide for the Reduction of NO by Activated Carbon. *Chinese Journal of Catalysis*, 32(5), 853–861.

Boutros, M., Gálvez, M. E., Onfroy, T. & Da Costa, P. (2014). Influence of Synthesis Parameters of SBA-15 Supported Palladium Catalysts for Methane Combustion and Simultaneous NOx Reduction. *Microporous and Mesoporous Materials*, 183, 1–8.

Brown, W. A. & King, D. A. (2000). NO Chemisorption and Reactions on Metal Surfaces: A New Perspective. *Journal of Physical Chemistry B*, 104(12), 2578–2595.

Burch, R. & Coleman, M. D. (1999). An Investigation of the NO/H2/O2 Reaction on Noble-

Metal Catalysts at Low Temperatures under Lean-Burn Conditions. *Applied Catalysis B: Environmental*, 23, 115–121.

Busca, G., Lietti, L., Ramis, G. & Berti, F. (1998). Chemical and Mechanistic Aspects of the Selective Catalytic Reduction of NOx by Ammonia over Oxide Catalysts : A Review. *Applied Catalysis B: Environmental*, 18(2), 1–36.

Cai, X., Sun, W., Xu, C., Cao, L. & Jang, Y. (2016). Highly Selective Catalytic Reduction of NO via SO2/H2O-Tolerant Spinel Catalysts at Low Temperature. *Environmental Science and Pollution Research*, 23, 18609–18620.

California Energy Commission. (2002). *Evaluation of Best Available Control Technology*.

Camposeco, R., Castillo, S., Mugica, V., Mejía-Centeno, I. & Marín, J. (2014). Role of V2O5-WO3/H2Ti3O7-Nanotube-Model Catalysts in the Enhancement of the Catalytic Activity for the SCR-NH3 Process. *Chemical Engineering Journal*, 242, 313–320.

Canter, N. (2012). Effective NOx Reduction without Using Precious Metals, in: *10th Annual CMF Plus: Seven of the industry's most innovative companies recap presentations from STLE's 2012 Commercial Marketing Forum. Tribology & Lubrication Technology*, (pp. 6–7). Afton Chemical.

Cao, F., Xiang, J., Su, S., Wang, P., Sun, L., Hu, S. & Lei, S. (2014). The Activity and Characterization of MnOx-CeO2-ZrO2/γ-Al2O3 Catalysts for Low Temperature Selective Catalytic Reduction of NO with NH3. *Chemical Engineering Journal*, 243, 347–354.

Caravaggio, G., Nossova, L. & Burich, R. (2016). Influence of Supports on Pd Catalysts for the Selective Catalytic Reduction of NOx with H2 and CO. *Emission Control Science and Technology*, 2(1), 10–19.

Castoldi, L., Matarrese, R., Lietti, L. & Forzatti, P. (2009). Intrinsic Reactivity of Alkaline and Alkaline-Earth Metal Oxide Catalysts for Oxidation of Soot. *Applied Catalysis B: Environmental*, 90, 278–285.

Cha, J. S., Choi, J. C., Ko, J. H., Park, Y. K., Park, S. H., Jeong, K. E., Kim, S. S. & Jeon, J. K. (2010). The Low-Temperature SCR of NO over Rice Straw and Sewage Sludge Derived Char. *Chemical Engineering Journal*, 156(2), 321–327.

Chan, L. K., Sarofim, A. F. & Beér, J. M. (1983). Kinetics of the NO-Carbon Reaction at Fluidized Bed Combustor Conditions. *Combustion and Flame*, 52, 37–45.

Chen, J., Cao, F., Qu, R., Gao, X. & Cen, K. (2015). Bimetallic Cerium-Copper Nanoparticles Embedded in Ordered Mesoporous Carbons as Effective Catalysts for the Selective Catalytic Reduction of NO with NH3. *Journal of Colloid and Interface Science*, 456, 66–75.

Cheng, Y., Song, W., Liu, J., Zheng, H., Zhao, Z., Xu, C., Wei, Y. & Hensen, E. J. M. (2017). Simultaneous NOx and Particulate Matter Removal from Diesel Exhaust by Gierarchical Fe-Doped Ce-Zr Oxide. *ACS Catalysis*, 7, 3883–3892.

Chiarello, G. L., Ferri, D., Grunwaldt, J. D., Forni, L. & Baiker, A. (2007). Flame-Synthesized LaCoO3-Supported Pd. 2. Catalytic Behavior in the Reduction of NO by H2 under Lean Conditions. *Journal of Catalysis*, 252(2), 137–147.

Choi, J., Pan, L., Zhang, F., Diulus, J. T., Asthagiri, A. & Weaver, J. F. (2015). Molecular

Adsorption of NO on PdO(101). *Surface Science*, 640, 150–158.

Chu, Y., Zhang, T., Guo, J., Liu, C., Yin, H., Zhu, X. & Liu, Y. (2015). Low Temperature Selective Catalytic Reduction of NO by C3H6 over CeOx Loaded on AC Treated by HNO3. *Journal of Rare Earths*, 33(4), 371–381.

Claesson, S., Donohue, J. & Schomaker, V. (1948). The Molecular Structure of Nitrogen Dioxide. A Reinvestigation by Electron Diffraction. *The Journal of Chemical Physics*, 16(3), 207–210.

Consul, J. M. D., Thiele, D., Veses, R. C., Baibich, I. M. & Dallago, R. M. (2004). Catalytic Decomposition of Nitrogen Oxides. *New Chemistry*, 1–19.

Costa, C. N., Savva, P. G., Andronikou, C., Lambrou, P. S., Polychronopoulou, K., Belessi, V. C., Stathopoulos, V. N., Pomonis, P. J. & Efstathiou, A. M. (2002). An Investigation of the NO/H2/O2 (Lean de-NOx) Reaction on a Highly Active and Selective Pt/La0.7Sr0.2Ce0.1FeO3 Catalyst at Low Temperatures. *Journal of Catalysis*, 209(2), 456–471.

Costa, C. N., Savva, P. G., Fierro, J. L. G. & Efstathiou, A. M. (2007). Industrial H2 -SCR of NO on a Novel Pt/MgO – CeO 2 Catalyst. *Applied Catalysis B: Environmental*, 75, 147–156.

Council of the European Communities. (1988). *Council Directive of 24 November 1988 on the Limitation of Emissions of Certain Pollutants into the Air from Large Combustion Plants*.

Deliyanni, E. & Bandosz, T. J. (2011). Effect of Carbon Surface Modification with Dimethylamine on Reactive Adsorption of NOx. *Langmuir*, 27(5), 1837–1843.

Deng, S., Meng, T., Xu, B., Gao, F., Ding, Y., Yu, L. & Fan, Y. (2016). Advanced MnOx/TiO2 Catalyst with Preferentially Exposed Anatase (001) Facet for Low-Temperature SCR of NO. *ACS Catalysis*, 6, 5807–5815.

Dollimore, D., Evans, T. A., Lee, Y. F., Pee, G. P. & Wilburn, F. W. (1992). The Significance of the Onset and Final Temperatures in the Kinetic Analysis of TG Curves. *Thermochimica Acta*, 196, 255–265.

Enders, A. & Lehmann, J. (2012). Comparison of Wet-Digestion and Dry-Ashing Methods for Total Elemental Analysis of Biochar. *Communications in Soil Science and Plant Analysis*, 43(7), 1042–1052.

Ertl;, G., Knozinger;, H., Schuth;, F. & Weitkamp, J. (2008). *Handbook of Heterogeneous Catalysis*.

Eugene, C., William, E. C. & James, R. D. (1959). Process for Catalytically Reducing Nitrogen Oxides in Industrial Stack Gases.

European Commission. (2006). *Reference Document on the Best Available Techniques for Waste Incineration*.

European Commission. (2016). *Emission Database for Global Atmospheric Research (EDGAR)*. Retrieved from http://edgar.jrc.ec.europa.eu/overview.php?v=431

European Environment Agency. (2010). *Nitrogen Oxides (NOx) Emissions*.

European Environment Agency. (2014). *Nitrogen Oxides Emissions*.

Evans, J.-M. M. G. Oç. ; E. H. (2007). *Inductively Coupled Plasma Spectrometry and Its Applications* (S. J. Hill, Ed.). Plymouth: Blackwell Publishing.

Fadoni, M. & Lucarelli, L. (2006). Temperature Programmed Desorption, Reduction, Oxidation and Flow Chemisorption for the Characterisation of Heterogeneous Catalysts, in: *Theoretical aspects, instrumentation and applications*, (pp. 177–225).

Fang, D., Xie, J., Hu, H., Yang, H., He, F. & Fu, Z. (2015). Identification of MnOx Species and Mn Valence States in MnOx/TiO2 Catalysts for Low Temperature SCR. *Chemical Engineering Journal*, 271, 23–30.

Feng, L., Xie, N. & Zhong, J. (2014). Carbon Nanofibers and Their Composites: A Review of Synthesizing, Properties and Applications. *Materials*, 7(5), 3919–3945.

Fioretos, K. a., Psofogiannakis, G. M. & Froudakis, G. E. (2011). Ab-Initio Study of the Adsorption and Separation of NOx and SOx Gases in Functionalized IRMOF Ligands. *Journal of Physical Chemistry C*, 115(50), 24906–24914.

Forzatti, P. (2001). Present Status and Perspectives in De-NOx SCR Catalysis. *Applied Catalysis A: General*, 222(1–2), 221–236.

Frank, B., Emig, G. & Renken, A. (1998). Kinetics and Mechanism of the Reduction of Nitric Oxides by H2 under Lean-Burn Conditions on a Pt-Mo-Co/Alpha-Al2O3 Catalyst. *Applied Catalysis B: Environmental*, 19, 45–57.

Fu, M., Li, C., Lu, P., Qu, L., Zhang, M., Zhou, Y., Yu, M. & Fang, Y. (2014). A Review on Selective Catalytic Reduction of NOx by Supported Catalysts at 100–300 °C—catalysts, Mechanism, Kinetics. *Catalysis Science & Technology*, 4, 14–25.

Fultz, B. & Howe, J. (2002). *Transmission Electron Microscopy and Diffractometry of Materials*. Berlin: Springer-Verlag Berlin Heidelberg.

Gandhi, H. S. & Shelef, M. (1973). The Adsorption of Nitric Oxide on Copper Oxides. *Journal of Catalysis*, 28, 1–7.

Gao, F., Tang, X., Yi, H., Zhao, S., Li, C., Li, J., Shi, Y. & Meng, X. (2017). *A Review on Selective Catalytic Reduction of NOx by NH3 over Mn–based Catalysts at Low Temperatures: Catalysts, Mechanisms, Kinetics and DFT Calculations*.

García-Cortés, J. M., Pérez-Ramírez, J., Illán-Gómez, M. J., Kapteijn, F., Moulijn, J. A. & Salinas-Martínez de Lecea, C. (2001). Comparative Study of Pt-Based Catalysts on Different Supports in the Low-Temperature de-NOx-SCR with Propene. *Applied Catalysis B: Environmental*, 30(3–4), 399–408.

Gomez-Garcia, M. A., Pitchon, V. & Kiennemann, A. (2005). Pollution by Nitrogen Oxides: An Approach to NOx Abatement by Using Sorbing Catalytic Materials. *Environment International*, 31(3), 445–467.

Gong, T., Qin, L., Zhang, W., Wan, H., Lu, J. & Feng, H. (2015). Activated Carbon Supported Palladium Nanoparticle Catalysts Synthesized by Atomic Layer Deposition: Genesis and Evolution of Nanoparticles and Tuning the Particle Size. *Journal of Physical Chemistry C*, 119, 11544–11556.

Goodsite, M., Wong Mei Ling, C., Hertel, O. & Moseholm, L. (2011). Responses to Air Pollution Based on Historical and Current Policies in the EU and ASEAN. *Global Environment*, 3.6, 150–182.

Gruber, M. & Hermann, K. (2013). Elementary Steps of the Catalytic NOx Reduction with NH3: Cluster Studies on Reactant Adsorption at Vanadium Oxide Substrate. *Journal of Chemical Physics*, 138(9).

Guan, B., Zhan, R., Lin, H. & Huang, Z. (2014). Review of State of the Art Technologies of Selective Catalytic Reduction of NOx from Diesel Engine Exhaust. *Applied Thermal Engineering*, 66(1–2), 395–414.

Haber, J., Block, J. H. & Delmon, B. (1995). Manual of Methods and Procedures for Catalyst Characterization (Technical Report). *Pure and Applied Chemistry*, 67(8–9), 1257–1306.

Hamada, H. & Haneda, M. (2012). A Review of Selective Catalytic Reduction of Nitrogen Oxides with Hydrogen and Carbon Monoxide. *Applied Catalysis A: General*, 421–422, 1–13.

Haneda, M. & Hamada, H. (2016). Recent Progress in Catalytic NO Decomposition. *Comptes Rendus Chimie*, 19(10), 1254–1265.

Haneda, M., Pusparatu, Kintaichi, Y., Nakamura, I., Sasaki, M., Fujitani, T. & Hamada, H. (2005). Promotional Effect of SO2 on the Activity of Ir/SiO2 for NO Reduction with CO under Oxygen-Rich Conditions. *Catalysis*, 229, 197–205.

Harris, D. C. (2010). *Quantitative Chemical Analysis*. China Lake: W.H. Freeman and Company.

Haxel, G. B., Hedrick, J. B. & Orris, G. J. (2002). *Rare Earth Elements — Critical Resources for High Technology*.

Hemmann, F., Jaeger, C. & Kemnitz, E. (2014). Comparison of Acidic Site Quantification Methods for a Series of Nanoscopic Aluminum Hydroxide Fluorides. *RSC Advances*, 4(100), 56900–56909.

Holder, J. V. (2002). Chapter 3: Chemistry and the Environment, in: *Handbook of Green Chemistry & Technology*, (pp. 28–55). London: Blackwell Science.

Hou, Y., Cai, G., Huang, Z., Han, X. & Guo, S. (2014). Effect of HCl on V2O5/AC Catalyst for NO Reduction by NH3 at Low Temperatures. *Chemical Engineering Journal*, 247, 59–65.

House, J. E. (1997). *Principles of Chemical Kinetics*. Dubuque: Wm. C. Brown Publishers.

Huai, L., He, C., Wang, H., Wen, H., Yi, W. & Liu, J. (2015). NO Dissociation and Reduction by H2 on Pd (111): A First-Principles Study. *Journal of Catalysis*, 322, 73–83.

Ilavsky, J., Zhang, F., et al. (2018). Development of Combined Microstructure and Structure Characterization Facility for in Situ and Operando Studies at the Advanced Photon Source. *Journal Of Applied Crystallography*, 51, 867–882.

Ilieva, L., Pantaleo, G., Velinov, N., Tabakova, T., Petrova, P., Ivanov, I., Avdeev, G., Paneva, D. & Venezia, A. M. (2015). NO Reduction by CO over Gold Catalysts Supported on Fe-Loaded Ceria. *Applied Catalysis B: Environmental*, 174–175, 176–184.

Imanaka, N. & Masui, T. (2012). Advances in Direct NO x Decomposition Catalysts. *Applied Catalysis A: General*, 431–432, 1–8.

Japke, E., Casapu, M., Trouillet, V., Deutschmann, O. & Grunwaldt, J. D. (2015). Soot and Hydrocarbon Oxidation over Vanadia-Based SCR Catalysts. *Catalysis Today*, 258, 461–

469.

Jeguirim, M., Tschamber, V., Brilhac, J. F. & Ehrburger, P. (2004). Interaction Mechanism of NO2 with Carbon Black: Effect of Surface Oxygen Complexes. *Journal of Analytical and Applied Pyrolysis*, 72, 171–181.

Jensen-holm, H., Castellino, F. & White, T. N. (2012). SCR DeNOx Catalyst Considerations When Using Biomass in Power Generation, in: *Power Plant Air Pollutant Control 'MEGA' Symposium*, (pp. 1–27).

Ji, Y., Xu, D., Bai, S., Graham, U., Crocker, M., Chen, B., Shi, C., Harris, D., Scapens, D. & Darab, J. (2017). Pt- and Pd-Promoted CeO2-ZrO2for Passive NOx Adsorber Applications. *Industrial and Engineering Chemistry Research*, 56, 111–125.

Johnson, T. V. (2009). Review of Diesel Emissions and Control. *International Journal of Engine Research*, 10, 275–285.

Johnsson, J. E. (1994). Formation and Reduction of Nitrogen Oxides in Fluidized-Bed Combustion. *Fuel*, 73(9), 1398–1415.

Kacimi, M., Ziyad, M. & Liotta, L. F. (2015). Cu on Amorphous AlPO4: Preparation, Characterization and Catalytic Activity in NO Reduction by CO in Presence of Oxygen. *Catalysis Today*, 241, 151–158.

Kane International. (2006). *KANE940 Hand-Held Combustion Analyser*.

Khwaja, M. A., Umer, F., Shaheen, N., Sherazi, A. & Haq Shaheen, F. (2012). *Air Pollution Reduction and Control in South Asia*. Islamabad.

Kijlstra, W. S., Brands, D. S., Poels, E. K. & Bliek, A. (1997). Mechanism of the Selective Catalytic Reduction of NO by NH3 over MnOx/Al2O3. I. Adsorption and Desorption of the Single Reaction Components. *Journal of Catalysis*, 171, 208–218.

Klose, W. & Rincón, S. (2007). Adsorption and Reaction of NO on Activated Carbon in the Presence of Oxygen and Water Vapour. *Fuel*, 86(1–2), 203–209.

Koebel, M. & Elsener, M. (1998). Selective Catalytic Reduction of NO over Commercial DeNOx-Catalysts: Experimental Determination of Kinetic and Thermodynamic Parameters. *Chemical Engineering Science*, 53(4), 657–669.

Lam, E. & Luong, J. H. T. (2014). Carbon Materials as Catalyst Supports and Catalysts in the Transformation of Biomass to Fuels and Chemicals. *ACS Catalysis*, 4, 3393–3410.

Łamacz, A., Krztoń, A. & Djéga-Mariadassou, G. (2013). Study on the Selective Catalytic Reduction of NO with Toluene over CuO/CeZrO2. A Confirmation for the Three-Function Model of HC-SCR Using the Temperature Programmed Methods and in Situ DRIFTS. *Applied Catalysis B: Environmental*, 142–143(2), 268–277.

Lázaro, M. J., Boyano, A., Gálvez, M. E., Izquierdo, M. T., García-Bordejé, E., Ruiz, C., Juan, R. & Moliner, R. (2008). Novel Carbon Based Catalysts for the Reduction of NO: Influence of Support Precursors and Active Phase Loading. *Catalysis Today*, 137(2–4), 215–221.

Lee, J., Kim, K. H. & Kwon, E. E. (2017). Biochar as a Catalyst. *Renewable and Sustainable Energy Reviews*, 77, 70–79.

Lee, S. M., Park, K. H., Kim, S. S., Kwon, D. W. & Hong, S. C. (2012). Effect of the Mn Oxidation State and Lattice Oxygen in Mn-Based TiO2 Catalysts on the Low-

Temperature Selective Catalytic Reduction of NO by NH 3. *Journal of the Air & Waste Management Association*, 62, 1085–1092.

Lee, Y. W., Kim, H. J., Park, J. W., Choi, B. U., Choi, D. K. & Park, J. W. (2003). Adsorption and Reaction Behavior for the Simultaneous Adsorption of NO-NO2 and SO2 on Activated Carbon Impregnated with KOH. *Carbon*, 41(10), 1881–1888.

Levasseur, B., Gonzalez-Lopez, E., Rossin, J. A. & Bandosz, T. J. (2011). Effect of Reduction Treatment on Copper Modified Activated Carbons on NOx Adsorption at Room Temperature. *Langmuir*, 27(9), 5354–5365.

Li, J., Chang, H., Ma, L., Hao, J. & Yang, R. T. (2011). Low-Temperature Selective Catalytic Reduction of NOx with NH3 over Metal Oxide and Zeolite Catalysts - a Review. *Catalysis Today*, 175(1), 147–156.

Li, J., Wang, S., Zhou, L., Luo, G. & Wei, F. (2014). NO Reduction by CO over a Fe-Based Catalyst in FCC Regenerator Conditions. *Chemical Engineering Journal*, 255, 126–133.

Li, N., Ma, X., Zha, Q., Kim, K., Chen, Y. & Song, C. (2011). Maximizing the Number of Oxygen-Containing Functional Groups on Activated Carbon by Using Ammonium Persulfate and Improving the Temperature-Programmed Desorption Characterization of Carbon Surface Chemistry. *Carbon*, 49(15), 5002–5013.

Li, Q., Yang, H., Ma, Z. & Zhang, X. (2012). Selective Catalytic Reduction of NO with NH3 over CuOx-Carbonaceous Materials. *Catalysis Communications*, 17, 8–12.

Li, S., Wang, X., Tan, S., Shi, Y. & Li, W. (2017). CrO3 Supported on Sargassum-Based Activated Carbon as Low Temperature Catalysts for the Selective Catalytic Reduction of NO with NH3. *Fuel*, 191, 511–517.

Li, Y. & Armor, J. N. (1991). Temperature-Programmed Desorption of Nitric Oxide over Cu-ZSM-5. *Applied Catalysis*, 76, L1–L8.

Li, Y., Li, G., Lu, Y., Hao, W., Wei, Z., Liu, J. & Zhang, Y. (2018). Denitrification Performance of Non-Pitch Coal-Based Activated Coke by the Introduction of MnOx–CeOx–M (FeOx, CoOx) at Low Temperature. *Molecular Catalysis*, 445, 21–28.

Lietti, L., Ramis, G., Berti, F., Toledo, G., Robba, D., Busca, G. & Forzatti, P. (1998). Chemical, Structural and Mechanistic Aspects on NOx SCR over Commercial and Model Oxide Catalysts. *Catalysis Today*, 42(1–2), 101–116.

Lindholm, A., Sjövall, H. & Olsson, L. (2010). Reduction of NOxover a Combined NSR and SCR System. *Applied Catalysis B: Environmental*, 98(3–4), 112–121. Retrieved from http://dx.doi.org/10.1016/j.apcatb.2010.05.019

Liu, C., Shi, J. W., Gao, C. & Niu, C. (2016). Manganese Oxide-Based Catalysts for Low-Temperature Selective Catalytic Reduction of NOx with NH3: A Review. *Applied Catalysis A: General*, 522, 54–69.

Liu, F., Yu, Y. & He, H. (2014). Environmentally-Benign Catalysts for the Selective Catalytic Reduction of NOx from Diesel Engines: Structure–activity Relationship and Reaction Mechanism Aspects. *Chemical Communications*, 50, 8445–8463.

Liu, H., Qiu, G., Shao, Y. & Riffat, S. B. (2010). Experimental Investigation on Flue Gas Emissions of a Domestic Biomass Boiler under Normal and Idle Combustion. *International Journal of Low-Carbon Technologies*, 88–95.

Liu, Z., Li, J. & Woo, S. I. (2012). Recent Advances in the Selective Catalytic Reduction of NOx by Hydrogen in the Presence of Oxygen. *Energy & Environmental Science*, 5(10), 8799.

Loferski, P. J. (2014). *Platinum-Group Metals [Advance Release]*.

Long, R. Q. & Yang, R. T. (2001). Temperature-Programmed Desorption/Surface Reaction (TPD/TPSR) Study of Fe-Exchanged ZSM-5 for Selective Catalytic Reduction of Nitric Oxide by Ammonia. *Journal of Catalysis*, 198, 20–28.

López, D., Buitrago, R., Sepúlveda-Escribano, A., Rodríguez-Reinoso, F. & Mondragon, F. (2007). Low-Temperature Catalytic Adsorption of NO on Activated Carbon Materials. *Langmuir*, 23, 12131–12137.

Ma, Z., Yang, H., Li, Q., Zheng, J. & Zhang, X. (2012). Catalytic Reduction of NO by NH3 over Fe-Cu-Ox/CNTs-TiO2 Composites at Low Temperature. *Applied Catalysis A: General*, 427–428, 43–48.

Marsh H. & Rodriguez-Reinoso F. (2006). *Activated Carbon*. UK: Elsevier.

Mears, D. E. (1971). Diagnostic Criteria for Heat Transport Limitations in Fixed Bed Reactors. *Journal of Catalysis*, 20(2), 127–131.

Mihet, M. & Lazar, M. D. (2014). Effect of Pd and Rh Promotion on Ni/Al2O3 for NO Reduction by Hydrogen for Stationary Applications. *Chemical Engineering Journal*, 251, 310–318.

Mihet, M., Lazar, M. D., Almasan, V. & Mirel, V. (2012). H2-SCR at Low Temperatures on Noble Metal Supported Catalysts, in: *AIP Conference Proceedings 2012*, (pp. 73–76).

MKS Instruments. (2013). *MKS G-Series Digital Mass Flow Controllers Instruction Manual G-Series Mass Flow Controllers*.

Mondt, J. R. (2000). *Cleaner Cars: The History and Technology of Emission Control Since the 1960s*. Warrendale: Society of Automotive Engineers.

More, P. M., Nguyen, D. L., Granger, P., Dujardin, C., Dongare, M. K. & Umbarkar, S. B. (2015). Activation by Pretreatment of Ag-Au/Al2O3 Bimetallic Catalyst to Improve Low Temperature HC-SCR of NOx for Lean Burn Engine Exhaust. *Applied Catalysis B: Environmental*, 174–175, 145–156.

Moreno-Castilla, C. & Pérez-Cadenas, A. F. (2010). Carbon-Based Honeycomb Monoliths for Environmental Gas-Phase Applications. *Materials*, 3(2), 1203–1227.

Moreno-Piraján, J. C., Tirano, J., Salamanca, B. & Giraldo, L. (2010). Activated Carbon Modified with Copper for Adsorption of Propanethiol. *International Journal of Molecular Sciences*, 11(3), 927–942.

Mrad, R., Aissat, A., Cousin, R., Courcot, D. & Siffert, S. (2015). Catalysts for NOx Selective Catalytic Reduction by Hydrocarbons (HC-SCR). *Applied Catalysis A: General*, 504, 542–548.

Murzin, D. & Salmi, T. (2005). *Catalytic Kinetics*. Elsevier. Retrieved May 29, 2017, from http://www.sciencedirect.com/science/book/9780444516053

Murzin, D., Salmi, T., Murzin, D. & Salmi, T. (2005a). Chapter 9 – Mass Transfer and Catalytic Reactions, in: *Catalytic Kinetics*, (pp. 341–418).

Murzin, D., Salmi, T., Murzin, D. & Salmi, T. (2005b). Chapter 7 – Heterogeneous Catalytic Kinetics, in: *Catalytic Kinetics*, (pp. 225–284).

Nanba, T., Kohno, C., Masukawa, S., Uchisawa, J., Nakayama, N. & Obuchi, A. (2003). Improvements in the N2 Selectivity of Pt Catalysts in the NO-H2-O2 Reaction at Low Temperatures. *Applied Catalysis B: Environmental*, 46(2), 353–364.

Neathery, J. K., Rubel, A. M. & Stencel, J. M. (1997). Uptake of NOx by Activated Carbons: Bench-Scale and Pilot-Plant Testing. *Carbon*, 35(9), 1321–1327.

Nevers, N. de. (1995). *Air Pollution Control Engineering*. Singapore: McGraw-Hill.

Norris, J. O. W. (2002). *Technologies Available for Measuring NOx*.

NRCCSR. (2012). *Replacing Critical Materials with Abundant Materials - the Role of the Chemical Sciences in Finding Alternatives to Critical Resources*.

O.Bennett, C. (1999). Experiments and Processes in the Transient Regime for Heterogeneous Catalysis. *Advances in Catalysis*, 44, 329–416.

Oh, S. H. & Carpenter, J. E. (1986). Platinum-Rhodium Synergism in Three-Way Automotive Catalysts. *Journal of Catalysis*, 98(1), 178–190.

Otto, K. & Shelef, M. (1970). The Adsorption of Nitric Oxide on Iron Oxides. *Journal of Catalysis*, 18, 184–192.

Park, S. M., Kim, M. Y., Kim, E. S., Han, H. S. & Seo, G. (2011). H2-SCR of NO on Pt-MnOx Catalysts: Reaction Path via NH3 Formation. *Applied Catalysis A: General*, 395(1–2), 120–128.

Pârvulescu, V. I., Grange, P. & Delmon, B. (1998). Catalytic Removal of NO. *Catalysis Today*, 46(4), 233–316.

Pasel, J., Käßner, P., Montanari, B., Gazzano, M., Vaccari, A., Makowski, W., Lojewski, T., Dziembaj, R. & Papp, H. (1998). Transition Metal Oxides Supported on Active Carbons as Low Temperature Catalysts for the Selective Catalytic Reduction (SCR) of NO with NH3. *Applied Catalysis B: Environmental*, 18(3–4), 199–213.

Patel, A., Rufford, T. E., Rudolph, V. & Zhu, Z. (2011). Selective Catalytic Reduction of NO by CO over CuO Supported on SBA-15: Effect of CuO Loading on the Activity of Catalysts. *Catalysis Today*, 166(1), 188–193.

Patel, A., Shukla, P., Rufford, T. E., Rudolph, V. & Zhu, Z. (2014). Selective Catalytic Reduction of NO with CO Using Different Metal-Oxides Incorporated in MCM-41. *Chemical Engineering Journal*, 255, 437–444.

Piumetti, M., Bensaid, S., Fino, D. & Russo, N. (2015). Catalysis in Diesel Engine NOx Aftertreatment: A Review. *Catalysis, Structure & Reactivity*, 1(4), 155–173.

Plens, A. N. A. C. O., Monaro, D. L. G. & Coutinho, A. R. (2015). Adsorption of SOx and NOx in Activated Viscose Fibers. *Annals of the Brazilian Academy of Sciences*, 87, 1149–1160.

Qi, G., Yang, R. & Rinaldi, F. (2006). Selective Catalytic Reduction of Nitric Oxide with Hydrogen over Pd-Based Catalysts. *Journal of Catalysis*, 237(2), 381–392.

Qian, K., Kumar, A., Zhang, H., Bellmer, D. & Huhnke, R. (2015). Recent Advances in

Utilization of Biochar. *Renewable and Sustainable Energy Reviews*, 42, 1055–1064.

Radic, D. B., Stanojevic, M. M., Obradovic, M. O. & Jovovi, A. M. (2017). Thermal Analysis of Physical and Chemical Changes Occuring during Regeneration of Activated Carbon. *Thermal Science*, 21(2), 1067–1081.

Regalbuto, J. R. & Ha, J. W. (1994). A Corrected Procedure and Consistent Interpretation for Temperature Programmed Reduction of Supported MoO3. *Catalysis Letters*, 29(1–2), 189–207.

Rezaei, F., Rownaghi, A. a, Monjezi, S., Lively, R. P. & Jones, C. W. (2015). SOx/NOx Removal from Flue Gas Streams by Solid Adsorbents: A Review of Current Challenges and Future Directions. *Energy & Fuels*, 29, 1–65.

Rodriguez-Mirasol, J., Ooms, A. C., Pels, J. R., Kapteijn, F. & Moulijn, J. A. (1994). NO and N20 Decomposition over Coal Char at Fluidized-Bed Combustion Conditions. *Combustion and Flame*, 99, 499–507.

Roy, S., Hegde, M. S. & Madras, G. (2009). Catalysis for NOx Abatement. *Applied Energy*, 86(11), 2283–2297.

Sager, U., Schmidt, W., Schmidt, F. & Suhartiningsih. (2013). Catalytic Reduction of Nitrogen Oxides via Nanoscopic Oxide Catalysts within Activated Carbons at Room Temperature. *Adsorption*, 19(5), 1027–1033.

Santillan-Jimenez, E., Miljković-Kocić, V., Crocker, M. & Wilson, K. (2011). Carbon Nanotube-Supported Metal Catalysts for NOx Reduction Using Hydrocarbon Reductants. Part 1: Catalyst Preparation, Characterization and NOx Reduction Characteristics. *Applied Catalysis B: Environmental*, 102(1–2), 1–8.

Savva, P. G. & Costa, C. N. (2011). Hydrogen Lean-DeNOx as an Alternative to the Ammonia and Hydrocarbon Selective Catalytic Reduction (SCR). *Catalysis Reviews*, 53(2), 91–151.

Serra, R. M., Aspromonte, S. G., Miró, E. E. & Boix, A. V. (2015). Hydrocarbon Adsorption and NOx-SCR on (Cs,Co) Mordenite. *Applied Catalysis B: Environmental*, 166–167, 592–602.

Shelef, M. & Gandhi, H. S. (1972). Ammonia Formation in Catalytic Reduction of Nitric Oxide by Molecular Hydrogen. *Industrial & Engineering Chemistry Product Research and Development*, 11(4), 393–396.

Shen, B., Chen, J., Yue, S. & Li, G. (2015). A Comparative Study of Modified Cotton Biochar and Activated Carbon Based Catalysts in Low Temperature SCR. *Fuel*, 156, 47–53.

Shen, Y., Ge, X. & Chen, M. (2016). Catalytic Oxidation of Nitric Oxide (NO) with Carbonaceous Materials. *RSC Advances*, 6, 8469–8482.

Shi, W., Zhang, J., Li, X., Zhou, J., Pan, Y., Liu, Q., Xu, Z. P. & Qian, G. (2017). Synergistic Effect between Surface Anhydride Group and Carbon-Metal Species during Catalytic Reduction of Nitric Oxide. *Energy and Fuels*, 31(10), 11258–11265.

Shibata, J., Hashimoto, M., Shimizu, K. I., Yoshida, H., Hattori, T. & Satsuma, A. (2004). Factors Controlling Activity and Selectivity for SCR of NO by Hydrogen over Supported Platinum Catalysts. *Journal of Physical Chemistry B*, 108(47), 18327–18335.

Shuit, S. H., Yee, K. F., Lee, K. T., Subhash, B. & Tan, S. H. (2013). Evolution towards the

Utilisation of Functionalised Carbon Nanotubes as a New Generation Catalyst Support in Biodiesel Production: An Overview. *RSC Advances*, 3(24), 9070.

Sing, K. S. W., Everett, D. H., Haul, R. A. W., Moscou, L., Pierotti, R. A., Rouquerol, J. & Siemieniewska, T. (1985). Reporting Physisorption Data for Gas/Solid Systems with Special Reference to the Determination of Surface Area and Porosity (Recommendations 1984). *Pure and Applied Chemistry*, 57(4), 603–619.

Singh, S., Nahil, M. A., Sun, X., Wu, C., Chen, J., Shen, B. & Williams, P. T. (2013). Novel Application of Cotton Stalk as a Waste Derived Catalyst in the Low Temperature SCR-DeNOx Process. *Fuel*, 105, 585–594.

Singoredjo, L., Slagt, M., Wees, J. van, Kapteijn, F. & Moulijn, J. A. (1990). Selective Catalytic Reduction of NO with NH3 over Carbon Supported Copper Catalysts. *Catalysis Today*, 7, 157–165.

Sorrels, J. L., Randall, D. D., Schaffner, K. S. & Fry, C. R. (2015). *Chapter 2: Selective Catalytic Reduction*.

Spivey, J. J. (1994). Carbon-Based Catalysts for the Low-Temperature Reduction of NO with NH3. *Annual Reports & Progress in Chemistry, Section C: Physical Chemistry*, (6), 155–176.

Sreekanth, P. M. & Smirniotis, P. G. (2008). Selective Reduction of NO with CO over Titania Supported Transition Metal Oxide Catalysts. *Catalysis Letters*, 122(1–2), 37–42.

Stenger, H. G. & Hepburn, J. S. (1987). NO Reduction by Al2O3-Supported Rhodium, Palladium, and Platinum. 1. Intrinsic Activities and Selectivities. *Energy and Fuels*, 1(5), 412–416.

Ström, L., Carlsson, P., Magnus, S. & Harelind, H. (2018). Surface Species and Metal Oxidation State during H2-Assisted NH3-SCR of NOx over Alumina-Supported Silver and Indium. *Catalysts*, 8(38), 1–14.

Su, W., Lu, X., Jia, S., Wang, J., Ma, H. & Xing, Y. (2015). Catalytic Reduction of NOx over TiO2-Graphene Oxide Supported with MnOx at Low Temperature. *Catalysis Letters*, 145(7), 1446–1456.

Sultana, A., Sasaki, M., Suzuki, K. & Hamada, H. (2013). Enhanced NOx Conversion with Decane over Ag/Al2O3 and Metal Supported ZSM-5 Composite SCR Catalysts. *Topics in Catalysis*, 56(1–8), 172–176.

Tabata, T., Kokitsu, M. & Okada, O. (1994). Study on Patent Literature of Catalysts for a New NOx Removal Process. *Catalysis Today*, 22(1), 147–169.

Taheri Najafabadi, A. (2015). Emerging Applications of Graphene and Its Derivatives in Carbon Capture and Conversion: Current Status and Future Prospects. *Renewable and Sustainable Energy Reviews*, 41, 1515–1545.

Tahir, M. A., Ahmad, I., Umer llyas, S., Waqas, S. & Javed, M. T. (2013). Selective Non-Catalytic Reduction of NOx (a Review Study). *NFC-IEFR Journal of Engineering & Scientific Research*, 145–150.

Tan, L. L., Ong, W. J., Chai, S. P. & Mohamed, A. R. (2013). Growth of Carbon Nanotubes over Non-Metallic Based Catalysts: A Review on the Recent Developments. *Catalysis Today*, 217, 1–12.

Thirupathi, B. & Smirniotis, P. G. (2011). Co-Doping a Metal (Cr, Fe, Co, Ni, Cu, Zn, Ce, and Zr) on Mn/TiO2 Catalyst and Its Effect on the Selective Reduction of NO with NH3 at Low-Temperatures. *Applied Catalysis B: Environmental*, 110, 195–206.

Thommes, M., Kaneko, K., Neimark, A. V., Olivier, J. P., Rodriguez-Reinoso, F., Rouquerol, J. & Sing, K. S. W. (2015). Physisorption of Gases, with Special Reference to the Evaluation of Surface Area and Pore Size Distribution (IUPAC Technical Report). *Pure and Applied Chemistry*, 87(9–10), 1051–1069.

Touloukian, Y. S., Kirby, R. K., Taylor, R. E. & Desai, P. D. (1975). Volume 1 : Thermal Conductivity - Metallic Elements and Alloys. *Thermophysical Properties of Matter-the TPRC Data Series.*, 1595.

Tu, B., Shi, N., Sun, W., Cao, L. & Yang, J. (2017). SO2-Tolerant and H2O-Promoting Pt/C Catalysts for Efficient NO Removal via Fixed-Bed H2-SCR. *Environmental Science and Pollution Research*, 24(1), 676–684.

Tufano, V. & Turco, M. (1993). Kinetic Modelling of Nitric Oxide Reduction over a High-Surface Area V205-Ti02 Catalyst. *Applied Catalysis B: Environmental*, 2, 9–26.

Ueda, A., Nakao, T., Azuma, M. & Kobayashi, T. (1998). Two Conversion Maxima at 373 and 573 K in the Reduction of Nitrogen Monoxide with Hydrogen over Pd/TiO2 Catalyst. *Catalysis Today*, 45, 135–138.

United Nations Economic Commission for Europe. (1979). *Protocol to the 1979 Convention on Long-Range Transboundary Air Pollution to Abate Acidification, Eutrophication and Ground-Level Ozone*.

United Nations Economic Commission for Europe. (2012). Status of Ratification of The 1999 Gothenburg Protocol to Abate Acidification, Eutrophication and Ground-Level Ozone as of 24 May 2012. *UNECE*. Retrieved August 13, 2017, from http://www.unece.org/env/lrtap/status/99multi_st.html

Väliheikki, A., Petallidou, K. C., Kalamaras, C. M., Kolli, T., Huuhtanen, M., Maunula, T., Keiski, R. L. & Efstathiou, A. M. (2014). Selective Catalytic Reduction of NOx by Hydrogen (H2-SCR) on WOx-Promoted CezZr1-ZO2 Solids. *Applied Catalysis B: Environmental*, 156–157, 72–83.

Wang, Lifeng; Chen, Hao; Yuan, Min-Hao; Rivillon, Sandrine; Klingenberg, Eric H.; Li, Jimmy Xianming; Yang, R. T. (2014). Selective Catalytic Reduction of Nitric Oxide by Hydrogen over Zn-ZSM-5 and Pd and Pd/Ru Based Catalysts. *Applied Catalysis B: Environmental*, 152–153, 162–171.

Wang, L., Yin, C. & Yang, R. T. (2016). Selective Catalytic Reduction of Nitric Oxide with Hydrogen on Supported Pd: Enhancement by Hydrogen Spillover. *Applied Catalysis A: General*, 514, 35–42.

Wang, W., McCool, G., Kapur, N., Yuan, G., Shan, B., Nguyen, M., Graham, U. M., Davis, B. H., Jacobs, G., Cho, K. & Hao, X. (Kelly). (2012). Mixed-Phase Oxide Catalyst Based on Oxidation in Diesel Exhaust. *Science*, 337, 832–836.

Wang, X., Wen, W., Su, Y. & Wang, R. (2015). Influence of Transition Metals (M = Co, Fe and Mn) on Ordered Mesoporous CuM/CeO2 Catalysts and Applications in Selective Catalytic Reduction of NOx with H2. *RSC Advances*, 5(77), 63135–63141.

White, J. L. (1971). Interpretation of Infrared Spectra of Soil Minerals. *Soil Science*, 112(1),

22–31.

Wilkinson, F. (1980). *Chemical Kinetics and Reaction Mechanisms*. London: Van Nostrand Reinhold Company.

Winter, E. R. S. (1971). The Catalytic Decomposition of Nitric Oxide by Metallic Oxides. *Journal of Catalysis*, 22(2), 158–170.

Xue, Y., Lu, G., Guo, Y., Guo, Y., Wang, Y. & Zhang, Z. (2008). Effect of Pretreatment Method of Activated Carbon on the Catalytic Reduction of NO by Carbon over CuO. *Applied Catalysis B: Environmental*, 79(3), 262–269.

Yahya, M. A., Mansor, M. H., Zolkarnaini, W. A. A. W., Rusli, N. S., Aminuddin, A., Mohamad, K., Sabhan, F. A. M., Atik, A. A. A. & Ozair, L. N. (2018). A Brief Review on Activated Carbon Derived from Agriculture By-Product, in: *AIP Conference Proceedings*, (pp. 1–8).

Yakub, I., Mohamad Said, K. A., Mohamed Amin, M. A., Ahmad Zauzi, N. S. & Mohamed Sutan, N. (2013). Characteristics of Carbon-Supported Catalysts Derived for Low-Temperature Selective Catalytic Reduction: A Short Review. *Proceedings of the 1st International Conference on Chemical, Nano and Sustainable Engineering*, 118–131.

Yang, J., Ma, H., Yamamoto, Y., Yu, J., Xu, G., Zhang, Z. & Suzuki, Y. (2013). SCR Catalyst Coated on Low-Cost Monolith Support for Flue Gas Denitration of Industrial Furnaces. *Chemical Engineering Journal*, 230, 513–521.

Yang, Y., Chiang, K. & Burke, N. (2011). Porous Carbon-Supported Catalysts for Energy and Environmental Applications: A Short Review. *Catalysis Today*, 178(1), 197–205.

Yin, C., Wang, L., Rivillon, S., Shih, A. J. & Yang, R. T. (2015). SCR of Nitric Oxide by Hydrogen over Pd and Ir Based Catalysts with Different Supports. *Catalysis Letters*, 145, 1491–1499.

Yoshinari, T., Sato, K., Haneda, M., Kintaichi, Y. & Hamada, H. (2003). Positive Effect of Coexisting SO2 on the Activity of Supported Iridium Catalysts for NO Reduction in the Presence of Oxygen. *Applied Catalysis B: Environmental*, 41, 157–169.

Yu, Q., Richter, M., Li, L., Kong, F., Wu, G. & Guan, N. (2010). The Promotional Effect of Cr on Catalytic Activity of Pt/ZSM-35 for H2-SCR in Excess Oxygen. *Catalysis Communications*, 11(11), 955–959.

Yu, T., Fan, D., Hao, T., Wang, J., Shen, M. & Li, W. (2014). The Effect of Various Templates on the NH3-SCR Activities over Cu/SAPO-34 Catalysts. *Chemical Engineering Journal*, 243, 159–168.

Yuan, D., Li, X., Zhao, Q., Zhao, J., Tadé, M. & Liu, S. (2014). A Novel CuTi-Containing Catalyst Derived from Hydrotalcite-like Compounds for Selective Catalytic Reduction of NO with C3H6 under Lean-Burn Conditions. *Journal of Catalysis*, 309, 268–279.

Zhang, J. J. & Samet, J. M. (2015). Chinese Haze versus Western Smog: Lessons Learned. *Journal of Thoracic Disease*, 7(1), 3–13.

Zhang, L., Aboagye, A., Kelkar, A., Lai, C. & Fong, H. (2014). A Review: Carbon Nanofibers from Electrospun Polyacrylonitrile and Their Applications. *Journal of Materials Science*, 49(2), 463–480.

Zhang, S., Liu, W., Wang, C., Zhu, C., Yang, S., Guo, M., Qiao, R., Stewart, P., Zhang, H., Gu,

X., Hexemer, A., Wang, Y. & Yang, W. (2016). Improving the NOx Decomposition and Storage Activity through Co-Incorporating Ammonium and Copper Ions into Mg/Al Hydrotalcites. *RSC Advances*, 6(51), 45127–45134.

Zhang, X. (2016). *Emission Standards and Control of PM2.5 from Coal-Fired Power Plant*.

Zulkurnai, N. Z., Mohammad Ali, U. F., Ibrahim, N. & Abdul Manan, N. S. (2017). Carbon Dioxide (CO2) Adsorption by Activated Carbon Functionalized with Deep Eutectic Solvent (DES), in: *IOP Conference Series: Materials Science and Engineering*.

APPENDICES

Appendix A: Supplementary information for Chapter 3 (Methodology)

Table A.1: Fragmentation and relative fragment intensities (RFI).

	RFI as found in MS library %												RFI from calibration experiment %											
Species	47	46	45	44	34	33	32	31	30	29	28	22	20	19	18	17	16	15	14	13	12	4	2	1
He																						100	10	
																						100	0.02	4.93
NO							0.2	0.4	100								1.5	2.4	7.5					
							0.41	0.36	100								1.40	2.53	5.34					
NO_2	1	37.0							100.0								22.3		9.6					
	0	11.7		6.6			12.9	0.4	100.0								4.7	6.4	4.4					
CO_2		0.4	1.3	100						0.1	11.4	1.2					8.5			0.1	6.0			
		0.37	1.11	100						0.08	10.78	1.60					17.55			0.04	7.98			
N_2O		0.2	0.7	100				0.1	31.1		10.8						5		12.9				0.1	
		0.25	0.83	100			1.60	0.16	27.76		11.98						7.61		14.16				1.45	
N_2										0.8	100								7.2					
										0.7	100								9.28					
CO									0.2	1.1	100						0.9		0.6		4.5			
											100													
O_2					0.4	0.1	100										11.4							
					0.39	0.08	100										11.97							
NH_3															0.4	100	80.0	7.5	2.2					
									2.2						6.3	100	78.1	3.1	0.9				0.7	
H_2																							100	10.0
																							100	28.96
H_2O													0.3	0.1	100	23	1.1						0.7	
											1.44		0.00	5.08	100	25.97	2.13						0.00	

Highlighted green RFI – overlapped base peak
Highlighted yellow RFI – unique indicator of gas present

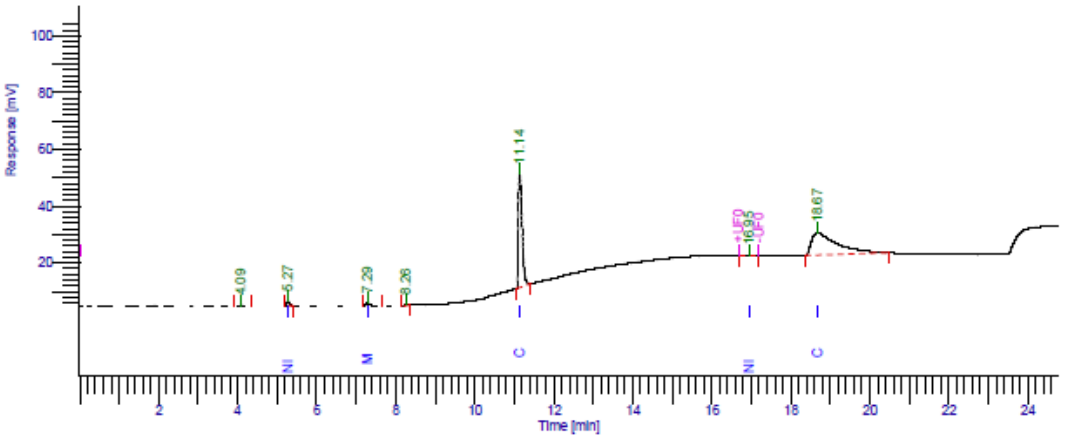

DEFAULT REPORT

Peak #	Component Name	Time [min]	Area [µV·s]	Height [µV]	Area [%]	Norm. Area [%]	BL	Amount (%)
1		4.089	3611.78	246.55	0.56	0.56	BB	0.0036
2	Nitrogen	5.272	7489.50	1655.33	1.16	1.16	BB	1.0624
3	Methane	7.288	9300.78	1096.93	1.44	1.44	BB	1.2204
4		8.255	1499.49	267.45	0.23	0.23	BB	0.0015
5	Carbon monoxide	11.136	263128.93	40025.12	40.72	40.72	BB	23.1717
6	Nitrous Oxide	16.947	0.07	3.66	1e-05	1e-05	MM	0.0000
7	Carbon dioxide	18.673	361091.89	7812.42	55.89	55.89	BB	40.2005
			646122.43	51107.45	100.00	100.00		65.6601

Figure A.1: Calibration curve for GCTCD molecular sieve column. Detector: TCD (100 °C), carrier gas: pure hydrogen (5 mL/min), oven ramp: 30 °C for 8 mins, increase to 300 °C at 40 °C/min and hold for 10 min.

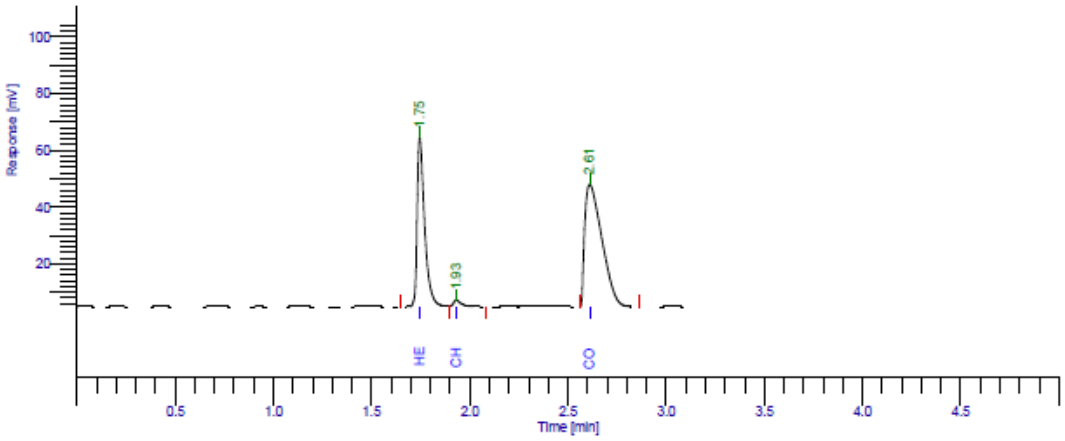

DEFAULT REPORT

Peak #	Component Name	Time [min]	Area [µV·s]	Height [µV]	Area [%]	Norm. Area [%]	BL	Amount (%)
1	He/Air/CO	1.745	158753.50	59749.68	37.17	37.17	BV	0.1588
2	CH4	1.931	6581.64	2398.99	1.54	1.54	VB	0.0066
3	CO2	2.611	261761.22	43056.43	61.29	61.29	BB	35.4702
			427096.36	105205.10	100.00	100.00		35.6355

Figure A.2: Calibration curve for GCTCD PLOT column. Detector: TCD (100 °C), carrier gas: pure hydrogen (5 mL/min), and oven ramp: 30 °C for 5 min.

Table A.2: Calibration certificate for KANE 940 combustion analyser of the following accuracy: ±2ppm NO for < 30 ppm, ±5ppm NO for > 30 ppm and ±5ppm < 100 ppm NO_2.

Gas value:	**Instrument reading**
O_2 5.08%	5.2%
NO 995 ppm	1000 ppm
CO 977 ppm	972 ppm
Applied value for NO (ppm)	**Instrument reading**
0	0
10	9
25	24
50	49
75	74
100	100
500	499

Section A.1: Sample calculation for NO_x at reference condition.

Oxygen correction factor, $f_{oxy} = \frac{21 - reference\ oxygen}{21 - measured\ oxygen}$

Concentration at reference conditions = measured concentration X f_{oxy}

In the case for using catalyst $PKSCu_{20}$ in 500 ppm NO + 4% H_2 + 1.5% O_2 at 200 °C,

Reference oxygen = 1.5%

Measured oxygen with KANE940 = 2.7%

NO measured concentration with KANE940 = 479 ppm

Therefore, the corrected NO concentration = 510 ppm

Table A.3: Calculation of heat of reaction at 300 °C.

	ΔHr(298)	**Cp (J/mol.K)**	
Component	**kJ/mol**	**298**	**573**
NO	91.2	29.86	30.51
H_2	0	28.84	29.32
N_2	0	29.12	30.1
N_2O	81.6	38.6	48.38
NH_3	-45.9	35.64	45.26
H_2O	-241.8	75.38	36.48
prod - react	-1387.5	96.96	-44.15
		$\int_{298}^{573} C_p dT$	-54.192
		ΔHr(573)	-1441.69

$$2NO + 2H_2 \rightarrow N_2 + 2H_2O$$

$$2NO + H_2 \rightarrow N_2O + H_2O$$

$$NO + \frac{5}{2}H_2 \rightarrow NH_3 + H_2O$$

$$\Delta H_R(T) = \Delta H_R(298K) + \int_{298}^{573} C_p dT$$

$$\int_{298}^{573} C_p dT = \left(C_{p,573}\right)(573\ K) - \left(C_{p,298}\right)(298\ K)$$

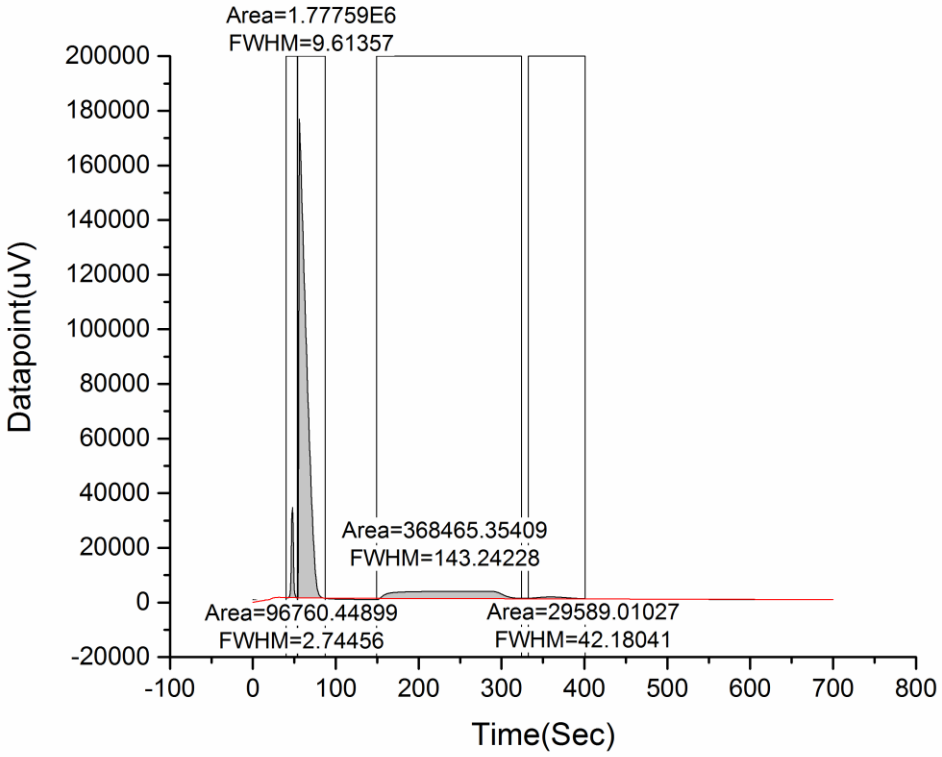

Figure A.3: GC-TCD calibration peak for 2,5-(bis(5-tert-butyl-2-benzo-oxazol-2-yl) thiophene (BBOT) with the area-under-the-peak in PTFE Porapaq Q (6x5mmx2m) column. Detector: TCD (65 °C), carrier gas: pure nitrogen (200 mL/min).

Table A.4: Inorganic content of PKS and PKSCu as obtained using ashing method coupled with ICPMS.

Element	PKS	PKSCu	**Element**	PKS	PKSCu
	mg/kg	**mg/kg**		**mg/kg**	**mg/kg**
Cu	6.3	110535.4	Tl	0.1	1.1
Ca	553.1	345.5	As	1.1	0.7
Mg	301.8	199.2	Mo	0.0	0.6
Fe	229.1	49.6	Ag	0.0	0.5
Al	235.9	34.5	Be	0.0	0.4
Zn	3.5	19.2	Ce	15.7	0.4
W	9.1	13.1	Te	0.0	0.2
Rb	21.5	7.8	Ga	2.0	0.2
Mn	6.2	5.9	Cr	0.9	0.1
Sr	10.3	5.8	Co	0.1	0.1
Pb	0.2	4.5	Cd	0.0	0.1
Li	0.5	3.2	U	0.0	0.0
Ba	4.3	3.0	Nd	0.0	0.0
V	3.8	2.9	Bi	0.0	0.0
B	13.9	2.6	Cu (wt%)	0.000626	11.05354
Ni	1.6	1.5			
Se	0.2	1.4			

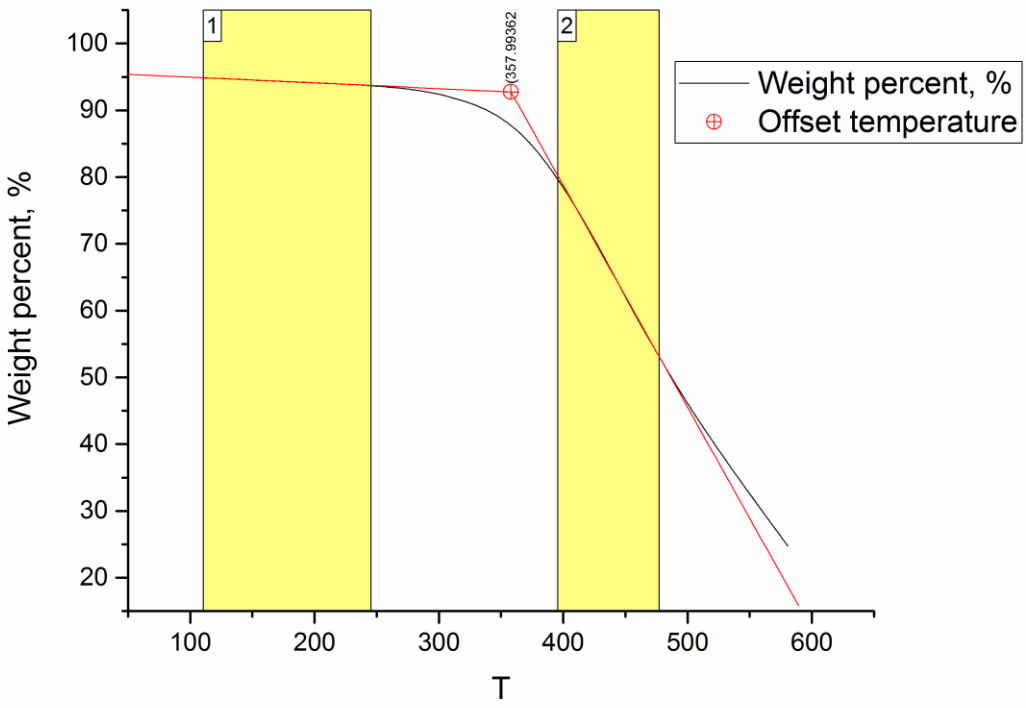

Figure A.4: An example of offset-temperature determination from TGA curve (for $PKSCu_{20}$) using OriginPro 2017. 5 mg sample was held at constant temperature of 30 °C for 4 minutes, heated to 110 °C at 40 °C/min and held at this temperature for 6 minutes, and further heated to 600 °C at 80 °C/min.

Appendix B: Supporting information for Chapter 4

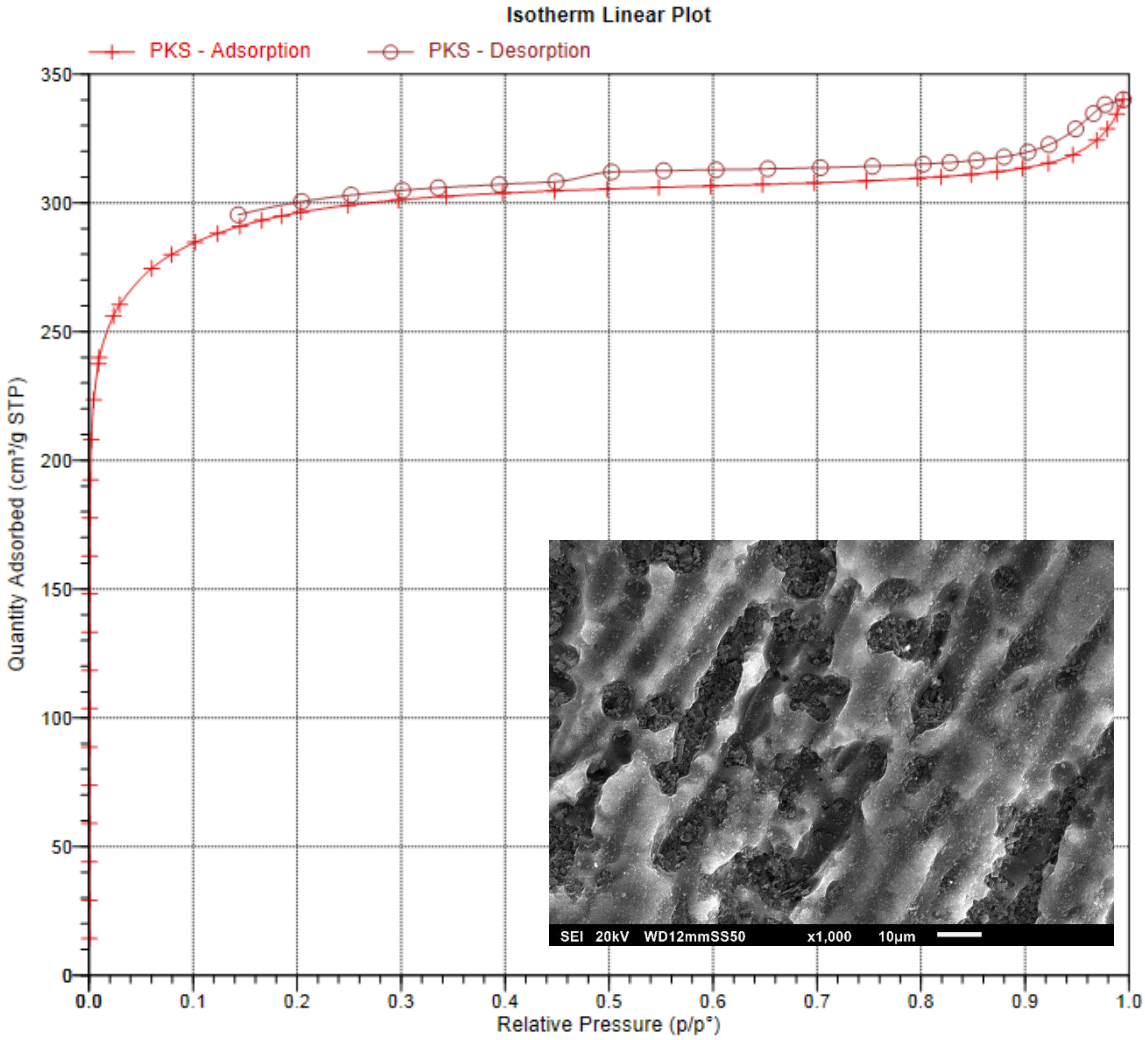

Figure B.1: Nitrogen adsorption-desorption isotherm over 0.1 g sample and 77 K, and (insert) SEM image at 1000 magnifications and 20 kV for PKS.

Table B.1: Peak properties obtained from OriginPro 2017 using Gaussian deconvolution method.

Species / Sample	Adsorbed NO_2			Adsorbed NO			Nitrosyls		
	Peak (°C)	FWHM	Area (X 10^{-9})	Peak (°C)	FWHM	Area (X 10^{-9})	Peak (°C)	FWHM	Area (X 10^{-9})
PKS	166	79.1	9.59	273	117.0	6.02	-		
	128*	56.9	0.06						
PKSCu	160	92.2	3.43	-			85	58.6	2.10
							115	30.7	0.27
PKSFe	-			134	109.3	1.22	87	67.0	0.85
PKSMn	117	88.2	1.17	210	123.8	0.70	73	58.0	0.70

FWHM = Full width at half maximum

*From desorption of NO_2

Appendix C: Supplementary information for Chapter 5

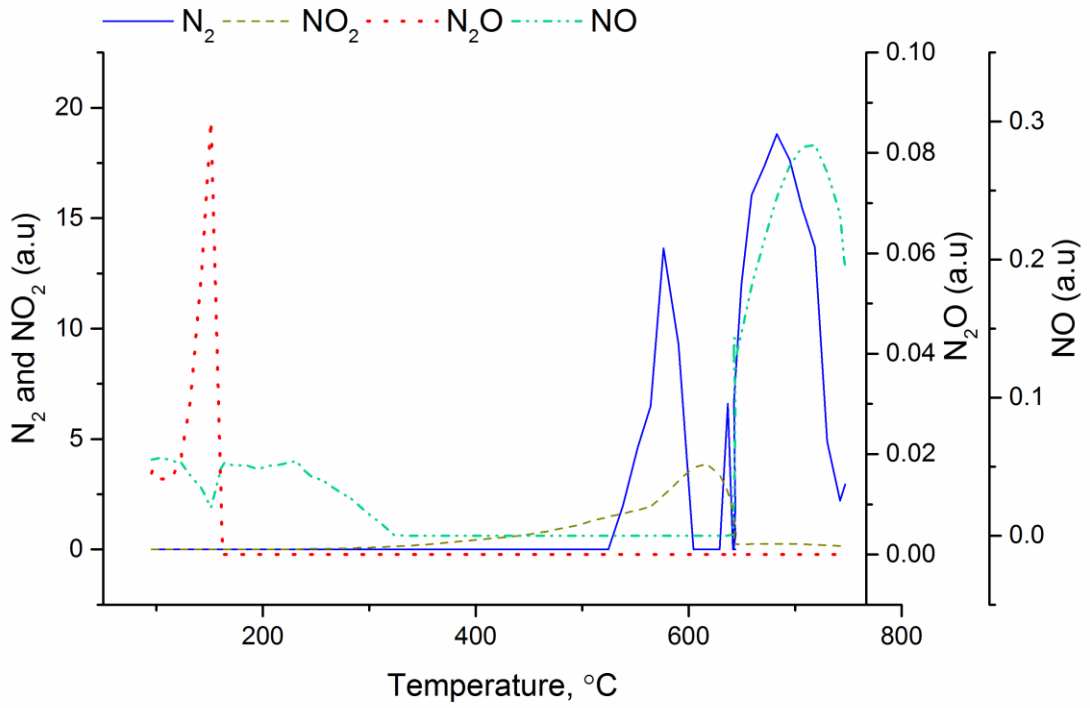

Figure C.1: Desorption profile for the undesorbed products from $PKSFe_{30}Cu_{10}$ in 500 ppm NO + 4% H_2 + 1.5% O_2 at 7,175 h^{-1}. The reaction was carried out at 300 °C for 2 h and cooled to 100 °C with the gas flow switched to pure helium at the same flow rate. After reaching 100 °C, the temperature was ramped at 5 °C/min until no more peak appeared.

Figure C.1 shows that the undesorbed products include nitrous oxide (N_2O), nitrogen dioxide (NO_2), nitric oxide (NO), and nitrogen (N_2). At temperature below 200 °C, N_2O was one of the products detected but it seemed that some of this gas was not completely desorbed due to the slow desorption constant. At about 200 °C, NO was also released making conversion low at this temperature, while at higher temperatures, NO experienced decomposition into nitrogen and oxidation to NO_2 (reaction with metal oxides or carbon surface functional groups).